The impact of alpha (α)-synuclein pathology on prefrontal cortex networks in a mouse model of Dementia with Lewy Bodies

Anastasia Dimitriou

Thesis submitted for the degree of Doctor of Philosophy at Newcastle University, Biosciences Institute

June 2024

Supervisors:

Dr Fiona LeBeau, Dr Gavin Clowry

Abstract

Dementia with Lewy Bodies (DLB) is caused by aggregated insoluble alpha(α)-synuclein (α-syn) in neurons and patients exhibit cognitive impairment involving the anterior cingulate cortex (ACC). Cortical network hyperexcitability has also been observed in DLB patients. Parvalbumin interneurons (PVIs) are critical for controlling excitability and normal cognitive function and are often surrounded by a specialised extracellular matrix, the perineuronal nets (PNNs). Loss of PVIs and PNNs occurs in Alzheimer's Disease but their role in DLB remains unclear. Neuroinflammatory changes may play an early role in DLB. In this thesis, I aimed to investigate hyperexcitability in the early stages of α-syn disease pathology in the ACC using hA30P transgenic mice expressing human α-syn. Changes in PVIs, PNNs, and glial cells in different disease stages were examined. In the A30P mice, I found hyperexcitability in ACC *in vitro* including frequent seizure-like events associated with PV activity. Additionally, immunofluorescence was conducted to examine the impact of hα-syn pathology on PVIs, PNNs, microglia, and reactive astrocytes in the ACC in young (2-4 months) and aged (10-12 months) A30P and control mice. A trend towards a decrease in the PVI number was revealed in young and aged A30P mice. Additionally, a significantly greater proportion of PNNs surrounding non-PV neurons was observed in young A30P animals. PV somas and PNNs contained hα-syn in young A30P mice and this expression increased with age. Neuroinflammation also increased in all aged animals showing a significant increase in the %area of GFAP+ astrocytes and reactive microglia. This thesis provided evidence of hyperexcitability potentially related to changes in PV neurons in the ACC and a shift in PNN localisation to surround presumed pyramidal neurons in young A30P mice which might be protective against hα-syn pathology. Additionally, the data suggested increased neuroinflammation correlated with age in the ACC in hA30P and control mice.

Acknowledgements

First and foremost, I would like to express my deepest gratitude to my supervisors at Newcastle University, Dr Fiona LeBeau and Dr Gavin Clowry, for their unwavering support, guidance, and advice throughout my research project. My PhD journey was different and special as I had to change labs halfway through. Fiona, who used to be on my progress panel, welcomed me into her lab and believed in me as a scientist and a person. Thus, I would like to say a particular thank you to her for helping me develop as a PhD student in Neuroscience, for always making me comfortable and for her good company during these last two years. Gavin, thank you for also being a great supervisor and for all your help with the immunohistochemistry experiments and analysis. To both of you, your invaluable knowledge and expertise played an instrumental role in shaping this research project.

I am also grateful to my progress panel, Dr Faye McLeod and Professor Adrian Rees, for their constructive feedback, thoughtful critiques and continuous support. Thank you for ensuring I am always on track and for your honest advice.

The work presented in this research project is my own, but I would also like to acknowledge the help of undergraduate and master's students that I have assisted in their co-supervision over these two years. For the data collection of the *in vitro* electrophysiology and immunohistochemistry experiments, I would like to thank Daisy McAllister, Youssef Sammouh, Annie Thomas, Sophie Cuthbertson, and Poppy Spiers. Annie Thomas assisted with the electrophysiology and immunohistochemistry data collection and analysis in Chapter 3 and some immunohistochemistry data collection and analysis in Chapter 4. Sophie Cuthbertson also assisted with the immunohistochemistry work in Chapter 3. Daisy and Youssef assisted with the electrophysiology data collection and analysis of the hyperexcitability experiments in Chapter 4. Lastly, Poppy has assisted with the immunohistochemistry work in Chapter 6. I am grateful for all the help you provided in this project as without all of you, I would not have delivered this research outcome in such a limited time.

A PhD journey is stressful, and you are required to make sacrifices to succeed but moral support from good friends keeps you going. Thus, I would like to acknowledge the great moments I had with all the lab members which made this experience for me more enjoyable. A special thank you goes to the lunch club

members. A particular thank you must go to Beth, even though I have known you for only two years, I am thankful for our friendship, your constant support and advice. Sorry to say but you will be stuck with me for more years to come! Lauren, our youngest PhD student in the lab, I am glad I met you and have come to call you a good friend, cannot wait for more memories together. Dave, thank you for all the help and wise advice, your blunt Scottish humour, and your awesome taste in music, happy to call you a true friend. Jean, we spent some great moments together and it was hard to make you laugh but I succeeded with my awful dad jokes, cannot wait to see you again. I would also like to thank the rest of the lab members including Ibtisam, Connie, Daipayan, Ashan, and Mark as well as Dr Bas for his Imaris analysis advice. A particular thank you also goes to the BioImaging unit at Newcastle University and specifically to Glyn Nelson who was always helping me with the confocal microscope.

On a personal note, I would like to thank my friends and family who are back home in Cyprus. To my parents, Andri and Panayiotis, and my younger brother Demetris, thank you for believing in me and letting me spread my wings and fly. I know being away for almost 10 years was not easy but my studies without your endless love and support would not have been possible. I did it, Mum and Dad, and now I will be able to finally get a job and become a “full adult”! I would also like to thank my cousin Kyriaki, who has been studying here in Newcastle, for all her continuous support, for calming me down during some stressful moments and for bearing my mood swings.

“And a new day will dawn for those who stand long, and the forests will echo with laughter.” - Led Zeppelin

Thank you all.

Impact of Covid-19 pandemic

The COVID-19 pandemic affected the initial stages of my PhD project, particularly during the early stages of global lockdowns and restricted access to the lab facilities. As my research involves hands-on lab work involving mouse tissue, the closure of research institutions led to a substantial pause in getting a personal licence for animal experiments as well as in data collection and experimental procedures. This interruption then required a reassessment of my project timelines and goals.

The pandemic also introduced new challenges related to the availability of resources and reagents, as supply chains were disrupted globally. This created additional delays in obtaining the necessary consumables and equipment for my research. Thus, I had to adapt my research strategy and prioritise tasks that could be completed remotely, such as literature review and writing. Although this allowed me to make progress in other areas, it limited my ability to begin the experiments of my project. In response to these challenges, I developed new skills in project management and remote collaboration, ensuring that I could still meet my research objectives despite the setbacks.

While the pandemic extended the timeline of my PhD, it also strengthened my resilience, adaptability, and problem-solving abilities. These experiences have equipped me to navigate unforeseen challenges in future research settings.

Conference Presentations

Work from this thesis was presented at the following conferences:

International Conference on Alzheimer's and Parkinson's Diseases (ADPD)

(Gothenburg, Sweden) March 2023, poster presentation

British Neuroscience Association

(Brighton, UK) April 2023, poster presentation

Federation of European Neuroscience Association

(Vienna, Austria) June 2024, poster presentation

Table of Contents

List of Figures

List of Tables

List of Abbreviations

3D	Three-dimensional
4-AP	4-Aminopyridine
A.U.	Arbitrary Units
A30P	Alanine to proline exchange in position 30
ACC	Anterior Cingulate Cortex
ACSF	Artificial cerebrospinal fluid
AD	Alzheimer's Disease
ADAMTS	A Disintegrin and Metalloproteinase with Thrombospondin motifs enzymes
AI	Agranular Insular area
AMPA	alpha-amino-3-hydroxy-5-methyl-4-isoxazole-propionic acid
AMPA-R	AMPA Receptor
ANOVA	ANOVA Analysis of variance
Aβ	Amyloid beta protein
BBB	Blood-brain barrier
BCAN	Brevican
BDNF	Brain-derived neurotrophic factor
C1q	Component 1 subcomponent q
CA 1,3	Cornu Ammonis 1, 3
CCL2	Chemokine (C-C motif) ligand 2
Ch ABC	Chondroitinase ABC
CNS	Central Nervous System
COX	Cyclooxygenase
CS4	Sulphation patterns in position 4 of CS chains
CS6	Sulphation patterns in position 6 of CS chains
CSF	Cerebrospinal fluid
CSPGs	Chondroitin sulphate proteoglycans
DLB	Dementia with Lewy Bodies
dlPFC	Dorsolateral Prefrontal Cortex
DNA	Deoxyribonucleic acid
dPFC	Dorsal Prefrontal Cortex

E/I	Excitation/Inhibition
EAAT1	Excitatory amino acid transporter 1
EAAT2	Excitatory amino acid transporter 2
ECM	Extracellular matrix
EEG	Electroencephalogram
eNOS	Endothelial NOS
Fc receptor	Fragment crystallisable receptor
fMRI	Functional Magnetic Resonance Imaging
GABA	Gamma-aminobutyric acid
$GABA_A$-R	GABA receptor type A
GABA-R	GABA receptor
GAD	Glutamic acid decarboxylase
GAGs	Glycosaminoglycans
GFAP	Glial fibrillary acidic protein
HA	Hyaluronan
HAS	Hyaluronan synthase
HD	Huntington's Disease
HSPGs	Heparan sulphate proteoglycans
Hyase	Hyaluronidase
hα-syn	Human α-synuclein
Iba-1	Ionized calcium-binding adaptor molecule 1
IFN-γ	Interferon-gamma
IHC	Immunohistochemistry
IID	Interictal discharges
IL	Infralimbic area
iNOS	Inducible NOS
IQR	Interquartile range
KA	Kainate
KA-R	Kainate receptor
KCC2	Potassium chloride cotransporter
LBD	Lewy Body Diseases
LBs	Lewy bodies
LFP	Local field potential

LIF	Leukemia inhibitory factor
LNs	Lewy neurites
LPS	Lipopolysaccharide
LTP	Long term potentiation
LTS	Low-threshold spiking
L-VDCC	L-type voltage-dependent calcium channels
MCI	Mild cognitive impairment
MD	Mediodorsal Nucleus
MDD	Major depressive disorder
MEG	Magnetoencephalography
mIPSC	Miniature inhibitory postsynaptic current
MMPs	Matrix metalloproteinases
mPFC	Medial Prefrontal Cortex
MSA	Multiple System Atrophy
NFIA	Nuclear factor IA
NHP	Non-human primates
NK-κB	Nuclear factor kappa-light-chain-enhancer of activated B cells
NMDA	N-methyl-D-aspartate
NMDA-R	NMDA receptor
nNOS	Neuronal NOS
NO	Nitric oxide
NOS	Nitric oxide synthase
NREM	Non-rapid eye movement sleep
OFC	Orbitofrontal Cortex
PBS	Phosphate buffer saline
PCC	Posterior Cingulate Cortex
PD	Parkinson’s Disease
PDD	Parkinson’s disease dementia
PET	Positron Emission Tomography
PFA	Paraformaldehyde
PFC	Prefrontal Cortex
PFF	Pre-formed fibrils
PL	Prelimbic area

PNNs	Perineuronal nets
pS129	Phosphorylation of α-syn at serine residue 129
PV	Parvalbumin
RBD	Rapid eye movement sleep behaviour disorder
RNS	Reactive nitrogen species
ROS	Reactive oxygen species
sACSF	Sucrose artificial cerebrospinal fluid
SD	Standard deviation
SEM	Standard error of the mean
SNARE	SNAP Receptor proteins
SST	Somatostatin
TGF-β1	Transforming growth factor β1
Thy-1	Thymocyte differentiation antigen 1
TIMPs	Tissue inhibitors of matrix metalloproteinases
TLR	Toll-like receptors
TMS	Transcranial magnetic stimulation
TNF-α	Tumour necrosis factor-α
tPA	Tissue plasminogen activator
TSPO	Translocator protein
TUNEL	Terminal deoxynucleotidyl transferase dUTP nick end labelling
VTA	Ventral Tegmental Area
WT	Wild type
α-syn	α-synuclein
β-syn	β-synuclein
γ-syn	γ-synuclein

Chapter 1. Introduction

1.1. General Introduction

Dementia originates from the Latin word “demens” which means “out of mind”. It is a clinical syndrome characterised by progressive cognitive decline and causes people to be unable to function independently (Sheehan, 2012; Chertkow *et al.*, 2013). People with dementia are affected by a variety of symptoms including memory loss, communication and language dysfunction, agnosia, apraxia, and impaired executive function (Duong *et al*., 2017). Dementia does not affect a specific age group as it has an impact across the lifespan of individuals, however, the ageing population is most likely affected by dementia as the incidence increases with age. Dementia is considered early-onset when affecting people under 65 years old and it is late-onset when it is diagnosed over 65 years old which is the majority of cases (Cunningham *et al.*, 2015).

The estimated number of people affected by dementia in the United Kingdom is currently more than 944,000 and it is a physical, emotional, and financial burden on patients, carers, and the wider society (NHS England). The number of dementia cases is estimated to increase in the coming decades, and as suggested by the National Health Service (NHS), the number of patients will rise to more than 1 million by 2030 due to the ageing population. The most common type of dementia is Alzheimer’s disease (AD) affecting 50-70% of the cases followed by vascular dementia accounting for 20% of cases, dementia with Lewy bodies up to 15 – 20 % and frontotemporal lobar dementia for 5% (Aarsland *et al.*, 2001; Jellinger and Attems, 2011; Cunningham *et al.*, 2015; Kane *et al.*, 2018). Each of these dementia subtypes encompasses different clinical symptoms underpinning different pathological mechanisms that complicate the diagnosis and treatment approaches.

"In the world of dementia, reality is a matter of perception. Our job is to inhabit their world, not force them into ours." - Naomi Feil, developer of Validation Therapy.

1.2. Alpha-synucleinopathy

1.2.1. *Dementia with Lewy Bodies*

Dementia with Lewy Bodies (DLB) is part of the Lewy body diseases (LBD) which are a group of synucleinopathies including Parkinson's disease (PD), Parkinson's disease dementia (PDD), and multiple system atrophy (MSA). These neurodegenerative disorders are characterised by a common pathological lesion which is the accumulation of aggregated insoluble α-synuclein (α-syn) protein in neurons and glial cells (Spillantini *et al.*, 1997; Galvin *et al*., 2001). The α-syn protein is a 14.5 kDa acidic protein composed of 140 amino acid residues and is encoded by the SNCA gene, belonging to the synuclein protein family including β-syn and γ-syn (Vasili *et al*., 2019). It was discovered and isolated from the synaptic vesicles of the electric organs of Torpedo californica, also known as the Pacific electric ray, in 1988 (Maroteaux *et al*., 1988). Later in 1997, the α-syn protein was characterised as the main component in Lewy bodies (LBs) and Lewy neurites (LNs) and the key features of the pathology of PD (Spillantini *et al.*, 1997). The importance of genetics in the disease was then demonstrated by Polymeropoulos and colleagues in 1997 who identified the first point mutation in the SNCA gene associated with autosomal familial PD (Polymeropoulos *et al.*, 1997).

Normal α-syn is involved in vesicle release and even though it is abundantly expressed in the blood cells and kidneys, it is mostly expressed in neuronal presynaptic terminals but also present in the nucleus. In the nucleus, α-syn is co-localised with the nuclear membrane and it is implicated in the regulation of synaptic membrane processes including neurotransmitter release by interacting with SNARE proteins (Tsigelny *et al.*, 2012; Bellucci *et al.*, 2016; Twohig and Nielsen, 2019). Interestingly, α-syn is not vital for the formation of synapses and survival of the cells as discovered from studies using α-syn knockout mice (Bisaglia *et al*., 2009). The α-syn protein is generally expressed in humans and rodents in the cerebral cortex, cerebellum, striatum, thalamus, hippocampus, and olfactory bulb (Burré, 2015; Twohig and Nielsen, 2019).

Under pathological conditions, α-syn becomes misfolded from monomers to oligomers and then aggregates into fibrils which turn into LBs (Fig. 1.1). Pathological

α-syn essentially undergoes a conformational change from a random coil structure to a cross-β sheet-rich amyloid structure (Outeiro *et al.*, 2019). The aggregated α-syn leads to the formation of LBs in neuronal somas and LNs in neuronal processes (Outeiro *et al.*, 2019). The LBs are spherical structures composed of a dense central core and a peripheral halo (Wakabayashi *et al.*, 2007). Additionally, apart from α-syn fibrils, LBs consist of other proteins (Wakabayashi *et al.*, 2013), lipids (Den Hartog Jager, 1969; Gai *et al.*, 2000) as well as membranous organelles such as lysosomal structures and damaged mitochondria (Forno and Norville, 1976; LS, 1986; Wakabayashi *et al.*, 1988; Hayashida *et al.*, 1993; Shahmoradian *et al.*, 2019). As the pathology progresses, apart from oligomerisation and fibrilisation there is increased phosphorylation of α-syn at serine 129 (pS129) found in both LBs and LNs which also increases with disease progression (Fujiwara *et al.*, 2002; Yuko *et al.*, 2003; Walker *et al.*, 2013; Kellie *et al.*, 2014; Ghanem *et al.*, 2022).

Clinical and autopsy studies have shown that DLB and PD patients demonstrate decreased dopamine terminals in the striatum (Braak *et al.*, 1994; Heiko Braak *et al.*, 2003; Adler and Beach, 2016). Additionally, it is suggested that synaptic damage is caused by α-syn oligomers, the toxic form of α-syn before further aggregation into LBs. Oligomers exert cytotoxicity by binding and inserting the lipid bilayer of the neuronal soma thus destroying the membrane integrity and forming pore-like structures (Tsigelny *et al.*, 2012; Fusco *et al.*, 2017; Froula *et al.*, 2019). These pores cause an increase in ionic influx inside the cell, especially calcium ions, which changes the ionic balance leading to cell death (Quist *et al.*, 2005; Angelova *et al.*, 2016; Fusco *et al.*, 2017). Oligomers can also cause mitochondrial dysfunction, endoplasmic reticulum stress, proteostasis dysregulation, synaptic impairment, apoptosis, and neuroinflammation (Kim *et al.*, 2009; Lorenzen *et al.*, 2014; Fusco *et al.*, 2017). These changes then contribute to progressive neuronal degeneration.

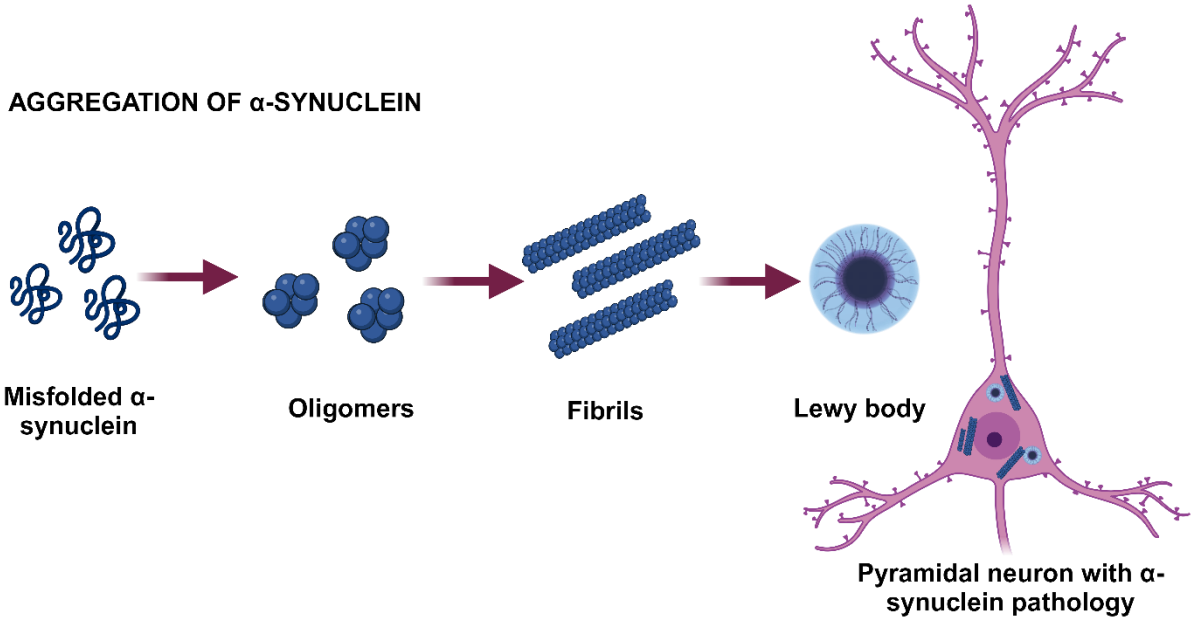

Figure 1.1. The misfolding of α-syn protein. Under pathological conditions, insoluble α-syn monomers are misfolded and aggregate into oligomers. The oligomers further aggregate into fibrils which could further turn into LBs. The α-syn oligomers and fibrils can be transmitted between neurons through synaptic interactions. The α-syn oligomeric structures are suggested to spread in a prion-like manner. This figure was created using Bio Render.

Patients suffering from DLB are first diagnosed with dementia and later with two or more symptoms including recurrent visual hallucinations, spontaneous extrapyramidal motor features, cognitive fluctuations and rapid eye movement sleep behaviour disorder (RBD) (McKeith, 2017). Cognitive fluctuations are spontaneous changes in cognition, attention, and arousal. Additionally, spontaneous extrapyramidal motor features are spontaneous parkinsonism characterised by continuous spasms and muscle contractions, a general increase in motor tone and involuntary motor activity as well as rigidity and bradykinesia (slowness of movement). Lastly, RBD is a dream enactment behaviour related to the loss of the rapid eye movement (REM) phase of sleep (McKeith, 2017).

Importantly, the spread of α-syn pathology in DLB differs from PD as initial symptoms in DLB reflect changes in the limbic system and neocortex as the patients manifest clinical dementia before the onset of motor symptoms (Outeiro *et al.*, 2019). While in PD, motor dysfunction occurs first, it is followed later in some cases by cognitive decline. German neurologist Heiko Braak (2003) analysed the disease's neuropathological progression based on post-mortem human brain tissue

examinations and characterised it into different Braak stages (Heiko Braak *et al.*, 2003). The first stage is identified with lesions originating in the olfactory bulb, anterior olfactory nucleus, and dorsal motor nucleus of the vagus nerve. In the second stage, lesions are spread to the lower raphe nuclei, the magnocellular parts of the reticular formation, and locus coeruleus. Furthermore, midbrain regions such as the substantia nigra pars compacta demonstrate increased pathology in the third stage. In Braak stage 4 pathology spreads to the mesocortex. Eventually, in stages 5 and 6, α-syn pathology reaches the neocortex, affecting first the prefrontal cortex and then the premotor, primary sensory areas, and the primary motor field (Braak *et al.*, 2003; Vasili *et al.*, 2019).

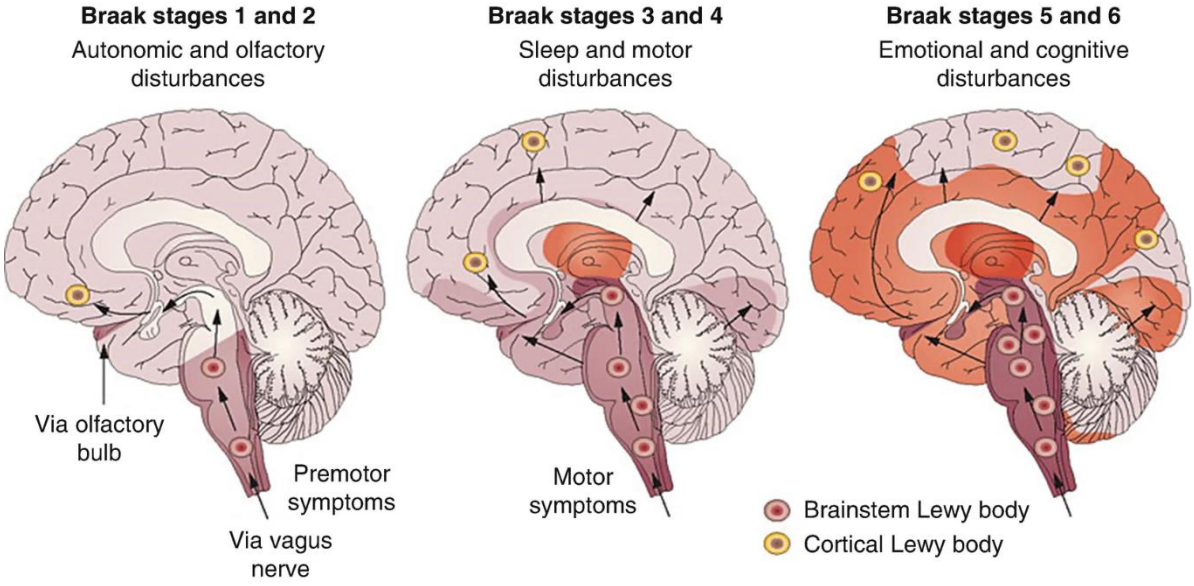

Figure 1.2. Braak stages describing α-syn pathology in a PD human brain. The progression of aggregated α-syn spread in the form of LBs is shown in Braak stages 1 – 6 in a PD human brain affecting connected brain areas. Figure taken from Doty, 2012 (Doty, 2012).

A preclinical study also characterised the spatiotemporal pattern of the α-syn pathology spread in the mouse brain. Henderson et al. (2019) injected α-syn pre-formed fibrils in the dorsal striatum of 3-month-old non-transgenic mice and analysed the pathology spread 1-, 3- or 6-months post-injection examining the abnormal misfolded (Syn506) and pS129 α-syn. A-syn was found to spread and accumulate in different brain areas, with those connected to the injection site most affected by

increased α-syn pathology. A “network diffusion” computational model based on a map of mouse brain areas and connection pathways helped with a more detailed investigation of the pathology spread. This revealed that the pattern of pathology spread was related to both the anatomical connections and endogenous levels of α-syn expression within a brain area (Henderson *et al.*, 2019). Therefore, these studies in mice suggest the increased spread of α-syn pathology over time between connected brain areas through neuronal connections.

To further study the impact of α-syn aggregation in different areas causing network and cognitive impairment, transgenic mouse models of α-synucleinopathies including DLB are necessary. These α-syn transgenic mouse models include the A53T, A30P, the double mutated A53T*A30P and human wild-type (WT) α-syn mice.

1.2.2. *Transgenic α-syn mouse models*

There are different α-syn transgenic mice overexpressing α-syn linked to familial forms of PD to study the α-syn pathology. One example would be the A53T transgenic mice expressing alanine-to-threonine mutation at amino acid position 53 in the α-syn SNCA gene (Polymeropoulos *et al.*, 1997). The A53T mice have been shown to develop α-syn intraneuronal inclusions, mitochondrial degeneration and cell death in neocortical areas, brainstem and spinal cord which might be related to their motor impairment and paralysis (Van Der Putten *et al.*, 2000; Giasson *et al.*, 2002; Lee *et al.*, 2002; Martin *et al.*, 2006). There are also double transgenic mice expressing combined point mutations in the α-syn gene including A53T and A30P which is the change of alanine-to-proline at amino acid position 30 (A53T*A30P mice). The A53T*A30P mice demonstrate dopaminergic neuronal loss and impairment in motor behaviour (Yan *et al.*, 2017; Kilpeläinen *et al.*, 2019). Kilpeläinen et al. (2019) discovered the expression of pathologic human α-syn (hα-syn) in cell somas, axons, and terminals in the nigrostriatal pathway in the A53T*A30P mice. Moreover, these animals demonstrated locomotor impairments at 7 - 9 and 13 - 23 months of age and a reduction in extracellular dopaminergic markers in the striatum and substantia nigra at 16 - 18 months of age (Kilpeläinen *et al.*, 2019). There are also transgenic mice expressing the non-mutated human WT α-syn related to sporadic PD. Cognitive impairment is present at an early stage and motor deficits at 14 - 15 months of age in

these mice correlated with α-syn overexpression throughout the brain (Chesselet et al., 2012; Magen et al., 2012).

In this thesis, the A30P α-syn transgenic mouse model was investigated. The A30P mutation is an autosomal dominant missense mutation in the SNCA gene, and it was initially discovered in a patient with familial PD reporting an aggressive early-onset form of the pathology. Kruger et al. (1998) identified the substitution of G-to-C at nucleotide position 88 resulting in alanine-to-proline exchange at amino acid position 30, the A30P mutation (Krüger *et al.*, 1998). Subsequently, Kahle and colleagues generated a transgenic mouse line harbouring the human A30P mutation to model PD (Kahle *et al.*, 2000, 2001). The A30P mouse model expresses the human mutant α-syn under the control of the Thymocyte differentiation antigen 1 (Thy-1) promoter. The Thy-1 promoter is Central Nervous System (CNS) neuron-specific and has a broad expression in all brain regions driving the overexpression of the hα-syn protein (Kahle *et al.*, 2000, 2001). Additionally, the Thy-1 promoter is a pan-neuronal marker originally presumed to have a predominant expression in the excitatory pyramidal cells in both the cortex and hippocampus (Feng *et al.*, 2000; Sugino *et al.*, 2005). At normal levels, human A30P α-syn was located in the synapses but also accumulated in the cell somas when overexpressed. In the A30P mice, mutant hα-syn is strongly expressed in the whole brain and is upregulated by the first month of age (Kahle *et al.*, 2000). The hα-syn is also expressed in a 3-fold higher expression level in the A30P mice compared to the endogenous α-syn protein (Kahle *et al.*, 2001).

The A30P mutation increases the aggregation of the hα-syn into oligomers and fibrils and the animals exhibit cognitive impairments and motor dysfunction by 12-14 months of age (Kahle et al., 2000, 2001). However, the A30P mice show neuronal degeneration and motor deficits without the formation of LBs as seen in PD and DLB patients although they do exhibit so-called Lewy-like neurites (Van Der Putten *et al.*, 2000; Martin *et al.*, 2006; Taylor *et al.*, 2014). Cognitive dysfunction has been reported at 12 months of age in the A30P mice associated with hα-syn overexpression and pathology in different brain areas (Freichel *et al.*, 2007). However, cognitive deficits and behavioural changes may occur earlier in the A30P mice. Decreased risk-taking behaviour has been demonstrated in 8-month-old A30P mice during the multivariate concentric square field test (Ekmark-Lewén *et al.*, 2018). These findings thus show that aggregation of hα-syn plays a key role in cognitive decline.

Lindström et al. (2014) showed that in the 12-month-old A30P mice, there was increased expression of hα-syn oligomers and protofibrils in the spinal cord which was related to obvious motor symptoms observed (Lindström *et al.*, 2014). In their later study, Ekmark-Lewén et al. (2018) demonstrated early PD-related symptoms in the A30P mice (Ekmark-Lewén *et al.*, 2018). Fine motor impairments were revealed in 2-month-old A30P mice following the beam test and progressed up to 11 months of age. Accumulation of hα-syn oligomers was discovered in the neuronal somas of 8-month and 11-month-old A30P mice as well as decreased tyrosine hydroxylase expression linked with the decrease in the dopaminergic system and possibly motor dysfunction (Ekmark-Lewén *et al.*, 2018). Previous studies in human post-mortem tissue have shown that acetylcholine in cortical areas, particularly the hippocampus in DLB and PDD patients, is reduced (Perry *et al.*, 1994; Tiraboschi *et al.*, 2000; Bohnen *et al.*, 2003). Following induced dopamine depletion, aged A30P mice have also shown decreased neurons expressing a cholinergic marker in the medial septum-diagonal band of the Broca complex (Szego *et al.*, 2013). However, future studies are required to elucidate the impact of α-syn pathology in cortical areas at an early stage in disease progression. Research using the A30P transgenic mouse model will help in the better understanding of α-syn induced toxicity in neural networks associated with cognitive dysfunction linked to DLB.

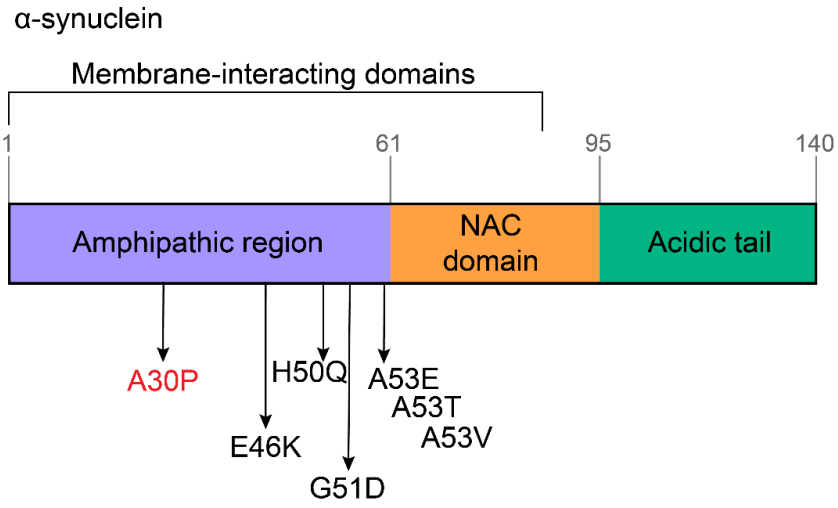

Figure 1.3. The domain structure of α-synuclein protein. The protein is composed of an N-terminal which is an amphipathic region, the central non-amyloid component (NAC) domain, and the acidic C-terminal. The amphipathic region includes the pathogenic mutations including the A30P mutation which is coloured in red.

1.3. The Prefrontal Cortex

1.3.1. *Structure and Function of the Prefrontal Cortex in human and mouse*

As the most complex organ of the human body, the human brain performs higher cognitive functions including intellectual function, memory, speech and language, complex perception, orientation, attention, judgment, planning, and decision-making. These mental processes constitute cognition, whereas behaviour is the manifestation of these cognitive functions (Tranel *et al*., 2003). As outlined in section 1.2.1, patients with DLB exhibit impaired cognitive functioning, for which various brain areas have been implicated, but primarily involves the prefrontal cortex (PFC). The PFC is the most anterior part of the frontal lobe and a key brain area exerting control of higher-order executive functions including working memory, decision-making, temporal processing, flexibility, and goal-directed behaviour (Miller and Cohen, 2001).

PFC in humans

The PFC constitutes approximately one-third of the human cerebral cortex (Siddiqui *et al.*, 2008). In human and non-human primates, PFC refers to the granular and orbital regions of the frontal cortex (Laubach *et al.*, 2018). The human PFC is divided into dorsomedial, dorsolateral, ventromedial, ventrolateral, anterior cingulate cortex (ACC), and orbitofrontal areas (Dalley *et al*., 2004; Siddiqui *et al.*, 2008). The Brodmann areas (BAs) defining the PFC are BA8-BA14 and BA44-BA47 which roughly correspond to the granular regions of PFC. The ACC is used to denote the agranular parts in the medial frontal cortex (Laubach *et al.*, 2018). The ACC is characterised as a midline, collar-formed structure surrounding the frontal area of the corpus callosum. It is considered a part of PFC since it receives projections from the MD nucleus (Carlén, 2017).

For more than 70 years, PFC has been characterised as the area of the cerebral cortex which receives projections from the mediodorsal nucleus (MD) of the thalamus. This division was based on research done by Rose and Woosley who used the

projection field of MD to explain the frontal cortex since MD targets a restricted frontal field, the orbitofrontal cortex (OFC), in primate and non-primate mammals (Rose and Woolsey, 1948). Research began to have a growing interest in elucidating the role of dorsolateral PFC (dlPFC) in humans and non-human primates with an increased rate of publications in the 1990s. Researchers were inspired and motivated by earlier investigations in the PFC of macaque monkeys led by Fuster in 1971 (Fuster and Alexander, 1971) as well as Goldman-Rakic in 1995 (Goldman-Rakic, 1995). Fundamental neuroimaging studies using PET and fMRI scans in humans characterised the PFC as crucial in higher-order cognitive processes including attention (Pardo *et al.*, 1991) and working memory (McCarthy *et al.*, 1994).

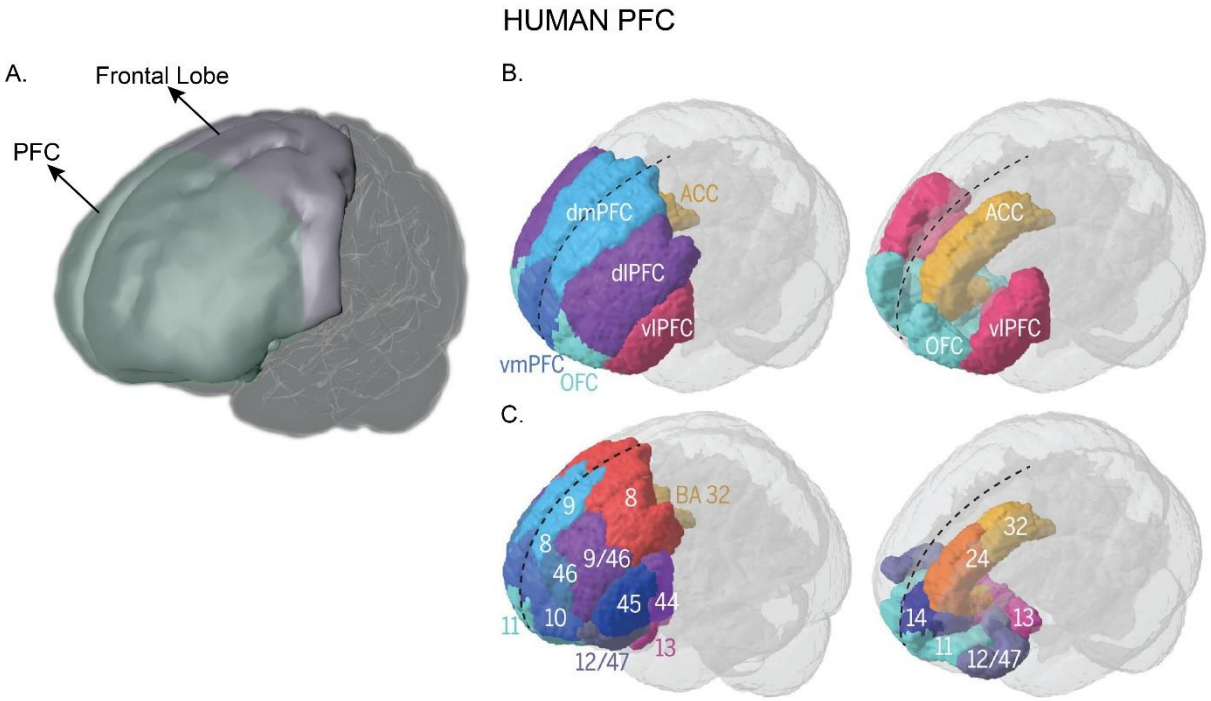

Figure 1.4. The human PFC. A. The green shaded area demonstrates the PFC located in the anterior part of the frontal lobe in humans. **B.** The PFC subdivisions include dorsomedial PFC (light blue), dorsolateral PFC (purple), ventromedial PFC (blue), ventrolateral PFC (pink), OFC (teal) and ACC (yellow). **C.** The PFC is divided into BAs. B & C are taken from Carlen, 2017 (Carlén, 2017).

PFC in mouse

There is a debate regarding the nomenclature of PFC and which areas it includes between humans, non-human primates, and rodents. The rodent equivalent PFC areas to humans are the ACC, prelimbic (PrL), infralimbic (IL), OFC, and agranular insular (AI) areas (Dalley *et al*., 2004). Additionally, the mediodorsal part of the rodent PFC has been known as the secondary motor area (MOs) (Carlén, 2017) In both mice and rats, fewer areas constitute the frontal lobe compared to primates, and the rodent PFC is agranular lacking layer 4 (Carlén, 2017; Le Merre *et al.*, 2021). Cytoarchitectonic investigations suggest homologies among the medial PFC (mPFC) and particularly the ACC in rodents, humans, and non-human primates (Vogt *et al.*, 2013; Vogt and Paxinos, 2014).

Following research in humans and non-human primates, the function of PFC was further elucidated with electrophysiology studies including multi-electrode recordings in rodents while performing behavioural tasks. This aided in the investigation of the role of PFC neurons in rodents during behaviour tasks dependent on the PFC (Jung *et al.*, 1998; Baeg *et al.*, 2003). PFC, as a higher cognitive area, exerts top-down control over downstream brain areas. The mouse PFC is a cortical area that receives input from the largest number of brain areas, but it also has reciprocal connectivity with projections to numerous brain regions. This makes the PFC a central player in various complex neuronal processes (Miller and Cohen, 2001). The PFC connections with the ventral hippocampus are important in working memory and with the amygdala and dorsomedial striatum for decision-making (Jobson *et al.*, 2021). Moreover, the mPFC connectivity with the dorsomedial thalamus and ventromedial striatum is essential for cognitive flexibility, and with subthalamic nuclei for processes involving attention (Jobson *et al.*, 2021).

Top-down signals from the mouse ACC control the visual cortex processing by modulating the function of inhibitory interneurons and exerting direct and di-synaptic inhibition (Kamigaki, 2019). Furthermore, feedback projections from the ACC to the visual cortex in mice convey information based on experiences for the prediction of imminent visual scenes when the animal is in a familiar environment. ACC-derived signals controlled and updated these predictions based on novel experiences (Fiser *et al.*, 2016; Leinweber *et al.*, 2017). The ACC is particularly important in executive

functions such as decision-making, attention, and cognitive control which are all critical for social cognition. The delivery of positive outcomes including reward, or negative outcomes involving punishment, to nearby conspecifics regulated the firing rate of neurons in ACC in both monkeys and rats (De Waal and Preston, 2017; Carrillo *et al.*, 2019; Hernandez-Lallement *et al.*, 2020). Information-sharing between individuals in a group and the resultant changes in ACC firing will help in emotion recognition for the appropriate actions to be carried out (De Waal and Preston, 2017; Carrillo *et al.*, 2019; Hernandez-Lallement *et al.*, 2020). In this thesis, we examined the neuronal networks in the ACC of A30P transgenic mice of DLB because of the key cognitive changes seen in DLB patients linked to ACC.

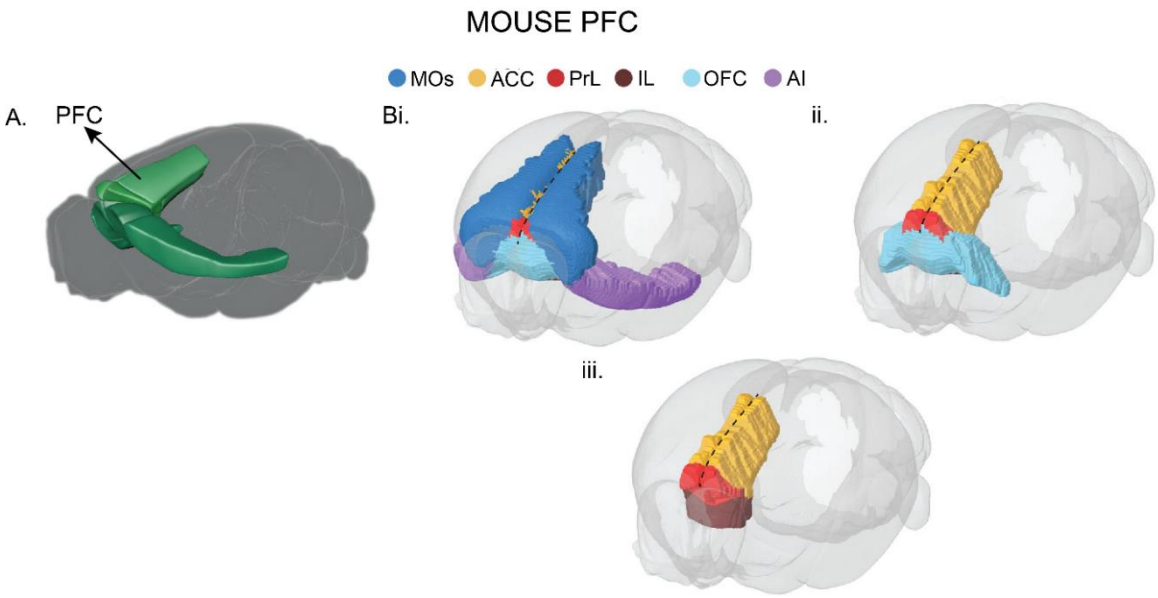

Figure 1.5. The mouse PFC. A. The green shaded area demonstrates the PFC in the mouse brain. **Bi**, **ii** and **iii** show the agranular PFC subdivisions including the secondary motor areas (Mos, blue), ACC (yellow), PrL (red), IL (brown), OFC (light blue) and AI (purple). Bi, ii and iii are taken from Carlen, 2017 (Carlén, 2017).

1.3.2. *Neurodegeneration in PFC*

The mPFC in rodents including ACC, PrL, and IL, as well as the ACC in humans, are of growing interest in neurodegeneration since patients with PD, AD, and Huntington's disease (HD) manifest impaired PFC cognitive abilities (Jobson *et al.*, 2021). The ACC, as discovered from PD post-mortem human studies, had a higher density of LBs compared to the frontal cortex which exhibited a mild LB pathology. The LB density in the ACC was also correlated with cognitive decline in PD patients with parkinsonism which preceded the cognitive impairment (Kövari *et al.*, 2003). Braak et al. (2000) demonstrated that the ACC together with the entorhinal cortex are early and severely impacted by the α-syn pathology in PD, which contributes to progressive personality changes and cognitive impairment patients develop (Braak *et al.*, 2000). Furthermore, synaptic and pathological changes in the ACC were associated with visual hallucinations observed in DLB patients, and there was reduced metabolism in the ACC in DLB and PD patients with dementia (Teaktong *et al.*, 2005; Yong *et al.*, 2007). Importantly, patients suffering from prodromal DLB revealed atrophy in their right ACC and bilateral insular areas and 93% of patients exhibited fluctuating cognition (Blanc *et al.*, 2016).

Schumacher et al. (2018), investigated the functional connectivity between and within brain networks during resting state of DLB patients using fMRI scans. They found decreased "within-network" connectivity particularly in the motor, temporal, and frontal networks including ACC of DLB patients compared to healthy controls. The ACC in DLB patients also demonstrated disconnection from the inferior temporal areas. This decreased activity of the ACC within the temporal pole network was rescued by compensatory mechanisms of increased ACC "between-brain" network connections within the temporal pole in DLB patients. This study proposes that impairment at the synaptic level in DLB leads to wide-ranging impairment of functional connectivity of the ACC with other brain regions, compared to healthy controls (Schumacher *et al.*, 2018).

Evidence in AD patients, who may seem cognitively normal, but have a high amyloid beta (Aβ) burden, suggested decreased functional connectivity between the mPFC including ACC, and the hippocampus. Also, in AD patients who progressed from mild cognitive impairment (MCI) to advanced clinical state of dementia, the mPFC

connectivity with other brain areas was greatly affected. There was decreased default mode network (DMN) functional connectivity with mPFC and parietal cortices or the posterior cingulate cortex (PCC) in those patients compared to controls. Moreover, there were no connections between the mPFC and the hippocampus (Jobson *et al.*, 2021). Other studies investigating the resting-state fMRI in AD patients found increased connectivity of the left hippocampus with dlPFC, and decreased connectivity between the right hippocampus, mPFC, and ventral ACC suggesting disrupted network connectivity within the hippocampus and with the PFC. This might indicate potential compensatory mechanisms between the PFC and downstream brain areas to prevent further cognitive impairments in AD (Wang *et al.*, 2006). Therefore, there is a clear indication that changes in PFC connectivity with other cortical and subcortical areas play a key role in DLB.

Mice with injected α-syn fibrils in the striatum exhibited behavioural impairment related to the PFC and amygdala functions including social dominance and fear conditioning (Stoyka *et al.*, 2020). Furthermore, α-syn inclusions were present primarily in the excitatory neurons of both PFC and amygdala but there was no neuronal loss in the PFC. Thus, α-syn inclusions could contribute to neuronal dysfunction, but not cell death, which contributes to behavioural dysfunction (Stoyka *et al.*, 2020). Further investigations have demonstrated that mice expressing the human WT α-syn under the Thy-1 promoter show impaired learning in rule-reversing tasks and spontaneous alteration along with raised anxiety levels which could be associated with PFC (Chesselet *et al.*, 2012; Magen *et al.*, 2012, 2015).

Moreover, dopaminergic degeneration contributes to cognitive dysfunction in PD. The ventral tegmental area (VTA) which is a source of dopaminergic neurons, projects to the PFC (Xu *et al.*, 2019). Evidence shows that in both PD patients and mouse models with VTA dopamine depletion, impaired behavioural performance is associated with mPFC functions, including the interval timing task which involves working memory and attention (Parker *et al.*, 2013). However, the impact of toxic pathologic α-syn on cognitive behaviour associated with prefrontal networks remains to be elucidated further.

1.4. Hyperexcitability in Dementia

1.4.1. *Hyperexcitability in AD and DLB.*

Hyperexcitability in AD, PD and DLB patients

Excess excitation is termed hyperexcitability and is observed in DLB, PD, and AD patients as well as in mouse models. Hyperexcitability is an epileptic phenomenon and can be seen consisting of abnormal poly-spikes evident in the electroencephalogram (EEG) in AD (Rabinowicz *et al.*, 2000; Palop and Mucke, 2009, 2010) and DLB (Morris *et al.*, 2015) patients and in some cases, full seizure activity occurred. Emerging evidence shows that there is an association between dementia and epilepsy, with the highest prevalence in AD cases (Stefanidou *et al.*, 2020; Szaflarski, 2021). Additionally, patients with dementia have a 2- to 10-fold increase in risk of developing seizures but also epileptic patients are prone to an increased risk of developing dementia (Stefanidou et al., 2020).

AD, DLB patients, or AD-DLB (combined pathology) patients exhibit increased seizure tendency when Aβ or α-syn pathology is present (Beagle et al., 2017). DLB and PD patients exhibit myoclonus which is an involuntary sudden brief jerk of the muscles resulting from a sharp transient in the contralateral sensory-motor cortex, as demonstrated on EEG recordings (Caviness et al., 2002, 2003). Myoclonus in DLB patients could be seen as reflecting excess excitability which might have emerged from chronic α-syn accumulation (Morris *et al.*, 2015). Morris et al. (2015) found that patients with myoclonus exhibited cognitive deficits at an earlier age than those without suggesting that hyperexcitability contributes to cognitive dysfunction (Morris *et al.*, 2015). Cortical α-syn aggregation was also increased in the sensorimotor cortex of PD patients who exhibited myoclonus, compared to the patients who did not (Caviness *et al.*, 2011). Myoclonus is also considered to be more severe and frequent in DLB patients compared to PD patients due to the worsening of α-syn pathology in the cortical regions (Louis *et al.*, 1997; Caviness *et al.*, 2003). Together these data support a link between abnormal cortical α-syn and network hyperexcitability.

Fluctuating consciousness is observed in DLB patients with symptoms similar to nonconvulsive seizures, including staring spells and speech disorganisation which

are a key feature of DLB (Mckeith *et al.*, 2017). In cognitive fluctuation episodes, it is challenging to distinguish between epileptic and non-epileptic symptoms which could result in the misdiagnosis of seizure activity (Morris et al., 2015). Visual hallucinations are also a prominent symptom of DLB and possibly related to changes in excitation levels in neuronal networks. Around 80% of DLB patients experience visual hallucinations and studies proposed that they might be linked with hyperexcitability in the visual cortex (Aarsland *et al.*, 2001; Archibald *et al.*, 2009). Taylor et al. (2011) investigated visual cortical excitability using transcranial magnetic stimulation (TMS) over the occipital lobe of DLB patients and healthy controls to generate phosphenes which are transient visual percepts. They found a strong relationship between the TMS visual cortical excitability measures and the severity level of visual hallucinations in DLB patients compared to controls (Taylor *et al.*, 2011).

These studies suggest a link between epilepsy and neurodegeneration. Protein aggregation in AD, PD and DLB leads to molecular changes in the neuronal networks as well as neuroinflammation triggering hyperexcitability (Cano *et al.*, 2021). Pathologic α-syn interacts with the mitochondrial membrane leading to mitochondrial changes, increased oxidative stress and mitochondrial dysfunction (Shen *et al.*, 2014; Ludtmann *et al.*, 2018). Additionally, oxidative stress contributes to the activation of neuroinflammatory responses which worsens neuronal damage (Trushina and McMurray, 2007; Nunnari and Suomalainen, 2012; Peng *et al*., 2020). The neuroinflammatory environment then causes ionic changes and disrupts the normal function of neurons including altered neuronal firing patterns and network hyperexcitability before cell death (Vezzani and Viviani, 2015; Estrada-Sánchez *et al*., 2017; Li *et al.*, 2023; Yu *et al*., 2023; Al-Musawi *et al.*, 2024).

Hyperexcitability in α-syn mouse models of neurodegeneration

Various studies examined hyperexcitability at neuron and network levels in different transgenic murine models of neurodegenerative disorders, most notably AD (Busche *et al.*, 2015; Palop and Mucke, 2016; Zhang *et al.*, 2016; Haberman *et al*., 2017). However, a few studies have discovered abnormal poly-spike activity in the cerebral cortex EEG in awake behaving α-syn transgenic mice (Morris et al., 2015;

Peters et al., 2020). Morris et al. (2015), observed hyperexcitability in WT hα-syn transgenic mice in the form of interictal spikes and intermittent seizures on EEG recordings and motor behaviour. These changes in activity due to hyperexcitability proposed an association with molecular changes in the hippocampus including decreased calbindin (important in calcium buffering) gene expression indicating increased hyperexcitability (Morris *et al.*, 2015). Calbindin depletion is suggested to be a sensitive indicator for excess excitability compared to scalp EEG recordings in which epileptiform events could be missed and also not detected in deep brain regions (Pillai and Sperling, 2006; Vossel *et al.*, 2013). Hyperexcitability was also seen in hippocampal slices taken from A30P mice aged 2-5 months where interictal-like discharges were recorded following kainate application to induce gamma frequency oscillations, something that was never seen in WT mice (Tweedy *et al*., 2021).

These findings suggest that increased network excitability may lead to severe cognitive decline in DLB. Therefore, by assessing hyperexcitability early before the cognitive impairments have developed, we might be able to understand the changes in neuronal network function that are responsible for the disease progression. Importantly, to date there are no detailed studies of the α-syn pathology affecting the PFC neuronal networks and whether this contributes to hyperexcitability and cognitive dysfunction in DLB. In this thesis, hyperexcitability and neuroinflammatory changes in the ACC neuronal networks will be examined in young A30P mice.

1.4.2. *Oscillatory activity and impairment in neurodegeneration*

Brain oscillations control the firing time between the neurons at the microscale and are involved in the synchronisation of communication between cortical networks at the macroscale. Brain rhythms of neural activity are categorised in different frequency bands including delta (1 - 4 Hz), theta (4 - 8 Hz), alpha (8 - 12 Hz), beta (15 - 30 Hz), gamma (30 - 90 Hz) and high gamma (>50 Hz) (Cole and Voytek, 2017). Neural oscillations are periodic variations in the local field potentials (LFPs). The LFPs are recordings of the extracellular voltage fluctuations generated from the membrane potential changes due to synaptic inputs to neurons in local neuronal networks. These voltage fluctuations involve both excitatory and inhibitory postsynaptic potentials (Jafari *et al*., 2020). All these types of oscillatory activity can also be evoked *in vitro*.

Siegel et al. (2012) demonstrated that coherent EEG oscillations between two distant brain areas contribute to functional communication in humans (Siegel *et al.*, 2012).

Slow-frequency oscillations such as delta, theta and alpha bands reflect the communication of large-scale neuronal networks between distant brain areas while high-frequency oscillations such as beta and gamma bands indicate the communication between local neuronal populations in neighbouring brain areas (Von Stein and Sarnthein, 2000; Siegel *et al.*, 2012). Gamma oscillatory activity, depending on the activated brain area, is important for the attentive processing of information, and active preservation of memory or conscious perception (Singer, 2001; Herrmann *et al*., 2004; Womelsdorf and Fries, 2006). On the other hand, beta oscillations are associated with movement-related activities such as movement observation, imagery and execution of movement and cognitive processes related to sensorimotor interaction (Neuper and Pfurtscheller, 2001; Kilavik *et al.*, 2013; Rossiter *et al.*, 2014).

Dysfunction in oscillatory activity in AD, PD and DLB

Oscillatory activity is disrupted in neurodegenerative disorders implying disruption of neuronal networks. EEG data has indicated a slowing of cortical oscillations from higher alpha (8 - 12 Hz) to lower theta (4 - 8 Hz) frequency bands in AD, DLB, and PDD patients (Andersson *et al.*, 2008; Bonanni *et al.*, 2008; Stylianou *et al.*, 2020). These changes in neuronal network oscillations were associated with clinical symptoms such as cognitive fluctuations (Andersson *et al.*, 2008; Bonanni *et al.*, 2008; Stylianou *et al.*, 2020). However, it is unclear how α-syn aggregation causes network and cognitive impairment. Most studies in human patients are primarily focused on oscillations in the theta and alpha band but it is important to investigate changes in high-frequency beta and gamma oscillations. Beta and gamma oscillations are critical for cognitive tasks involving attention and memory functions (Clayton *et al*., 2015; Watrous *et al.*, 2015; Zheng *et al.*, 2016) and investigations in AD patients showed impairments in the gamma oscillatory activity (Herrmann and Demiralp, 2005; Başar *et al.*, 2016).

Findings from AD patients suggested decreased fast oscillatory activity including alpha, beta, and gamma oscillations in the posterior regions based on

resting-state EEG and magnetoencephalography (MEG) recordings. On the other hand, delta and theta oscillations were increased during the resting state (Babiloni *et al.*, 2004; Schnitzler and Gross, 2005; Rossini *et al.*, 2006, 2007; Yener and Başar, 2013; Ishii *et al.*, 2018). Importantly, studies have shown that gamma-band stimulation in the brain improves memory function and could be considered a potential treatment method for neurodegenerative disorders (Clements-Cortes *et al.*, 2016; Herrmann *et al.*, 2016; Lozano *et al.*, 2016; Posporelis *et al.*, 2018; Vosskuhl *et al*., 2018).

The role of network oscillations was also studied in transgenic animals. Previous investigation in our lab revealed that the young A30P mice (2.5-4 months old) had decreased Up-state (depolarisation) duration and increased frequency of the slow oscillations (<1Hz) activity recorded during non-rapid eye movement (NREM) sleep under anaesthesia in the mPFC and CA1 of the hippocampus (Stylianou *et al.*, 2020). The altered slow frequency oscillation activity might suggest an early network dysfunction, potentially due to pathological hα-syn, at 2.5-4 months of age which could be linked to future impairments in cognitive behaviour (Stylianou *et al.*, 2020). Impaired gamma oscillations were reported in aged >9+-month-old A30P transgenic mice. Robson et al. (2018) recorded the gamma oscillatory activity in the hippocampus of A30P mice aged between 2 and 16 months old *ex vivo* (Robson *et al.*, 2018). They showed a significant reduction in the power of gamma oscillations in the 9-16-month-old A30P mice compared to the 2-6-month-old A30P mice associated with reduced mitochondrial function. Even though the hα-syn was already expressed in the young 2-month-old A30P mice, the deficiencies in gamma oscillation power were obvious in the older animals as pathology progresses with age leading to cognitive dysfunction (Schell *et al.*, 2009; Robson *et al.*, 2018). However, whether the overexpression of hα-syn contributes to changes in beta and gamma frequency oscillations in the ACC of young A30P mice has not been examined. This will be an important area to investigate in this thesis.

Neuronal network dysfunction involving PV interneurons in neurodegeneration

The highly interconnected local PFC microcircuit networks, in both humans and mice, consist of excitatory and inhibitory neurons. In the mouse PFC there are

approximately 82% excitatory glutamatergic neurons and 17% inhibitory GABAergic interneurons (Erö *et al.*, 2018). Pyramidal cells are the most common type of excitatory neurons in the cerebral cortex (Elston *et al.*, 2011). There are also inhibitory GABAergic long-range neurons and interneurons that strictly target neighbouring cells to control activity in the local network. One of the most abundant subtypes of GABAergic interneurons is the parvalbumin (PV)-expressing interneurons which express the calcium-binding protein parvalbumin. PV interneurons are implicated in executive functions such as learning, memory, and planning and are important in the cognitive functioning of PFC (Cho *et al.*, 2015; Kim *et al.*, 2016a; Lagler *et al.*, 2016; Tremblay *et al.*, 2016). PV interneurons shape the activity of neuronal circuits by releasing the inhibitory neurotransmitter GABA which binds to pre- and post-synaptic receptors. Complex neural functions controlled by the PV interneurons include feedforward and feedback inhibition as well as lateral inhibition (Pouille and Scanziani, 2001; Pouille *et al.*, 2009; Espinoza *et al.*, 2018). Importantly, PV interneurons exert these types of inhibition and control excitatory cell output by primarily exerting somatic inhibition on the postsynaptic neuron (Hu *et al.*, 2014; Tremblay *et al.*, 2016). Data from paired recordings by Packer and Yuste (2011) showed that a single PV interneuron connected with almost every nearby pyramidal neuron to control their activity (Packer and Yuste, 2011).

PV interneurons are crucial for the generation and synchronisation of high-frequency oscillations (Buzśaki and Wang, 2012). The coordinated interaction between excitation and inhibition gives rise to high-frequency gamma rhythms (30 - 80 Hz) (Buzśaki and Wang, 2012). It has been shown that PV interneurons in the mouse mPFC synchronised activity and increased the power of slow (30 - 40 Hz) gamma oscillations during attention (Kim *et al.*, 2016b). Compared to other inhibitory interneurons, PV interneurons are more excitable and have higher mean firing rates contributing to synchronising principal neuron outputs into neural assemblies (Avermann *et al.*, 2012; Pala and Petersen, 2015; Badin *et al.*, 2017). The balance between excitation and inhibition (E/I balance) in cortical circuits is implicated in the modulation of neuronal oscillations and it is crucial for optimal information processing and, thus optimal cognitive functioning (Atallah and Scanziani, 2009; Xue *et al.*, 2014). However, this E/I balance is not stable, therefore, the inhibitory neurons are required to respond appropriately to any cortical state fluctuations and excitatory inputs (Le

Roux *et al.*, 2008; den Boon *et al.*, 2015). Electrophysiological studies on mPFC mouse brain slices suggested that the PV interneurons mediate feedforward inhibition in neural circuits which is important for sustaining the E/I balance (Lee *et al.*, 2014). Overall, the PV interneurons are considered the input regulators, critical for serving all higher mental functions.

Changes in the function of PV interneurons could be associated with deficient gamma activity. There are decreased PV interneuron numbers in the hippocampus of AD (Brady and Mufson, 1997) and DLB (Bernstein *et al.*, 2011) patients according to post-mortem studies which may be related to changes in network activity and cognitive impairment. Palop and Mucke (2016) showed that loss of PV neuronal function in AD transgenic mouse models was correlated with impairments in network oscillations (Palop and Mucke, 2016). However, there are very few investigations looking at interneuron changes as disease pathology progresses in transgenic mouse models of DLB and PD. The impaired gamma frequency activity and hyperexcitability reported in the A30P mice could be related to changes in the PV neuronal function (Robson *et al.*, 2018; Tweedy *et al.*, 2021). Discrepancies in the literature also exist concerning the effect of α-syn on interneurons and its co-localisation within the soma. Taguchi et al. (2014), revealed that GABAergic inhibitory neurons which were glutamic acid decarboxylase positive (GAD+) had weak expression levels of α-syn but α-syn was highly expressed in the presynaptic terminals of excitatory neurons in hippocampal mouse cultures (Taguchi *et al.*, 2014). Another study also showed minimal α-syn aggregation in the PV interneurons following α-syn fibril injection in the mouse striatum (Stoyka *et al.*, 2020). It could be possible that pathologic α-syn indirectly affects the activity of interneurons, mainly through excitatory synaptic interactions. Interneuron impairment and decreased inhibitory transmission can lead to altered E/I balance, leading to increased excitation, and the generation of aberrant network excitability. However, the role of α-syn pathology in hyperexcitability needs to be investigated further.

1.5. Perineuronal Nets

Important structures that could also play a role in regulating network hyperexcitability are the perineuronal nets (PNNs) which were first described by Golgi in 1898. Initially, PNNs were considered as staining artefacts of coagulated pericellular fluids by Ramon y Cajal. However, in the 1980s with new staining methodologies, there was renewed interest in these structures (Celio *et al.*, 1998). The PNNs are now known to be condensed extracellular matrix (ECM) structures that are present in several brain regions including the cerebral cortex, hippocampus, and amygdala in humans (Adams *et al.*, 2001; Morawski *et al.*, 2004, 2012; Baig *et al.*, 2005),rodents (Galtrey *et al.*, 2008; Gogolla *et al.*, 2009; Yamada *et al.*, 2015), sheep (Fowke *et al.*, 2018), and monkeys (Adams *et al.*, 2001; Mueller *et al.*, 2016; Grey *et al.*, 2023)(Celio *et al.*, 1998; Kwok *et al.*, 2011). PNNs surround the soma, axon initial segment, and proximal dendrites of specific neurons, mainly around PV interneurons (Dityatev *et al.*, 2007; Sigal *et al.*, 2019; Kaushik *et al.*, 2021). However, PNNs also surround excitatory neurons in rodents in brain regions such as amygdaloid nuclei, pyriform cortex, dorsal tenia tecta and medial entorhinal cortex (Alpár *et al.*, 2006; Lensjø *et al.*, 2017; Morikawa *et al.*, 2017). Additionally, neurons with the typical morphology of pyramidal cells in the human PFC have been seen surrounded by PNNs (Enwright *et al.*, 2016; Alcaide *et al.*, 2019).

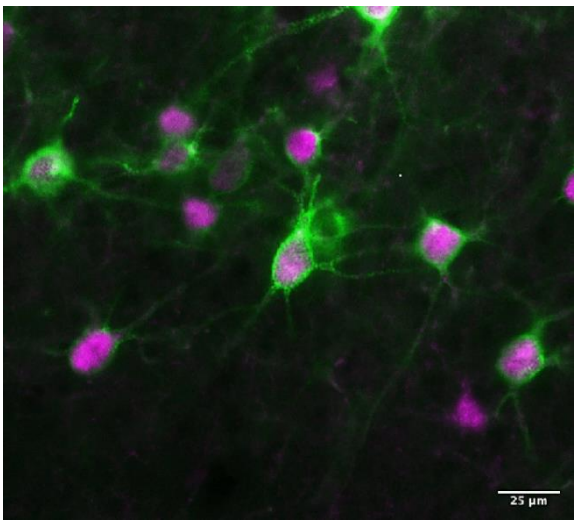

Figure 1.6. Perineuronal nets surrounding PV interneurons. PNNs are shown in green around PV interneurons in magenta in the mouse primary somatosensory cortex (Bucher et al., 2021).

1.5.1. *Formation and development of the Perineuronal Net structures*

The composition of the PNN structure

The PNNs are composed of chondroitin sulphate proteoglycans (CSPGs) which are synthesised by neurons (Chelini *et al.*, 2018; Testa *et al*., 2019; Tanti *et al.*, 2022) as well as astrocytes, oligodendrocytes, oligodendrocyte precursors, and microglia (Chelini *et al.*, 2018; Testa *et al*., 2019; Tanti *et al.*, 2022). The CSPGs comprise a core protein that is composed of up to three globular domains and chains of chondroitin sulphate glycosaminoglycans (GAGs) that are covalently attached. Additionally, the repeated pairs of disaccharide units that make up the GAG chains have sulphation patterns in position 6 (chondroitin chains, CS6) or position 4 (CS4) (Kjellén and Lindahl, 1991; Künze *et al*., 2021) which is crucial for the relationship of PNNs and other molecules including orthodenticle homeobox 2 or semaphorin 3A (Testa *et al*., 2019). The four known CSPGs that are found in PNN structures are aggrecan, versican, neurocan, and brevican (Haunsø *et al.*, 1999).

The backbone component of PNNs is hyaluronan (HA) and it is critical for PNN integrity. HA is a big unsulphated GAG composed of D-glucuronic acid and N-acetylglucosamine. The CSPGs are non-covalently attached to the HA chains. Additionally, the interactions between the HA and CSPGs are stabilised by link proteins and tenascin-R allows for increased aggregation between the CSPGs (Katarzyna *et al*., 2021) (Fig. 1.7). Furthermore, the CSPGs and HA are important in modulating the intracellular signalling pathways. Both structures interact with different membrane receptors including the HA cell surface adhesion receptor CD44, leucocyte common antigen-related receptor, epidermal growth factor receptor, integrins, etc (Yu *et al*., 2018).

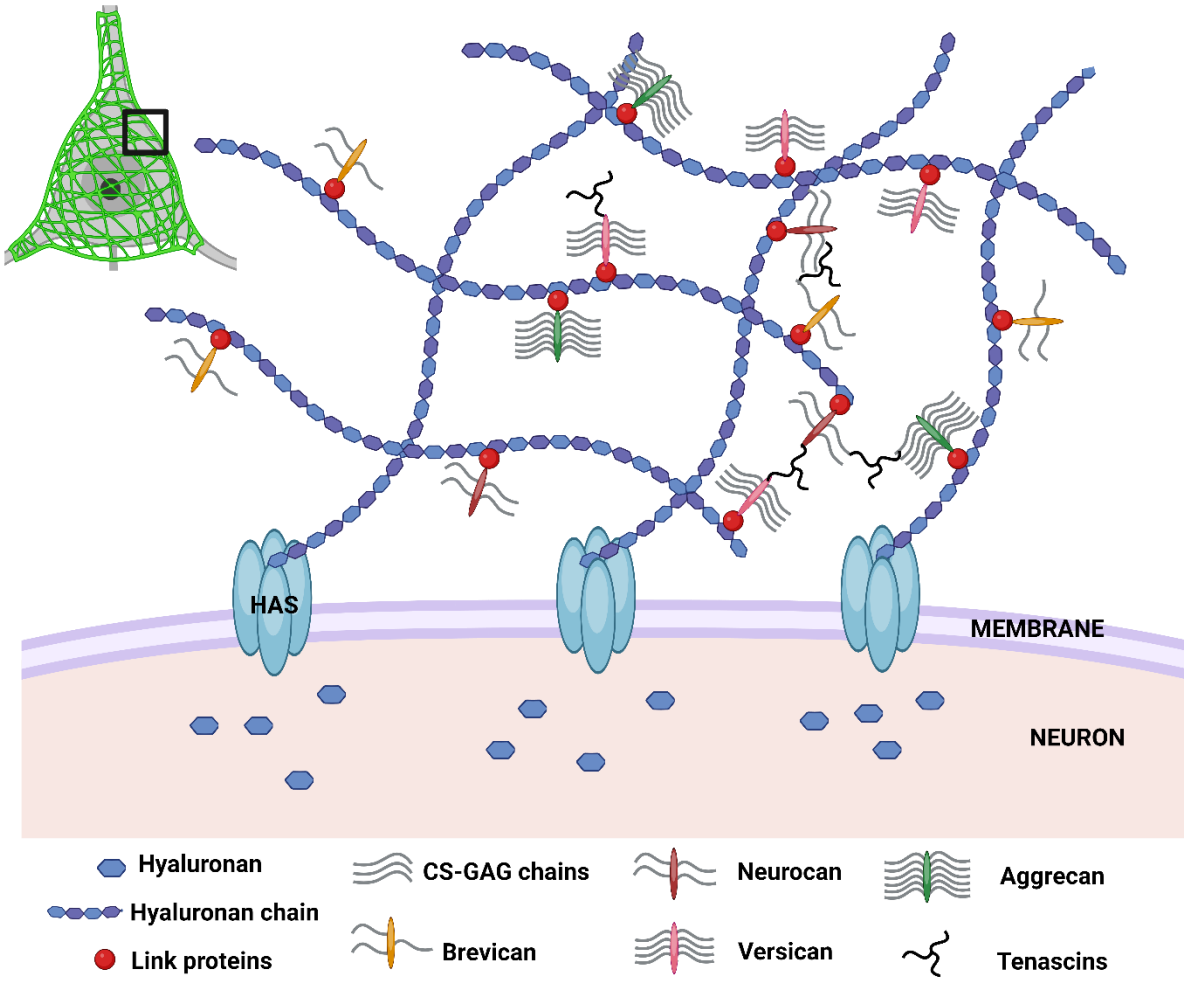

Figure 1.7. Structural composition of the PNNs. A schematic representation of the composition of ECM molecules of PNNs surrounding a neuron (green net structure) is shown. PNNs are composed of hyaluronan chains synthesised by the hyaluronan synthases (HAS) located on the neuronal membrane. There are four types of CSPGs found in PNNs including brevican, neurocan, versican and aggrecan. The CSPGs consist of a core protein and chondroitin sulphate chains of glycosaminoglycans (CS-GAG). The CSPGs are non-covalently attached to the hyaluronan chains with link proteins and tenascins. This figure was created using Bio Render.

The formation and development of PNNs

The formation of PNNs occurs during development in an activity-dependent manner. *In vitro* electrophysiology studies revealed that the PNN formation is dependent on AMPA receptor activity and L-type voltage-dependent calcium channels (L-VDCC) in hippocampal cultures (Dityatev *et al.*, 2007). In humans, the PNNs appear at two months of age and are fully developed and mature around eight years of age (Rogers *et al.*, 2018). PNNs start to get assembled during the first two to three postnatal weeks in mice and are fully formed by the sixth postnatal week. During the first few postnatal weeks, important molecules composing the immature ECM, including tenascin-C and neurocan decrease in expression. However, other molecules such as aggrecan, brevican, versican, phosphacan, tenascin-R and Hapln1 (HA-binding protein) have increased expression (Song and Dityatev, 2018; Balashova *et al.*, 2019). The timings of PNN formation and maturation differ in each brain area. In the mouse barrel cortex, the PNNs appear between postnatal days 10 and 20 and have a mature density and distribution by around postnatal day 30 (Nowicka *et al.*, 2009). On the other hand, the PNN-like structures in the mouse PFC start to appear on postnatal days 14 – 21 and have a mature density and distribution between postnatal days 28 and 56 (Ueno *et al.*, 2017).

PNN maturation around PV interneurons in rodents coincides with the end of critical periods along with synaptogenesis, synaptic refinement, and maturation of neural networks (Sorg *et al*., 2016; Carceller *et al*., 2020; Souter and Kwok, 2020). In different brain areas, PV neuronal circuits mature at different time points during development resulting in the sequential emergence of critical periods. The maturation of PV interneurons is determined by genetic programs and experiences based on environmental stimuli (Morales *et al*., 2002; Cancedda *et al.*, 2004; Sale *et al.*, 2004; Southwell *et al.*, 2010; Tang *et al.*, 2014; Baroncelli *et al.*, 2016). During development, neuronal synapses on PV interneurons are stabilised in the PNN lattice perforations preventing synaptic plasticity and rearrangements (Tommaso Pizzorusso *et al.*, 2002; Chaunsali *et al*., 2021).

PNNs undergo marked alterations during brain processes requiring plasticity such as memory formation and consolidation (Banerjee *et al.*, 2017; Shi *et al.*, 2019). It has been shown that auditory fear memory acquisition leads to raised PNN numbers

in the hippocampus, auditory cortex, and ACC (Banerjee *et al.*, 2017; Shi *et al.*, 2019). Specifically, Banerjee et al. (2017) found an increase in mRNA levels of PNN components 4 hours after fear conditioning (Banerjee *et al.*, 2017). During prenatal and postnatal development, the ECM undergoes structural remodelling implicating changes involving the production and degradation of its components (Hockfield *et al.*, 1990; Morawski *et al.*, 2009; Pintér *et al.*, 2020). ECM remodelling is increased through different processes including cell division, migration, inflammation, and injury (Bronner-Fraser, 1986; Nagano *et al*., 1993; Saksela and Laiho, 1997; McKeon *et al*., 1999; Théry *et al.*, 2005; Bonnans *et al*., 2014; George and Geller, 2018; Yamada *et al.*, 2019). Enzymes such as matrix metalloproteinases (MMPs) and their tissue inhibitors (TIMPs), tissue plasminogen activator (tPA), plasminogen activator inhibitor, metalloproteinases of ADAMTS family and the hyaluronidase and chondroitinase family are important for the ECM structural changes (Custod and Young, 1968; Lorenzl *et al.*, 2003; Baba *et al.*, 2009; Fanne *et al.*, 2010; Wang *et al*., 2017; Yamakage *et al.*, 2019; Cabral-Pacheco *et al.*, 2020; Mohamedi *et al.*, 2020). During processes such as ocular dominance plasticity and fear conditioning, the activity of MMP-9 is overexpressed leading to the breakdown of PNNs (Dubey *et al.*, 2017).

1.5.2. *Effects of PNN breakdown on neuronal networks*

PNN manipulation methods

Studies on the disruption of PNNs beyond the critical period showed that the breakdown of PNNs reactivates neuroplasticity resembling that seen during juvenile stages (Tommaso Pizzorusso *et al.*, 2002; Wang and Fawcett, 2012; Rowlands *et al.*, 2018; Fawcett *et al*., 2019). PNN manipulation methods include genetic modifications such as gene deletions of PNN components, antibodies blocking the PNN inhibitory action, and enzymatic degradation of ECM molecules (Kwok *et al.*, 2008; Carulli *et al.*, 2010; Howell and Gottschall, 2012; Romberg *et al.*, 2013; Yang *et al.*, 2017). Chondroitinase ABC (Ch ABC) is one of the enzymes that non-specifically cleaves the PNN proteoglycans, disrupting PNN structure and function. Ch ABC promotes the digestion of CS-GAGs and this increases neuronal plasticity in neocortical regions including the visual and auditory cortex (Pizzorusso *et al.*, 2002; Deepa *et al.*, 2006;

Happel *et al.*, 2014; Rowlands *et al.*, 2018; Tewari and Sontheimer, 2019). The enzyme hyaluronidase (hyase) is also used for the PNN breakdown allowing the random cleavage of the glycosidic bonds in the HA, a major component of both loose and condensed ECM. However, hyase also breaks the glycosidic bonds in chondroitin and CSs. Ch ABC and hyase enzymes cause long-lasting changes in the ECM including transient loss of PNNs (McRae and Porter, 2012).

PNN degradation contributes to hyperexcitability and changes in behaviour

The PNNs have been characterised as protective “scaffolds” around the surrounding cells and their composition varies in different brain regions. It is still unclear whether PNNs are found solely around PV basket interneurons or around PV chandelier interneurons as well (Favuzzi *et al.*, 2019). The array of proteoglycans and polysaccharides on the PNNs provides a strong negative charge to the neurons. The excitability of the PV interneurons is controlled by the PNNs which thus indirectly control GABAergic inhibition (Chaunsali *et al*., 2021). The PV interneurons surrounded by PNNs are fast-spiking neurons with a firing frequency of 100 - 800 Hz (Hu *et al*., 2014) and their PNNs play a key role in their spiking activity by decreasing the membrane capacitance (Balmer, 2016; Favuzzi *et al.*, 2017; Tewari *et al.*, 2018). PNNs have been characterised as “ion filters” that can change the ion mobility in the extracellular space. The negative ionic charges produced by PNNs protect the PV interneurons, preventing negatively charged extracellular glutamate from entering the extracellular space around the cell. Therefore, PNNs protect PV interneurons from glutamate excitotoxicity that can result in cell death. Cleavage of the PNN structures makes the neurons vulnerable to excitotoxicity (Okamoto *et al*., 1994; Tewari *et al.*, 2018). Additionally, PNNs control the intracellular chloride concentrations through the Gibbs-Donnan forces in hippocampal neurons as increased intracellular chloride concentrations change the ionic gradient contributing to hyperexcitability (Glykys *et al.*, 2014).

Condensed HA controls the ion exchange at a subcellular level between synaptic and extrasynaptic sites by limiting the movement of AMPA receptors (AMPA-Rs) (Frischknecht *et al.*, 2009). The activity of calcium channels at dendritic sites is

also controlled by HA perisynaptically in the PNNs to enable their use-dependent synaptic plasticity (Kochlamazashvili *et al.*, 2010). Previous research showed that mice lacking HA synthase exhibited an epileptic phenotype (Arranz *et al.*, 2014). Enzymatic digestion of HA using hyase in hippocampal neuronal cultures resulted in a delay in the development of epileptic activity (Vedunova *et al.*, 2013). Additionally, Balashova et al. (2019) demonstrated the occurrence of seizures in 40% and 50% of mice following 48 and 72 hours of hyase bilateral intrahippocampal injections. Importantly, the hyase-treated mice exhibited memory improvements. This could be associated with synaptic reformation and changes in the ratio of inhibitory and excitatory neuronal connections underlying changes in plasticity (Balashova *et al.*, 2019).

Evidence in the PrL area of mPFC in adult mice showed that PV interneurons surrounded by PNNs had increased PV expression compared to PV interneurons without PNNs (Carceller *et al.*, 2020). The PNN breakdown with Ch ABC however led to a decreased density of PV inhibitory puncta which contributed to changes in the E/I balance by reducing the gamma oscillatory activity (Carceller *et al.*, 2020). Although PNNs predominantly surround PV interneurons, there is a limited expression of PNNs around somatostatin (SST)-expressing interneurons throughout the brain (McRae *et al.*, 2010; Berretta *et al.*, 2015). Chu et al. (2018) reported changes in PV and SST interneuron function following Ch ABC-dependent PNN removal in the barrel cortex of juvenile mice. Particularly, the PNN breakdown led to decreased input resistance, decreased resting membrane potential, and faster firing rate of action potentials of fast-spiking (FS) PV interneurons as well as changes in their spontaneous synaptic inputs. Additionally, the loss of PNNs caused changes in the rebound depolarizations of low-threshold spiking (LTS) SST interneurons and decreased frequency of their spontaneous synaptic inputs. Thus, these findings highlight the important role of PNNs in the intrinsic and synaptic functions of inhibitory interneurons (Chu *et al.*, 2018).

The PNN protein BCAN is critical for regulating the localisation of potassium channels and AMPA-R levels in the excitatory synapses of the PV interneurons in the hippocampus (Favuzzi *et al.*, 2017). PV interneurons surrounded by BCAN are better adjusted to higher spiking frequencies by demonstrating higher maximum firing frequency, less spike frequency adaptation, narrower AP half-width, and earlier fast after-hyperpolarisation time. However, in the absence of BCAN protein, PV

interneurons exhibit increased intrinsic excitability by lowering the AP threshold and latency to the first AP. This also leads to impairments in spatial working memory and short-term memory (Favuzzi *et al.*, 2017). The manipulation of other PNN components also affects neuronal activity and plasticity levels. The genetic depletion of neurocan has been shown to cause deficits in the hippocampal LTP (Zhou *et al.*, 2001; Fawcett *et al.*, 2022). However, aggrecan knock-out mice exhibited memory and spontaneous object recognition test improvements (Rowlands *et al.*, 2018). Also, tenascin-R knockout mice showed a faster adjustment in reversal learning, improvements in working memory, and enhanced novel object recognition (Morellini *et al.*, 2010). Therefore, PNN manipulation might also be beneficial to memory contributing to memory modification and strengthening (Fawcett *et al*., 2019).

1.5.3. *Role of PNNs in the PFC*

Investigation of PNNs in the PFC has been the centre of attention as changes in the PNNs are involved in the pathogenesis of schizophrenia (Bitanihirwe and Woo, 2014; Enwright *et al.*, 2016; Alcaide *et al.*, 2019; Sultana *et al.*, 2021). The PNNs in human PFC are increased in the peripubertal period until late adolescence which is also the age at which schizophrenia symptoms first occur. The changes in PNNs of patients with schizophrenia are found to be specific to PFC. Some studies showed decreased density and labelling of PNNs in the dlPFC of patients with schizophrenia (Mauney *et al.*, 2013; Enwright *et al.*, 2016) and others showed significant reductions in patients with psychosis, compared to those without (Alcaide *et al.*, 2019). There is also a decrease in the density of PV interneurons in layer 4 in BA9 of PFC as discovered from post-mortem brain examinations of schizophrenic patients (Mauney *et al.*, 2013; Enwright *et al.*, 2016). Schizophrenia is associated with an imbalance between E/I neurotransmission leading to impairments in the function of PV interneurons. It has, therefore, been hypothesised that there is a potential link between the depletion of PNNs and their protective role with the exposure of the fast-spiking PV interneurons to oxidative stress (Cabungcal *et al*., 2013; Fawcett *et al*., 2022).

Local Ch ABC infusion in mPFC enhanced performance during a touchscreen trial-unique nonmatching-to-location assay (TUNL) task in rats (Anderson *et al.*, 2020). This task depends on mPFC but is also an automated test of location memory relying

on hippocampal activity (Anderson *et al.*, 2020). PNNs also regulate the stabilisation of grid cell activity supporting navigation and spatial memory in a familiar environment. Removal of PNNs decreased grid cell activity, following novel spatial learning which can be associated with decreased PV neuronal activity leading to overlapping spatial representations (Christensen *et al.*, 2021).

1.5.4. *PNNs in Epilepsy*

There are changes in the diffused and condensed ECM observed in human post-mortem studies from patients with epilepsy and rodent models of epilepsy. Studies on temporal lobe epilepsy animal models (Naffah-Mazzacoratti *et al.*, 1999; Mcrae *et al.*, 2012; Pollock *et al.*, 2014; Rankin-Gee *et al.*, 2015; Favuzzi *et al.*, 2017; Härtig *et al.*, 2017; Kim *et al.*, 2017) and human tissue (Perosa *et al.*, 2002; Favuzzi *et al.*, 2017; Kim *et al.*, 2017) demonstrated the abnormal expression of ECM components as well as PNN disruption and decreased density of both PNNs and PV interneurons. Therefore, disruption or dysfunction of the PNNs and overall ECM around the PV interneurons changes the neuronal spiking activity. Disruption of PNNs also decreases inhibition leading to increased seizure activity.

In a mouse model of Theiler's murine encephalomyelitis, a virus infection-induced epilepsy, Patel et al. (2023) discovered raised levels of CSPG expression in the dentate gyrus of the hippocampus and amygdala. The researchers primarily noticed a de novo CSPG expression around the excitatory neurons linked to the seizure formation. Additionally, this increased CSPG expression around the dentate granule cells led to the increased extracellular concentration of potassium and calcium which caused depolarisation of the resting membrane potential of the neurons, thus increasing neuronal excitability (Patel *et al.*, 2023).

1.5.5. *The impact of Ageing on PNNs*

Ageing impacts the density of PNNs in some brain regions, as well as the sulphonation patterns of GAGs, resulting in a decrease in plasticity in aged animals (Foscarin *et al.*, 2017; Ueno *et al.*, 2018). Increased PNN and PV neuronal density

were observed particularly in the ventral OFC and ACC in 12-month-old WT mice compared to 2-month-old mice. Interestingly, however, the brain areas with the strongest age-related increase in PNNs and PV interneurons were the somatosensory, visual, and auditory cortices (Ueno *et al.*, 2018). This suggests that the PFC did not have a strong increase in PNNs to maintain plasticity in the neuronal networks and preserve cognitive functioning (Ueno *et al.*, 2018). It is thought that fewer PNNs allow for new synaptic interactions to occur in the neuronal networks, allowing rapid synaptic modifications that are necessary for optimal cognitive functioning throughout the lifespan.

It is well established that memory is affected during ageing. The sulphation patterns of the chondroitin sulphate components of PNNs can influence memory loss in ageing. The chondroitin 4-sulphates (CS4) are inhibitory against neuronal plasticity whereas the chondroitin 6-sulphates (CS6) allow for plasticity and regeneration (Wang *et al.*, 2008; Lin *et al.*, 2011; Miyata *et al.*, 2012). Therefore, balanced CS4 and CS6 sulphation patterns are crucial for controlling neuroplasticity. Following the end of juvenile critical periods, the sulphation patterns remain stable but change during ageing including the loss of CS6 in 20-month-old rodents. On the other hand, the concentration of CS4 is not affected (Foscarin *et al.*, 2017; Yang *et al.*, 2021). Transgenic C6-sulphotransferase knockout mice, which express very low concentrations of CS6, exhibit object recognition and spontaneous alternation memory impairments as early as 3 months of age. This level of performance in the 3-month-old mice is similar to that of 20-month-old mice that are not genetically modified. Additionally, the expression C6-sulphotransferase restored the CS6 levels in the aged animals which was followed by the restoration of the object memory loss associated with ageing (Yang *et al.*, 2021). Thus, balanced levels between the CS4 and CS6 are critical in the regulation of memory mediated by the PNNs.

Evidence suggests that the HA chains have different functions depending on their length. Low molecular weight HA acts as a pro-inflammatory whereas high molecular weight HA is an anti-inflammatory (D'Agostino *et al.*, 2017). During ageing and other pathological conditions such as ischemic and traumatic brain damage, the quantity of HA is altered (Jenkins and Bachelard, 1988; Al'Qteishat *et al.*, 2006; Cargill *et al.*, 2012). Particularly, it is degraded into smaller fragments causing the release of other PNN components, including aggrecan, into the soluble ECM (Sugitani *et al.*,

2021). Future studies will need to address whether these changes in HA during ageing have an impact on memory as it is still unknown.

1.5.6. *PNNs in Neurodegeneration*

Nissl and Alzheimer first proposed the involvement of PNNs in neurodegenerative diseases and later the researchers Besta, Belloni, and Donaggio. Besta suggested that the perineuronal net structures are not part of the neuron and that they may be produced by glia (Celio *et al.*, 1998). In the 1930s, Bellani and Donaggio investigated dementia, diffuse gliosis, and psychiatric cases and noticed alterations in PNNs and the neuropil (Piez, 1997). As outlined above, PNNs are vital for the protection of neurons and their synaptic connections against environmental stressors (Reichelt *et al.*, 2019). The degradation of PNNs is associated with a range of neurodegenerative disorders including AD (Suttkus *et al.*, 2016; Crapser, Spangenberg, *et al.*, 2020), PD (Suttkus *et al.*, 2012, 2016; Sancandi *et al.*, 2018), and HD (Crapser, Ochaba, *et al.*, 2020), and may contribute to cognitive impairment (Pintér and Alpár, 2022). In post-mortem examinations of AD patients, there was decreased PNN expression, and the neurons exhibiting pathological lesions, including tau protein and neurofibrillary tangles, lacked PNNs (Wen *et al.*, 2018). The neuroprotective role of PNNs was demonstrated in rodent cortical neurons, including PV neurons, *in vitro.* The PNN-surrounded neurons showed resistance to cell death when incubated with exogenous monomeric Aβ1-42 peptide compared to when neurons were pre-treated with Ch ABC which led to neuronal death (Miyata *et al*., 2007).

PNNs are also implicated in the exacerbation of AD pathology. The binding of the PNN components heparan sulphate proteoglycans (HSPGs) to Aβ is associated with plaque pathology affecting the processing and clearance of the beta-amyloid precursor protein (Scholefield *et al.*, 2003; Liu *et al.*, 2016). Additionally, proteoglycans found in tangles encourage aggregation of tau protein and contribute to the prion-like spread of tau pathology (Goedert *et al.*, 1996; Holmes *et al.*, 2013). HA is also very important in cognitive impairment linked to vascular dementia while its upregulation has been linked to stroke (Dityatev *et al.*, 2009). Particularly, the HA synthases HAS 1 and 2 and the hyaluronidases Hyal 1 and 2 are upregulated in cells from stroke and peri-infracted brain areas (Sherman *et al.*, 2015).

The PNN proteoglycan agrin is implicated in α-syn pathology in PD by increasing α-syn protein insolubility (*in vitro*). Furthermore, in human tissue, agrin co-localised with abnormal α-syn in LBs (Liu *et al.*, 2005). Elevated HSPG concentrations contribute to the progression of LB pathology and amyloid plaque formation (Ramachandran and Udgaonkar, 2011; Mehra *et al.*, 2018). The GAGs, side chains of proteoglycans, contribute to the formation of pathological α-syn (Mehra *et al.*, 2018). Particularly, the α-syn pathology is triggered by excess GAG concentrations, GAG long polymer isoforms, increased protein-to-GAG ratio, charge density, and specific sulphate group orientation which progressed pathology. The generation of different GAG types causes changes in the structure of α-syn fibrils as well as cytotoxicity which affects the uptake of α-syn by the cell (Mehra *et al.*, 2018).

It is debated whether the digestion of PNNs in neurodegeneration is a compensatory mechanism for the neurons to be more plastic and form new synapses which then could reduce cognitive impairment (Romberg *et al.*, 2013; Végh *et al.*, 2014; Yang *et al.*, 2015). Consistent with this protective role, research suggests that object recognition was repaired following disruption of PNNs in the perirhinal cortex of tauopathy mouse models, and enzymatic degradation of PNNs with Ch ABC led to restored hippocampal function (Yang *et al.*, 2015; Fu and Ip, 2017). Additionally, object recognition memory was normalised in the perirhinal cortex of AD transgenic mice with balanced levels between the CS6 and CS4 CSPGs following the antibody blockade of the inhibitory CS4 CSPGs (Yang *et al.*, 2017). However, future studies are required to address the role of PNNs in other neurodegenerative disorders including DLB. There is currently no research concerning the role of PNNs in transgenic α-syn mouse models of PD or DLB, which makes this an important area to investigate in this project.

1.6. Role of Neuroinflammation in DLB

Apart from neurons in the brain, there are also glial cells which are critical for optimal cognitive function. There are four different glial types in the CNS including microglia, astrocytes, oligodendrocytes, and neuron-glial antigen 2 (NG2)-glia which are their progenitors (Kimelberg and Nedergaard, 2010; Hesdorffer *et al.*, 2011; Baulac *et al.*, 2015; Jäkel and Dimou, 2017). It is suggested that the glial cell population is 50% of all cells in the brain in humans, primates and rodents (Reemst *et al.*, 2016).

1.6.1. *Microglia*

The microglia structures were first characterised as rod cells ("Stabchenzellen") in human tissue by Franz Nissl in the late 19th century who described them as reactive glial elements which were of migratory, phagocytic, and proliferative nature. Ramon y Cajal named them the "third element of the nervous system" for their discrimination from neurons and neuroglia. The name "microglial cell", referring to their small soma size, was given by his student del Rio-Hortega in 1919 who based the name on the Cajal's "third element" concept to characterise further the non-neuronal, non-astrocytic third element which was different from neuroectodermal oligodendroglia or oligodendrocytes (Ginhoux *et al.*, 2013). He also discovered that these structures are phagocytes that eliminate dendritic spines and cell debris but also network with different cells in the brain parenchyma (Gao *et al.*, 2023).

In human brains, the detection of microglia-like cells with different morphologies can be seen from approximately three post-conception weeks, but their maturation continues throughout gestation (Hutchins *et al.*, 1990; Rezaie and Male, 1999; Rezaie *et al.*, 2005). The differentiation of the microglial populations is detected at 35 weeks of gestation (Esiri *et al*., 1991). Del Rio-Hortega also proposed that during the perinatal period in humans, blood monocytes enter the CNS and contribute to the increase in microglia which replace the embryonic microglial cells (Ginhoux *et al.*, 2013). Based on this, fundamental evidence in rats suggests that the microglial structures derive from circulating monocytes which enter the brain during development. These circulating monocytes are believed to have an ameboid microglial structure which then adopts a ramified shape (Ling, 1976). Perry et al. in 1985 discovered that macrophage-

like cells extravasated into the brain parenchyma and were localised in “hot spots” which were observed on embryonic day 16 (E16) in mice. After entering the brain, these macrophages underwent a series of transformations which led to their final ramified microglial structure (Perry *et al*., 1985). The microglia numbers increase dramatically after birth in rodents (Alliot *et al*., 1999; Tambuyzer *et al*., 2009).

Studies in mice showed that microglia have a critical role during development since they help in shaping neural circuits via phagocytosis of dendritic spines. Following an injury to the CNS, microglia phagocytose and remove the invading pathogens or any threat to the CNS including microbes, dead cells, protein aggregates, and antigen particles (Colonna and Butovsky, 2017). Microglia can be found in different forms in the CNS depending on their activity state. In the resting state, microglia have a ramified shape with several branches and processes (Fig. 1.8). These long processes contribute to the continuous motion of microglia travelling long distances in large brain regions (Davalos *et al.*, 2005; Nimmerjahn *et al*., 2005; Wake *et al.*, 2009). Microglia interact with neurons, astrocytes as well as blood vessels and are important in tracking the functional state of their synapses (Reemst *et al.*, 2016; Colonna and Butovsky, 2017). During injury, microglia in the close vicinity are stimulated and move towards the injured area where their morphology changes into an amoeboid shape. Their soma is enlarged, and processes become smaller when the microglia are activated and this is linked to phagocytosis and their proinflammatory function (Colonna and Butovsky, 2017).

The activation of microglia has in the past been categorised as classical (M1) which is pro-inflammatory or alternative (M2) which is anti-inflammatory and healing (Fig. 1.8) (Appel *et al.*, 2011; Sica and Mantovani, 2012). However, this terminology is now considered out of date. M1 activation tends to be neurotoxic and is triggered by the Toll-like receptor (TLR) and Interferon-gamma (IFN-γ) signalling pathways. Pro-inflammatory cytokines are derived from pathogens in the CNS or damaged cells inducing the M1 activation of resting microglia. The activated microglia express pro-inflammatory cytokines and chemokines including tumour necrosis factor-α (TNF-α), interleukins (IL)-6, IL-1β, IL-12, and chemokine (C-C motif) ligand 2 (CCL2). Additionally, the M1 microglia express NADPH oxidase which is critical for producing superoxide, ROS and nitric oxidase which generates nitric oxide (NO) from arginase. On the other hand, the anti-inflammatory M2 activation of neuroprotective microglia is

triggered by the release of IL-4, IL-13, IL-10, and fragment crystallisable (Fc) receptor ligation by immunocomplexes and apoptotic cell detection (Saijo et al., 2013). Evidence also suggests that the release of the pro-inflammatory cytokines including IL-6, TNF-α, and NO is suppressed by the anti-inflammatory cytokine IL-4 (Park *et al.*, 2005; Zhao *et al.*, 2006).

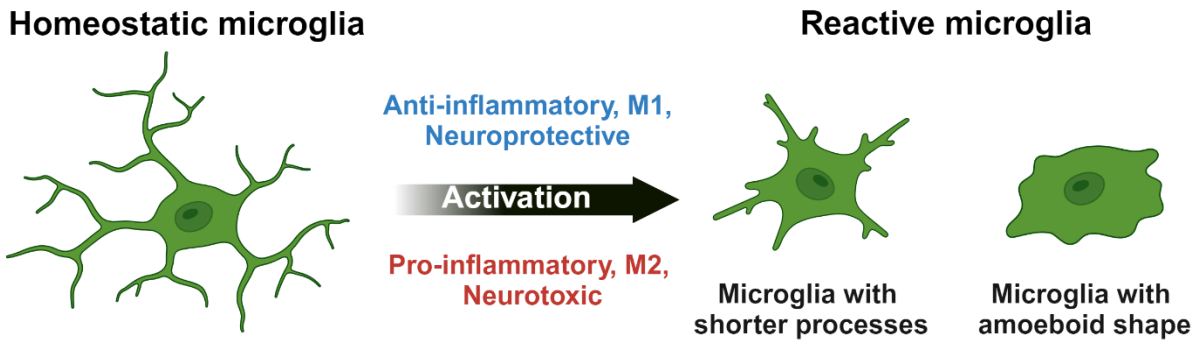

Figure 1.8. Microglial activation. Homeostatic microglia during resting state are activated and become reactive adopting morphological changes including shortening of processes and transformation into an amoeboid shape. There are two types of microglial activation: 1) anti-inflammatory known as M1 which is neuroprotective and 2) pro-inflammatory known as M2 which is neurotoxic. This figure was created using Bio Render.

1.6.2. *Astrocytes*

Homeostatic functions of astrocytes

Astrocytes are another important glial cell and the most abundant in the brain making up 20 - 40% of cells (Herculano-Houzel, 2014; Colombo and Farina, 2016; von Bartheld *et al*., 2016). Rudolph Virchow was the first researcher to define astrocytes in 1846 as a homogeneous cell population supporting neuronal functions (Molofsky and Deneen, 2015; Perez-Nievas and Serrano-Pozo, 2018). In previous years, astrocytes have been characterised as “glue” providing structural support in the neural circuits by stabilising and holding together neuronal elements. However, this is now thought to be an oversimplification of their role in brain function. As their name suggests, astrocytes are star-shaped structures with long-branched processes. The

terminating processes of astrocytes contact different synapses and are known as the perisynaptic astrocytic processes (Araque *et al.*, 1999). Interestingly, an astrocyte can contact up to 100,000 synapses in a mouse brain whereas it can contact over a million synapses in the human brain (Halassa *et al.*, 2007).

Recent transcriptomic studies suggested that there are distinct subtypes of astrocytes differing in their morphology and function depending on the brain region (Zeisel *et al.*, 2018; Batiuk *et al.*, 2020). Astrocytes are categorised based on their morphology, distribution, and function into fibrous astrocytes and protoplasmic astrocytes (Wang and Bordey, 2008). Fibrous astrocytes prevalently exist in the white matter and are composed of long non-branched processes with end-feet contacting the nodes of Ranvier and blood vessels (Fig.1.9). On the other hand, protoplasmic astrocytes are found in grey matter and have a branched morphology with their processes contacting synapses and their end-feet contacting blood vessels. Astrocytes then interact with different cells in the neural networks by contacting synaptic terminals, dendrites, and dendritic spines with their processes (Wang and Bordey, 2008). Both astrocytic populations once activated express the glial fibrillary acidic protein (GFAP), the main intermediate filament protein contributing to their astrocytic cytoskeleton (Marín-padilla, 1995; Wilhelmsson *et al.*, 2006; Brozzi *et al.*, 2009; Saur *et al.*, 2014). Additionally, GFAP sustains the mechanical strength of astrocytes while it provides support to the contacting neurons and blood-brain barrier (BBB) (Eng *et al*., 2000). Importantly, astrocytes express different GFAP isoforms as well as other intermediate filament proteins such as nestin and vimentin (Wang and Bordey, 2008; Kamphuis *et al.*, 2012).

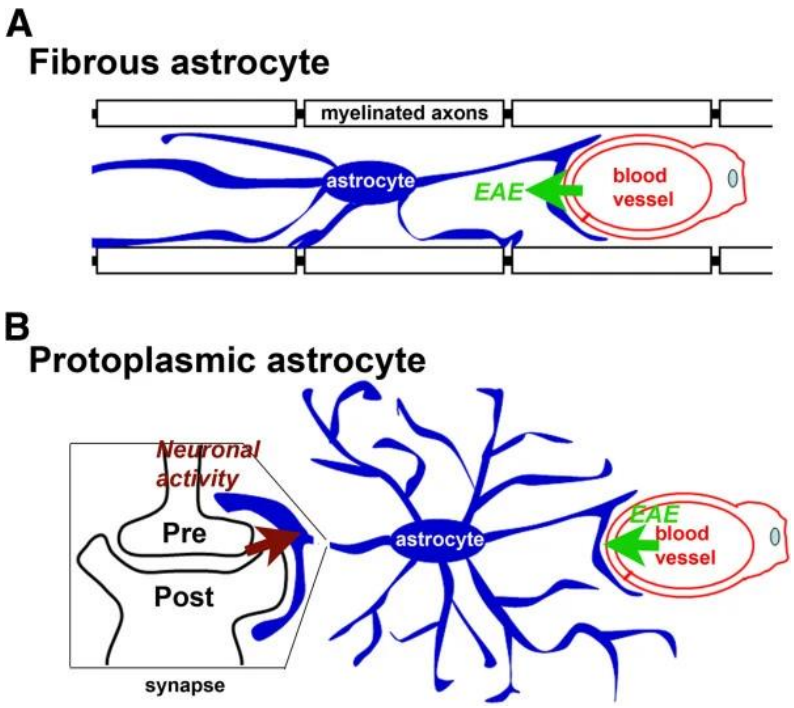

Figure 1.9. Fibrous and protoplasmic astrocytes. A. Fibrous astrocytes are shown contacting nodes of Ranvier and blood vessels in white matter. **B.** The protoplasmic astrocytes are more ramified and contact both blood vessels and neuronal synapses found in grey matter. This figure was taken from Jukkola et al., 2013 (Jukkola *et al.*, 2013).

Astrocytes play a key role in critical functions in the brain including inflammation, oxidative stress, neuronal metabolism, energy supply, neuronal synaptic function, plasticity support, neurotransmitter extracellular balance, water and ion extracellular homeostasis, maintenance of BBB as well as blood flow control (Volterra and Meldolesi, 2005; Abbott *et al*., 2006; Bak *et al*., 2006; Iadecola and Nedergaard, 2007; Pellerin *et al.*, 2007; Gordon *et al*., 2007; Vezzani *et al.*, 2011; Haj-Yasein *et al.*, 2012; Devinsky *et al.*, 2013; Serlin *et al.*, 2015; Falkowska *et al.*, 2015; De Pittà *et al*., 2016; Vasile *et al*., 2017; Boison and Steinhäuser, 2018; Hussaini and Jang, 2018; Chen *et al.*, 2020). Having such a pivotal position between different neuronal types, astrocytes control the extracellular ionic concentrations as well as the neurotransmitter uptake and release. Astrocytes express high levels of potassium channels and function as spatial buffers during the extracellular release of potassium ions caused by neuronal action potential firing (Paulson and Newman, 1987; Kim *et al*., 2019). Particularly, astrocytes take up and transport the extracellular potassium ions located on the synapses of neurons and release them through their end feet onto the blood

vessels. This ionic transfer is important for the management of regional cerebral blood flow (Paulson and Newman, 1987; Kim *et al*., 2019).

The role of astrocytes in neurotransmission

Astrocytes also play a key role in neurotransmission. GABA is rapidly taken by astrocytes, and this controls GABA levels in the synapse and prevents the spread of GABA (Kinney and Spain, 2002). Also, astrocytes control the excitatory glutamatergic signalling. The glutamate transporters excitatory amino acid 1 (EAAT1) and 2 (EAAT2) found on astrocytes are responsible for the uptake of glutamate from the synaptic cleft (Kinney and Spain, 2002). Apart from this critical role of astrocytes in the management of neurotransmission, they also release gliotransmitters and modulators including the amino acids glutamate, glycine, D-serine, and GABA, and the nucleotide ATP (Kimelberg *et al.*, 1990; Parpura *et al.*, 1994; Pellerin and Magistretti, 1994; Schell *et al.*, 1997; Do *et al.*, 1997; Desai *et al*., 1999; Barakat and Bordey, 2002; Krzan *et al.*, 2003; Newman, 2003; Zhang *et al.*, 2003; Angulo *et al.*, 2004; Fellin and Carmignoto, 2004; Gordon *et al.*, 2005; Jean *et al*., 2008; Eulenburg and Gomeza, 2010; Jiménez-González *et al.*, 2011; Yoon and Lee, 2014; DiNuzzo, 2016; Shibasaki *et al.*, 2017; Bardóczi *et al.*, 2017; Beltrán-Castillo *et al.*, 2017). Astrocytes are also involved in the facilitation of spontaneous focal calcium transients and might transmit calcium to neighbouring astrocytes (Nimmerjahn *et al.*, 2004; X. Wang *et al.*, 2006; Takata and Hirase, 2008; Hoogland *et al.*, 2009; Perea *et al*., 2009; Kuga *et al.*, 2011).

The role of astrocytes in neuroinflammation

Similar to microglia, astrocytes are also involved in the phagocytosis of synapses and the elimination of debris (Gomez-Arboledas *et al.*, 2018; Jung and Chung, 2018). Different chemicals, toxins, oxidative stress, or pathogens cause resting astrocytes to become reactive. Molecules that trigger astrocytic activation include the transforming growth factor β1 (TGF-β1) (Ongali *et al.*, 2018), leukaemia inhibitory factor (LIF) (Zhou *et al.*, 2017), and ciliary neurotrophic factor (Wang *et al.*, 2020). Epilepsy, stroke, traumatic brain injury and neurodegeneration are all

conditions that trigger astrocytic activation leading to reactive astrogliosis (Sofroniew, 2015; Escartin *et al*., 2019). There are two types of astrocytic activation including A1 and A2 astrocytes (Fig. 1.10). Both A1 and A2 reactive astrocytes demonstrate morphological changes and reversible alterations in gene expression, cell hypertrophy and glial scar generation (Anderson *et al*., 2014). A1 astrocytes are pro-inflammatory and neurotoxic, and their activation is induced by activated neuroinflammatory microglia. The secretion of component 1 subcomponent q (C1q), TNF-α, and IL-1α by the activated microglia leads to the formation of A1 reactive astrocytes (Liddelow and Barres, 2017; Liddelow *et al.*, 2017). The A1 astrocytic phenotype secretes neurotoxins and releases neuroinflammatory markers including ROS, IL-1β, and TNF-α contributing to the loss of synaptogenesis, oligodendrocyte induction, and cell death (Liddelow and Barres, 2017; Lee *et al.*, 2019).

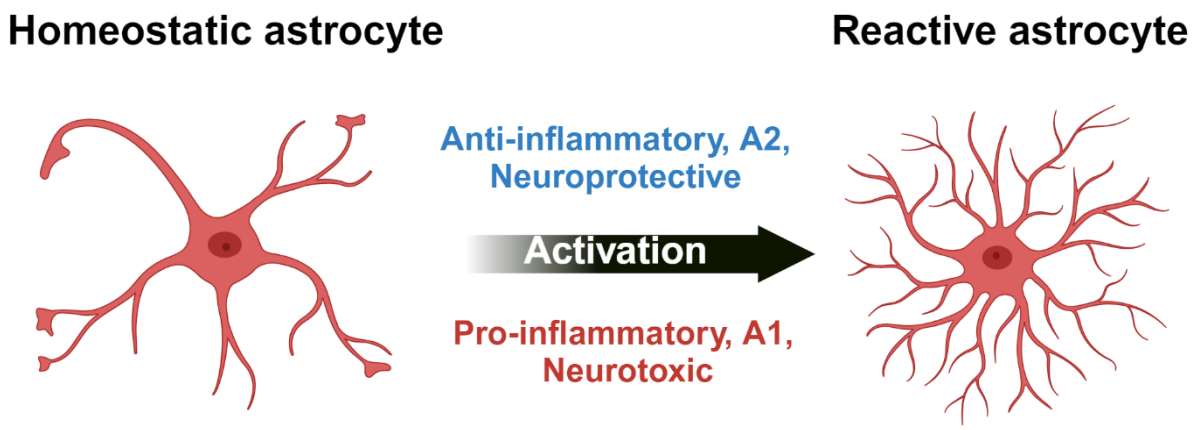

Figure 1.10. Astrocytic activation. The homeostatic astrocytes (with end-feet) during the resting state once activated become reactive and show an increased ramification of their processes. There are two types of astrocytic activation: 1) anti-inflammatory known as A2 which is neuroprotective and 2) pro-inflammatory known as A1 which is neurotoxic. This figure was created using Bio Render.

On the other hand, A2 reactive astrocytes are thought to be mainly anti-inflammatory and neuroprotective, and their activation is caused by microglia following brain injury (Anderson *et al*., 2014; Liddelow *et al.*, 2017). Important for the shift of resting astrocytes into an A2 reactive state is the nuclear factor IA (NFIA) which induces human glial competency and turns astrocytes into a more neuroprotective phenotype (Tchieu *et al.*, 2019). The A2 astrocytes form a glial scar by surrounding the injured site and sealing the affected BBB (Liddelow *et al.*, 2017). Reactive astrocytes

demonstrate GFAP, vimentin, nestin, and inducible nitric oxide (iNOS) upregulation (Robel, 2017; Verhoog *et al.*, 2020).

There is communication between astrocytes and microglia. Research shows that following injury, astrocytes send signals to direct the microglial processes to the affected site (Davalos *et al.*, 2005). Furthermore, the astrocytic release of GABA reduces the inflammatory responses of the microglia (Lee *et al*., 2011). However, microglia also influence astrocytic behaviour and there is a bilateral communication between these two glial cells (Liddelow and Barres, 2017; Jha *et al.*, 2019). As mentioned earlier, microglia drive the activation of astrocytes, and they can influence the shift into a neurotoxic or neuroprotective phenotype (Burda and Sofroniew, 2017). This is crucial in different neurological diseases involving neuroinflammation as the bidirectional signalling between microglia and astrocytes can cause persistent inflammatory responses exacerbating the disease condition (Liddelow and Barres, 2017; Liddelow *et al*., 2017). Furthermore, both astrocytes and microglia cooperate to control the pruning of neuronal synapses and the elimination of apoptotic cells (Colonna and Butovsky, 2017).

1.6.3. *Changes in glial cells and neurodegeneration*

Glial cell function under normal conditions acts as a defence mechanism and is important for immune response and tissue repair in the CNS (Wyss-Coray and Mucke, 2002). However, under pathological conditions including endogenous ones such as genetic mutation and protein aggregation, or environmental ones like infection, trauma, and drugs, neuroinflammation becomes persistent (Glass *et al.*, 2010; Kempuraj *et al.*, 2016; Stephenson *et al.*, 2018). Sustained neuroinflammation involving microglia and astrocytes can be damaging and toxic as it prevents regeneration of synaptic function and contributes to the pathogenesis of neurodegeneration (Kempuraj *et al.*, 2016; Russo and McGavern, 2016).

Neuroinflammation in AD

Sustained inflammatory responses involving microglia and astrocytes are reported in AD. Both activated microglia and reactive astrocytes were observed to interact with Aβ and undergo morphological changes highlighting neuroinflammatory responses toward protein aggregation (Glass *et al.*, 2010). There is a bidirectional relationship between Aβ pathology and microglia and astrocytes. Microglial and astrocytic metabolism impairment causes the accumulation of Aβ (Yan *et al.*, 2013; Hickman *et al.*, 2018). On the other hand, Aβ triggers the activation of microglia and astrocytes through TLRs leading to the release of neuroinflammatory mediators and neurodegeneration (Glass *et al.*, 2010; Kempuraj *et al.*, 2016). Even though microglia can have a neuroprotective role as they can eliminate Aβ and tau, increased interaction between Aβ and pro-inflammatory cytokines diminishes this neuroprotective ability of microglia (Takata *et al.*, 2010; Asai *et al.*, 2015; Hickman *et al.*, 2018). Examination of post-mortem human tissue from AD patients revealed increased microglial activation within brain areas with Aβ plaques compared to cortical regions without (Liu and Hong, 2003; Dal Bianco *et al.*, 2008). Clusters of reactive microglia were observed near the Aβ plaques in different brain areas not only in human post-mortem tissue but also in AD mouse models (Bouvier *et al.*, 2016; Savage *et al*., 2019).

In the early stages of AD pathology, Aβ plaques are surrounded by neuroprotective anti-inflammatory microglia. However, because of increased pathology as the disease stages progress, neuroprotective microglia shift to the neurotoxic pro-inflammatory phenotype (Jimenez *et al.*, 2008; Tang and Le, 2016). Evidence shows that in the CSF of AD patients, who initially were diagnosed with MCI, there were increased levels of the pro-inflammatory cytokine TNF-α and decreased levels of the anti-inflammatory cytokine TNF-β. In contrast, patients with MCI who did not progress to AD did not express these changes in TNF-α and TNF-β cytokines (Tarkowski *et al.*, 2003). Additionally, in AD there is generally an early induction of neuroinflammation with a slow increase of pro-inflammatory cytokines IL-1β, IL-6, and TNF-α while the expression levels of IL-18, MCP-1, and IP-10 peak at later stages during the disease pathology (Brosseron *et al.*, 2014). The microglia-induced pro-inflammatory cytokines contribute to the decreased phagocytic activity of microglia and

their transformation into the neurotoxic phenotype (Kwon and Koh, 2020). Further evidence highlights the role of microglia in AD pathology as tau phosphorylation is increased by pro-inflammatory microglia which worsens the pathology (Lee *et al.*, 2010).

Astrocytes, as outlined above in section 1.6.2, also undergo morphological changes during pathological conditions in neurodegenerative disorders including AD and PD where an increase in GFAP expression is observed (Tzeng *et al.*, 2005; Sofroniew, 2009; Członkowska and Kurkowska-Jastrzebska, 2011; Lopategui Cabezas *et al.*, 2014). Pro-inflammatory A1 astrocytes proliferate in numbers in neurodegeneration and become toxic to neurons (Liddelow *et al.*, 2017). Aβ activates the advanced glycation end products receptors/NF-κB pathway which is critical for the transcription of astrocytic pro-inflammatory mediators like IL-1β, IL-6, iNOS, and TNFα cytokines and chemokines. Furthermore, oxidative stress, ROS, and reactive nitrogen species (RNS) are generated following Aβ production from astrocytes (González-Reyes *et al.*, 2017). Elevated expression levels of the protein C1q occur following changes in neuronal gene expression from immature astrocytes in AD and this contributes to synaptic removal (Stevens *et al.*, 2007).

Neuroinflammation in PD

Persistent neuroinflammation involving microglia and astrocytes contributes to the pathogenesis of PD. The activation of these two glial cells is controlled by proteins involved in familial forms of PD including α-syn, parkin, DJ-1, and ATPase (Glass *et al.*, 2010; Oksanen *et al.*, 2019). Activated pro-inflammatory microglia, caused by aggregated α-syn, contribute to the post-translational modifications of α-syn including its phosphorylation (pS129) (Reynolds *et al.*, 2009; Barkholt *et al.*, 2012; Béraud *et al.*, 2012). Research on post-mortem human brain tissue from PD patients showed that there was increased microglia activation in the hippocampus and substantia nigra (Rocha *et al.*, 2015). Activated microglia in these brain areas also had an amoeboid reactive shape (Imamura *et al.*, 2003). A spread of reactive microglia across all brain areas was noticed in PET scans done in PD patients (Gerhard *et al.*, 2006). Interestingly, microglial activation was observed in early-diagnosed PD patients

underpinning the induction of neuroinflammatory responses early in the disease (Gerhard *et al.*, 2006). Activated microglia attempt to retain homeostasis in the CNS by phagocytosing and degrading aggregated α-syn through lysosomes or facilitate its transfer to other microglia via tunnelling nanotubes (Choi *et al.*, 2020; Scheiblich *et al.*, 2021)

In the early stages of PD, microglial activation is associated with the loss of dopaminergic terminals and evidence suggests that neuroinflammatory responses are induced before the loss of dopaminergic neurons (Reish and Standaert, 2015; Kwon and Koh, 2020). Dopaminergic neurons affected by the α-syn pathology release toxic aggregated α-syn which activates the pro-inflammatory microglia. The reactive microglia then release pro-inflammatory mediators including TNF-α, NO, and IL-1β which drive the neuroinflammatory responses and worsening of disease progression (Zhang *et al.*, 2005; Hirsch and Hunot, 2009; Rojanathammanee *et al*., 2011; Tang and Le, 2016). There is an increase in the pro-inflammatory markers associated with microglia activation including iNOS, cyclooxygenase (COX), and the phagocytosis marker CD68 in PD patients (Hunot *et al.*, 1996; Knott *et al*., 2000; Doorn *et al.*, 2014). Importantly, microglia are targeted by α-syn through exosomes derived from neurons which enable the spread of pathological α-syn from neuron to neuron and neuroinflammation (Colonna and Butovsky, 2017; George *et al.*, 2019).

Injection of α-syn pre-formed fibrils (PFF) in the striatum of A30P transgenic mice revealed the spread and accumulation of pS129 from the injection site as well as induction of microglia and development of hindlimb paralysis not evident in the WT (Gentzel *et al.*, 2021). The same study also showed that brain areas with increased accumulation of pS129 had intense Iba-1 staining (ionised calcium-binding adaptor molecule 1, pan macroglia marker), highlighting an increase in microglia (Gentzel *et al.*, 2021). Further evidence indicates that injection of α-syn PFF and lipopolysaccharide (LPS, induces bacterial infection) in the striatum of a PD mouse model showed increased microglial activation, accumulation of aggregated α-syn, and neurodegeneration. Importantly, the administration of a microglial inhibitor (PLX5622) reduced the expression of Iba-1+ microglia and decreased α-syn toxicity and degeneration of dopaminergic neurons in the PFF-injected mice (Lai *et al.*, 2024). These studies highlight the contribution of activated microglia to the α-syn pathology and the role of their neuroinflammatory responses in neurodegeneration.

On the other hand, the role of astrocytes in the α-syn pathology has not yet been fully elucidated. Similar to microglia, astrocytes might be involved in the phagocytosis and elimination of misfolded aggregated α-syn from the extracellular space (Jung and Chung, 2018). This hypothesis is based on investigations of PD patient brain tissue demonstrating α-syn inclusions in astrocytes and neurons (Wakabayashi *et al.*, 2000; Hishikawa *et al.*, 2001; Braak *et al*., 2007). However, there is evidence showing the uptake of α-syn by astrocytes through an endocytosis mechanism dependent on TLR4 (Braidy *et al.*, 2013; Fellner *et al.*, 2013; Rannikko *et al*., 2015). Additionally, localisation of the taken α-syn in lysosomes implies its degradation by astrocytes (Lee *et al.*, 2010). Examination of post-mortem human tissue of PD patients revealed reactive astrocytes in substantia nigra and it has been suggested that astrocytes are implicated in the neurodegeneration of dopaminergic neurons (Miklossy *et al.*, 2006; Booth *et al*., 2017).

1.6.4. *Changes in glial cells in DLB*

Neuroinflammation in DLB patients post-mortem

Neuroinflammation including elevated microglial activation has been mostly shown in post-mortem brains of AD patients (Rivera et al., 2005; Dal Bianco et al., 2008; Nielsen et al., 2013; Lastres-Becker et al., 2014; Lue et al., 2015; Rangaraju et al., 2015; Walker and Lue, 2015; Satoh et al., 2016). However, there are fewer post-mortem studies focused on microglial and astrocytic activation in DLB patients. Microglial activation was not observed in the hippocampus and pulvinar of DLB patients post-mortem compared to controls (Bachstetter et al., 2015; Streit and Xue, 2016; Erskine et al., 2018; Amin et al., 2020; Rajkumar et al., 2020). However, increased levels of GFAP protein were discovered in the pulvinar area of DLB patients post-mortem suggesting elevated astrocytic activation (Erskine et al., 2018). Importantly, post-mortem examinations in DLB cases only revealed changes related to pathology at the end course of the disease. There might be changes in neuroinflammatory markers, however, during the earlier stages of the pathology which need to be considered.

Neuroinflammation in early DLB

Evidence shows that neuroinflammation occurs in the early stages of neurodegenerative disorders including the prodromal DLB. The prodromal stage in DLB is a stage before dementia has developed which includes mild cognitive deficits as well as motor symptoms/signs, sleep disorders, autonomic impairment, and neuropsychiatric disruption (McKeith *et al.*, 2020). PET imaging revealed increased microglial activation in the substantia nigra of patients with RBD, a confirmed prodromal stage in α-synucleinopathies (Stokholm *et al.*, 2017). To better understand neuroinflammatory changes in the brain, the examination of cytokine concentrations in the CSF of patients is important. The levels of the pro-inflammatory cytokine IL-6 are decreased in the CSF of DLB patients compared to AD patients and healthy controls (Wennström *et al.*, 2015). Furthermore, research shows there is an association between CSF IL-6 levels and CSF α-syn levels but not with cognitive test scores. This contradicts other findings showing no differences in the IL-6 or IL-1β concentration between DLB, AD patients, and healthy controls (Amin *et al.*, 2022). There are probably distinct immune reactions for AD and DLB. In AD patients, the glycoprotein YKL-40 which is expressed in glial cells has an increased expression in the CSF of patients whereas this change is not seen in the CSF of prodromal and established DLB patients (Craig-Schapiro *et al.*, 2010; Morenas-Rodríguez *et al.*, 2019). Interestingly, in the CSF of DLB patients with AD pathology there was an increased concentration of YKL-40 highlighting the difference in inflammatory responses in different pathologies (Morenas-Rodríguez *et al.*, 2019).

Changes in the peripheral immune system in neurodegeneration can also be demonstrated by investigating blood-based biomarkers. In patients exhibiting MCI and LB pathology (probable LB pathology diagnosed using Diagnostic and Statistical Manual of Mental Disorders 5 criteria and dopaminergic imaging) as well as AD patients with MCI, there were increased concentrations in the plasma cytokines IL-1β, IL-2, IL-4, and IL-10 and decreased TNF-α levels compared to healthy controls and patients with dementia. An increase in cognitive impairment was associated with decreased plasma concentrations of IL-1β, IL-2, and IL-4 while the levels of IL-6 and

TNF-α were increased across all patients including DLB patients with parkinsonism and DLB patients with MCI (King *et al.*, 2018).

PET scan imaging of amyloid and microglial activation (using PK11195) *in vivo* was used by Surendranathan et al. (2018) to investigate peripheral blood cytokine concentrations in people with probable DLB and DLB patients. In prodromal DLB patients, there was enhanced microglial activation in areas that were later affected by pathology, including the caudate nucleus, cuneus, anterior orbital gyrus, and superior frontal gyrus areas compared to DLB patients with moderate or severe cognitive impairment. Furthermore, there were increased levels of peripheral cytokines implicated in T-cell function including macrophage inflammatory protein 3 (MIP 3), IL-2, and IL-17A, and decreased IL-8 levels in the serum of DLB patients compared to healthy controls. Importantly, the difference between prodromal DLB patients and DLB patients with cognitive impairment was the increased IL-2 levels, which were found only in prodromal DLB. However, the peripheral cytokine concentrations did not correlate with microglial activation or amyloid deposition (Surendranathan *et al.*, 2018). This provides evidence of microglial activation in the early stages of DLB which decreases with cognitive decline and the increase in peripheral inflammatory cytokines in DLB patients.

Another study using PET imaging combined with PK11195 binding *in vivo* also showed increased microglial activation in the substantia nigra and putamen in the early stages of DLB and PD patients (within one-year onset). Both DLB and PD patients had increased CSF protein carbonylation suggesting CNS protein modifications linked to oxidative stress (Iannaccone *et al.*, 2013). It is suggested that hypometabolism in the occipital area precedes abnormalities in the nigrostriatal pathway in the early stages of DLB. Huang et al. (2015) by using Fludeoxyglucose (FDG) PET imaging, discovered that mild DLB patients exhibited hypometabolism in the temporal brain areas, ACC, inferior orbital area, thalamus, and caudate nucleus compared to normal controls. In demented DLB patients, however, there was extensive hypometabolism in the cortex implicating the occipital cortex (Huang *et al.*, 2015).

Overall, neuroinflammation can be assessed at the prodromal DLB stage by investigation methods involving blood cytokines and PET imaging. Evidence supports the induction of neuroinflammatory responses in DLB involving microglial activation,

which is enhanced at early disease stages, and then declines as cognitive impairment progresses. This decrease in microglial activation might be reflected in the post-mortem human brain tissue examinations since inflammation declines in the advanced stages of the disease. However, there is no evidence of neuroinflammation in the ACC in the early stages of DLB. Thus, the role of glial cells in the ACC in the A30P transgenic mouse model of DLB will be examined in this thesis to elucidate potential differences in different disease stages.

1.6.5. *The relationship between neuroinflammation and PNNs in neurodegeneration*

In AD patient post-mortem brain tissue and mouse models, PNNs are degraded by microglia activated by cell damage which then phagocytose the neuronal debris (Crapser, Spangenberg, *et al.*, 2020). This process is initiated by the secretion of proinflammatory cytokines, reactive oxygen species, and proteinases by the microglia (Kettenmann *et al.*, 2013). These proteinases include MMPs, which are ECM-cleaving enzymes that digest PNNs, and expose the neurons to oxidative stress (Pirbhoy *et al.*, 2020). The activated microglia also interact with the now-exposed neurons and remove synapses.

Fragments of PNNs have been observed inside microglia in the subiculum of the 5xFAD mouse model of AD and in patients, which is a critical brain area in memory and is affected early in AD (Crapser, Spangenberg, *et al.*, 2020). Thus, microglia play a critical role in the degradation of PNNs by directly “attacking” them through MMPs and then engulfing them. Chronic depletion of microglia before and during plaque progression, as shown in AD mouse models, promoted the recovery of dendritic spine loss as well as the prevention of neuronal and PNN loss (Spangenberg *et al.*, 2016; Crapser, Spangenberg, *et al.*, 2020). Even though PNNs act as a shield around the surrounding neurons, which is thought to prevent tau uptake, their loss caused by microglial activation reduces their protective role (Baig *et al.*, 2005; Suttkus *et al.*, 2016; Crapser, Ochaba, *et al.*, 2020; Crapser, Spangenberg, *et al.*, 2020). It is also suggested that the PNN loss in AD is proportional to the Aβ plaque burden in both AD patients and transgenic mice (Fawcett *et al.*, 2019; Crapser, Spangenberg, *et al.*,

2020). Therefore, reactive microglia triggered by the Aβ aggregation contribute to cognitive decline by degrading the PNNs.

The PNN component HA is also associated with AD pathology and has been shown to accumulate mainly at the perimeter of plaques. Increased accumulation of HA is associated with the activation of CD44+ astrocytes which exacerbates AD pathology (Akiyama *et al.*, 1993; Sherman *et al.*, 2002, 2015; Bourguignon *et al.*, 2007). HA, overload impacts the BBB by decreasing the blood flow, thus decreasing glucose and oxygen supply to the neurons leading to ischaemia (Akiyama *et al.*, 1993; Sherman *et al.*, 2002, 2015; Bourguignon *et al.*, 2007; Pintér and Alpár, 2022). The PNN structure and activity are affected by hyperphosphorylated tau causing the formation of dysfunctional PNNs with abnormally short HA molecules (Li *et al.*, 2017). This pathologic remodelling of PNNs has been shown to trigger a positive feedback loop by activating inflammation which worsens tissue damage in post-mortem examinations of AD patients (Akiyama *et al.*, 2000; Reed *et al.*, 2019).

The interplay between neuroinflammatory markers, including reactive microglia and astrocytes, and PNNs has been studied mainly in AD. However, it is still unknown whether α-syn pathology in DLB promotes PNN degradation by reactive microglia. The impact of hα-syn overexpression on the PNNs surrounding PV interneurons in the ACC will be investigated in this thesis.

1.7. Aims of the thesis

The aims of the thesis are summarised below.

- Test the hypothesis that ACC in A30P mice would exhibit hyperexcitability and gliosis in the early stages of α-syn pathology.

- Explore whether changes in PV inhibitory interneurons and/or PNNs are impacted by human mutant α-syn.

- Investigate whether ACC shows evidence for neuroinflammatory changes in either young or aged A30P mice.

Chapter 2. General Methods

2.1. Animal Provision

The (Thy-1)-h[A30P]αSYN mice (referred to hereafter as A30P) have a C57BL/6 background and were kindly provided by Prof. Philipp Kahle, University of Tübingen, Germany. A colony was established at the internal animal facilities at Newcastle University's Comparative Biology Centre. Homozygous mice were crossed with C57BL/6 mice to produce the F1 generation. From the F1 generation of heterozygous mice, the homozygous A30P mice were then crossed together to produce the homozygous A30P mouse line. To regenerate the homozygous A30P mouse breeding line, homozygous offspring from the previous lines, which were not from the same progenitors, were crossed. Mice were ear notched after they were weaned (~21 days) and samples were genotyped (Transnetyx Inc., Tennessee, USA) before two separate lines were generated for wild-type (WT) and homozygous A30P mice. The A30P mouse line is regenerated every 5 - 6 generations.

The A30P mice exhibit severe motor deficits from ~16 months onwards and there is premature death from around 17-18 months (Freichel *et al.*, 2007). Hence, the animals used in this thesis were between the ages of 2 months and 12 months. The mice were categorised into two different age groups: 2 - 4 months and 10 - 12 months (for both WT and A30P mice). Mice aged between 2 - 4 months were used to investigate changes in neuronal networks early in α-syn pathology and aged 10 - 12 months mice were used since at this age, the A30P mice develop cognitive deficits and not motor symptoms which follow after (Kahle *et al.*, 2000, 2001). Data were compared within and between the two age groups as the same mice were not used longitudinally. Some C57BL/6 mice were purchased from external sources (Charles River) for the 2–4-month age group when the availability of WT mice was low.

The project procedures described were performed according to the UK Animals (Scientific Procedures) Act 1986, and the European Union Directive 2010/63/EU under the provision of appropriate personal and project licenses. All animals used for the project were maintained on a 12-hour light/dark cycle with unlimited access to food and water and environmental enrichment in same-sex groups no larger than 6 mice. Wherever possible, animals were not housed alone for longer than 24 hours.

2.2. *In vitro* Electrophysiology

2.2.1. *Preparation of acute brain slices*

Animals were anaesthetised with inhaled isoflurane (IsoFlo 100% w/w; Zoetis, UK) followed by an intramuscular injection of ketamine (Ketabel 100 mg/ml; used at 0.25 ml >100 mg/kg) and xylazine (Xylacare 20 mg/ml). Before proceeding with any operations, the reflexes were checked via pedal and tail withdrawal. Once all reflexes had ceased, the abdominal cavity and ribcage were opened for heart exposure and the left ventricle of the heart was pierced with a needle. An incision was made in the right atrium and a transcardial perfusion of chilled, carbogenated (95% O_2 / 5% CO_2) sucrose artificial cerebrospinal fluid (sucrose ACSF) was performed with 30 ml solution at an approximate rate of 0.5 ml/sec.

The sucrose ACSF (sACSF) solution was prepared using distilled water by dilution of 252 mM sucrose, 3 mM KCl, 1.25 mM NaH2PO4, 24 mM NaHCO3, 1 mM MgSO4, 1.2 mM CaCl2 and 10 mM glucose. Regular ACSF was prepared by use of 126 mM NaCl instead of 252 mM sucrose. All chemicals were stored according to supplier recommendations and details of each chemical are described in Table 2.4. The stock solutions were maintained for 2 - 3 weeks to allow daily preparation of regular or sACSF. Fresh ACSF solution was prepared on the experimental day, whilst sACSF was prepared the day before and kept refrigerated for a maximum of 48 hours.

Following intracardial perfusion with sACSF, the animal was decapitated to separate the head from the spinal cord and the skull was exposed with an incision. Further dissection of the skull revealed the brain which was removed. The brain was then placed into a petri dish of chilled, carbogenated sACSF and trimmed in half using a razor blade to section off the prefrontal cortical area. The rostral portion of this sectioned part of the brain containing the PFC was then glued to the chuck of a Leica VT1000 vibrating blade microtome (Leica Microsystems, Germany) and the brain was covered in chilled, carbogenated sACSF. The frontal part of the brain was sectioned in 450 µm thick coronal slices which were collected in a petri dish of chilled, carbogenated sACSF. The slices were then trimmed to isolate the ACC and PFC regions and both hemispheres were used.

The prefrontal slices were categorised according to the anterior-to-posterior axis based on plates 21, 23, 25 and 30 from Paxinos and Franklin, 2001 mouse brain atlas, 2nd edition. The slices categorised as plates 21, 23, 25 and 30 were chosen for the *in vitro* electrophysiology experiments for the ACC since the following slices were too posterior (Fig. 2.1). Additionally, these slices were selected as they consist of the ACC triangle area and no other mPFC regions including the PrL and IL areas.

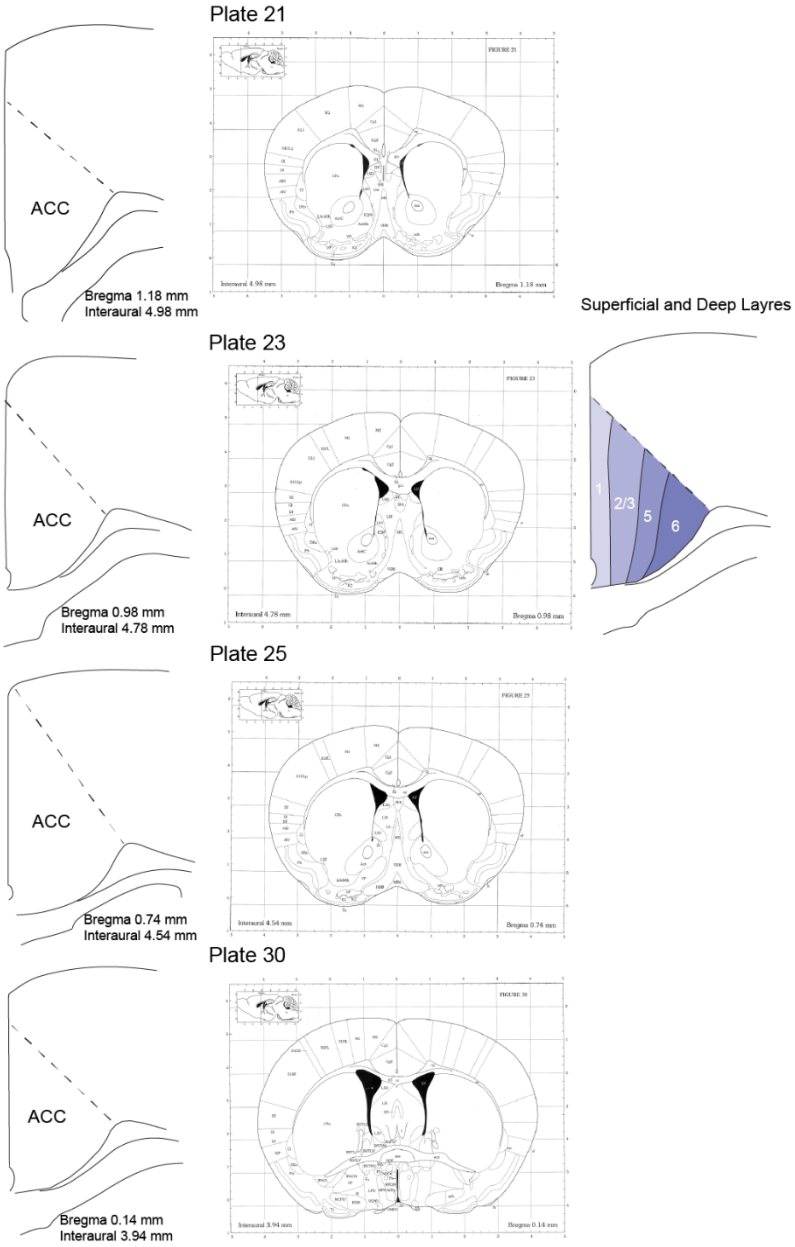

Figure 2.1. Classification of the mouse ACC slices in different anterior-to-posterior axis locations. The slices of the ACC have been classified according to plates 21, 23, 25 and 30 from the Paxinos and Franklin, 2001, 2nd edition mouse brain atlas. On the right, the ACC deep layers 5, 6 and the superficial layers 1, 2/3 are shown.

2.2.2. *Slice maintenance*

Once the ACC slices were prepared, they were transferred to an interface holding chamber maintained at room temperature in carbogenated normal ACSF (126 mM NaCl instead of sucrose). The chamber was covered with parafilm and left for 1 hour for the slices to recover and to allow sufficient time for the washing of the water-soluble anaesthetics isoflurane, ketamine, and xylazine (Dickinson *et al.*, 2003).

Following this 1-hour incubation, a maximum of 3 slices were transferred to an interface recording chamber, supplied with a continuous flow (~1.2 ml/min) of carbogenated normal recording ACSF through a Gilson Minipuls3 pump. The chamber was maintained at a temperature of 30 – 31 °C using a heater (FH16-D; Grant Instruments Ltd, UK), with temperature measurements taken by infrared thermometer before and throughout the experiment. To maximise slice use, multiple rigs with one recording chamber and two electrodes on each were used simultaneously. Additionally, the experiments described in this thesis were performed within 6 hours following slice preparation.

2.2.3. *Data acquisition*

Glass microelectrodes (1.2 mm OD, 0.94 mm ID, 100 mm L; 30-0050 G120TF-10, Harvard Apparatus Ltd., UK) were used for extracellular local field potential (LFP) recordings. The electrodes were pulled using a P-97 Flamming/Brown puller (Sutter Instrument Co., USA). This produced electrodes with a resistance of approximately 2 - 5 mΩ. The electrodes were then filled with ACSF and placed in a holder attached to a head-stage preamplifier held in place by a micromanipulator.

Each rig had 2 micromanipulators, and thus 2 channels. Electrodes were positioned using the micromanipulator and inserted into the ACC of the mouse PFC. Each of the 2 electrodes was inserted into ACCs from a separate slice and data were recorded with an Axoclamp-2B amplifier (Axon Instruments Inc., UK). The activity was filtered through a band-pass filter using Neurolog external filters at 0.001 kHz high pass and 0.4 kHz low pass. Data was re-digitised at 10 kHz using an ITC-16 interface (Digitimer, UK). The electrical mains noise at 50 Hz was removed using a HumBug

(Digitimer, UK) and data were recorded using the AxoGraph software (Version 1.8, Axon Instruments Inc., USA) and analysed offline.

2.2.4. *Data analysis*

Oscillations in the ACC were evoked using 800 nM kainate (KA) which was bath-applied to the circulating carbogenated ACSF. Oscillatory activity was obvious 30 minutes-1 hour following the KA application and stabilised 3 hours post-application i.e. area power readings were +/- 10% at 3 x 10-minute intervals. In most cases, the electrodes were moved positions around the deep layers of ACC to find clear oscillatory activity. The data were analysed using Axograph's power spectrum analysis to examine the oscillation power, peak amplitude, and peak frequency (Fig. 2.2).

Using the AxoGraph's Fast Fourier Transform algorithms, power spectral density analysis was performed using 8192 bins resolution. The data were represented by frequency (Hz) and power (μV^2 / Hz) over a 60-second recording trace. For each trace, the area under the curve (area power; μV^2/Hz) and peak frequency (Hz) were measured between 15 and 90 Hz to study both beta and gamma oscillations in the ACC. The area power indicates the oscillation strength within the 15 – 90 Hz frequency band.

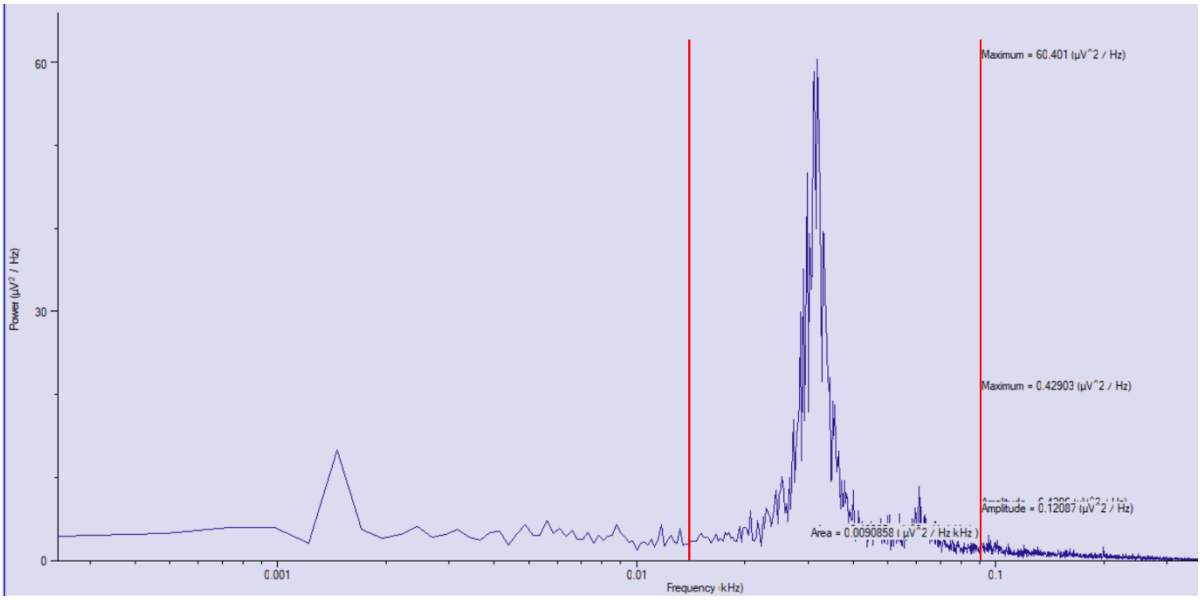

Figure 2.2. Example power spectrum of 15 – 90 Hz oscillation in the ACC. Oscillatory activity in the 15 – 90 Hz area (red line indicators) was analysed using the power spectrum in Axograph. The power spectrum analysis shows measurements including area power (μV^2/Hz), peak amplitude (μV^2), and peak frequency (Hz).

To investigate hyperexcitability in the ACC, the bath application of gabazine (antagonist of $GABA_A$ receptors) or 4-aminopyridine (4-AP, voltage-gated potassium channel blocker) was used in the circulating carbogenated ACSF. The two pharmacological compounds drive hyperexcitability under different mechanisms. Recordings were taken post-drug application for 4 hours and the hyperexcitability events were analysed. Depending on the experiment, three different forms of hyperexcitable events were manually measured including simple interictal discharges (IIDs) a single population spike event, and complex IIDs with two or more population spike events. The seizure-like activity was defined as any spike activity lasting longer than 5 seconds consisting of a combination of both simple and complex IIDs (Fig. 2.3).

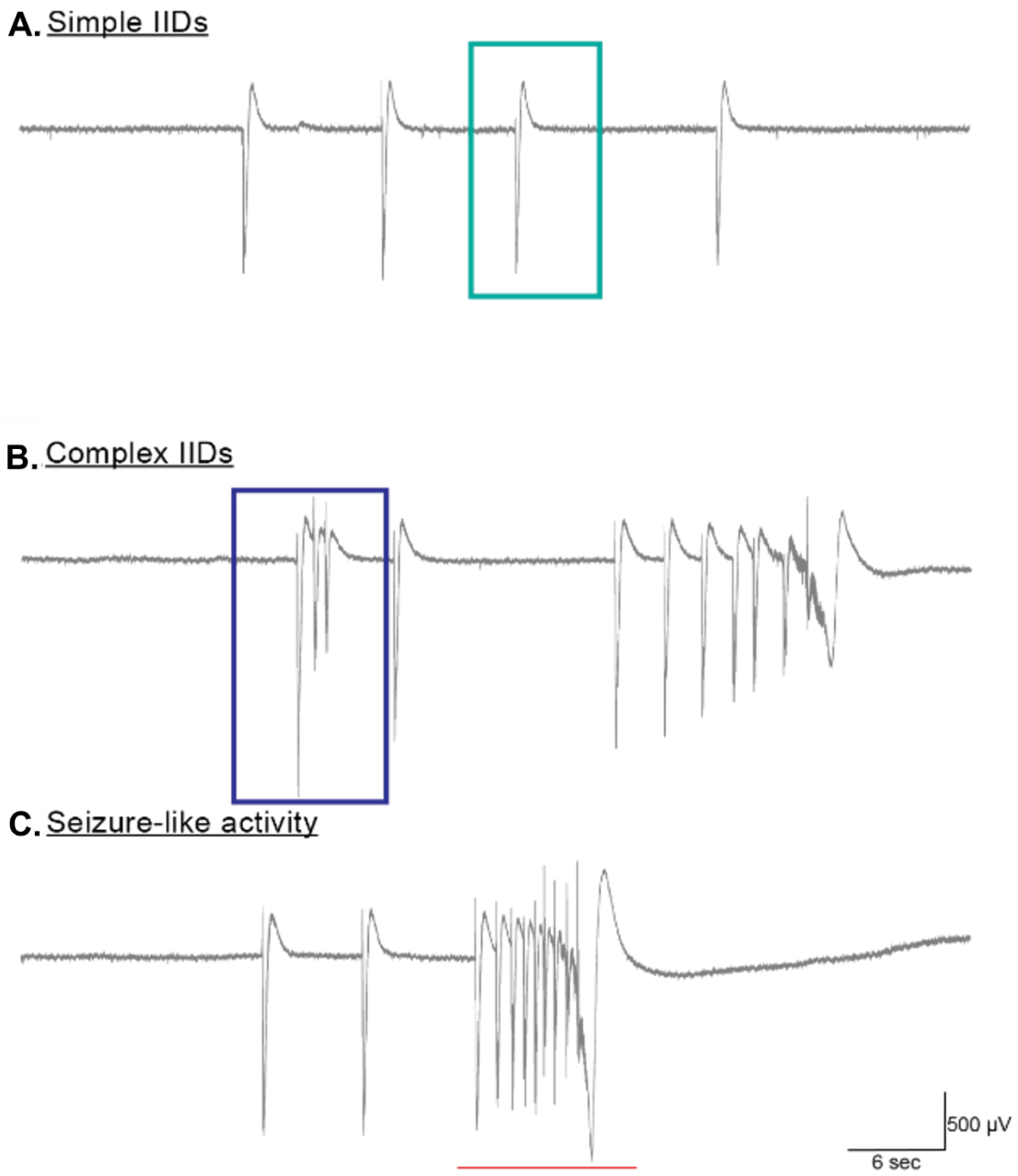

Figure 2.3. Example traces of hyperexcitable events in the ACC. Hyperexcitability events were classified as (**A**) simple IIDs, (**B**) complex IIDs and (**C**) seizure-like activity. **A.** The teal box shows an example IID event consisting of a single population spike event. **B.** The blue box shows an example complex IID event consisting of two or more population spike events. **C.** The red line indicates a seizure-like event consisting of multiple spike events with simple and complex IIDs lasting longer than 5 seconds. This is a modified version of Fig. 4.6.

2.2.5. *Pharmacological and chemical compounds*

All compounds used for the experiments were stored according to the manufacturer's recommendations. Water-soluble compounds were constituted in distilled water, and the stock solutions were kept frozen (-20°C) or refrigerated (4°C), depending on manufacturer instructions and frequency of use. All the drugs (Table 2.2) were applied in the bath through the circulating carbogenated ACSF to reach the prefrontal slices in the chamber within minutes.

Chemical Name	Formula	Vendor
Sodium chloride	NaCl	Merck (57653)
Potassium chloride	KCl	BDH (101985M)
Sodium dihydrogen orthophosphate	NaH_2PO_4	BDH (307164T)
Magnesium sulphate	$MgSO_4$	Merck (M7506)
Calcium chloride dihydride	$CaCl_2$.2H2O	Merck (5080)
Glucose	$C_6H_{12}O_6$	VWR Chemicals (101176K)
Sucrose	$C_{12}H_{22}O_{11}$	Merck (50389)

Table 2.1. List of chemical compounds used for the *in vitro* electrophysiology experiments.

Compound name	Chemical name	Mechanism of action	Vendor
Kainic acid (kainate, KA)	(2S,3S,4S)-3-(Carboxymethyl)-4-prop-1-en-2-ylpyrrolidine-2-carboxylic acid	KA receptor agonist and partial AMPA receptor agonist	Hello Bio (HB0355-10mg)
Gabazine (SR-95531)	2-(3-carboxypropyl)-6-(4-methoxyphenyl)-2,3-dihydropyridazin-3-iminium bromide	Selective, competitive GABAA receptor antagonist	Hello Bio (HB0901-10mg)
4-Aminopyridine (4-AP)	pyridin-4-amine	Potassium channel blocker	Merck (275875)

Table 2.2. List of pharmacological compounds used for the *in vitro* electrophysiology experiments.

2.3. Free-floating Immunohistochemistry (IHC)

2.3.1. *Transcardial perfusions with paraformaldehyde*

Animals were anaesthetised as outlined above for acute slices (Chapter 2.2.1) with inhaled isoflurane (IsoFlo 100% w/w; Zoetis, UK) followed by an intramuscular injection of ketamine (Ketabel 100 mg/ml; used at 0.25 ml >100 mg/kg) and xylazine (Xylacare 20 mg/ml; used at 0.25 ml >10 mg/kg). Before proceeding with any operations, the reflexes were checked via pedal and tail withdrawal. Once all reflexes ceased, the abdominal cavity and ribcage were opened to expose the heart, and the left ventricle of the heart was pierced with a needle. An incision was made in the right atrium and transcardial perfusion was performed by first circulating 50 ml of 0.9% saline solution for blood removal and then 50 ml of paraformaldehyde (PFA, 4% diluted in PBS, Merck) was inserted at an approximate rate of 0.5 ml/sec. An incision was made to expose the skull and collect the brain. The cerebellum was removed, and the remaining brain was transferred to a tube containing 4% PFA solution which was stored in the fridge overnight before being changed into 30% sucrose phosphate buffered saline solution (PBS 0.1M) for two days. For longer storage in the freezer, the brain was then transferred to cryopreservant solution (300 ml glycerol, 300 ml ethylene glycol, 200 ml 0.3M PBS, 200 ml of deionised H_2O). Before brain sectioning, the cryopreservant solution was changed into a 30% sucrose solution and the brain was stored in the fridge overnight.

2.3.2. *Free-floating IHC-Immunofluorescence*

Whole brains from PFA-perfused mice were stored in buffered PFA (4%, Merck) overnight before being transferred to 30% sucrose PBS for two days. Brains were then sectioned at 40 µm using a freezing stage microtome. The 40 µm sections were collected in a well plate in which each well contained PBS (0.1M). For longer storage, the PBS solution was changed to cryopreservant solution. Otherwise, a blocking solution containing 0.1M PBS, 0.3% Triton-X (Acros Organics, 327371000), and 5% donkey serum (Merck, S30-100) was added to the sections to be blocked before the addition of primary antibodies or lectin (300 µl in each well). The blocking was

performed for 5 hours at room temperature (RT) and the well plate was positioned on a shaker to prevent non-specific antibody binding and reduce background staining.

Following tissue blocking, the sections were incubated with primary antibodies and lectin diluted in the blocking solution (Table 2.3) overnight with medium agitation in a cold room (4°C). The next day, the sections were returned to RT and the primary antibody/lectin solution was removed. Then, the sections were washed 3 x PBS 0.1 M for 10 minutes per wash on the shaker. Following this washing step, the PBS 0.1M was removed from the sections and the fluorescent secondary antibodies and avidin were diluted in the blocking solution (Table 2.4) and added to the sections (300 µl in each well). The sections were incubated with the secondary antibody/avidin solution for 3 hours at RT in the dark with medium agitation. The secondary antibody/avidin solution was then carefully removed from the sections, and they were washed twice with PBS 0.1M for 10 minutes on the shaker. Following the two PBS washes, a solution of PBS 0.1M containing Hoechst (1:5,000, Sigma-Aldrich, D9542) was added (300 µl in each well) and incubated in the dark for 10 minutes for all nuclei staining. This Hoechst solution was then removed, and the sections were washed 1 x PBS 0.1M for 10 minutes. Sections were mounted onto gelatine-subbed microscope slides according to an anterior-to-posterior axis order and left to dry for 5 mins before being cover-slipped using Fluoromount-G (Invitrogen, 15586276) mounting media. Imaging was performed using the Leica SP8 DLS confocal microscope or the Zeiss Axio Imager apotome 2.

The same procedures including 30% sucrose PBS storing and sectioning were applied for the ACC slices (450 µm) previously used in the *in vitro* electrophysiology experiments. The 450 µm ACC slices were re-sectioned into 40 µm sections using a freezing stage microtome and the same procedure of free-floating IHC followed.

Target	Host	Concentration	Vendor	Serum used
Parvalbumin (PV)	Mouse	1:500	Merck (SAB4200545)	Donkey 5%
Nacetylgalactosamine sugar (PNNs)	Biotinylated Wisteria Floribunda Lectin (WFA)	1:500	Vector Laboratories (B-1355-2)	Donkey 5%
GFAP (reactive astrocytes)	Rabbit	1:2,000	Dako (Z0334)	Donkey 5%
Iba-1 (microglia)	Goat	1:1,000	Abcam (ab5076)	Donkey 5%
iNOS (nitric oxide synthase) a marker of reactive microglia	Rabbit	1:200	Abcam (ab3083470)	Donkey 5%
c-Fos (nuclear phosphoprotein) a marker of neuronal activity	Rabbit	1:500	Abcam (ab222699)	Donkey 5%
α-synuclein (human)	Rat	4:500	Enzo (ALX-804-258-LC05)	Donkey 5%

Table 2.3. List of primary antibodies and lectin used in this thesis. Detailed description of antibody and lectin name and target, host, concentration, vendor (reference number) and the serum used for each.

Target	Concentration	Vendor	Serum used
Donkey anti-mouse IgG Alexa Fluor 568	1:500	Invitrogen (A10037)	Donkey 5%
Donkey anti-mouse IgG Alexa Fluor 647	1:500	Invitrogen (A10037)	Donkey 5%
Streptavidin, fluorescein	1:100	Vector Laboratories (SA-5001-1)	Donkey 5%
Donkey anti-rabbit IgG Alexa Fluor 568	1:500	Invitrogen (A10042)	Donkey 5%
Donkey anti-goat IgG Alexa Fluor 488	1:500	Invitrogen (A11055)	Donkey 5%
Donkey anti-rat IgG Alexa Fluor 647	1:500	Invitrogen (A48272)	Donkey 5%

Table 2.4. List of secondary antibodies and streptavidin used in this thesis. Detailed description of antibody and avidin target, concentration, vendor (reference number) and serum used for each.

2.3.3. *Data acquisition*

The sections from the IHC experiments were mainly imaged using the Leica SP8 DLS confocal microscope. The microscope settings used for all images include the lasers OP SL 552, OP SL 488, Diode 638 and Diode 405 depending on the secondary antibody/avidin combinations. Additionally, the magnification of 20x and zoom at 2, equal to 40x, was used for all images. Three sections per animal and one hemisphere of ACC from Paxinos and Franklin mouse atlas plates ranging from plates 21 - 30 were imaged with the method of 3 z-stack boxes as shown in Figure 2.4. I selected 3 regions of interest (ROIs) to image including ROIs 1 and 3 covering the superficial layers of the ACC, and ROI 2 covering the deep layers of the ACC.

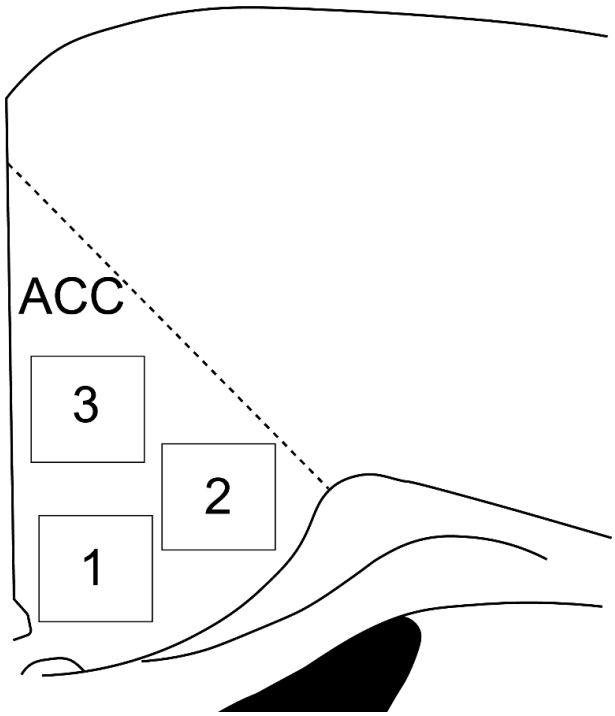

Figure 2.4. Imaging method of the ACC. Three 3 z-stack boxes of 40x magnification were imaged under the confocal microscope. The z-stack locations were ROIs 1, 2 and 3 to capture the superficial and the deep ACC.

2.3.4. *IHC Data analysis*

Densitometric analysis was performed using either FIJI (Image J) version 2.14.0 or Imaris version 9.8.2 software, depending on the research questions for each IHC experiment.

Analysis using FIJI software

For the results shown in Chapter 3, the data were analysed using FIJI to investigate the % area and intensity of PV and PNN expression as well as the % area and count of c-Fos expression in the ACC. The channels PV, PNN and c-Fos were pseudo-coloured as red, cyan, and green respectively to help with analysis. FIJI software was also used in Results Chapter 6 to examine the % area and intensity of the expression of GFAP+ astrocytes and Iba-1+ microglia as well as the % area of iNOS expression and its co-localisation with Iba-1+ microglia.

For all analyses, brightness, and contrast (B and C) as well as threshold values were calibrated and averaged for each channel. The z-stack images were first collapsed in 2D and transformed into 8-bit. The image processing started by applying the average B and C values for each channel and then the background noise was removed in each image. For the background noise removal, the background was subtracted, and the median filter was applied. Then, the average threshold values for each channel were applied using the default threshold option and further noise was removed using de-speckle. Finally, the particle analysis was performed by adjusting the size, and circularity according to the particles of interest for each staining and an outline image was provided. The results included both the % area and intensity (referred to as mean on FIJI) measurements for the analysis of PV, PNN, c-Fos, Iba-1 and GFAP expression. Additionally, for the c-Fos analysis, following the threshold process, the image was converted to a mask to apply the overlay mask option in the particle analysis for accurate counting.

Analysis using Imaris software

Imaris software, which allows for a three-dimensional (3D) detailed analysis, was used in Results Chapter 5. The aim was to investigate the interactions between PV interneurons, PNNs and hα-syn in the ACC in 3D for a detailed co-localisation analysis. The channels PV and PNN were pseudo-coloured for better demonstration and analysis purposes as green and cyan, respectively. The B and C, and threshold values were averaged across all sections in young and aged animals for each channel and were the same for all images in each age group. Additionally, the PNN channel in young animals and PV and PNN channels in aged animals have undergone background subtraction before the mask generation. After creating masks for each channel, the count, volume, and intensity were analysed according to each variable.

2.4. Statistical analysis

All statistical analyses were performed using GraphPad Prism software (USA, version 10.1.2.234). Significance was determined as * for $p < 0.05$, ** for $p < 0.01$ and *** for $p < 0.001$. The sample sizes for animals (N) and slices/sections (n) are presented in text and figure legends. Similar approaches were used for both the *in vitro* electrophysiology and IHC data.

Data normality was examined using the Shapiro-Wilk test and if data were found to be normally (Gaussian) distributed, then parametric tests were performed. However, if the data were not normally distributed, non-parametric tests were applied. Parametric data were plotted in bar charts presenting the standard error of the mean (SEM) whereas non-parametric data was plotted in boxplots presenting the median and interquartile range (IQR, Q1 – Q3). Individual values in the plots are represented in black dots.

Unpaired t-tests were performed for parametric data and the comparison of two samples independent of each other. The Mann-Whitney test was applied to non-parametric data as an unpaired t-test alternative. For the comparison of the effect of two independent variables on one dependent variable, a two-way ANOVA (mixed models) test was used for parametric data. If data showed significance ($p < 0.05$), multiple comparisons were performed for post hoc examinations using the Holm-Sidak test or Fisher's LSD test. Non-parametric data were transformed into a logarithmic scale which allowed for normal distribution and the application of a two-way ANOVA (mixed models) test. The log transformation of data was performed on base 10 using two methods: 1) $\log_{10}(x)$ or 2) $\log_{10}(x+1)$. The log transformation using method 2 was applied to data with 0s.

Chapter 3. Neuronal network activity and neuroinflammation markers under control and pathological conditions in the ACC of young WT mice.

3.1. Introduction

The ACC plays an important role in cognitive, motor, and emotional functions. Evidence from fMRI studies showed that the ACC and other brain areas including the insular cortex, secondary somatosensory cortex, nuclei in the tegmentum, and hypothalamus are involved in the integration of internal and external stimuli to control attention. The ACC contributes to controlling the expression of emotional states (Cera *et al.*, 2019). Cognitive functions involving the ACC are impaired in neurodegenerative disorders including AD and PD and it is one of the earliest brain regions affected by Aβ deposits accumulating from an early stage in AD patients (Braak and Braak, 1991; Zhou *et al.*, 2012). Additionally, PD post-mortem tissue investigations showed high LB density in the ACC of patients correlating with cognitive decline (Kövari *et al.*, 2003). In PD, the ACC is affected early by the α-syn pathology leading to personality changes and impaired cognitive functioning (Braak et al., 2000).

As outlined in Introduction, fine-tuning between excitation and inhibition is required in the neural networks of the ACC. Impaired E/I balance leads to excess excitation, also termed hyperexcitability, and contributes to seizure activity observed in DLB, PD, AD patients, and mouse models (Palop and Mucke, 2010; Caviness *et al.*, 2011; Busche *et al.*, 2015; Morris *et al.*, 2015). Hyperexcitability is observed as abnormal poly-spikes in the EEG and, in some cases, there was full seizure activity in AD (Palop and Mucke, 2010) and DLB (Morris *et al.*, 2015) patients. Numerous cortical brain areas are hyperexcitable in AD (Palop and Mucke, 2010; Bonanni *et al.*, 2016), DLB (Bonanni *et al.*, 2016) and PD (Rodriguez-Oroz *et al.*, 2009; Helmich *et al.*, 2012) including the hippocampus, basal ganglia, and entorhinal cortex (Bonanni *et al.*, 2008).

Hyperexcitability in the PFC, particularly the ACC, has been underexplored in neurodegeneration. As a higher cognitive area, the ACC connects with regions commonly affected by neurodegeneration, such as the hippocampus, amygdala, thalamus, and basal ganglia (Öngür and Price, 2000; Summerfield *et al.*, 2005; Haber and Knutson, 2009; Fanselow and Dong, 2010; Etkin *et al.*, 2011; Deture and Dickson, 2019; Nikolenko *et al.*, 2020; Rao *et al.*, 2022). In rodents, pyramidal neurons in layers (L) 2/3 and 5 drive projections to cortical and subcortical areas, with L5 crucial for output (Gabbott *et al.*, 2005). PV, SST, and VIP (vasoactive intestinal peptide)-

expressing interneurons in L2/3 and L5 regulate the E/I balance of these pyramidal neurons (Pan *et al.*, 2016; Johnson *et al.*, 2020; Rupert and Shea, 2022). Inputs to the ACC include projections to L1 from the thalamus and cortical association areas synapsing on the apical dendrites of pyramidal neurons (Hoover and Vertes, 2007; Anastasiades *et al.*, 2020; Leow *et al.*, 2022; Xue *et al.*, 2022), L2/3 receives inputs from other PFC regions (Zingg *et al.*, 2014), and L5 inputs from the amygdala (Shi *et al.*, 2022; Becker *et al.*, 2023). The thalamus also sends signals to L6, modulating feedback to deep brain areas (Gabbott *et al.*, 2005). Therefore, the ACC may be indirectly involved in pathology through this highly interconnected network, but future studies need to address this in more detail.

Hyperactivity has been widely studied in the hippocampus and other cortical regions, but its occurrence in the ACC remains largely unexplored (Myers *et al.*, 2018; Codadu *et al.*, 2019; Codadu, Parrish and Trevelyan, 2019). In humans, epilepsy affecting the cingulate cortex (area 24) is linked to cognitive impairment and psychiatric conditions such as obsessive-compulsive disorder (Levin and Duchowny, 1991; Bancaud and Talairach, 1992; Guarnieri *et al.*, 2005). *In vitro* studies in rats have shown that 4-AP induces hyperactivity in the ACC, generating IIDs through glutamatergic and $GABA_A$ receptor ($GABA_A$-R) activation, with IIDs appearing rapidly before the onset of ictal activity (Panuccio *et al.*, 2009). However, whether hyperactivity, including IIDs and seizure-like activity, occurs in the ACC of mice has not been investigated. Therefore, this chapter aims to determine whether the ACC in WT mice generates ictal discharges and/or IIDs and to characterise this activity. This is required before we can assess hyperexcitability in the A30P mice.

One potential mechanism underlying the hyperexcitability is neuroinflammation. To explore this, we assessed whether abnormal excitation in the ACC could drive an inflammatory response. The bidirectional relationship between microglia and astrocytes amplify the release of pro-inflammatory toxic cytokines, potentially contributing to hyperexcitability (Kempuraj *et al.*, 2016; Russo and McGavern, 2016; Kwon and Koh, 2020). These glial cells play a crucial role in maintaining neurotransmission homeostasis, and their activation disrupts neurotransmitter systems. Impaired glutamate clearance and potassium buffering by glial cells lead to elevated extracellular glutamate levels, which are involved in neuronal hyperexcitability (Lobsiger and Cleveland, 2007; Vargas *et al.*, 2008; Heneka *et al.*,

2015; Colombo and Farina, 2016; Liddelow *et al.*, 2017). The ACC is particularly responsive to painful stimuli, and neuroinflammation linked to activated microglia and astrocytes in this region has been mostly investigated in studies focusing on chronic neuropathic pain and pain-evoked aversive memory in rodents (Li *et al.*, 2022; Iqbal *et al.*, 2023a). However, no studies to date have specifically investigated glial cell activation associated with hyperexcitability in the ACC.

This chapter investigates whether the ACC in mice exhibits hyperexcitability, including seizure-like activity, as previously observed in the rat ACC (Panuccio *et al.*, 2009) and mouse hippocampus (Myers *et al.*, 2018; Codadu *et al.*, 2019; Codadu, Parrish and Trevelyan, 2019). Using *in vitro* ACC slices from young WT mice, pre-ictal IIDs and seizure-like events (ictal events) were examined following 4-AP application. The study also assessed PV interneuron and PNN expression to explore changes related to E/I imbalance. c-Fos protein expression was analysed, as its upregulation in neuronal nuclei has been linked to seizure activity in brain regions including the mPFC and cingulate cortex in rodents (Morgan *et al.*, 1987; Yang *et al.*, 2019; Akdağ *et al.*, 2023). Additionally, glial responses, including microglia and reactive astrocytes, were studied to assess neuroinflammation under these hyperexcitable conditions. This chapter provides a foundational understanding of ACC network activity under induced epileptic conditions before extending the investigation to the A30P transgenic mouse model.

3.2. Aims

- To investigate the species-specific induction of hyperexcitability including seizure-like events following 4-AP in the mouse ACC as previously shown in the rat ACC.

- Determine whether increased excitability affected inhibitory interneurons and PNNs.

- Determine whether there is glial cell activation following 4-AP-induced hyperexcitability in the ACC of young WT animals.

3.3. Methods

3.3.1. *In vitro Electrophysiology*

The acute slice preparation for *in vitro* electrophysiology experiments followed the protocol outlined in Chapter 2.2.1. ACC slices were obtained from young WT mice (2 - 4 months old, N = 5: 4 males, 1 female), and slice maintenance followed the protocol in Chapter 2.2.2. Baseline LFP recordings (10 minutes) were taken from the deep ACC layers of each hemisphere in two rigs. In one rig, 4-AP (75 µM) was added to the circulating ACSF and remained throughout the experiment. The other rig contained a separate set of slices with the corresponding ACC hemispheres exposed only to ACSF (control slices). There were in total n = 5 control and n = 5 4-AP ACC slices in these experiments, with the placement of slices alternated between rigs on subsequent experimental days. LFP recordings were taken every 30 minutes during the 3-hour incubation in 4-AP or ACSF to monitor neuronal network activity. The 3-hour 4-AP incubation ensured sufficient time for measurable network activity and protein expression changes. Following the experiment, slices from both conditions were fixed with PFA for IHC experiments to investigate protein expression changes.

The baseline activity and the recordings following 4-AP or ACSF incubation were acquired and analysed using the AxoGraph software according to Chapters 2.2.3 and 2.2.4, respectively. For the analysis, the hyperexcitable events were counted and categorised as simple IIDs (consisting of one population spike event), complex IIDs (consisting of two or more population spike events). Hyperexcitable events longer than 5 seconds were categorised as seizure-like events (Fig. 2.3). The average seizure-like event duration was also measured.

3.3.2. *Free-floating IHC-Immunofluorescence*

Following slice fixation with PFA, the ACSF-exposed and 4-AP-exposed ACC slices were re-sectioned and stained with different antibody and lectin-avidin combinations following the protocol in Chapter 2.3.2. The aim was to examine microglia and reactive astrocytes as well as PV inhibitory interneurons, PNNs, and c-Fos protein as a neuronal activity marker. One set of WT ACSF and 4-AP sections

was immunolabelled with the primary-secondary antibody/lectin-avidin combination 1 and the other set of sections was stained with combination 2 (Table 3.1). The ACC sections were then imaged under the Leica SP8 DLS confocal microscope at 40x magnification (20x magnification and zoom at 2) following the 3-z-stack-box method in Chapter 2.3.3 (Fig. 2.4). FIJI densitometric analysis was performed according to Chapter 2.3.4. Astrocytes around blood vessels were excluded from the analysis.

Staining Combination 1	
Primary Antibody/Lectin	**Secondary Antibody/Avidin**
Mouse anti-PV	Donkey anti-mouse Alexa Fluor 647
Biotinylated WFA lectin	Streptavidin fluorescein (498)
Rabbit anti-c-Fos	Donkey anti-rabbit Alexa Fluor 568
Staining Combination 2	
Goat anti-Iba-1	Donkey anti-goat Alexa Fluor 488
Rabbit anti-GFAP	Donkey anti-rabbit Alexa Fluor 568

Table 3.1. IHC staining combinations used on the ACSF and 4-AP ACC sections following the *in vitro* electrophysiology experiments.

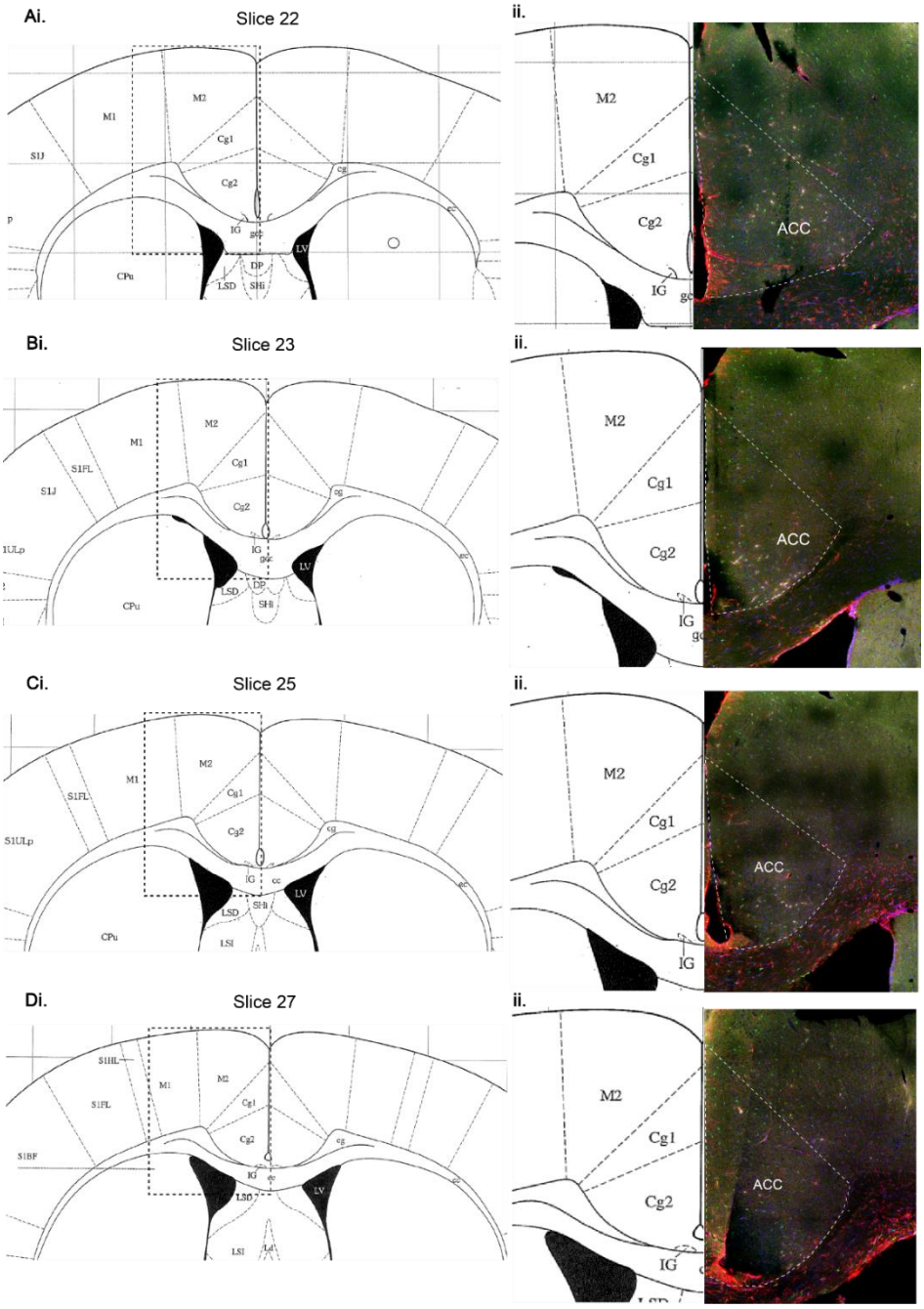

Figure 3.1. Different ACC slices across the anterior-to-posterior axis and optimisation of microglia and astrocyte staining. Optimisation staining was performed before the staining of fixed slices from the electrophysiology experiments to confirm successful microglia and astrocyte labelling in the mouse ACC. The ACC sections selected for IHC were within the range of plates 21 - 30 based on the numbering system given by Paxinos and Franklin mouse atlas, 2001 (Cingulate-Cg 1 and 2 refer to ACC). All sections were stained with Iba-1 (green) and GFAP (red) to investigate microglia and reactive astrocytes, respectively in the ACC in different locations. **Ai.** Sections 22, interaural 4.90 mm, bregma 1.10 mm. **Bi.** Section 23, interaural 4.78 mm, bregma 0.98 mm. **Ci.** Section 25, interaural 4.54 mm, bregma 0.74 mm. **Di.** Section 27, interaural 4.30 mm, bregma 0.50 mm. **Aii – Dii.** Enlarged view of squared areas and respective ACC section stained with Iba-1 (green), GFAP (red) and Hoechst stain for nuclei (blue).

3.4. Results

3.4.1. *4-AP evoked Hyperexcitability in the ACC of young WT animals.*

I first wanted to determine whether the ACC in young WT mice shows epileptic-like activity similar to that seen in the mouse hippocampus and rat ACC, before assessing this in the young A30P mice.

Simple and Complex IIDs in the ACC following 4-AP application

During the baseline recordings before the 4-AP application, no hyperexcitable events of any type were seen. Following the application of 75 µM 4-AP both simple and complex IIDs were observed. The median time to onset of the first simple IID and complex IID was 10.68 minutes (-2.19, 33.44) and 15.17 minutes (2.94, 35.27) in 4-AP, respectively (N = 5 mice, n = 5 slices). Network activity was recorded following 4-AP application for 3 hours and compared to the slices bathed only in ACSF which did not demonstrate such events (Fig. 3.2D). In the presence of 4-AP, there was a trend towards an increase in the total count of simple IIDs over the 3-hour recording, but this did not reach statistical significance (Fig. 3.2Di, ACSF 0 (0,0) vs 4-AP 2 (-3.57,11.97), $p > 0.05$, Mann-Whitney, N = 5, n = 5 ACSF slices, n = 5 4-AP slices). The 4-AP-exposed slices had a total of 21 simple IIDs while the ACSF-exposed slices had 0 simple IIDs. There was, however, a statistically significant increase in the total count of complex IIDs in the 4-AP-exposed slices with 61 IIDs in total compared to the ACSF-exposed ACC slices which had 0 complex IIDs (Fig. 3.2Dii, median ACSF 0 vs 4-AP 2, $p < 0.01$, Mann-Whitney, N = 5, n = 5 ACSF slices, n = 5 4-AP slices).

These results demonstrated that as reported in the rat ACC (Ren *et al.*, 2018), the mouse ACC also evokes a range of IID activity in response to 4-AP application *in vitro*.

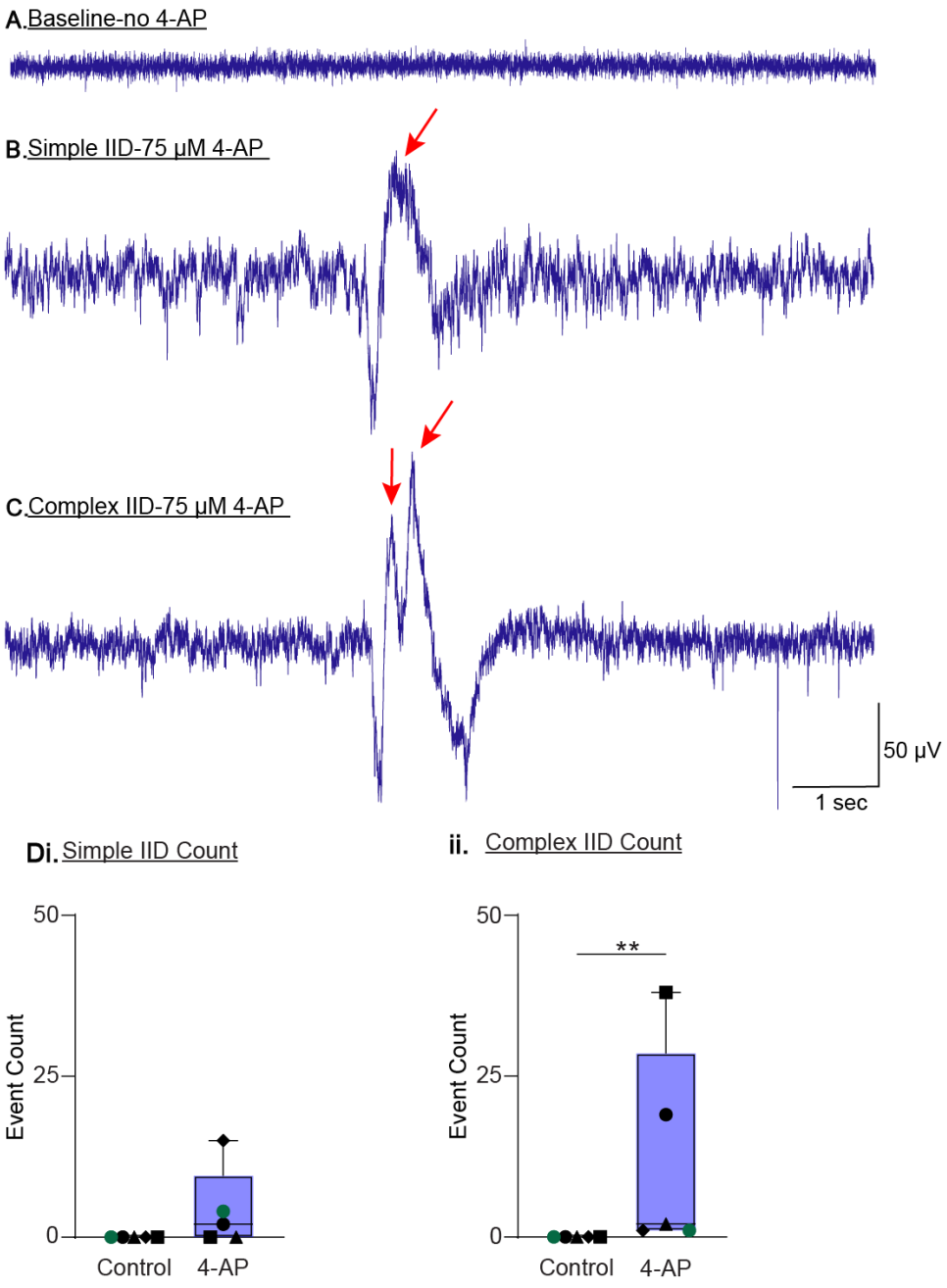

Figure 3.2. Simple and Complex types of IID activity in the ACC of young WT mice. A. Example of a baseline trace from extracellular LFP activity recorded before 4-AP application. **B – C.** Example traces of LFP activity recorded from a 4-AP slice demonstrating a (**B**) simple IID and (**C**) complex IID event 30 minutes post 75 µM 4-AP application. The red arrows point to (**B**) the single population spike event comprising a simple IID and (**C**) the two population spike events comprising a complex IID. **D.** The count of (**i**) simple IIDs and (**ii**) complex IIDs over the 3-hour recording for both the ACSF control (grey) and 4-AP (blue) slices. Data points represent median values from WT male mice (black) and from a WT female mouse (green) and each symbol refers to a different mouse.

Seizure-like events in the ACC following 4-AP application

The total count of seizure-like events recorded in the ACC in both the ACSF- and 4-AP-exposed slices throughout the 3-hour experiment was analysed. The median time to onset of the first seizure-like events was 15.5 minutes (3.38, 35.5) following 4-AP application (N = 5, n = 5 4-AP slices). As outlined above no hyperexcitable activity was recorded in slices incubated only in the ACSF (Fig. 3.3A). There was a statistically significant increase in the total count of seizure-like events in the 4-AP slices over the 3-hour experiment compared to the ACSF slices, which had none (Fig. 3.3Bi, median ACSF 0 vs 4-AP 65, $p < 0.05$, Mann-Whitney, N = 5, n = 5 ASFC slices, n = 5 4-AP slices). The median count in 10-minute bins of seizure-like events recorded across all slices during the 3-hour 4-AP experiment was further analysed over time. Seizure activity began around 15 minutes post-4-AP application and progressively increased from 30 to 50 minutes before slightly decreasing after 60 minutes of incubation (Fig. 3.3Bii). The median count of seizure-like events in the 4-AP-exposed slices over the 3-hour recording period was 2.62 (SD = 1.34, SEM = 0.30), compared to 0 in the ACSF-exposed slices.

A statistically significant increase was shown for the median duration of seizure-like events in the ACC of slices in 4-AP compared to the ACSF slices which had no seizure activity (Fig. 3.3Ci, ACSF 0 vs 4-AP 7.37, $p < 0.05$, Mann-Whitney, N = 5, n = 5 ASFC slices, n = 5 4-AP slices). The median duration in 10-minute bins of all seizure-like events recorded in ACSF and 4-AP was analysed over the 3 hours. No activity was observed during the first 10 minutes following the 4-AP application. Seizure-like events began at around 15 minutes and steadily increased in duration until 40 minutes (Fig. 3.3Cii). Thereafter, both the event count and duration stabilised, followed by a slight decrease during the final 30 minutes.

Overall, these findings indicate that the ACC generates IID and seizure-like activity at least in male mice *in vitro,* similar to that reported in other brain regions in mice. Hyperexcitability in the ACC of 2-4-month-old WT mice induced by 4-AP was presented in simple and complex frequent short bursts as well as seizures lasting longer than 5 seconds.

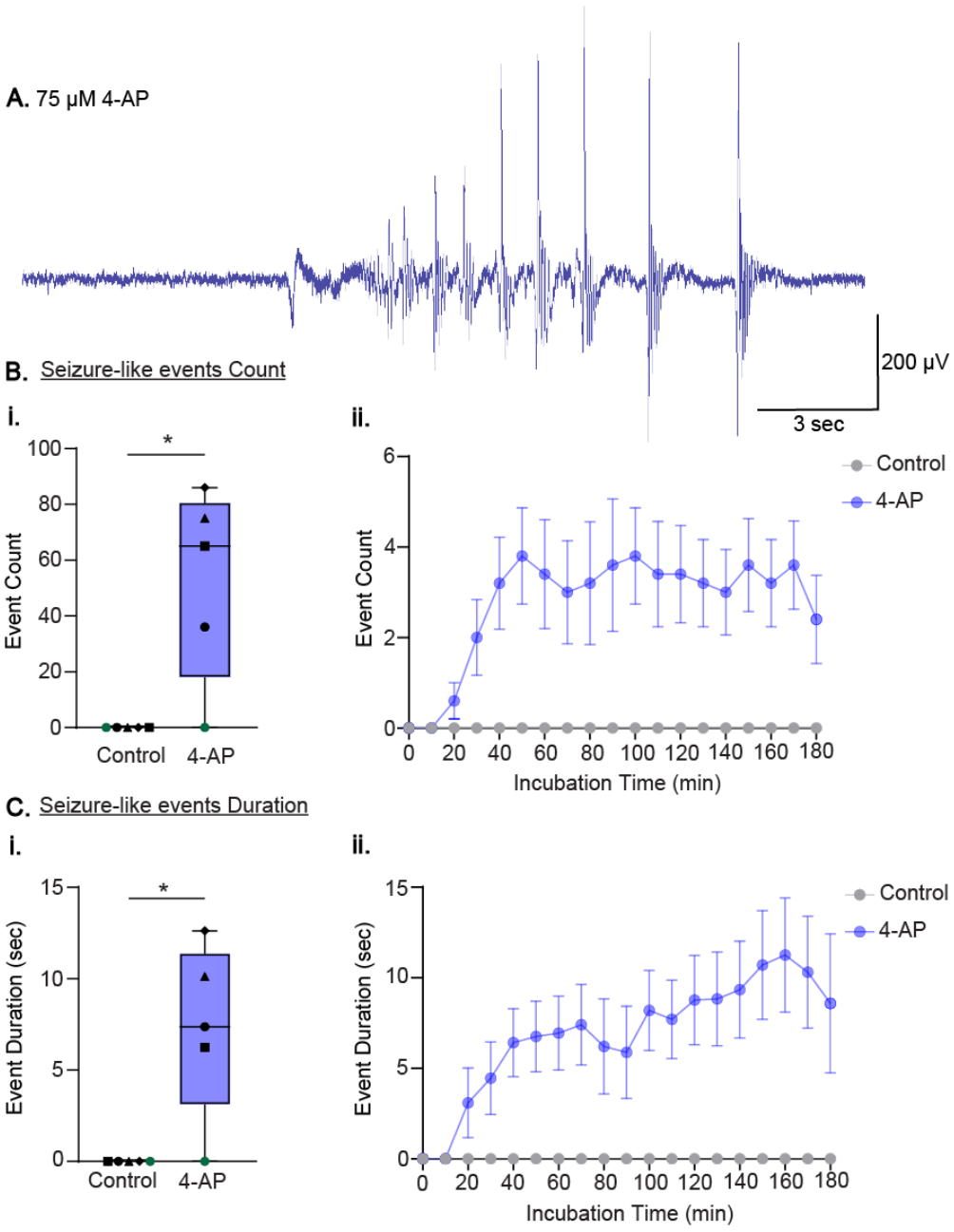

Figure 3.3. Seizure-like events recorded in the ACC of young WT mice following 4-AP application. A. Example of extracellular LFP activity trace recorded from the ACC showing an example 4-AP-induced seizure-like event with multiple population spikes lasting longer than 5 seconds after 30 minutes in 4-AP. **Bi.** The total count over the 3-hour recording of seizure-like events is shown for the ACSF control (grey) and 4-AP (blue) slices. Data points represent median values from WT male mice (black) and from a WT female mouse (green) and each symbol refers to a different mouse. **Bii.** The median count in 10-minute bins of all seizure-like events from all slices is shown over the 3 hours for each time point. **Ci.** The median duration of all seizure-like events over the 3-hour recording in the ACSF control and 4-AP slices is demonstrated. **Cii.** Group data plot showing the median duration in 10-minute bins of all events recorded during each time point.

3.4.2. *Increased PV expression following 4-AP-induced hyperexcitability in the ACC of young WT mice.*

PV interneurons are involved in 4-AP-induced neuronal network hyperexcitability (Shiri *et al.*, 2015; Yekhlef *et al.*, 2015; Chang *et al.*, 2018; Codadu *et al.*, 2019). We thus investigated potential differences in the expression of PV interneurons and PNNs between all ACSF- and 4-AP-incubated sections from young WT mice. PV expression was evident in the soma, processes and as punctate labelling at synaptic terminals of PV interneurons along with WFA+ PNN expression in the ACC in both conditions (Fig. 3.4, PV in red, PNNs in cyan). A detailed quantification of PV neuronal somas and PNNs in the ACC was performed and will be discussed in Chapter 5.

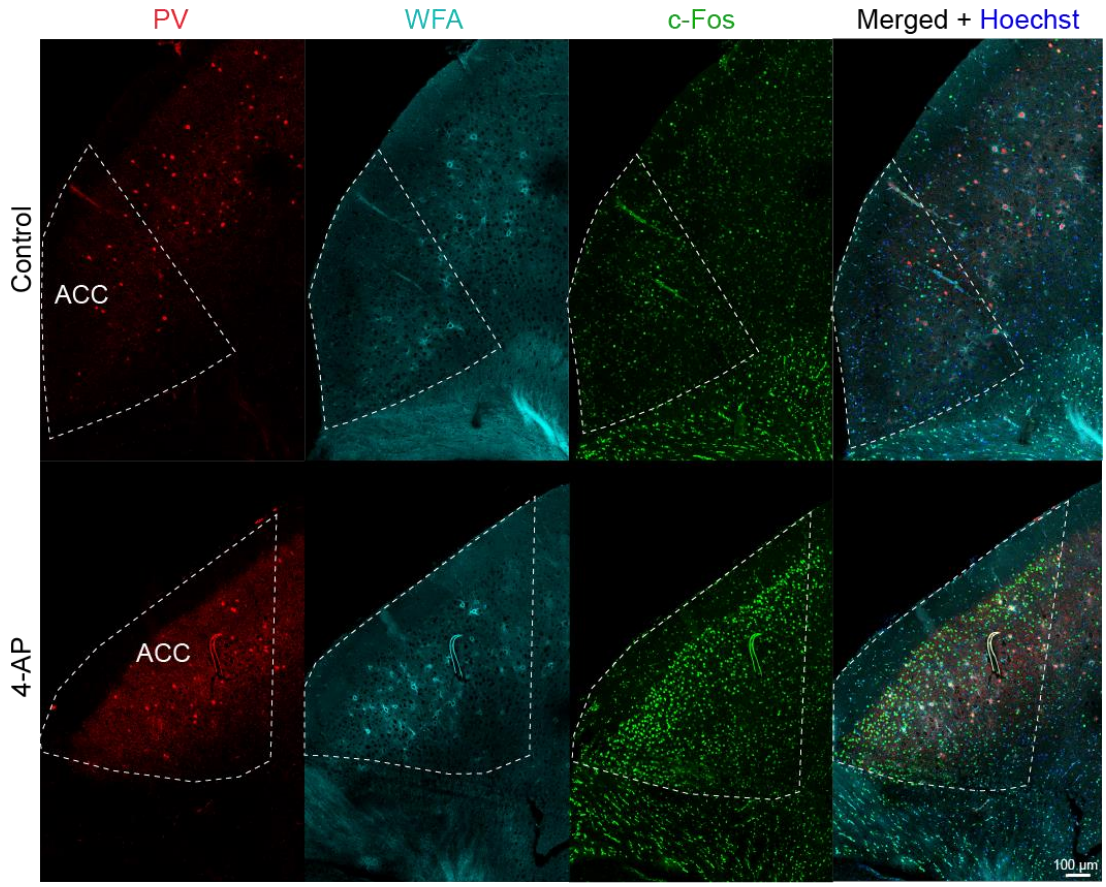

Figure 3.4. Expression of PV interneurons, PNNs and c-Fos in the ACC of ACSF and 4-AP sections in young WT mice. PV neuronal somas and processes are stained in red, WFA+ PNNs in cyan, c-Fos in green, and all Hoechst+ nuclei in blue in the ACC of ACSF (control) and 4-AP sections. Scale bar at 100 µm.

Results indicated a statistically significant increase in the median % area of PV expression in the ACC of 4-AP sections compared to ACSF sections (Fig. 3.5Bi, ACSF 0.98% (-0.27, 3.67) vs 4-AP 10.20% (2.73, 19.78), $p < 0.05$, Mann-Whitney, N = 5, n = 6 ACSF sections, n = 8 4-AP sections). A significant increase in intensity levels of PV expression was also shown in the 4-AP sections (Fig. 3.5Bii, ACSF 137.1 a.u. (134.4, 141) vs 4-AP 147.7 a.u. (142, 150.1), $p < 0.01$, Mann-Whitney, N = 5, n = 6 ACSF sections, n = 8 4-AP sections). The increase in PV expression was noted in the somas, dendrites, and synaptic terminals of ACC sections in the 4-AP-exposed slices compared to controls, highlighting the enhanced PV expression due to increased activity evoked by 4-AP. However, we found no significant differences between the median count of PV neuronal somas between the 4-AP and ACSF sections (ACSF 10.67 (1.81, 15.64) vs 4-AP 6.67 (3.02, 11.89), $p < 0.05$, Mann-Whitney, N = 5, n = 6 ACSF sections, n = 8 4-AP sections).

Some PV somas were surrounded by PNNs, but there were also PV somas not surrounded by any PNNs (Fig. 3.5A, enlarged view). Details of PV/PNN proportion are detailed in Chapter 5. No statistically significant differences were shown in the median % area and intensity of WFA+ PNN expression in the ACC between the two conditions (Fig. 3.5Ci and ii, % area: ACSF 0.02% (-0.03, 0.16) vs 4-AP 0.05% (0, 0.29), intensity: ACSF 64.50 a.u. (37.99, 77.64) vs 4-AP 63.96 a.u. (45.84, 72.32), $p > 0.05$, Mann-Whitney, N = 5, n = 6 ACSF sections, n = 8 4-AP sections).

To investigate the impact of the increased activity outlined above, a global measure of c-Fos was analysed across all cell types which is an indirect activity marker (Fig.3.4 and 3.5, c-Fos in green). A trend toward increased median % area and count of c-Fos expression was observed in the 4-AP sections relative to ACSF sections (Fig. 3.5Di and ii, % area: ACSF 0.92% (-0.03, 2.27) vs 4-AP 1.96% (0.19, 5.06), count: ACSF 23.50 (0.09, 62.36) vs 4-AP 48 (10.35, 96.86), $p > 0.05$, Mann-Whitney, N = 5, n = 6 ACSF sections, n = 8 4-AP sections).

Overall, these findings suggest that 4-AP evoked hyperexcitability in the ACC of young WT mice leading to significantly increased PV expression.

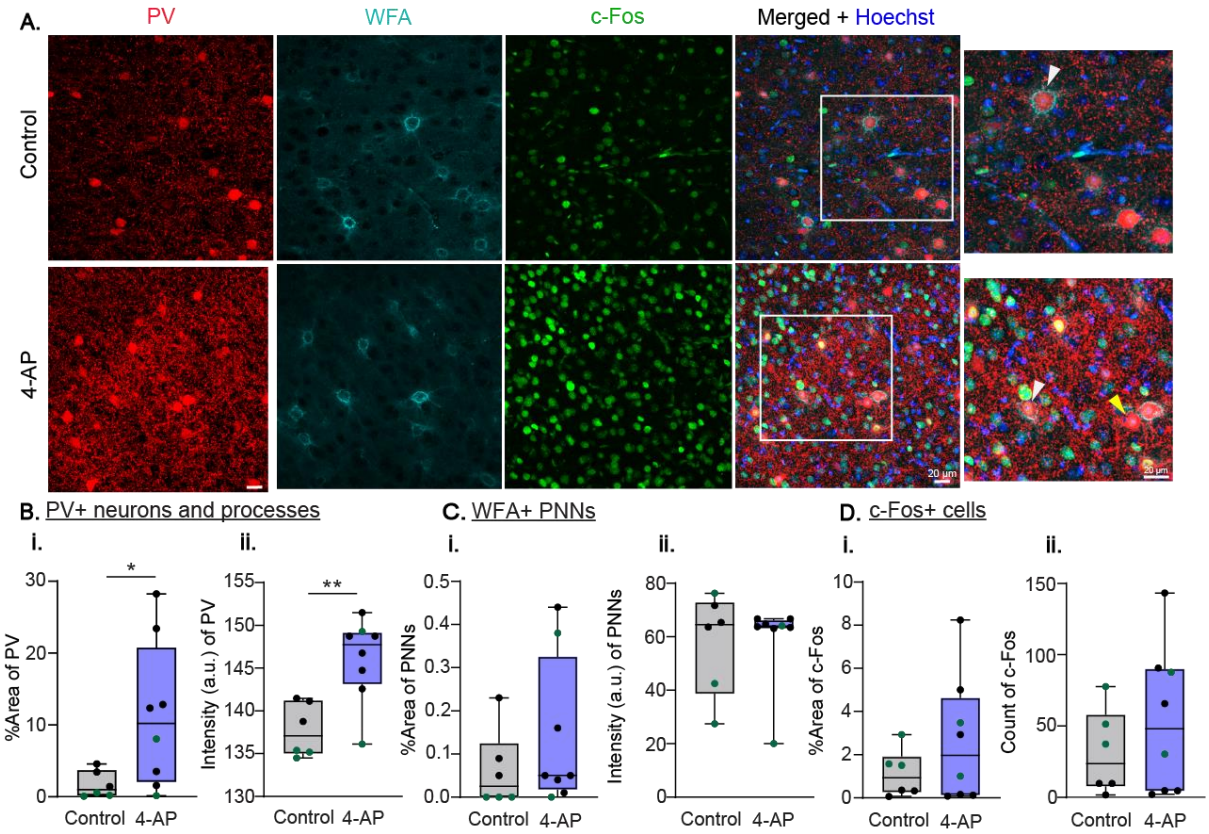

Figure 3.5. PV interneurons, PNNs and c-Fos in the ACC of ACSF and 4-AP sections from young WT mice. These are collapsed z-stack image examples (maximum projection) of 40x magnification taken from the superficial ACC layers. **A.** The expression of PV including neuronal somas and processes (red), WFA+ PNNs (cyan), c-Fos+ cells (green) and all nuclei (Hoechst, blue) in the ACC of ACSF (control) and 4-AP sections. The arrowheads in the enlarged view of the merged images show some PV somas surrounded by PNNs (white arrows) and not surrounded by PNNs (yellow arrows). **B - D.** The median (**i**) % area and (**ii**) intensity (a.u.; arbitrary units) or count of (**B**) PV, (**C**) PNN and (**D**) c-Fos expression are shown for the ACC in control (grey) and 4-AP (blue) sections are shown. Each data point represents the median value per ACC section, with male mice in black and female mice in green.

3.4.3. *No changes in the expression of neuroinflammatory markers induced by 4-AP in the ACC of young WT mice.*

Neuroinflammation in the ACC under induced 4-AP epileptic conditions *in vitro* in 2-4-month-old WT mice was then investigated in all incubated slices. The expression of microglia in the ACC sections from the young WT mice was confirmed using the pan-macrophage marker Iba-1 (Waller *et al.*, 2019) (Fig. 3.6, Iba-1+ microglia in green). Also, the expression of GFAP confirmed the presence of reactive astrocytes in the ACC (Yang and Wang, 2015) (Fig. 3.6, astrocytes in red).

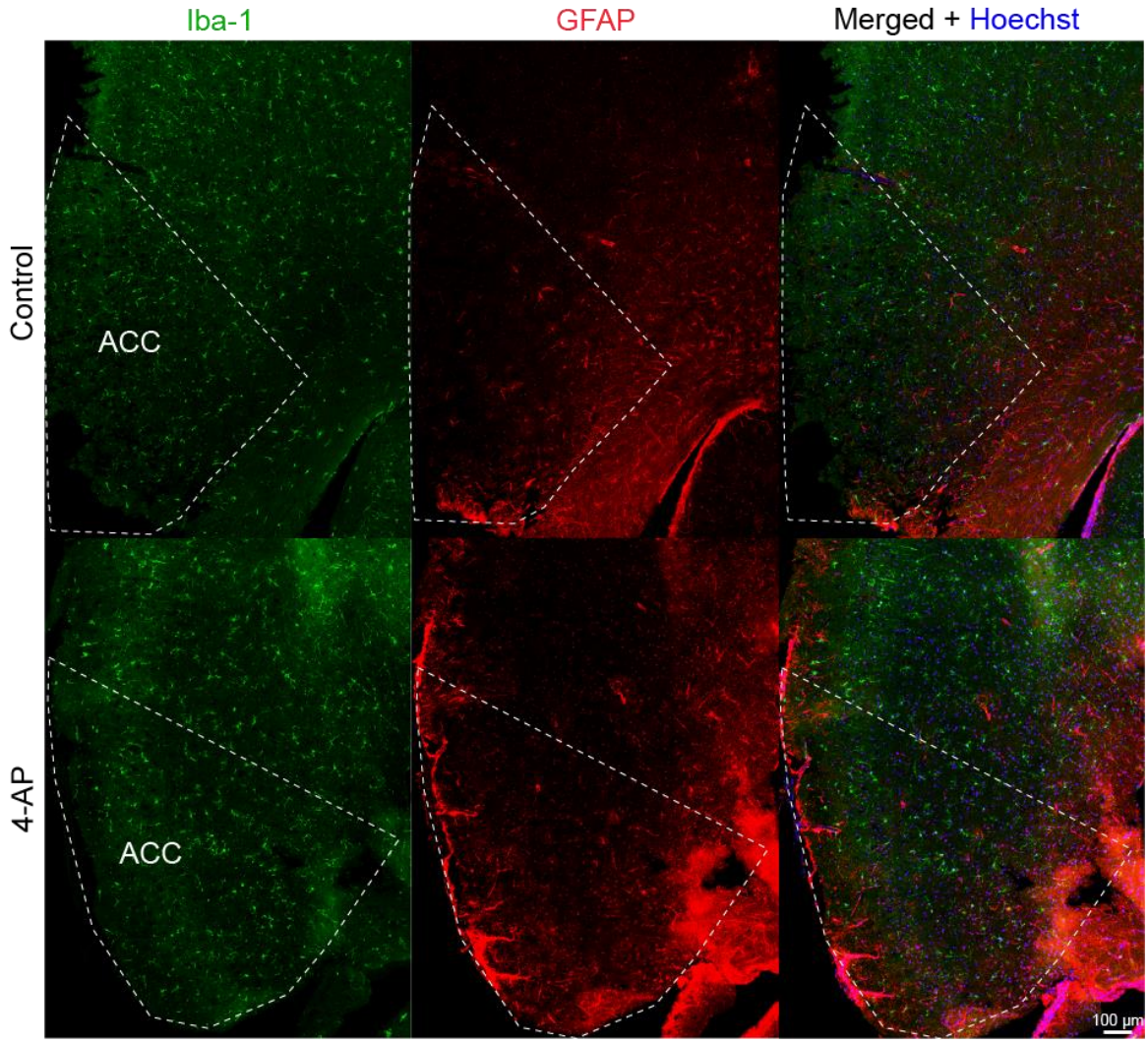

Figure 3.6. Expression of microglia and reactive astrocytes in the ACC of control and 4-AP sections in young WT mice. All Iba-1+ structures, including microglia, are shown in green, GFAP+ astrocytes in red, and all Hoechst+ nuclei in blue in the ACC of ACSF (control) and 4-AP sections. Scale bar at 100 µm.

No statistically significant differences were found in the median % area or intensity of Iba-1 between the ACSF and 4-AP sections (Fig. 3.7Bi and ii, % area: ACSF 0.71% (0.38, 1.13) vs 4-AP 0.77% (0.44, 1.05), intensity: ACSF 130.2 a.u. (124.2, 135.4) vs 4-AP 128.2 a.u. (92.29, 145), $p > 0.05$, Mann-Whitney, N = 5, n = 6 ACSF sections, n = 8 4-AP sections).

Similarly, no statistically significant differences were shown for the median % area and intensity of GFAP expression (Fig. 3.7Ci and ii, % area: ACSF 0.47% (0.08, 1.31) vs 4-AP 0.62% (0.37, 0.80), intensity: ACSF 113.2 a.u. (111.2, 115.1) vs 4-AP 112.3 a.u. (109.9, 114.2), $p > 0.05$, Mann-Whitney, N = 5, n = 6 ACSF sections, n = 8 4-AP sections).

Therefore, these data showed that the 3-hour 4-AP-induced hyperexcitability did not alter Iba-1+ microglia or GFAP+ astrocyte expression in the ACC of young WT mice compared to untreated sections.

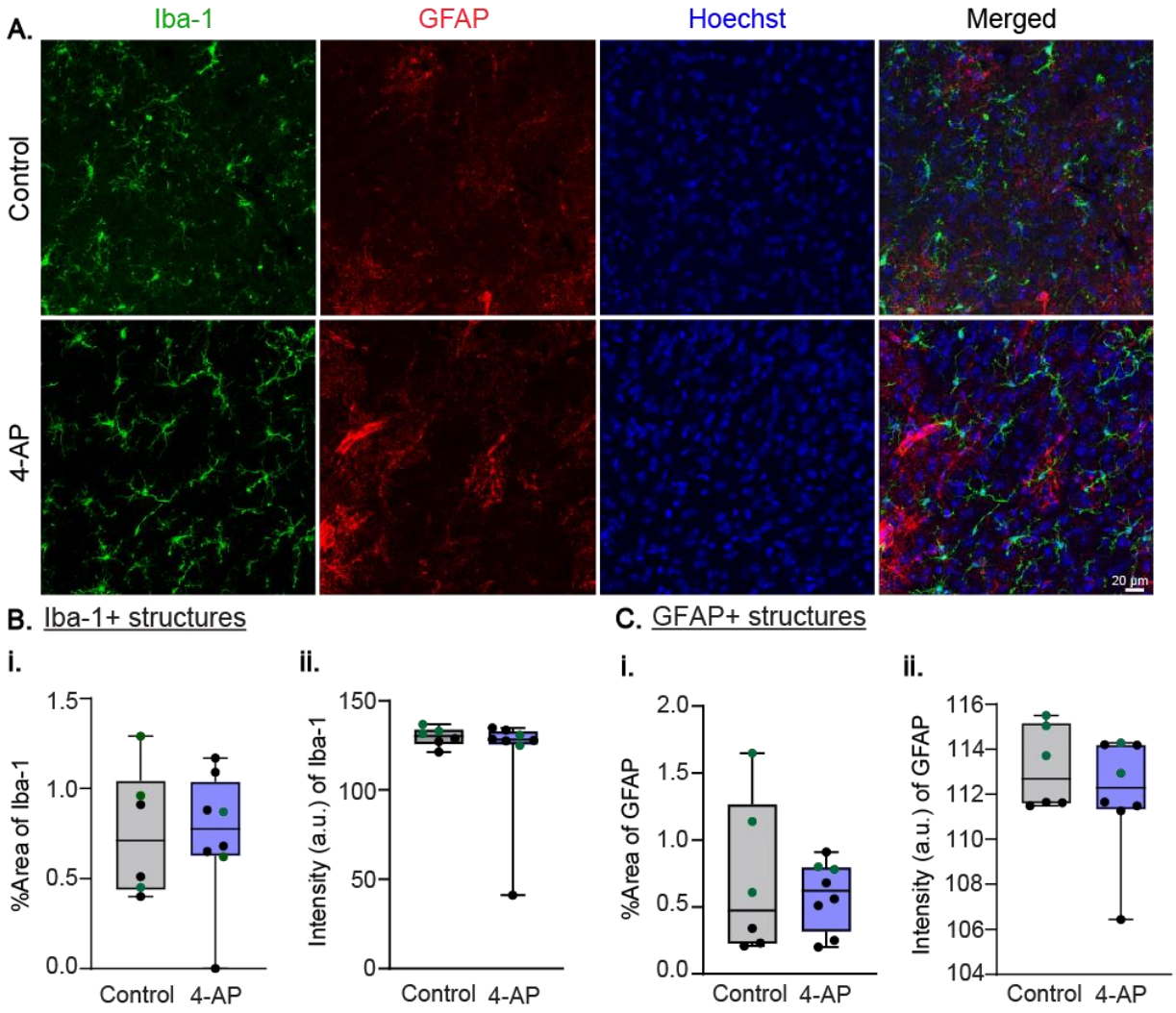

Figure 3.7. Iba-1+ microglia and GFAP+ astrocytes in the ACC of ACSF and 4-AP sections from young WT mice. These are collapsed 40x z-stack image examples (maximum projections) from the superficial ACC layers. **A.** The expression of all Iba-1+ structures, including microglia (green), GFAP+ reactive astrocytes (red) and all Hoechst nuclei (blue) in the ACC of ACSF (control) and 4-AP sections. **B - C.** The median (**i**) % area and (**ii**) intensity (a.u.) of (**B**) Iba-1 and (**C**) GFAP expression are shown for control (grey) and 4-AP (blue) sections. Each data point represents the median value per ACC sections, with male mice in black and female mice in green.

3.5. Discussion

3.5.1. *Summary of the main findings in Chapter 3*

- Trend towards an increase in the count of simple IIDs and complex IIDs were significantly increased in the ACC of young WT mice during 3 hours of 4-AP.
- The count and duration of seizure-like events significantly increased during 4-AP incubation.
- Seizure-like events in the ACC were first observed around 15 minutes in 4-AP.
- PV expression was significantly increased following the 4-AP-induced increase in ACC neuronal activity.

3.5.2. *Hyperexcitability was shown in the deep ACC layers in young WT mice following 4-AP.*

Hyperexcitable activity has been observed in the form of abnormal poly-spikes both *in vivo* in the cortex (Morris *et al.*, 2015; Peters *et al.*, 2020) and *in vitro* in the hippocampus (Tweedy *et al.*, 2021) in α-syn transgenic mouse models. To date, there is no data to my knowledge looking at induced hyperexcitability in the ACC in control mice. To understand the function of neural network activity in the ACC under altered E/I balance conditions, hyperexcitability was induced using 4-AP in WT mice *in vitro*. WT mice were studied in the project at first to elucidate the hyperexcitability mechanisms and patterns in a non-transgenic background which would then help to examine hyperexcitability in the A30P transgenic animals.

4-AP is a voltage-gated potassium channel inhibitor (Kv1 channels) causing an increase in action potential duration, and thus depolarisation, leading to epileptiform activity (Yao and Tseng, 1994; Zhang and McBain, 1995; Coetzee *et al.*, 1999; Gutman *et al.*, 2005). Importantly, 4-AP increases the excitation of both excitatory and inhibitory neurons (Lévesque *et al.*, 2013; Hamidi and Avoli, 2015; Avoli *et al.*, 2016; Shiri *et al.*, 2016; González *et al.*, 2018). A concentration of 75 μM 4-AP was applied and circulated to the mouse ACC slices which has been characterised as a “transition” 4-AP concentration (Myers *et al.*, 2018). In the mouse hippocampus, during this “transition” concentration there are IIDs and seizure-like events but these are not as

long-lasting or of as high frequency as those occurring during higher 4-AP concentrations (Myers *et al.*, 2018). The *in vitro* electrophysiology experiments reported here showed that the deep layers of ACC in young 2-4-month-old WT mice could generate both IID and seizure-like activity using 4-AP. Particularly, hyperexcitability in the neural networks was observed in three different forms starting from simple and complex IIDs which then led to seizure-like events over the 3-hour incubation. The seizure-like events were obvious around 15 minutes following the 4-AP bath application and kept increasing in both frequency and duration for 40 minutes. At 3 hours of 4-AP incubation, the seizure-like events decreased in both frequency and duration possibly caused by compensatory mechanisms of neural networks highlighting metabolic and homeostatic regulation.

In vitro studies in the rat hippocampus using 4-AP showed three types of synchronous field potential discharges. These included GABA-mediated IIDs occurring at lower frequencies (0.05 to 0.25 Hz) and IIDs occurring at higher frequencies (0.25 to 0.5 Hz) originating in CA3 and mainly driven by glutamate receptors reflecting faster excitatory events. Additionally, there were long-lasting seizure-like events which originated in the entorhinal cortex and propagated to the hippocampus (Avoli *et al.*, 2002). Furthermore, 4-AP-induced IIDs and seizure-like events *in vitro* were also seen in other rat brain areas, including the amygdala and parahippocampal cortex (Avoli *et al.*, 1996, 2002; Klueva *et al.*, 2003) as well as the ACC (Panuccio *et al.*, 2009). Panuccio et al. (2009) found that the bath application of 4-AP in rat ACC slices induced fast-onset IIDs leading to the formation of ictal activity (Panuccio *et al.*, 2009). However, there is limited evidence on 4-AP-driven hyperexcitability in the ACC, especially in mice, as most *in vitro* studies have examined the hippocampus. Multielectrode array recordings showed fast-frequency IIDs driven by the CA3 hippocampal region and slow-frequency IIDs induced by 4-AP in young mice (2 - 3 weeks old). 4-AP also caused long-lasting seizure-like activity in the neighbouring neocortical areas which did not propagate to the hippocampus (Gonzalez-Sulser *et al.*, 2011). An early induction of IIDs has also been shown in the mouse hippocampus following 4-AP application *in vitro* highlighting the increased seizure susceptibility using the 4-AP model (Codadu *et al.*, 2019). Our findings in the ACC demonstrating IID and seizure-like activity driven by 4-AP are, therefore, consistent with other findings from *in vitro* electrophysiology examinations in rodents.

3.5.3. *Hyperexcitability evoked by 4-AP might be associated with increased PV expression in the ACC of young WT mice.*

PV interneurons

PV and PNN expression was investigated to examine differences in the ACC following hyperexcitability induced by 4-AP. The results demonstrated a statistically significant increase in the PV expression in the ACC following 4-AP. Therefore, our findings possibly suggest the involvement of PV interneurons in modulating the hyperexcitable network activity. Importantly, PV expression is activity-dependent, thus there is an increase in PV expression as well as PV messenger RNA when there is an increase in PV neuronal activity (Page *et al.*, 2019). Different ion channels found in the PV interneurons are involved in their unique signalling and firing properties. Some of these ion channels are the voltage-gated potassium channels Kv1 and Kv3 which are critical in membrane repolarisation and hyperpolarisation (Shah and Aizenman, 2014). The Kv3 channels are localised on the PV neuronal somas, but their increased expression on the axon terminals contributes to the fast release of the inhibitory neurotransmitter GABA at the synaptic terminals (Rudy and McBain, 2001; Goldberg *et al.*, 2005; Richardson *et al.*, 2022). The Kv1 channels are found on the soma and axon initial segment of PV interneurons and are important in exerting control of the action potential firing threshold and neuronal excitability (Goldberg *et al.*, 2008; Campanac *et al.*, 2013). As a Kv1 potassium channel inhibitor, 4-AP prolongs depolarisation leading to the accumulation of excitatory neurotransmitter release. This then triggers the depolarisation of neighbouring neurons and increases spontaneous action potential firing causing hyperexcitability (Armstrong and Loboda, 2001).

It is suggested that the epileptic activity generated by 4-AP is driven by the inhibitory neurons (Shiri *et al.*, 2015; Yekhlef *et al.*, 2015; Chang *et al.*, 2018; Codadu *et al.*, 2019). This is hypothesised to implicate a cascade of events including pyramidal cell chloride-loading and further rises in potassium efflux through the potassium chloride cotransporter KCC2 (Viitanen *et al.*, 2010; Schevon *et al.*, 2012; González *et al.*, 2018; de Curtis *et al.*, 2019). Before seizure generation, there is an increase in the intracellular chloride concentration in principal neurons followed by increased

GABAergic neurotransmission (Lillis *et al.*, 2012). This leads to an overload of potassium concentration extracellularly which acts as a positive feedback loop favouring excitation in neural networks leading to seizure formation (Traynelis and Dingledine, 1988; Somjen, 2002; Fröhlich *et al.*, 2008; Krishnan and Bazhenov, 2011; González *et al.*, 2015).

Evidence based on 4-AP seizure models *in vitro* shows that this increase in the extracellular potassium levels, before the onset of seizure-like events, is linked with increased levels of interneuron activity (Yekhlef *et al.*, 2015; Librizzi *et al.*, 2017). Yekhlef et al. (2015) discovered that *in vitro* optogenetic stimulation of PV and SST interneurons in the presence of 4-AP caused interictal and preictal spikes which were rapidly followed by seizure-like events in the medial entorhinal cortex of adult mice. This would, therefore, explain the increase in PV expression observed in the ACC following 4-AP-induced hyperexcitability, suggesting an increase in PV activity. In this study, I did not look at SST neurons, but exploring their potential role in 4-AP-induced activity would be interesting to assess in the future. An earlier study also showed that the optogenetic stimulation of PV interneurons in the hippocampus of mice and rats contributed to the initiation of after-discharges during the clonic phase of the seizures, while their silencing decreased the number of after-discharges (Ellender *et al.*, 2014).

Hyperexcitability also led to a trend towards an increase in the c-Fos protein in the ACC following 4-AP incubation. The c-Fos protein is a proto-oncogene expressed in activated neurons after voltage-gated calcium entry into the cells. Additionally, there is a fast and transient induction of the c-Fos protein following excitation in the neural networks (Bullitt, 1990). Hyperexcitability then critically contributes to the accumulation of c-Fos in the neuronal nucleus, which is consistent with the trend towards an increase of c-Fos we observed in the 4-AP slices (Zhang *et al.*, 2002; Shimojo *et al.*, 2020a). In future work, it would be interesting to compare the activation of c-Fos by 4-AP between pyramidal neurons and PV interneurons.

Perineuronal Nets

PNNs are usually found to surround fast-spiking PV interneurons in the cortex, and their array of proteoglycans and polysaccharides provides a strong negative

charge to the neurons (Seeger *et al.*, 1994; Morawski *et al.*, 2005; Suttkus *et al.*, 2016). In the ACC of WT mice, we observed PNNs around PV interneurons. The excitability of the PV interneurons is controlled by their PNNs which indirectly control the GABAergic inhibition through regulation of PV neuronal activity and synaptic integration. In view of our findings showing an increase in PV expression, we thought we might also see an upregulation of WFA+ PNN expression. An upregulation in PNN expression might improve the E/I imbalance and the increased excitability of PV interneurons induced by 4-AP.

Changes in PNNs under epileptic conditions, including the upregulation of their components and disruption of their structure, have been shown in animal models and human tissue. PNN disruption affects the PV interneurons since decreased PV neuronal density was observed (Naffah-Mazzacoratti *et al.*, 1999; Perosa *et al.*, 2002; McRae *et al.*, 2012; Pollock *et al.*, 2014; Rankin-Gee *et al.*, 2015; Favuzzi *et al.*, 2017; Härtig *et al.*, 2017; Kim *et al.*, 2017). The time in which there are changes in PNNs following hyperexcitability is also important. Increased WFA binding was observed in the hippocampus of a kindled mouse model of epilepsy following 15 days of pentylenetetrazole ($GABA_A$-R antagonist) injections (Ueno, Suemitsu, *et al.*, 2019). Our preliminary analysis of WFA+ PNNs showed no statistically significant differences in the % area and intensity measurements following 3 hours of 4-AP incubation. However, potential changes in PNNs during prolonged epileptic conditions with longer recording time, and/or higher 4-AP concentrations, could be assessed in future studies.

Our findings might also indicate a protective role of the PNNs towards the PV interneurons in controlling their activity under epileptic conditions. On the other hand, hyperexcitability might have affected the PV interneurons since there was increased PV expression correlated with increased PV activity. Changes in PV expression could also imply potential changes in the ECM molecules of PNNs leading to the dysregulation of ion buffering in the cell which might have affected the spiking activity of PV interneurons. However, we do not have any evidence showing changes in the expression or quantification of PNN components, including the CSPGs, from our investigation. Importantly, there is no evidence in the literature demonstrating the change of PNN structures induced by hyperexcitability caused by 4-AP *in vitro*.

3.5.4. *No effect of 4-AP incubation on the neuroinflammatory markers in the ACC of young WT animals.*

Neuroinflammatory responses can be beneficial to repair tissue from damage and remove cellular debris under normal conditions. However, sustained and persistent neuroinflammation prevents the regeneration of functional connections potentially contributing to the pathogenesis of neurodegeneration (Kwon and Koh, 2020). Increased neuroinflammatory responses, involving microglial and astrocytic activation, play a role in hyperexcitability observed in different neurodegenerative disorders (Vicente *et al*., 2024). It is suggested that increased neuronal activity and seizures are triggered by neuroinflammation and impaired glial immunoinflammatory function contributes to generating seizure activity (Devinsky *et al.*, 2013a; Pracucci *et al.*, 2021).

In this pilot study, following the 4-AP-induced hyperexcitability including seizure-like activity in the ACC of young WT mice, we also assessed whether there were changes in the expression of microglia and astrocytes. However, no significant changes were found for the Iba-1 and GFAP expression. Unpublished work from our lab has discovered a trend towards an increase of Iba-1+ microglia but no changes in GFAP+ astrocytes in the rat ACC following incubation with kainate (KA, agonist of KA glutamate receptors) and PCP (NMDA antagonist) *in vitro* compared to ACC slices incubated only in KA. It is known that PCP induces schizophrenia-like psychosis and research shows dysregulation of neuroinflammation in animal models and patients of schizophrenia (Mouri *et al.*, 2007; Tarasov *et al.*, 2019; Laricchiuta *et al.*, 2024). Even though the neural networks in the ACC underwent changes in their E/I balance following the 4-AP application, in this study, we did not see any obvious effect of 4-AP in microglia and astrocytes during these experiments. It is possible that the hyperactivity we observed in the ACC might not have reached a threshold necessary to trigger glial cell activation, thus neuroinflammation. However, this does not exclude the contribution of glial cells to the formation of the hyperexcitable state with more long-term hyperexcitability compared to 3 hours.

Studies investigating the role of neuroinflammation in hyperexcitability showed that there is a crosstalk between microglia and astrocytes which increases seizure

activity (Verhoog *et al.*, 2020; Li *et al.*, 2023). Sano et al. (2021) showed that there was Iba-1+ microglial activation and release of proinflammatory cytokines following status epilepticus in the mouse hippocampus. Microglial activation played a critical role in the induction of GFAP+ astrocytic activation increasing seizure susceptibility (Sano *et al.*, 2021). The function of astrocytes might be influenced by the 4-AP application. 4-AP-mediated stimulation causes increased intracellular calcium concentrations affecting astrocytes which possess voltage-gated potassium channels and voltage-gated calcium channels (Wu *et al.*, 2009; Kasatkina, 2016). However, neuroinflammation in the ACC has been mostly examined in chronic neuropathic pain (Li *et al.*, 2022; Iqbal *et al.*, 2023) as well as major depressive disorder (MDD) (Cotter *et al.*, 2001; Setiawan *et al.*, 2015) and schizophrenia (Stark *et al.*, 2004). Even though we found no significant changes in the expression of Iba-1+ microglia and GFAP+ astrocytes following 4-AP, potential changes in the shape of glial cells may have occurred but were not detected in our analysis. On the other hand, it might be possible to see marked changes in both microglia and astrocytes, using a higher 4-AP concentration or longer incubation period.

3.6. Conclusions

This chapter demonstrated that ACC generates hyperexcitable activity induced by 4-AP that was similar to that observed in other cortical regions in the young WT animals *in vitro*. Hyperexcitability in the ACC was observed as both simple and complex IIDs, which then led to seizure-like events. The induced epileptic conditions in the ACC were associated with a statistically significant increase in PV expression and a potential increase in the nuclear accumulation of c-Fos protein. Increased PV expression might be related to increased PV activity via raised intracellular calcium concentrations. There were no statistically significant changes in glial cells, including microglia and reactive astrocytes, following 4-AP incubation which could have been observed in other more hyperexcitable brain regions such as the hippocampus. Overall, the findings in this chapter provide fundamental knowledge about neural network activity in the ACC associated with hyperexcitability in young WT animals which would be critical for investigation in the hα-syn transgenic A30P animals.

Chapter 4. Neuronal network activity in the ACC in young pre-symptomatic A30P mice and WT control.

4.1. Introduction

Fast-frequency oscillations, including beta and gamma frequencies, facilitate communication between local neuronal populations in neighbouring brain areas (Von Stein and Sarnthein, 2000; Siegel *et al.*, 2012). As outlined in Introduction Chapter 1.4.2, beta oscillations are linked to movement-related activities (observation, imagination, and execution) and sensorimotor-associated cognitive processes (Neuper and Pfurtscheller, 2001; Kilavik *et al.*, 2013; Rossiter *et al.*, 2014). Gamma oscillations, in contrast, are associated with attentive information processing and the active maintenance of memory or conscious perception (Singer, 2001; Herrmann *et al*., 2004; Womelsdorf and Fries, 2006). The ACC, a higher-order cognitive region, regulates top-down control of downstream areas and supports attention, decision-making, cost-benefit analysis, and emotional regulation (Ridderinkhof *et al.*, 2004; Etkin *et al.*, 2011; Shackman *et al.*, 2011; Holroyd and Yeung, 2012; Rushworth *et al.*, 2012; Shenhav *et al*., 2013; Ullsperger *et al.*, 2014; Holroyd and McClure, 2015; Verguts *et al*., 2015; Laubach *et al*., 2015; Kolling *et al.*, 2016). Electrophysiological studies in humans (Li *et al.*, 2018; Crespo-García *et al.*, 2022) and animals (Narayanan and Laubach, 2006; Rothé *et al.*, 2011) highlight the importance of high-frequency oscillations in these cognitive and emotional processes controlled by the ACC.

In neurodegenerative disorders including AD (Babiloni *et al.*, 2004; Herrmann and Demiralp, 2005; Schnitzler and Gross, 2005; Rossini *et al.*, 2006, 2007; Andersson *et al.*, 2008; Bonanni *et al.*, 2008; Yener and Başar, 2013; Başar *et al.*, 2016; Ishii *et al.*, 2018), PD (Schnitzler and Gross, 2005; Andersson *et al.*, 2008; Bonanni *et al.*, 2008) and DLB (Andersson *et al.*, 2008; Bonanni *et al.*, 2008), the oscillatory activity is disrupted because of changes in excitation and inhibition in the neuronal networks. However, most studies investigated dysfunction in theta and alpha slow-frequency oscillations but beta and gamma frequency oscillations are also important in cognitive processes which are impaired in neurodegeneration (Herrmann and Demiralp, 2005; Clayton *et al*., 2015; Watrous *et al.*, 2015; Başar *et al.*, 2016; Zheng *et al.*, 2016). In AD patients, there is decreased alpha, beta and gamma frequency oscillatory activity (Babiloni *et al.*, 2004; Herrmann and Demiralp, 2005;

Schnitzler and Gross, 2005; Rossini *et al.*, 2006, 2007; Yener and Başar, 2013; Başar *et al.*, 2016; Ishii *et al.*, 2018). Importantly, there is limited understanding of beta and gamma oscillation impairments in DLB. These oscillations can be studied both *in vivo* and *in vitro* using control and rodent disease models. While gamma oscillations have been examined in A30P transgenic mice, previous studies have focused mainly on the hippocampus, leaving the ACC unexplored (Robson *et al.*, 2018). Therefore, this chapter investigates beta and gamma oscillations in the ACC of young A30P mice.

Impairments in E/I balance can also lead to neuronal hyperexcitability leading to the seizure activity seen in AD (Palop and Mucke, 2010; Busche *et al.*, 2015), PD (Caviness *et al.*, 2011) and DLB (Morris *et al.*, 2015) patients as well as animal models. Different brain regions showed hyperexcitability in neurodegeneration including the hippocampus, DMN, and entorhinal cortex but limited investigations exist for the ACC (Bonanni *et al.*, 2008, 2016; Rodriguez-Oroz *et al.*, 2009; Helmich *et al.*, 2012; Palop and Mucke, 2016). Cognitive fluctuations and impaired attention in DLB patients might be associated with impairments in the ACC. In post-mortem tissue of prodromal DLB patients, of whom 93% exhibited fluctuating cognition, there was atrophy in the right ACC and bilateral insular areas (Blanc *et al.*, 2016). Also, high levels of neuronal α-syn pathology including LBs have been shown in the ACC associated with cognitive decline (Kövari *et al.*, 2003; Yamasaki *et al.*, 2019). Further studies are necessary to elucidate network dysfunction leading to hyperexcitability in ACC in DLB, and whether this leads to network oscillation changes.

Neuronal network changes involving PV neuronal dysfunction can lead to deficiencies in gamma oscillations and hyperexcitability. In post-mortem examinations of AD (Brady and Mufson, 1997) and DLB (Bernstein *et al.*, 2011) patients decreased PV neuronal densities were observed in the hippocampus. A reduction of PV expression was also reported in AD animal models and a loss of neurons expressing the GABA-synthesizing enzyme glutamate decarboxylase 67 (GAD 67) (Takahashi *et al.*, 2010; Krantic *et al.*, 2012; Silva Albequerque *et al.*, 2015; Huh *et al.*, 2016; Mahar *et al.*, 2016; Cattaud *et al.*, 2018; Choi *et al.*, 2018; Petrache *et al.*, 2019).

The breakdown of PNNs in AD is thought to contribute to PV neuronal dysfunction and loss. In AD post-mortem brains and animal models, activated microglia release enzymes that degrade PNNs, leaving neurons vulnerable to a toxic

environment (Crapser, Spangenberg, *et al.*, 2020; Reichelt, 2020; Wang *et al.*, 2023). Sustained neuroinflammation may further accelerate neuronal degeneration, as activated microglia and reactive astrocytes release pro-inflammatory cytokines, leading to oxidative stress, excitotoxicity, and neuronal network dysfunction (Kempuraj *et al.*, 2016; Russo and McGavern, 2016). As discussed in Introduction Chapter 1.6.3, neuroinflammation occurs early in AD, PD, and DLB, driving the progression of neurodegeneration (Tarkowski *et al.*, 2003; Glass *et al.*, 2010; Craig-Schapiro *et al.*, 2010; Brosseron *et al.*, 2014; Wennström *et al.*, 2015; Stokholm *et al.*, 2017; Morenas-Rodríguez *et al.*, 2019; Oksanen *et al.*, 2019; Amin *et al.*, 2022; Gao *et al.*, 2023). However, whether early neuroinflammation in the mouse ACC contributes to neuronal network dysfunction involving PV interneurons and PNNs in DLB remains unknown.

Here, we examined KA-evoked high-frequency oscillations, gabazine- and 4-AP-induced IIDs, seizure-like activity, and the expression of markers for interneurons, PNNs, and neuronal activation in young pre-symptomatic A30P mice and WT controls. In 4-AP-exposed ACC slices, we assessed glial cell expression alongside neuronal markers to identify genotype-specific differences. This study aimed to detect early network changes in 2-4-month-old A30P mice, a prodromal stage of hα-syn pathology (Chapter 1.2.2).

4.2. Aims

- To investigate fast network oscillations as well as gabazine-induced and 4-AP-induced IID activity in the ACC of young A30P mice compared to the WT.

- To determine differences in the PV inhibitory interneurons, PNNs and glial cells following 4-AP-induced hyperexcitability in the ACC of young A30P mice compared to WT.

4.3. Methods

4.3.1. *In vitro electrophysiology*

The acute slice preparation for the *in vitro* electrophysiology experiments was performed as previously described in Chapter 2.2.1.

Oscillation experiments

ACC slices were obtained from 2-4-month-old WT mice (N = 9: 7 males, 2 females, n = 13 slices total) and A30P mice (N = 8: 5 males, 3 females, n = 16 slices total), and slice maintenance followed the protocol in Chapter 2.2.2. Baseline LFP recordings of 10 minutes were taken from one ACC hemisphere in each slice. After baseline, 800 nM KA (from a 1 mM stock) was bath-applied to the circulating ACSF to induce oscillatory activity, which was sustained throughout the experiment.

Three types of recordings were conducted:

- **Oscillation mapping experiments**: To assess oscillatory activity across different ACC layers, 60-second recordings were taken from the superficial (L1, 2/3) and deep layers (L5, 6) of the ACC, 3 hours after KA application, once oscillations had stabilised.
- **Oscillation build-up experiments**: Continuous 30-minute recordings were taken from the deep layers of the ACC for up to 4 hours post-KA application to capture the development of oscillatory activity over time.
- **Stable oscillation recordings**: After 3 hours of KA application, stable oscillatory activity in the deep ACC layers was recorded for 30 minutes, with additional recordings continuing up to 5 hours post-KA.

Oscillatory activity was considered stable when area power and peak frequency measurements remained within ±10% over 30 minutes. For all experiments, 60-second traces were analysed using power spectrum analysis (15 - 90 Hz) to examine area power ($\mu V^2/Hz$), peak amplitude (μV^2), and peak frequency (Hz), as described in

Chapter 2.2.4. The 15 - 90 Hz range was selected to capture both beta and gamma frequency oscillations.

Gabazine- and 4-AP-induced hyperexcitability experiments

ACC slices were obtained from young 2-4-month-old WT mice (Gabazine: N = 3 including 2 males, 1 female, n = 6 slices total; 4-AP: N = 6 including 3 males, 3 females, n = 22 slices total) and A30P mice (Gabazine: N = 3 including 1 male, 2 females, n = 4 slices total; 4-AP: N = 3 including all females, n = 12 slices total total). Slice maintenance followed the protocol described in Chapter 2.2.2, and baseline recordings of 10 minutes were taken from each ACC hemisphere in both rigs, with all LFP recordings from the deep layers of the ACC.

For the Gabazine experiments, gabazine was bath-applied to the circulating ACSF starting at a concentration of 100 nM, with increases every 30 minutes up to 20 µM (100 nM, 250 nM, 500 nM, 1 µM, 10 µM, 20 µM). Recordings were taken every 30 minutes over a 3-hour period. For the 4-AP experiments, 4-AP was applied at an initial concentration of 25 µM, increasing by 25 µM every 15 minutes, up to 100 µM (25 µM, 50 µM, 75 µM, 100 µM). Recordings were taken every 15 minutes over a 1-hour period, after which the slices were fixed with PFA for free-floating IHC experiments.

The baseline activity and recordings post-drug application were acquired and analysed using AxoGraph software as outlined in Chapters 2.2.3 and 2.2.4. Hyperexcitable events were categorized as simple IIDs (one negative/positive going peak), complex IIDs (one big positive/negative peak followed by smaller positive/negative peaks), and seizure-like events (activity longer than 5 seconds) (Fig. 2.3). For the 4-AP experiments, only the count of seizure-like events and average seizure duration were measured.

4.3.2. *Free-floating IHC-Immunofluorescence*

The 4-AP-exposed ACC slices were PFA-fixed, re-sectioned and stained following the protocol in Chapter 2.3.2. One set of WT and A30P ACC sections was immunolabelled with the staining combination 1 and the other set of ACC sections was stained with the staining combination 2 (Table 4.1). The ACC sections were then imaged under the confocal microscope at 40x magnification as mentioned in Chapter 2.3.3 (Fig. 2.4). The densitometric analysis was performed using FIJI software according to Chapter 2.3.4.

Staining Combination 1	
Primary Antibody/Lectin	**Secondary Antibody/Avidin**
Mouse anti-PV	Donkey anti-mouse Alexa Fluor 647
Biotinylated WFA lectin	Streptavidin fluorescein (498)
Rabbit anti-c-Fos	Donkey anti-rabbit Alexa Fluor 568
Staining Combination 2	
Goat anti-Iba-1	Donkey anti-goat Alexa Fluor 488
Rabbit anti-GFAP	Donkey anti-rabbit Alexa Fluor 568

Table 4.1. IHC staining combinations used for the A30P and WT 4-AP ACC sections following the *in vitro* electrophysiology experiments.

4.4. Results

4.4.1. *KA-induced network oscillatory activity in the superficial and deep ACC layers in young WT mice.*

These mapping experiments were first conducted as a pilot study to investigate the 15 - 90 Hz oscillatory activity in both superficial and deep layers of the ACC. The goal was to explore how oscillatory activity varied across different ACC layers, but also make a comparison from anterior to posterior regions, as defined by the Paxinos and Franklin mouse brain atlas.

For each ACC slice, baseline activity was first recorded prior to KA. Following 3 hours of KA application, oscillatory activity was mapped across the ACC. We used one electrode per slice which was systematically moving from layer to layer within the same slice and recorded 60-second traces of the oscillatory activity in each layer. This allowed for a detailed exploration of oscillatory patterns across the superficial (L2/3) and deep (L5/6) layers. We investigated ACC oscillatory activity in young WT mice and noticed heterogeneity in the KA-evoked oscillatory activity with oscillations having mixed frequency peaks or a single frequency peak (Fig. 4.1).

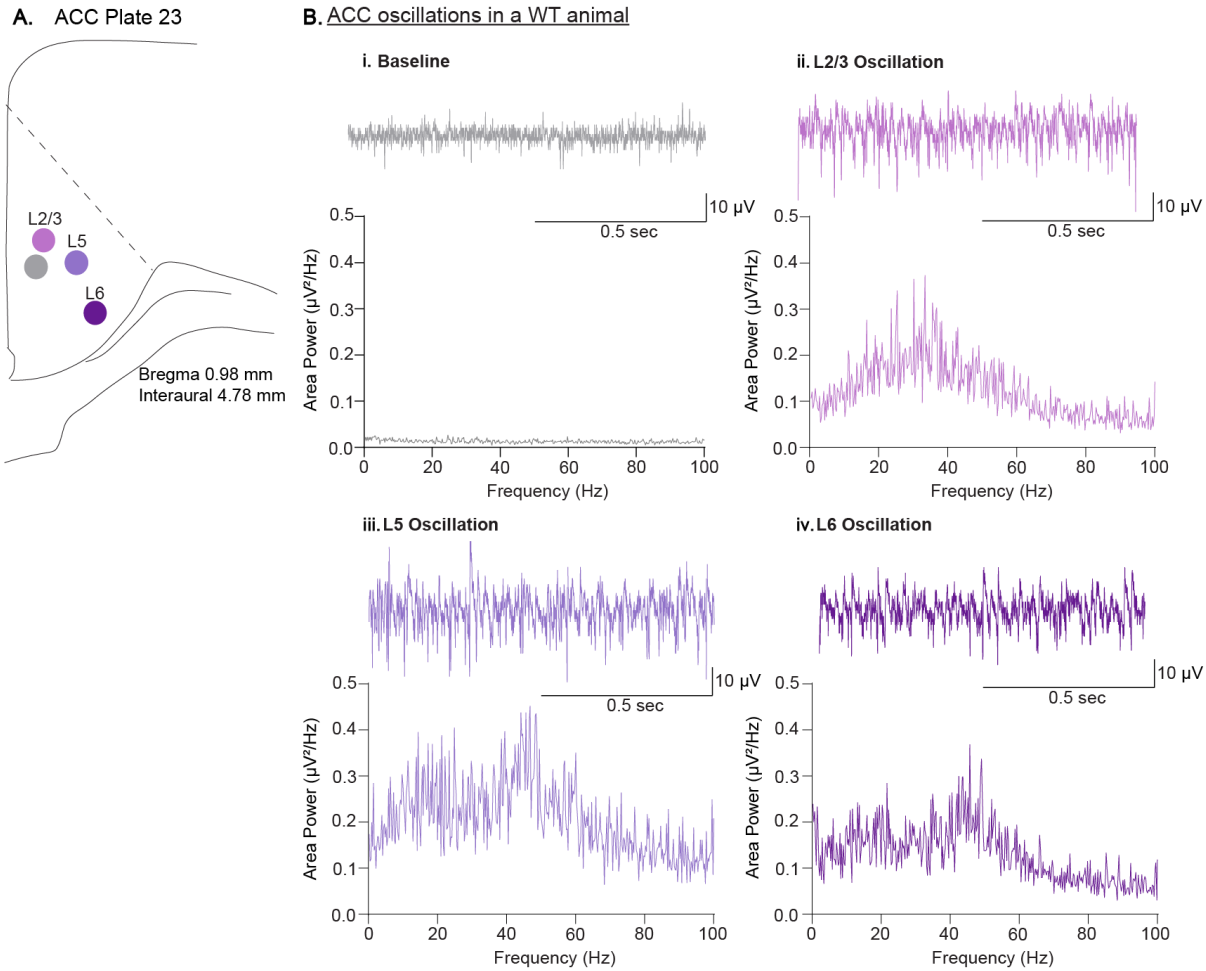

Figure 4.1. Example of fast oscillations in superficial and deep ACC layers of a young WT mouse. A. The locations of baseline (grey) and KA-evoked oscillation (pink, lavender, purple) recording locations are demonstrated on the ACC plate diagram. **B.** Traces and power spectra showing the area power ($\mu V^2/Hz$) against the frequency (Hz) are demonstrated for the recorded LFP activity in the ACC. Baseline activity (**i**), shown in grey, was recorded before the application of 800 nM KA to ACC (plate 23) of a young WT mouse. Example oscillation in (**ii**) superficial L2/3 following 3 hours of KA application is shown in pink and example oscillations in deep (**iii**) L5 and (**iv**) L6 are shown in lavender and purple, respectively.

In my recordings, I found gamma frequency peaks, but also oscillations of mixed beta and gamma frequencies. In the A30P and WT mice, there were 25% and 30% of beta 15 – 32.99 Hz oscillations, respectively, from the total of the 15 – 90 Hz oscillations in the ACC and the rest were gamma 33 – 90 Hz oscillations. We used this frequency classification of beta and gamma oscillations as it is a bimodal distribution of these frequencies previously reported in the rat ACC (Adams *et al.*, 2017; Dennis *et al.*, 2023).

From all ACC slices used in the *in vitro* electrophysiology mapping experiments, including plates 21, 23, 25 and 30 (based on Paxinos and Franklin mouse brain atlas, 2001, Chapter 2.2.1, Fig. 2.1), only slices corresponding to plate 30 did not oscillate as well as the others. This is demonstrated in Figure 4.2 for the percentage of the total oscillations recorded in all plates in the WT (A) and A30P (B) mice. From the total of all oscillations plates 23 and 25 showed more oscillatory activity recorded in the ACC in both genotypes compared to plate 30 (Fig. 4.2A WT: plate 21; 24.2%, plate 23; 27.3%, plate 25; 40.9%, plate 30; 7.6%, B A30P: plate 21; 22.1%, plate 23; 39.7%, plate 25; 25%, plate 30; 13.2%). Additionally, we recorded more 15 – 90 Hz frequency oscillations in the deep L5 and 6 compared to the superficial L2/3 in the ACC in both WT and A30P mice (Fig. 4.3A WT: L5,6; 87.9%, L2/3; 12.1%, B A30P: L5,6; 85.3%, L2/3; 14.7%).

Following this pilot mapping study in the ACC, the area power, peak amplitude, and frequency of stable 15 – 90 Hz oscillations were next quantified in the deep ACC layers of young A30P and WT mice within ACC plates 21, 23, and 25.

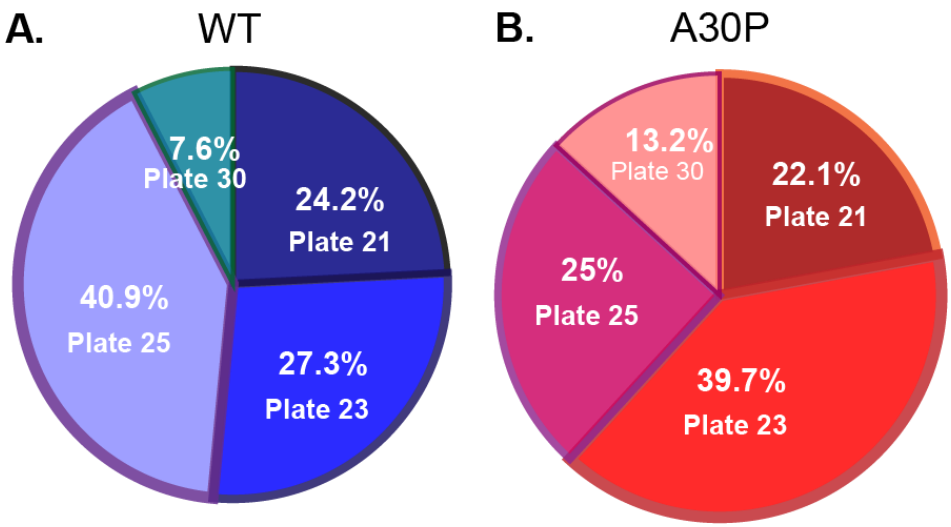

Figure 4.2. Percentages of KA-evoked 15 – 90 Hz frequency oscillations in each ACC plate during mapping experiments. A. Pie chart showing the % total oscillations for plate 21 (deep blue), 23 (blue), 25 (lavender) and 30 (teal) for all WT mice. **B.** Pie chart showing the % total oscillations for plate 21 (brown), 23 (orange), 25 (pink) and 30 (peach) for all A30P mice.

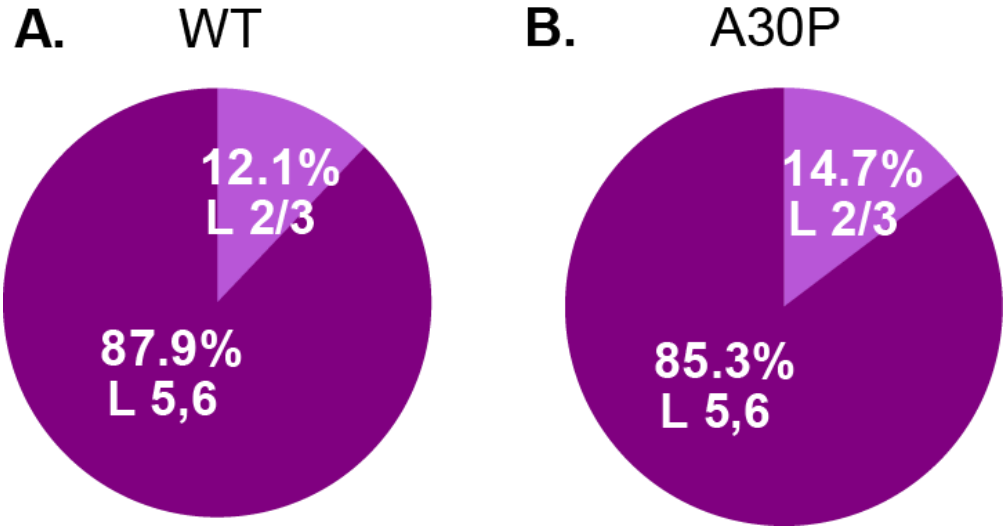

Figure 4.3. Percentages of KA-evoked 15 – 90 Hz frequency oscillations in the superficial and deep ACC layers during mapping experiments. A. Pie chart showing the % of all oscillations observed in superficial (L2,3 lavender) and deep layers (L5,6 purple) of the ACC in the WT mice. **B.** Pie chart showing the % total oscillations for the superficial and deep ACC layers in the A30P mice.

4.4.2. *Differences in oscillation power between young A30P and WT mice in the deep ACC layers.*

Stability of ACC oscillatory activity

To determine when oscillatory activity stabilised in the deep layers of the ACC in young A30P and WT mice *in vitro*, LFP activity was recorded every 30 minutes following the bath application of 800 nM KA for up to 4.5 hours (270 minutes). The area power, peak amplitude, and peak frequency of the 15 - 90 Hz oscillatory activity in four WT ACC slices and one A30P ACC slice are shown in grey and red lines, respectively, in Figure 4.4A (N = 4 WT mice, N = 1 A30P mice). Baseline recordings showed no oscillatory activity (Fig. 4.4B, black lines on power spectra). Unfortunately, humidity and breeding issues in the CBC resulted in a limited number of A30P mice, and therefore, the build-up analysis was primarily conducted on WT mice. From the recorded oscillatory activity, I observed that the area power increased over time and reached a stable state after 3 hours (180 minutes) of KA application in the ACC of young WT mice. However, there were not enough oscillations recorded from the same ACC location to fully quantify this.

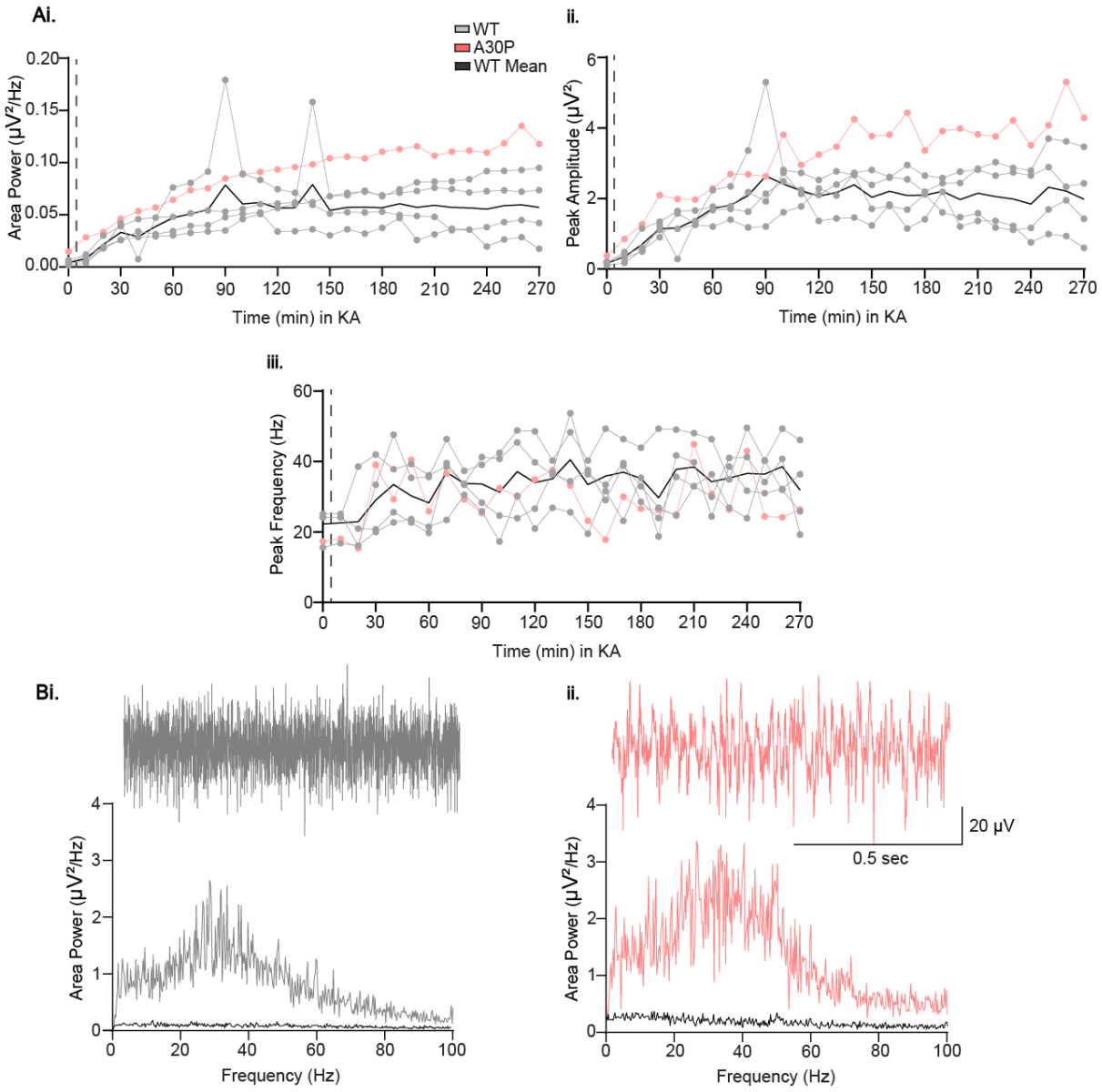

Figure 4.4. Fast oscillatory activity in the deep ACC layers for a 4.5-hour duration (270 minutes) in KA in young WT and A30P mice. A. Individual (**i**) area power (μV^2/Hz), (**ii**) peak amplitude (μV^2) and (**iii**) peak frequency (Hz) of fast 15 - 90 Hz oscillations in four WT ACC slices (grey) and one A30P ACC slice (red) were plotted every 10 minutes in 800 nM KA. The mean line of the WT ACC slices is shown in black. The dotted line indicates the baseline activity before 800 nM KA was applied. **B.** Example traces and power spectra of oscillatory activity in the deep layers of (**i**) a WT ACC slice (area power: 0.07 μV^2/Hz, peak amplitude: 2.2 μV^2, peak frequency: 35.4 Hz) and (**ii**) an A30P ACC slice (area power: 0.11 μV^2/Hz, peak amplitude: 3.37 μV^2, peak frequency: 26.61 Hz) at 180 minutes in KA are shown. The baseline power spectra before the KA application are shown in black.

Oscillation power in the ACC of young A30P and WT mice

Differences in oscillation power in the deep ACC layers between young A30P and WT mice were analysed. The median area power, peak amplitude, and peak frequency from the last 3 stable points of each oscillation were quantified for each ACC slice. No significant differences were found in the median area power of 15 - 90 Hz oscillations (Fig. 4.5A, WT 0.22 μV^2/Hz (0.17, 0.49) vs A30P 0.22 μV^2/Hz (0.15, 0.43), $p > 0.05$, Mann-Whitney, WT: N = 7; 6 males, 1 female /n = 9, A30P: N = 7; 4 males, 3 females/n = 13). Median peak amplitude also showed no significant differences (Fig. 4.5B, WT 11.83 μV^2 (5.28, 32.50) vs A30P 13.98 μV^2 (6.22, 26.77), $p > 0.05$, Mann-Whitney, WT: N = 7; 6 males, 1 female /n = 9, A30P: N = 7; 4 males, 3 females/n = 13). Similarly, no significant differences were observed in the median peak frequency (Fig. 4.5C, WT 41.10 Hz (31.53, 47.18) vs A30P 40.93 Hz (35.19, 44.74), $p > 0.05$, Mann-Whitney, WT: N = 7; 6 males, 1 female /n = 9, A30P: N = 7; 4 males, 3 females/n = 13).

Overall, mostly fast gamma frequency oscillations were recorded in the deep layers of ACC in young male and female mice but no differences between the two genotypes.

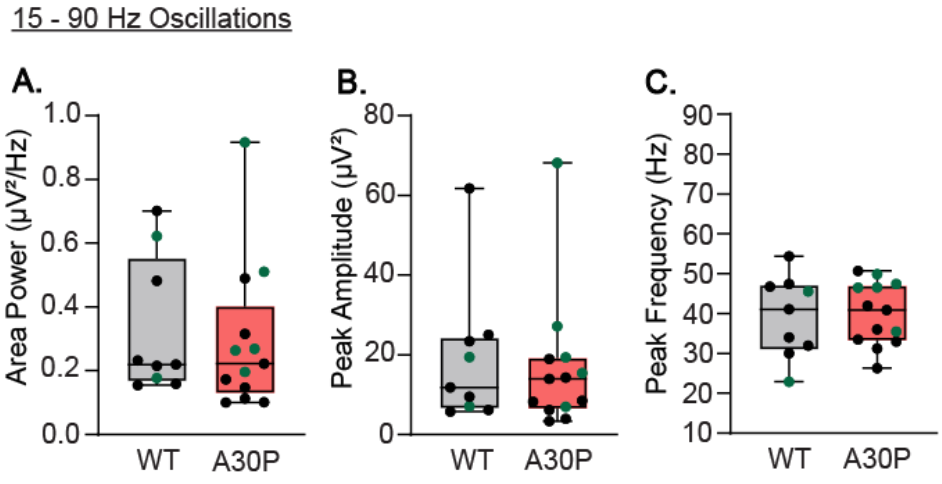

Figure 4.5. Stable oscillatory activity in the 15 – 90 Hz frequency band evoked by KA in the deep ACC layers in young A30P and WT mice. The (**A**) area power (μV^2/Hz), (**B**) peak amplitude (μV^2) and (**C**) peak frequency (Hz) of fast 15 - 90 Hz oscillations are demonstrated separately for the young WT (grey) and A30P (red) ACC slices. Data points represent the median values for each slice from male mice (black) and female mice (green).

4.4.3. *Gabazine-induced hyperexcitability is concentration-dependent and more pronounced in the deep ACC layers of young A30P mice compared to WT mice.*

Gabazine, a $GABA_A$-R antagonist, was used *in vitro* in ACC slices of young A30P and WT mice to investigate the role of inhibition in the ACC neuronal networks. Gabazine was bath-applied with concentrations increasing every 30 minutes from 100 nM to 20 μM to determine whether there were different hyperexcitability/seizure thresholds between young A30P and WT mice. Our recordings showed simple and complex IIDs and seizure-like activity in the deep layers of the ACC following gabazine application (Fig. 4.6Aii-iv). The distinction between simple and complex IIDs was performed qualitatively by examining the traces of these events as shown in the examples in Figure 4.6.

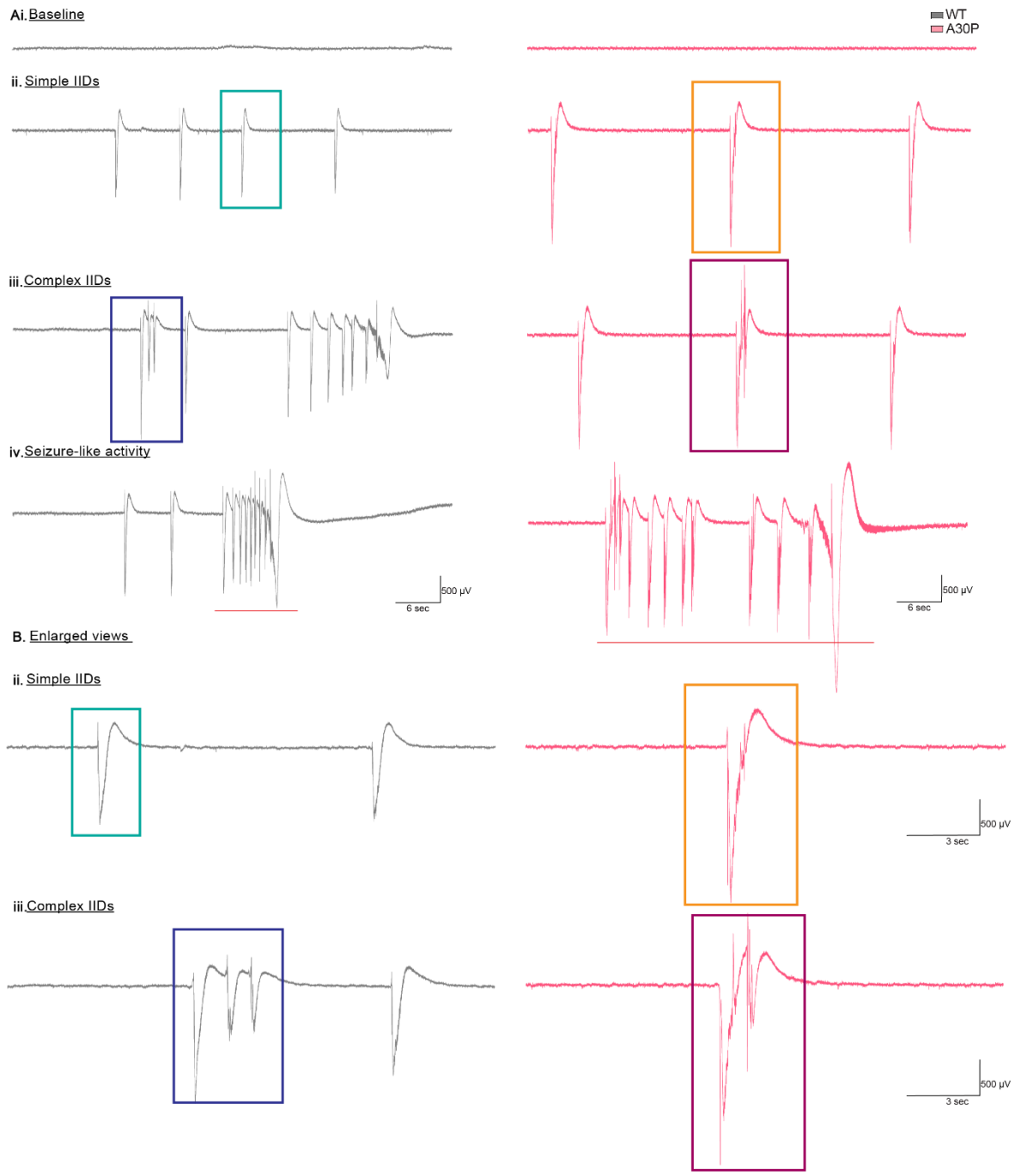

Figure 4.6. Simple IIDs, complex IIDs and seizure-like activity induced by gabazine in the deep layers of ACC in young A30P and WT mice. A. Example traces of (**i**) baseline activity, (**ii**) gabazine-induced simple IIDs, (**iii**) complex IIDs and (**iv**) seizure-like activity recorded in WT (grey) and A30P (red) ACC slices. Red underline indicates a single seizure-like event. In each trace, there are multiple spike events occurring with a mixture of simple IIDs and complex IIDs. **B.** Enlarged views of the boxes in **A** showing the example (**i**) simple IID consisting of one spike event (WT: teal box, A30P: orange box) and the complex IID consisting of more than two population spike events (WT: blue box, A30P: purple box).

To compare hyperexcitability in ACC slices between young A30P and WT mice, the total counts of simple IIDs, complex IIDs, and seizure-like events were recorded for each slice at each concentration over 30-minute recordings (Fig. 4.7A – C). Due to non-normally distributed data, even after log transformation, a two-way ANOVA test could not be applied (Fig. 4.7). In young WT mice, simple IIDs increased in frequency following 500 nM gabazine compared to A30P mice (Fig. 4.7A, WT: N = 3 mice/n = 6 slices, A30P: N = 3 mice/n = 4 slices). In contrast, in young A30P mice, there was a switch to more complex IIDs which were not seen in WT mice (Fig. 4.7B). Seizure-like events were observed only at 20 µM gabazine but there was no difference between the genotypes (Fig. 4.7C).

An example ACC slice from a young A30P mouse had very few simple IIDs, more complex IIDs and seizure-like events (Fig. 4.7, red, circle data points). Another A30P mouse slice showed only simple IIDs and no complex IIDs but had seizure-like events (Fig. 4.7, red, square data points). On the other hand, a few example ACC slices from the young WT mice had only simple IIDs and seizure-like events but no complex IIDs (Fig. 4.7, grey, triangle data points).

Overall, the results showed that gabazine induced IIDs and seizure-like activity in the deep ACC layers of both young A30P and WT mice. WT mice exhibited a trend toward more simple IIDs, while A30P mice showed an increase in the number of complex IIDs suggesting hyperexcitability. Seizure-like events occurred in both genotypes following the application of 20 µM gabazine, likely due to both the high concentration and prolonged exposure, as it was applied after 2.5 hours of treatment.

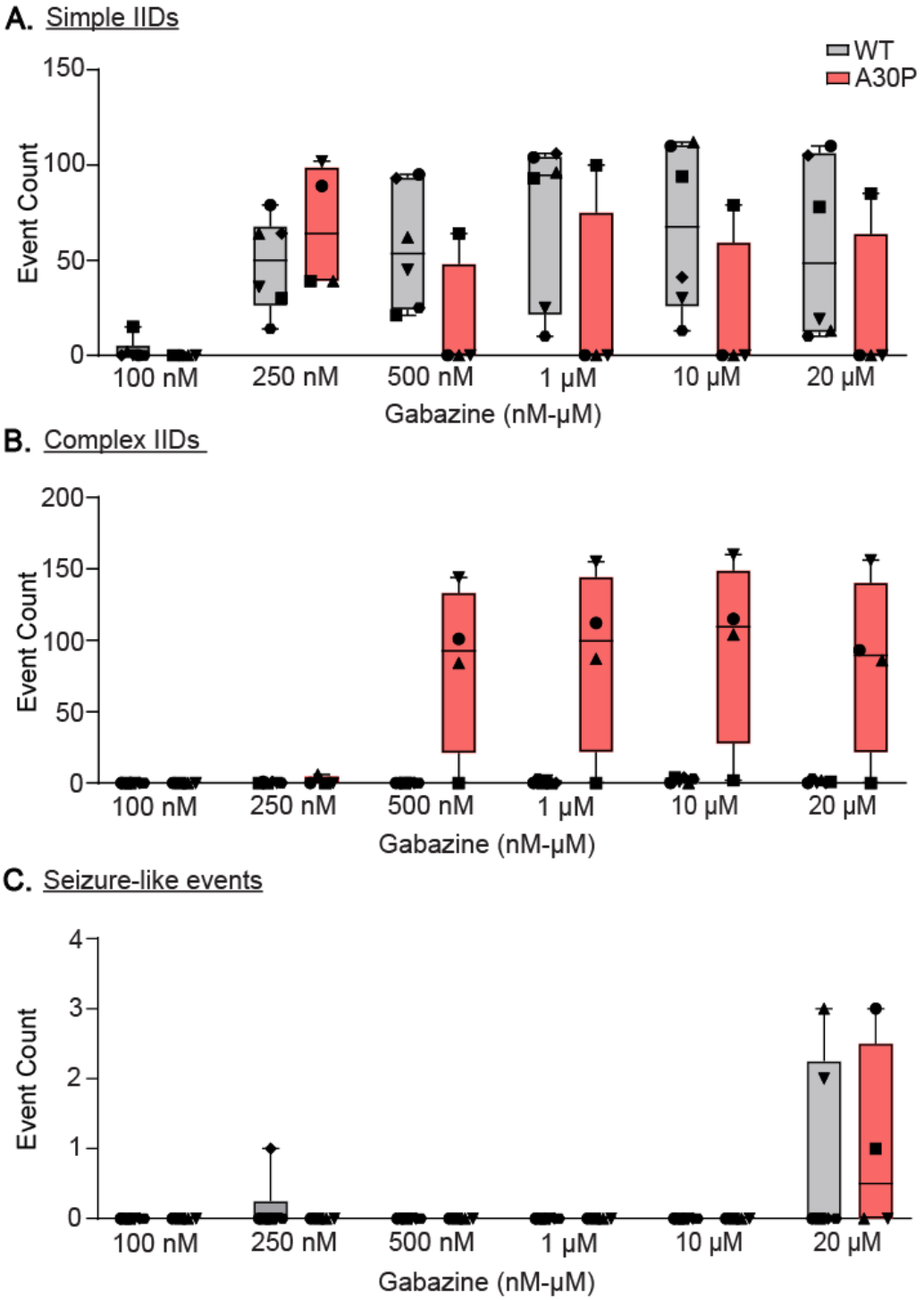

Figure 4.7. Simple IIDs, complex IIDs and seizure-like events during each gabazine concentration in the deep ACC layers in young A30P and WT mice. The total counts for (**A**) simple IIDs, complex IIDs (**B**) and (**C**) seizure-like events are shown during each 100 nM, 250 nM, 500 nM, 1 µM, 10 µM and 20 µM gabazine concentration between the WT (grey) and A30P (red) mice. Each data point represents the total number of events in a single slice and each symbol refers to a different slice.

4.4.4. *4-AP-induced hyperexcitability, PV and PNN expression and neuroinflammatory markers in the ACC of young A30P mice.*

Seizure-like activity induced by 4-AP in the ACC of young A30P and WT mice

Increasing concentrations of 4-AP (25 µM, 50 µM, 75 µM, and 100 µM) were sequentially applied to ACC slices from young A30P and WT mice, with each concentration lasting 15 minutes following baseline recordings. LFP activity in the deep ACC layers revealed IIDs and seizure-like events evoked by 4-AP in both genotypes. However, only seizure-like events were analysed, as distinguishing between simple and complex IIDs was challenging due to less distinct IID patterns seen with 4-AP compared to gabazine.

The seizure-like activity appeared at 50 µM 4-AP in both A30P and WT mice *in vitro*. As demonstrated in Figure 4.8, the 4-AP-induced seizure-like events began with an IID, which developed into a full seizure lasting longer than 5 seconds, followed by multiple IIDs resembling late recurrent discharges. This pattern of activity was observed in both A30P and WT ACC slices. When compared to the results from Chapter 3, where 75 µM 4-AP-induced seizure-like events were analysed, the seizure-like activity with varying 4-AP concentrations appeared to last longer, particularly at higher concentrations. The median count and duration of seizure-like events during different 4-AP concentrations in the ACC slices in both genotypes were also analysed.

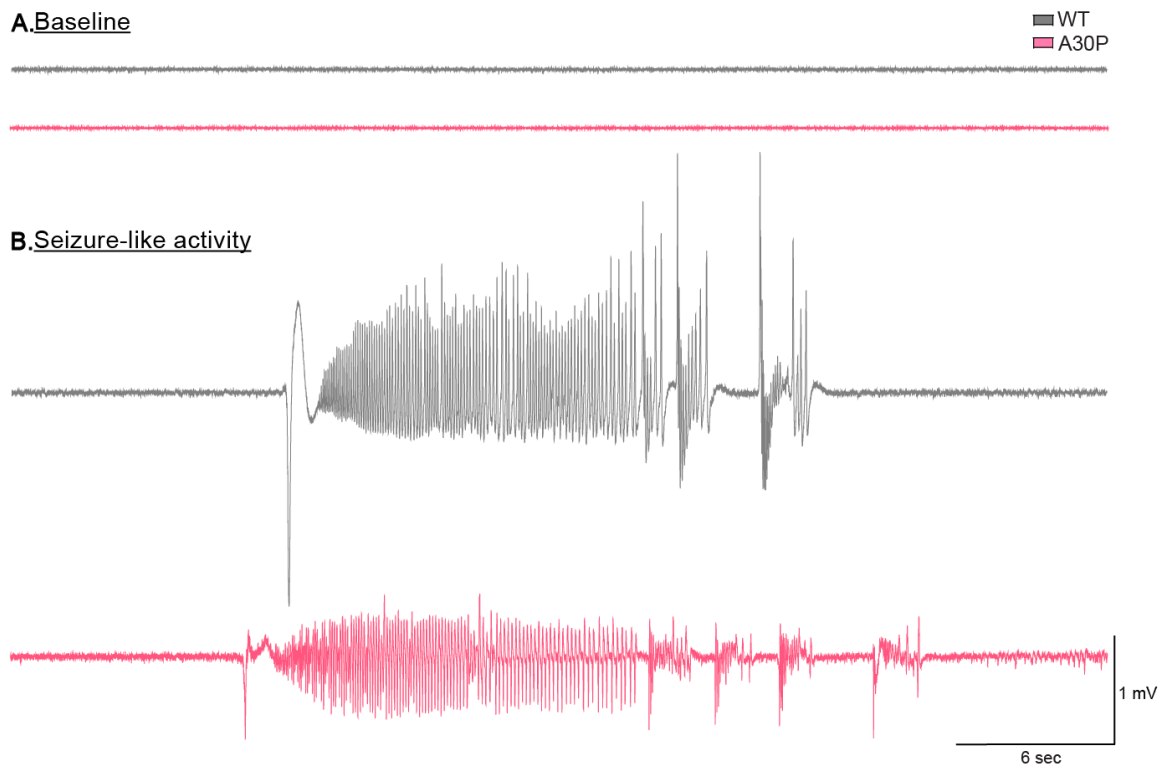

Figure 4.8. Seizure-like activity evoked by 4-AP in the deep ACC layers in young A30P and WT mice. Example traces of (**A**) baseline activity and (**B**) 4-AP-evoked seizure-like activity recorded in a WT (grey) and an A30P (red) ACC slice.

The data for the median count of seizure-like events at each 4-AP concentration were not normally distributed, which could be attributed to variability between the animals. Statistical analysis showed no significant differences in the median count of seizure-like events between A30P and WT mice for each 4-AP concentration (Fig. 4.9A, $p > 0.05$, Mann-Whitney, WT: N = 6 mice/n = 22 slices in total, A30P: N = 3 mice/n = 12 slices in total). The median duration of seizure-like events during each 4-AP concentration showed no significant differences in event duration were found between young A30P and WT mice (Fig. 4.9B, $p > 0.05$, Mann-Whitney, WT: N = 6 mice/n = 22 slices in total, A30P: N = 3 mice/n = 12 slices in total).

4-AP induced IIDs and seizure-like events in the deep ACC layers of both A30P and WT mice, with activity appearing at 50 µM. Event counts increased with higher 4-AP concentrations, but no significant differences were found between the genotypes, indicating similar levels of network excitability.

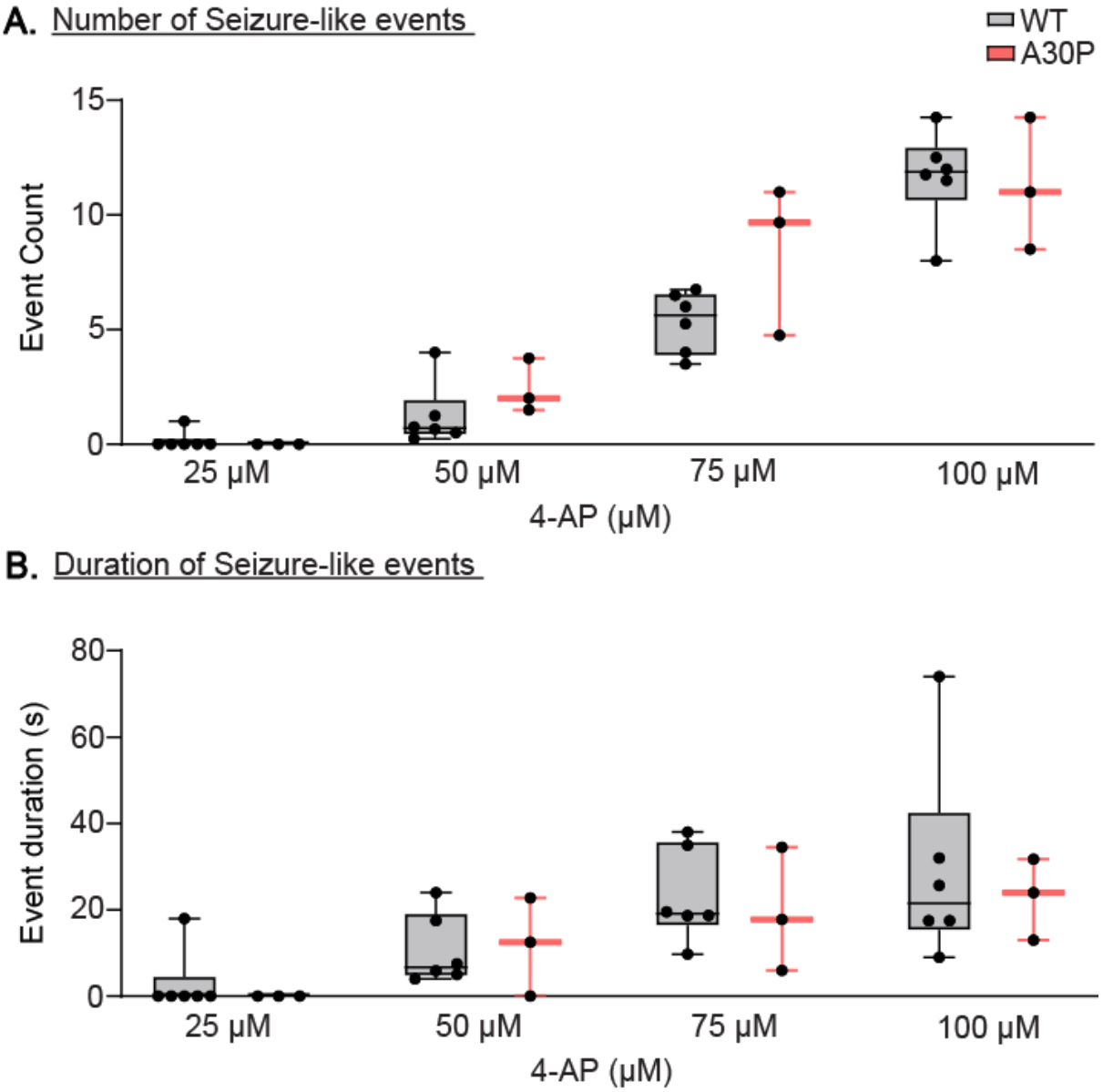

Figure 4.9. Seizure-like activity in the ACC in A30P and WT mice following 50 µM, 75 µM and 100 µM 4-AP. A. The median count of seizure-like events in the ACC slices is shown between the WT (grey) and A30P (red) animals during the different 4-AP concentrations. Each data point represents the median count of events from all slices per animal. **B.** The median event duration (seconds) of seizure-like events is demonstrated for the ACC of WT and A30P mice during each 4-AP concentration. Each data point represents the median duration of all seizure-like events from all slices per animal.

PV, PNN and c-Fos expression in the ACC of young A30P and WT mice following 4-AP

We compared PV, PNN, and c-Fos expression in the ACC between young A30P and WT mice after 4-AP exposure. Slices were fixed following the experiments of 1 hour of 4-AP incubation. PV expression in interneurons, WFA expression in PNNs, and global c-Fos expression were confirmed in the 4-AP-exposed ACC sections in both genotypes (Fig. 4.10). No statistically significant differences were found in either the median % area or intensity between A30P and WT mice (Fig. 4.10Bi and ii, % area: WT 4.26% (1.08, 18.49) vs A30P 3.17% (-2.35, 13.7), intensity: WT 99.5 a.u. (89.54, 107.6) vs A30P 100 a.u. (95.77, 106.6), $p > 0.05$, Mann-Whitney, WT N = 4 mice/n = 8 slices, A30P N = 3 mice/ n = 6 slices).

The median % area and intensity of WFA+ PNN expression in the 4-AP-exposed ACC sections showed no statistically significant differences between the two genotypes (Fig. 4.10Ci and ii, % area: WT 0.115% (0, 0.29) vs A30P 0.13% (-0.2, 0.75), intensity: WT 59.67 a.u. (42.42, 66.7) vs A30P 59.69 a.u. (58.39, 60.34), $p > 0.05$, Mann-Whitney, WT N = 4 mice/n = 8 slices, A30P N = 3 mice/ n = 6 slices).

The global c-Fos expression in all cell types in the ACC sections was analysed to assess changes associated with 4-AP-induced hyperexcitability. While no statistically significant differences were found between young A30P and WT mice, there was a trend toward increased median % area and count of c-Fos expression in A30P mice (Fig. 4.10Di and ii, % area: WT 1.62% (0.68, 2.71) vs A30P 2.20% (0.24, 4.18), count: WT 41.5 (16.57, 66.93) vs A30P 49.17 (2.09, 102), $p > 0.05$, Mann-Whitney, WT N = 4 mice/n = 8 slices, A30P N = 3 mice/ n = 6 slices).

Overall, the A30P slices showed a trend toward reduced PV % area and a trend towards increased global c-Fos expression following 4-AP. PV interneurons surrounded by PNNs were observed, but these interactions will be explored in Chapter 5.

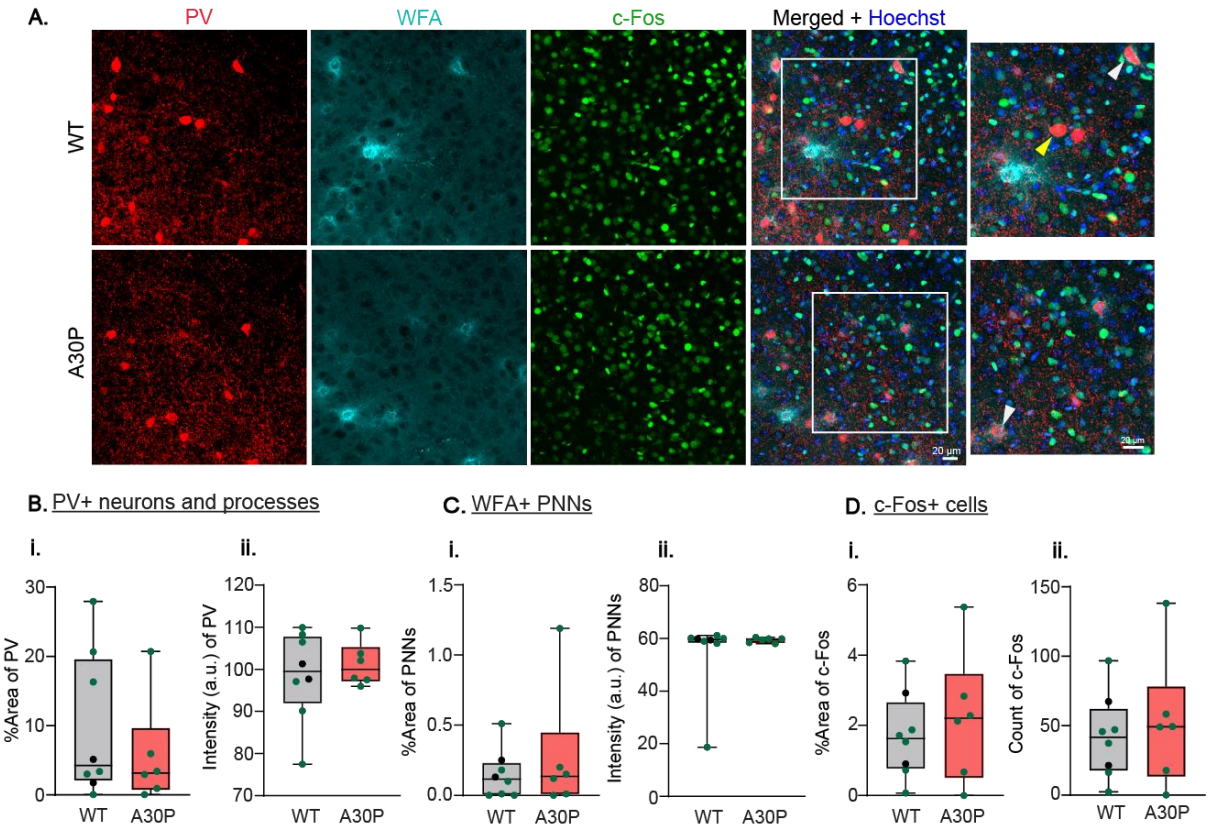

Figure 4.10. PV neurons and processes and PNNs in the ACC of 4-AP-exposed sections taken from young A30P and WT mice. These are collapsed z-stacks at 40x magnification taken from the deep ACC layers. **A.** The expression of PV including neuronal somas and processes (red), WFA+ PNNs (cyan), c-Fos+ cells (green) and all nuclei (Hoechst, blue) in the ACC of 4-AP-exposed WT and A30P ACC sections. The arrowheads in the enlarged view of the merged image show some PV somas surrounded by PNNs (white arrows) and not surrounded by PNNs (yellow arrow). **B - D.** The median (**i**) % area and (**ii**) intensity (a.u.; arbitrary units) or count of (**B**) PV, (**C**) PNN and (**D**) c-Fos expression are shown for the ACC in WT (grey) and A30P (red) sections are shown. Each data point represents the median values per ACC slice across the superficial and deep layers, with male mice in black and female mice in green.

Neuroinflammation markers in the ACC of young A30P and WT mice following 4-AP

Iba-1+ microglia and GFAP+ reactive astrocytes were assessed in 4-AP-exposed slices from young A30P and WT mice. Chapter 3.4.3 showed no changes in microglia or astrocytes in WT ACC after 75 µM 4-AP. Here, concentration-dependent effects of 4-AP were examined and compared between A30P and WT mice, which had not been previously analysed.

Iba-1+ microglia and GFAP+ astrocytes were detected in the ACC of 4-AP-exposed sections from both A30P and WT mice (Fig. 4.11A). No statistically significant differences were found between the two genotypes in either the median % area or intensity of Iba-1+ microglia. There was, though, a trend towards increased Iba-1 expression in the young A30P mice observed (Fig. 4.11Bi and ii, % area: WT 1% (-0.27, 3.69) vs A30P 2.07% (1.33, 3.03), intensity: WT 126.5 a.u. (121, 135.1) vs A30P 131 a.u. (125.2, 135.7), $p > 0.05$, Mann-Whitney, WT: N = 4 mice /n = 6 slices, A30P: N = 3 mice/n = 8 slices).

A trend towards an increased median % area of GFAP expression was shown in the A30P mice. Additionally, there was a statistically significant increase in median GFAP intensity in the 4-AP-exposed ACC sections of A30P mice compared to the WT (Fig. 4.11Ci and ii, % area: WT 0.50% (-0.25, 2.84) vs A30P 0.80% (0.80, 1.54), $p > 0.05$, intensity: WT 121.9% (119.4, 125.1) vs A30P 124% (122.7, 126.2), $p < 0.05$, Mann-Whitney, WT: N = 4 mice /n = 6 slices, A30P: N = 3 mice/n = 8 slices).

Overall, no significant changes in the % area of Iba-1+ microglia or GFAP+ astrocytes were found in the ACC between young A30P and WT mice after 4-AP-induced hyperexcitability. However, a trend towards increased Iba-1 and GFAP % area was observed in A30P mice, along with a significant increase in GFAP expression, possibly suggesting heightened astrocytic activation compared to WT.

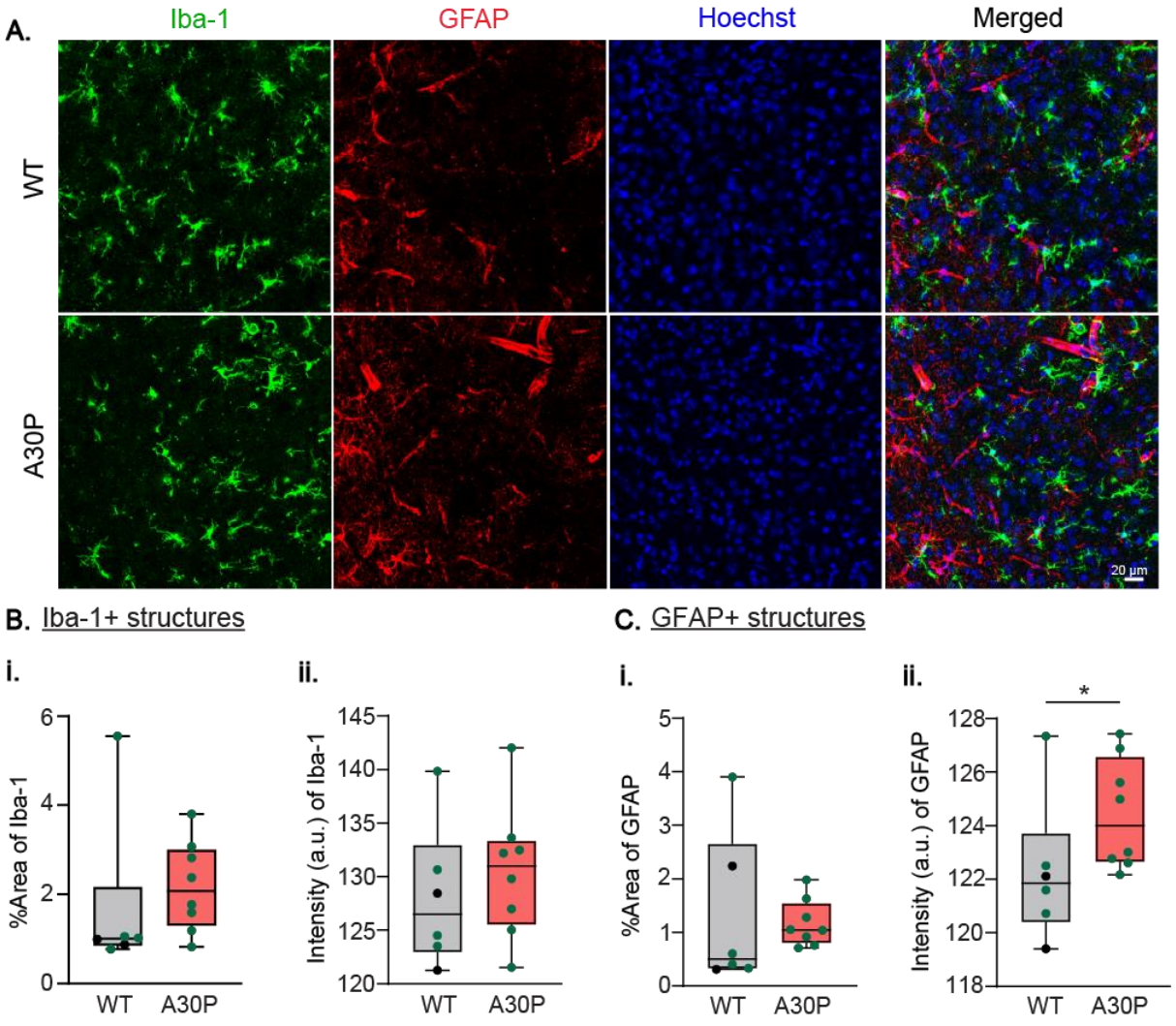

Figure 4.11. Microglia and reactive astrocytes in the ACC of 4-AP-exposed sections taken from young A30P and WT mice. These are collapsed z-stacks at 40x magnification taken from the deep ACC layers. **A.** The expression of all Iba-1+ structures, including microglia (green), GFAP+ reactive astrocytes (red) and all nuclei (Hoechst, blue) in the ACC of 4-AP-exposed sections in the WT and A30P mice is shown. Scale bar at 20 µm. **B - C.** The median (**i**) % area and (**ii**) intensity (a.u.) of (**B**) Iba-1 and (**C**) GFAP expression are shown for the 4-AP-exposed ACC in WT (grey) and A30P (red) sections. Each data point represents the median values per ACC slice across the superficial and deep layers, with male mice in black and female mice in green.

4.5. Discussion

4.5.1. *Summary of the main findings in Chapter 4.*

- Fast gamma KA-evoked oscillations were observed in the deep ACC layers of both young A30P and WT mice, with no significant differences in area power, peak amplitude, or frequency, though A30P mice showed a trend towards higher peak frequency.
- Simple IIDs appeared in ACC in both genotypes during all gabazine concentrations, with A30P mice showing more complex IIDs at 500 nM gabazine and seizure-like events in both genotypes after 20 µM gabazine.
- Seizure-like events occurred at 50 µM 4-AP in both A30P and WT ACC, with no significant differences in count or duration between genotypes, though events increased in both WT and A30P mice over time.
- A trend towards a lower % area of PV and higher global c-Fos expression was seen in 4-AP-exposed ACC slices of A30P mice compared to WT.
- No significant change in Iba-1+ microglia expression was found, but GFAP expression of reactive astrocytes significantly increased in A30P ACC slices after 4-AP-induced hyperexcitability.

4.5.2. *Fast gamma KA-evoked oscillations in the deep layers of mouse ACC but no differences between young pre-symptomatic A30P and WT.*

Theta, beta, and gamma frequency oscillations have been observed in the rodent ACC *in vitro* (Steullet *et al.*, 2014; Adams *et al.*, 2017; Dennis *et al.*, 2023) and *in vivo* (Ye *et al.*, 2023) and have been associated with cognitive functions. Studies have demonstrated that beta and gamma frequency oscillations in the ACC in mice (Steullet *et al.*, 2014) and rats (Adams *et al.*, 2017; Dennis *et al.*, 2023; Ye *et al.*, 2023) were evoked by KA. KA is an agonist activating the glutamatergic KA-Rs and binds with higher affinity than glutamate leading to stronger or more prolonged excitatory effects, with potential implications for both normal and pathological brain function (Falcón-Moya *et al.*, 2018; Lauri *et al.*, 2021; Chałupnik and Szymańska, 2023). KA-Rs are found both pre- and post-synaptically in various regions of the CNS, including

the cortex and hippocampus, where they are present on principal neurons such as pyramidal cells and inhibitory interneurons. These receptors when activated by KA modulate both glutamatergic and GABAergic synaptic transmission (Rodriguez-Moreno *et al*., 2000; Ali *et al.*, 2001; Christensen *et al.*, 2004; Jin and Smith, 2011; Chałupnik and Szymańska, 2023). Activation of KA-Rs on pyramidal neurons results in increased glutamatergic transmission contributing to the excitatory drive which is important in the generation of network oscillations (Whittington *et al*., 1995; Lauri *et al.*, 2006, 2021; Bartos *et al*., 2007; Vesikansa *et al.*, 2007; Gonzalez-Burgos and Lewis, 2008). Additionally, activation of KA-Rs on GABAergic interneurons leads to an increased release of GABA, which acts on $GABA_A$-Rs on both pyramidal neurons and inhibitory interneurons modulating network synchrony (Rodríguez-Moreno *et al*., 1997; Frerking *et al*., 1999; Mulle *et al.*, 2000; Ali *et al.*, 2001; Cossart *et al.*, 2001; Ren *et al.*, 2007; Mathew *et al*., 2008). The dual activation of KA-Rs and $GABA_A$-Rs leads to both excitatory and inhibitory effects in the network. In the ACC, the network oscillatory activity in the beta and gamma frequency range relies on both $GABA_A$ and glutamatergic AMPA receptors (Steullet *et al.*, 2014). Thus, the KA-evoked activation of interconnected pyramidal neurons and fast-spiking interneurons results in synchronised oscillations (Whittington *et al.*, 2011).

The number of studies investigating fast oscillatory activity evoked by KA in the ACC in mice is very limited. Oscillatory activity in the ACC in the A30P transgenic mice has not previously been examined. Therefore, in this chapter, we investigated KA-evoked fast oscillations in the ACC of young (2 - 4 months) pre-symptomatic A30P mice and compared them to young WT mice, aiming to determine whether early neuronal network impairments occur in the deep layers of the ACC in pre-symptomatic A30P mice. However, no differences were observed in the area power, peak amplitude, or peak frequency of the 15 – 90 Hz oscillations between the two genotypes. Similar findings were reported in the hippocampus of young A30P mice, where no differences in the power of carbachol (cholinergic agonist)-evoked gamma (20 – 80 Hz) oscillations were found compared to WT mice (Robson *et al.*, 2018). Conversely, another study found increased area power in KA-evoked fast gamma oscillations in the hippocampus of young pre-symptomatic A30P mice compared to WT (Tweedy *et al.*, 2021). Additionally, a higher concentration of KA (800 nM) was required to evoke fast oscillatory activity in the mouse ACC, similar to the rat ACC

(Adams *et al.*, 2017; Dennis *et al.*, 2023), compared to the hippocampus, where 100 nM KA is typically sufficient (Tweedy *et al.*, 2021). Therefore, these findings might suggest that hippocampal neuronal networks generate bigger fast frequency oscillations evoked by KA than the ACC with an increased area power between the young A30P and WT mice which was not evident in our experiments.

Tweedy et al. (2021) showed hyperexcitability, including IIDs, in CA3 hippocampal networks in the young 2-5-month-old A30P mice induced by high concentrations of KA (150 nM and 200 nM) suggesting an association with the hα-syn pathology occurring at early stages in disease progression (Tweedy *et al.*, 2021). However, even though we used a higher KA concentration, we did not observe KA-evoked network hyperexcitability in the deep layers of ACC in the young A30P mice underlying the difference in neuronal networks between brain areas in this transgenic mouse model. These data, therefore, suggest that ACC may be less susceptible than the hippocampus to hα-syn-induced excitability changes in the young A30P mice.

4.5.3. *Gabazine concentration-dependent effects on neuronal network activity in the deep layers of ACC in young A30P mice.*

GABAergic signalling is critical in regulating balanced levels between excitation and inhibition and in synchronising neuronal network activity (Buzsáki and Draguhn, 2004; Pavlov *et al.*, 2009; Griguoli and Cherubini, 2017). Dysfunctions in GABAergic neurotransmission lead to hyperexcitability and epileptic activity (Dichter and Ayala, 1987; Galarreta and Hestrin, 1998; Nelson and Turrigiano, 1998; Timofeev *et al.*, 2004). GABAergic dysfunction is one of the hallmarks of neurodegeneration. Fundamental post-mortem investigations on AD patients revealed decreased GABA concentrations in different brain areas including the hippocampus, amygdala and cingulate cortex (Rossor *et al.*, 1982; Ellison *et al.*, 1986; Sasaki *et al.*, 1986; Perry *et al.*, 1987). Evidence in AD animal models showed an early decrease in GABAergic interneurons in the hippocampus causing hyperexcitability (Ramos *et al.*, 2006; Levenga *et al.*, 2014; Najm *et al.*, 2019). Early-stage PD patients also demonstrated GABAergic dysfunction during PET scans in putamen and frontal cortex (Takashima *et al.*, 2022). Decreased GABAergic neurotransmission has been observed in the primary visual cortex of DLB patients related to recurrent complex visual hallucinations

(Khundakar *et al.*, 2016). However, whether there are dysfunctions in GABAergic neurotransmission leading to excess excitability in the ACC in the early stages of DLB is unknown.

This chapter examined hyperexcitability in the ACC of young pre-symptomatic A30P mice by disrupting GABAergic signalling. To alter the E/I balance, I applied gabazine, a competitive antagonist of GABA neurotransmitter that binds to $GABA_A$-Rs and blocks inhibitory GABAergic transmission (Johnston, 1996; Ueno *et al.*, 1997). My results revealed that young A30P mice exhibited a clear shift from simple to complex IIDs evoked by gabazine indicating enhanced network excitability. The observed shift towards complex IIDs and increased excitation in pre-symptomatic A30P mice following gabazine supports the hypothesis of impaired GABAergic control or increased excitation linked to hα-syn pathology.

As seen in the hippocampus of young A30P and WT mice, IIDs were observed following 250 nM and 500 nM gabazine, the ACC also showed IIDs at similar gabazine concentrations (Tweedy *et al.*, 2021). The IIDs were seen during 250 nM gabazine but the A30P mice showed a greater increase in overall IID activity (including both simple and complex IID) after 500 nM gabazine than the WT (Tweedy *et al.*, 2021). This pattern of gabazine-induced hyperexcitability has also been reported in AD mouse models (Busche and Konnerth, 2016; Petrache *et al.*, 2019). However, gabazine-evoked IIDs have not previously been examined in the mouse ACC, particularly in A30P mice. Our findings, therefore, reveal an increase in gabazine-induced IIDs but not seizure-like events in the ACC of young A30P mice, potentially linked to hα-syn overexpression. The higher count of complex IIDs in A30P mice suggests an overall increase in network excitability in the ACC compared to WT, which has not been previously reported.

4.5.4. *4-AP induced seizure-like activity and a trend in decreased PV expression and significantly increased GFAP expression in the ACC of young A30P mice.*

Hyperexcitability including IIDs leading to the generation of seizure-like activity has been previously seen in the ACC in rats *in vitro*, but not in the mouse ACC (Panuccio *et al.*, 2009). In Chapter 3, we showed that 75 µM 4-AP induced simple and complex IIDs as well as seizure-like activity in the deep layers of ACC of young WT mice after a 3-hour incubation. Here, we aimed to determine whether the deep layers of the ACC in young pre-symptomatic A30P mice would exhibit greater 4-AP-induced hyperexcitability compared to WT mice. To assess this, increasing concentrations of 4-AP were applied to ACC slices *in vitro*, over a shorter 1-hour period, allowing us to examine concentration-dependent effects on neuronal network activity in 2-4-month-old A30P and WT mice. Seizure-like events were observed following 50 µM 4-AP in both genotypes.

The difference in incubation times between Chapter 3 (3 hours) and the experiments in this chapter (1 hour) could have significantly affected the dynamics of hyperexcitability. Prolonged exposure in Chapter 3 may have allowed for a more extensive disruption of inhibitory circuits and a progressive build-up of hyperexcitability. In contrast, the shorter, stepwise approach here, in Chapter 4, with increasing concentrations, might not have fully exposed potential differences in the circuitry's long-term responses. Extending the duration of these concentration-dependent experiments might further elucidate differences in synaptic and network excitability between young A30P and WT mice, which were hinted at by the trend toward greater excitability in A30P mice at lower concentrations.

PV, PNN and c-Fos expression following 4-AP-induced hyperexcitability

Research suggests that 4-AP-evoked hyperexcitability is generated from both excitatory neurons and inhibitory interneurons (Shiri *et al.*, 2015; Yekhlef *et al.*, 2015; Chang *et al.*, 2018; Codadu *et al.*, 2019). 4-AP inhibits Kv1 potassium channels, which are important in repolarising neurons after an action potential. When Kv1 channels are

blocked, neurons have a reduced ability to return to their resting membrane potential, leading to prolonged depolarisation. This prolonged depolarisation increases excitatory neurotransmitter release and, crucially, facilitates the depolarisation of nearby neurons within the network, as excitatory signals are sustained for longer periods and spread more easily through synaptic connections (Armstrong and Loboda, 2001; Pathak *et al*., 2016).

Evidence shows that stimulation of PV interneurons is involved in the interictal and preictal spikes following 4-AP application *in vitro* leading to seizure-like events (Yekhlef *et al.*, 2015). The excitability of PV interneurons is controlled by their surrounding PNNs, which are critical in the regulation of PV neuronal activity and integration of their synaptic contacts (Chaunsali *et al*., 2021). PNNs regulate PV neuronal activity by stabilising synaptic inputs and limiting synaptic plasticity, thus maintaining the balance of excitatory and inhibitory signals. This ensures the optimal function of PV interneurons in controlling network activity and modulating neuronal circuits (Favuzzi *et al.*, 2017; Hayani *et al*., 2018; Cisneros-Franco and De Villers-Sidani, 2019).

Earlier, we showed a significant increase in the PV expression and a trend towards increased in global c-Fos expression in the ACC of 4-AP-exposed slices of young WT mice compared to the ACSF-exposed slices (Chapter 3.4.2). However, these results were shown following the incubation of ACC slices in 75 µM 4-AP and obtained only from young WT mice. Therefore, we further examined changes in PV, PNN and c-Fos expression in all cell types following 4-AP-induced hyperexcitability in the ACC between young pre-symptomatic A30P and WT mice. In these experiments, slices were fixed 30 minutes after reaching the maximal concentration of 100 µM 4-AP so the conditions were slightly different. We found a trend towards decreased % area of PV expression in the A30P mice compared to the WT. This is interesting as an increased PV expression, associated with increased calcium activity, following 4-AP was expected to be observed in the A30P mice which tend to be more hyperexcitable than the WT (Tweedy *et al.*, 2021). On the other hand, this trend in decreased PV expression in the ACC of young A30P mice might imply compensatory mechanisms to counterbalance increased excitability evoked by 4-AP.

A trend towards increased global c-Fos expression was also observed in the ACC of young A30P mice following 4-AP-induced hyperexcitability compared to the WT suggesting increased neuronal network activity. It is known that there is c-Fos accumulation in the neuronal nucleus under hyperexcitable conditions (Zhang *et al.*, 2002; Shimojo *et al.*, 2020b). Studies have also shown increased c-Fos expression following seizure activity in the rodent mPFC including the cingulate cortex (Morgan *et al.*, 1987; Yang *et al.*, 2019; Akdağ *et al.*, 2023). We previously demonstrated a non-significant increase in the c-Fos expression following 4-AP in the ACC of WT animals which might have been correlated with the increased PV expression (Chapter 3.4.2). We did not find any significant differences in the % area and intensity of PNNs in the ACC between A30P and WT mice following 4-AP-induced hyperexcitability from our analysis. However, potential structural changes in PNNs require a more detailed investigation.

Microglia and reactive astrocytic expression following 4-AP

Evidence shows that increased neuroinflammation contributes to the generation of hyperexcitability in neurodegenerative disorders (Devinsky *et al.*, 2013; Pracucci *et al.*, 2021; Vicente *et al*., 2024). A relationship between microglial activation and astrocytic activation is also suggested to increase seizure susceptibility (Sano *et al.*, 2021). There are no studies showing changes in neuroinflammation including microglia and astrocytes implicated in hyperexcitability in the mouse ACC in DLB. Thus, we assessed whether there were any effects of 4-AP-induced hyperexcitability on the Iba-1 and GFAP expression in the ACC between young A30P and WT mice.

A trend towards increased Iba-1 expression and a statistically significant increase in GFAP intensity was observed in the ACC of young A30P mice following 4-AP exposure, compared to WT. This neuroinflammatory response was not seen in the earlier examination of 4-AP-exposed and ACSF-exposed ACC slices of young WT mice (Chapter 3.4.3). These findings suggest a potential increase in microgliosis and reactive astrogliosis in the ACC of young pre-symptomatic A30P mice, possibly linked to hα-syn pathology contributing to hyperexcitability. Notably, GFAP+ astrocytes in the ACC of A30P mice showed a more ramified morphology with more processes compared to the astrocytes in the WT mice after 1-hour 4-AP exposure, suggesting a

more reactive state. Astrocytes may be particularly sensitive to 4-AP-induced changes, as fluctuations in intracellular potassium and calcium levels can affect their voltage-gated potassium and calcium channels (Wu *et al.*, 2009; Kasatkina, 2016). However, more investigations are needed to elucidate whether there are any changes in Iba-1+ microglia and GFAP+ astrocytes under non-epileptic conditions in the ACC of young A30P mice. This question will also be investigated in this thesis (see Chapter 6).

Overall, we observed that seizure-like activity induced by 4-AP led to a trend towards decreased PV expression and an increase in neuroinflammatory markers in the ACC of young A30P mice compared to the WT. The lower PV expression might underlie subtle dysfunction in PV interneurons in the young pre-symptomatic A30P mice. Even though there was an increase in the Iba-1 and GFAP expression in the A30P mice, no differences in seizure-like activity were detected between the two genotypes. It is possible that a longer 4-AP exposure may be required to reveal significant changes in Iba-1 and GFAP expression, indicating enhanced microgliosis and astrogliosis, which could contribute to increased hyperexcitability in A30P mice.

4.6. Conclusions

Overall, the results in Chapter 4 showed that fast gamma frequency oscillations, as well as mixed beta and gamma frequency oscillations, could be evoked by KA in the deep layers of the ACC. However, there were no differences in the oscillation power, peak amplitude, or peak frequency between the two genotypes. Hyperexcitability was generated by gabazine and 4-AP in the ACC in both genotypes. The A30P mice showed a shift from simple IIDs to complex IIDs following gabazine, suggesting a potential increase in network excitability associated with hα-syn. We also found no differences in the 4-AP-evoked seizure-like activity between A30P and WT mice. The 4-AP-induced hyperexcitability, however, led to a trend towards a decrease in PV expression and an increase in global c-Fos expression in the ACC of A30P mice. Additionally, there was a potential increase in glial cell expression including microglia and reactive astrocytes in the A30P mice following 4-AP compared to the WT. These changes observed in the young A30P animals during the induced epileptic conditions could be, therefore, associated with hα-syn upregulation and a susceptibility to increased hyperexcitability.

Chapter 5. PV interneurons and PNNs in the ACC of young pre-symptomatic and aged A30P mice.

5.1. Introduction

PV-expressing interneurons are critical for cognitive functions, including learning, memory, and planning (Tremblay *et al*., 2016). PNNs surround most cortical PV interneurons, though the number of PNNs varies across different brain regions (Ueno *et al.*, 2017). While PNNs primarily surround PV interneurons, they also surround some excitatory neurons sparsely in the cortex (Carceller *et al.*, 2022). The formation of PNNs around PV interneurons limits further plasticity by stabilising the neuronal synapses surrounding the cell (Chaunsali *et al*., 2021). These PNNs are essential for maintaining PV interneuron function and preserving the E/I balance within neural networks (Carceller *et al.*, 2020). Removing PNNs has been shown to lower input resistance, resting membrane potential, and action potential peaks in fast-spiking PV interneurons (Chu *et al.*, 2018).

The ECM concentration and structure of PNNs are affected by age, which also impacts the function and density of PV interneurons. In the PFC of 12-month-old mice, both PNN and PV interneuron numbers increase compared to those in 2-month-old mice, contributing to reduced plasticity (Ueno *et al.*, 2018). Increased PNN levels suggest a decrease in synaptic plasticity, as PNNs prevent the formation of new synaptic connections and the modification of existing ones (Sorg *et al.*, 2016; Ueno *et al.*, 2018). While ageing affects PNN and PV interneuron function, neurodegeneration also disrupts PNNs, contributing to cognitive decline. In disorders like AD (Suttkus *et al.*, 2016; Crapser, Spangenberg, *et al.*, 2020), PD (Suttkus *et al.*, 2012, 2016; Sancandi *et al.*, 2018), and HD (Crapser, Ochaba, *et al.*, 2020), PNN degradation correlates with cognitive impairments (Reichelt, 2020; Pintér and Alpár, 2022). Post-mortem examinations in AD patients show decreased PNNs, with neurons exhibiting tau pathology and neurofibrillary tangles notably lacking PNN coverage (Wen *et al.*, 2018). This evidence suggests that PNNs may protect certain neurons against oxidative stress and neurodegeneration.

The impact of pathological α-syn on PV interneurons and PNNs remains poorly understood. A significant reduction in PV neuronal density has been shown in the hippocampus of DLB post-mortem cases compared to controls, suggesting α-syn

pathology may affect these cells (Bernstein *et al.*, 2011). Although α-syn aggregates primarily in excitatory neurons, it may indirectly affect inhibitory interneurons through excitatory synaptic interactions (Ghiglieri *et al*., 2018; Calabresi *et al.*, 2023). In mouse hippocampal cultures, α-syn is predominantly found in the presynaptic terminals of excitatory neurons and weakly expressed in GAD+ inhibitory interneurons (Taguchi *et al.*, 2014). Previous work in our lab indicated that human α-syn was present in the somas of about 25% of PV interneurons in the hippocampus of young A30P mice, though no significant changes in PV expression intensity were observed (Tweedy *et al.*, 2021). In PD, excess PNN components have been shown to enhance α-syn pathology by promoting α-syn deposition (Huynh *et al.*, 2019; Pintér and Alpár, 2022). Specifically, increased amounts of the PNN component GAGs, which are proteoglycan side chains, can exacerbate α-syn pathology through factors like polymer length, α-syn ratio, charge density, and sulphate group orientation (Mehra *et al.*, 2018). To date, there are no detailed studies on whether PNNs protect PV interneurons in the ACC from α-syn pathology, making this an important are to investigate in this thesis.

In this chapter, we will investigate potential changes in the count and expression of PV interneurons and PNNs, along with their association, in the ACC of both young pre-symptomatic and aged A30P mice compared to the age-matched WT controls. We will also assess the laminar distribution of PV interneurons and PNNs in the superficial and deep layers of the ACC. To explore the potential neuroprotective role of PNNs against hα-syn pathology, as they are implicated in neurodegenerative processes, we will examine whether hα-syn co-localises to the soma of PV interneurons and their surrounding PNNs in both young and aged A30P mice. This analysis aims to elucidate age- and pathology-related shifts in the ACC neuronal networks that may contribute to neurodegenerative vulnerability starting from pre-symptomatic disease stages.

5.2. Aims

- To investigate the number and degree of co-localisation of PV interneurons and PNNs in the ACC of young and aged A30P and WT mice.

- To assess whether hα-syn is present in PV interneurons and PNNs in the ACC of young and aged A30P mice.

5.3. Methods

5.3.1. *Free-floating IHC-Immunofluorescence*

Fixed mouse brains were sectioned in 40 µm sections as described in Chapter 2.3.2. The sections used in IHC experiments were chosen from specific ACC locations including plates 21 - 30 according to plates 21 - 30 from Paxinos and Franklin mouse brain atlas, 2001 (Fig. 2.1). For all experiments 5 A30P and 5 age-matched WT male mice were selected for two different age groups: 1) young animals 2 - 4 months-old and 2) aged animals 10 - 12 months-old. The IHC protocol was carried out as described in Chapter 2.3.2 with the primary-secondary antibody and lectin-avidin combinations as shown in Table 5.1. To stain for the hα-syn, we used an antibody which binds onto the mutated hα-syn in the A30P mice instead of the endogenous murine α-syn. Three ACC sections, and one hemisphere per section, were analysed for each animal (N = 5 mice for each WT or A30P group/ n = 3 sections per animal).

Staining Combination	
Primary Antibody/Lectin	**Secondary Antibody/Avidin**
Mouse anti-PV	Donkey anti-mouse Alexa Fluor 568
Biotinylated WFA lectin	Streptavidin fluorescein (498)
Rat anti-α-synuclein (hα-syn)	Donkey anti-rat Alexa Fluor 647

Table 5.1. Primary and secondary antibody as well as lectin-avidin combinations used for this chapter.

5.3.2. *Data analysis using Imaris software*

The ACC sections were imaged under the Leica SP8 DLS confocal microscope using the 3-z-stack box method (40x magnification) as described in Chapter 2.3.3. ROIs 1 and 3 were combined for the analysis of the superficial layers of ACC and ROI 2 for the deep layers.

The images were analysed using the Imaris software for a 3D analysis as described in Chapter 2.3.4. Surface masks were created for each channel including

PV somas (green), PNNs (cyan) and Hoechst+ nuclei (blue) as well as a spot mask for hα-syn (red). Only PV somas and PNNs which had nuclei were analysed (Fig. 5.1). For the PV soma surface mask, any parts of proximal dendrites were removed for the accurate analysis of the soma. An additional surface mask was created to analyse the total PV neuronal signal including the PV somas and processes. Also, for the PNN surface mask, each PNN was manually differentiated if located within a group of PNNs following mask generation. Masks for co-localisation combinations were also created for 1) PV somas with PNNs, 2) hα-syn in PV somas, 3) hα-syn in PNNs, 4) hα-syn in PV nuclei and 5) hα-syn in all nuclei.

The co-localisation combinations of PV somas with PNNs and Hoechst with PV somas were done using the “Shortest distance to surfaces-surfaces” filter set at 0 µm (Fig 5.2). Also, the co-localisations of hα-syn with PV somas, PNNs and Hoechst were performed using the MATLAB tool “Find Spots close to Surface” and the shortest distance of hα-syn mask was set at 0 µm (Fig. 5.3). This allowed analysis of the hα-syn that touched, but also was found inside, the object of interest. The average count, volume and intensity were analysed accordingly for each variable.

5.3.3. *Statistical analysis*

If data were normally distributed, they are plotted as mean +/- SEM and parametric t-tests or two-way ANOVA are used. Much of the data, however, were non-parametric so plotted as box plots with median and IQR. Paired statistical comparisons were performed with the Mann-Whitney U test. Some data were log-transformed to normalise the data and two-way ANOVAs were performed when data were normally distributed. Post hoc comparisons were then made using Fisher’s LSD test.

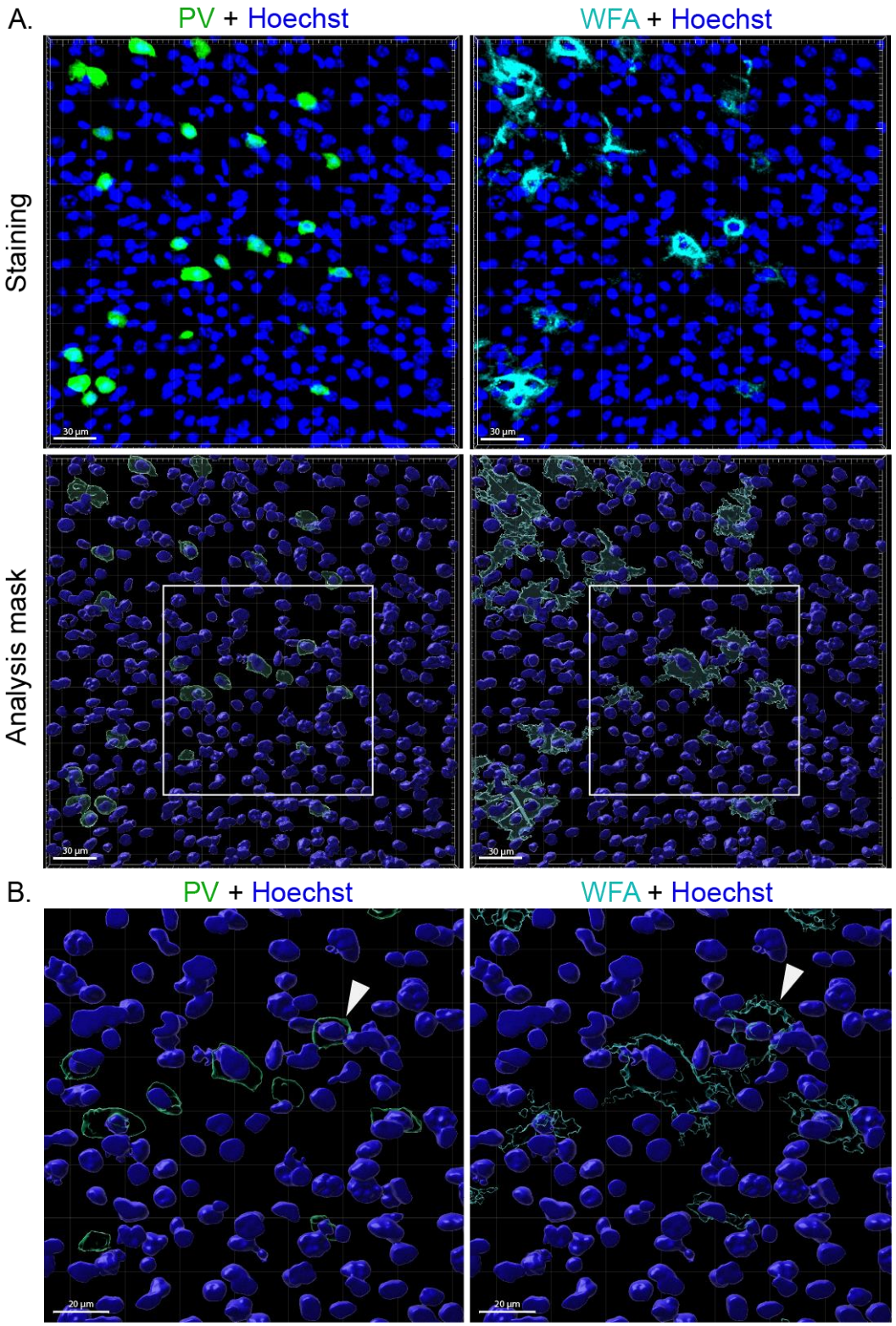

Figure 5.1. Selection of PV somas and PNNs for analysis. The (**A**) whole and (**B**) enlarged views of staining and analysis mask images are shown on Imaris for the PV somas (green) and PNNs (cyan) co-localising with Hoechst+ nuclei (blue) are shown. Only the PV+ somas and PNNs that had a clear nucleus inside were chosen for the analysis (examples shown with white arrowheads). Scale bars at 30 µm and 20 µm**.**

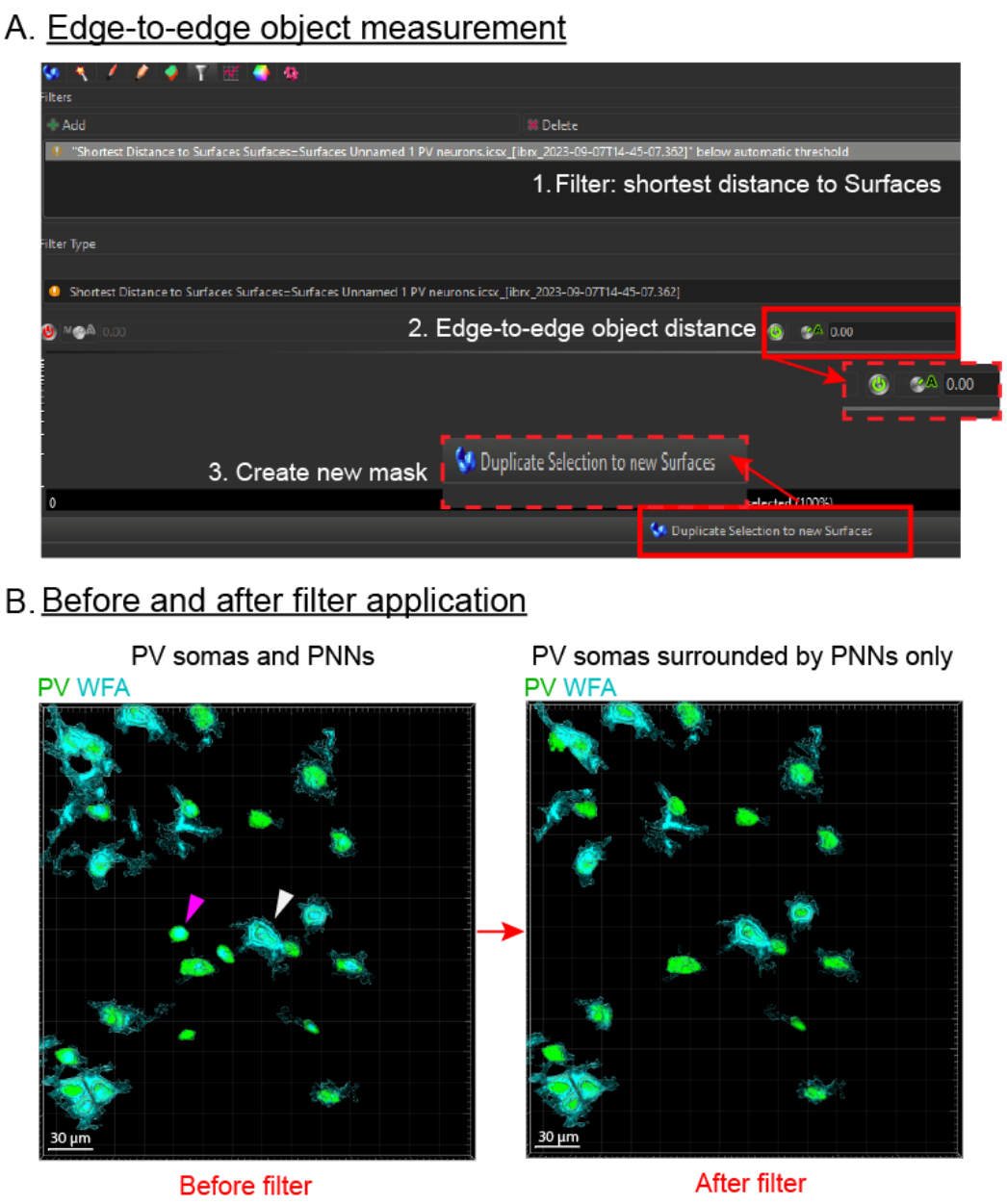

Figure 5.2. Co-localisation analysis method 1 using the "Shortest distance to surfaces" filter. A. The stepwise approach by applying the "shortest distance to surfaces" filter was used to examine PV somas (surface) co-localising with PNNs (surface) on Imaris. To select the PV somas that co-localised with PNNs, the distance of 0 µm is set as the edge-to-edge object measurement distance (boxed in red). The selected surfaces that co-localised were duplicated to create a new mask and analysed separately from the total PV somas and PNNs. The same filter was applied to find the PNNs co-localising with PV somas. **B.** On the left, all the PV somas (green) and PNNs (cyan) are shown before the filter application. There were PV somas without PNNs (pink arrow) and PV somas with PNNs (white arrow). On the right, following the filter application, only the PV somas with PNNs are shown. Scale bars at 30 µm.

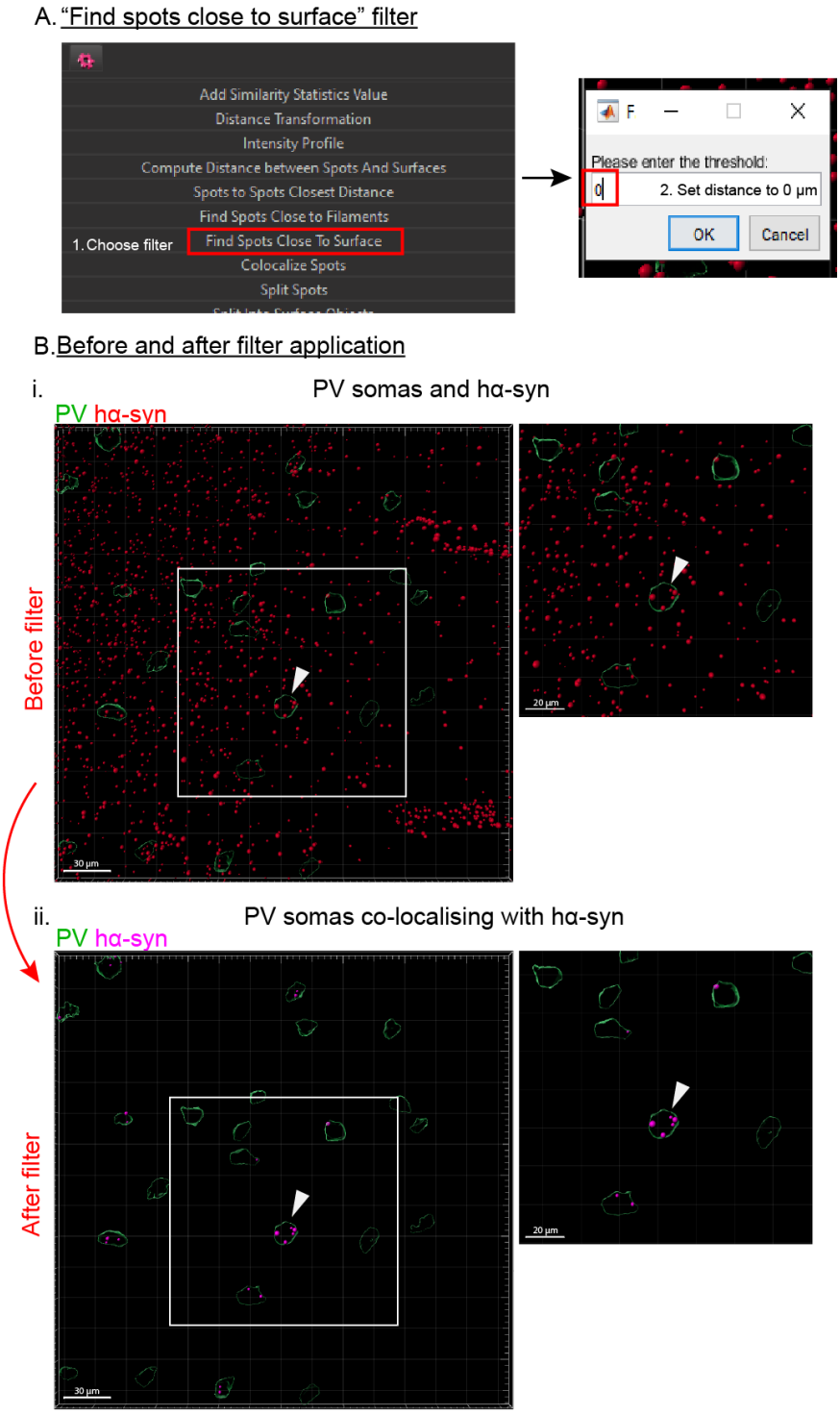

Figure 5.3. Co-localisation analysis method 2 using the "Find spots close to surface" filter. A. The "find spots close to surface" tool was used on Imaris to examine the hα-syn co-localising with the PV somas but also PNNs and Hoechst+ nuclei. The distance 0 µm was set to find the hα-syn (spots mask) that was within a distance of 0 µm and below in the surface of interest. **B.** From the (**i**) total hα-syn signal (spots, red) only the (**ii**) hα-syn that touched and was within the PV somas (surface, green) was selected and shown in pink after the filter application. The white arrows show an example PV soma co-localising with hα-syn. Scale bars at 30 and 20 µm.

5.4. Results

5.4.1. *Hα-syn expression and PV-expressing interneurons in the ACC of young A30P and WT mice*

While hα-syn aggregation in PV interneurons has been observed in the hippocampus of A30P mice (Tweedy *et al.*, 2021), its effects on PV interneurons and PNNs in the ACC, particularly in DLB, remain unclear. Here, we assess their interactions in A30P and WT mice across different ages.

Before investigating PV interneurons in the ACC, we first verified the hα-syn expression in the ACC of A30P mice, as this had not been previously examined. As expected, no hα-syn expression was detected in the WT (control) mice. In contrast, A30P mice showed marked hα-syn staining, with clear expression throughout the ACC and the broader cortex (Fig. 5.4). The staining pattern in the A30P mice was primarily intracellular, with hα-syn localised within neuronal somas, suggesting cytoplasmic accumulation which is typical of hα-syn aggregation, as seen in the magnified view in Figure 5.4B (white arrows). We also observed distinct hα-syn puncta within the neuropil which could reflect synaptic terminals where hα-syn may accumulate. This hα-syn cytoplasmic and punctate distribution is consistent with the intracellular aggregation seen in other synucleinopathies, indicating that hα-syn might affect both within neurons and across synaptic networks.

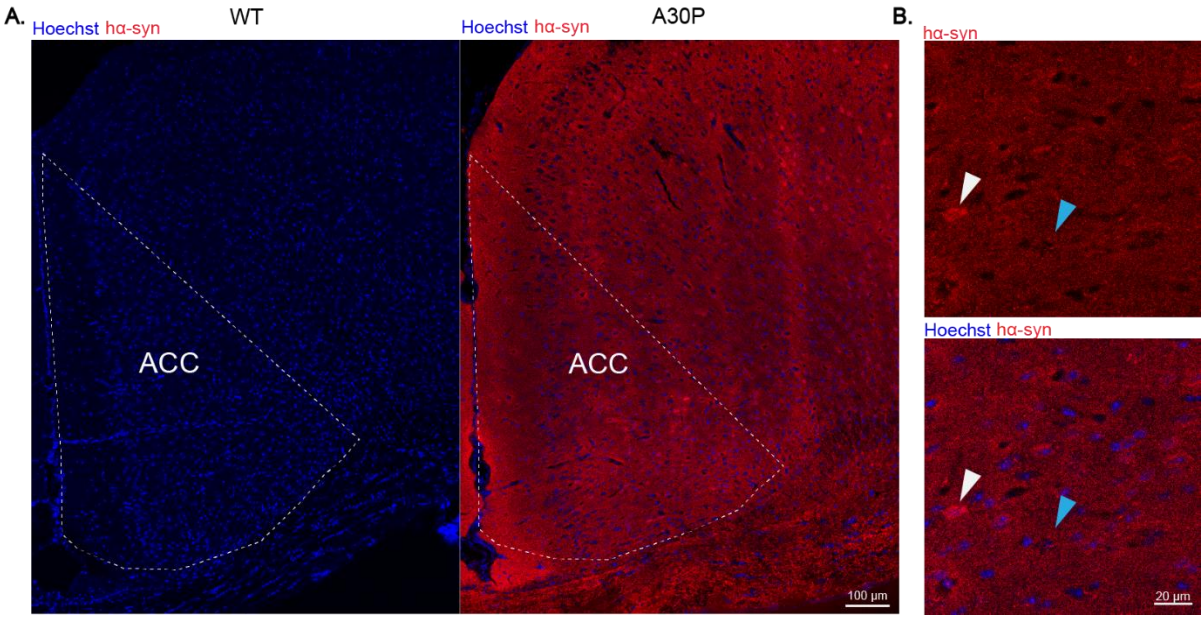

Figure 5.4. Expression of the hα-syn in the ACC of A30P and WT mice. A. Tile-scan (single z-plane) images of the ACC in an example WT mouse (left) without hα-syn expression, showing all Hoechst+ nuclei (blue), compared to an A30P mouse (right) with hα-syn expression (red). **B.** Magnified single z-plane images (maximum intensity projection) from the ACC of the A30P mouse, showing detailed hα-syn labelling (with and without Hoechst co-staining) indicating clustering within cells (white arrows) and synaptic terminals (blue arrows). Scale bars at 100 µm and 20 µm.

PV interneurons were sparsely distributed across all layers in the ACC with no laminar differences or obvious distribution patterns seen in the WT mice (Fig. 5.5). However, in the A30P mice, PV interneurons appeared to be mainly clustered in the deep layers of the ACC. Additionally, in Figure 5.5, the PV expression in the ACC of A30P mice was greatly decreased compared to the WT, but this was not observed in all A30P mice. The PV expression was measured and calculated in volume and total intensity of the PV interneurons, including somas and processes, in both young A30P and WT mice. The count, volume and intensity of PV somas only were also measured in both genotypes.

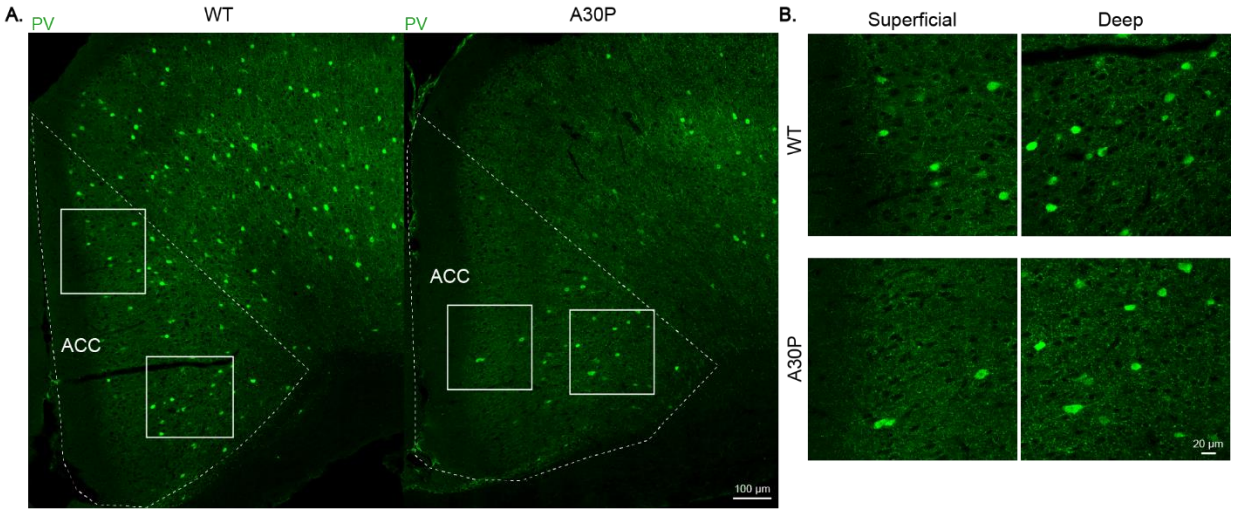

Figure 5.5. Expression of PV in the ACC of young A30P and WT mice. A. Tile-scan (single z-plane) images showing the PV-expressing interneurons and PV puncta in the ACC of an example WT (left) and an A30P (right) mouse. **B.** Magnified single z-plane images of the squared areas demonstrating the structure of the PV interneurons and synaptic interactions in more detail for the WT and A30P mice in superficial and deep ACC layers.

The median count, volume, and intensity for PV interneurons (including somas and processes) and PV somas only across all ACC sections were calculated and compared between young A30P and WT mice. In young A30P mice, there was a trend towards an increased median volume and intensity of PV interneurons compared to WT (Fig. 5.6Ai and ii, volume: WT 18,829 μm^3 (7,148, 33,674) vs A30P 21,780 μm^3 (8,780, 39,000), intensity: WT 16,912,947 a.u. (4,517,803, 36,586,492) vs A30P 20,301,234 a.u. (3,102,567, 46,458,052), $p > 0.05$, Mann-Whitney, N/n = 5/3). For PV somas, however, young A30P mice showed a trend towards a decreased median count, volume, and intensity compared to young WT (Fig. 5.6Ci and ii, count: WT 10.22 (8.04, 14.58) vs A30P 9.33 (7.64, 11.78), volume: WT 5,726 μm^3 (3,527, 7,959) vs A30P 4,212 μm^3 (2,697, 5,278), intensity: WT 6,565,620 a.u. (3,044,830, 11,543,699) vs A30P 4,776,908 a.u. (2,180,215, 8,129,199), $p > 0.05$, Mann-Whitney, N/n = 5/3).

These findings suggest that the A30P mice had fewer PV+ cell somas as indicated by a reduced cell count, and that the PV+ somas present also exhibited lower expression of PV. However, there was more PV+ expression in the processes compared to the WT.

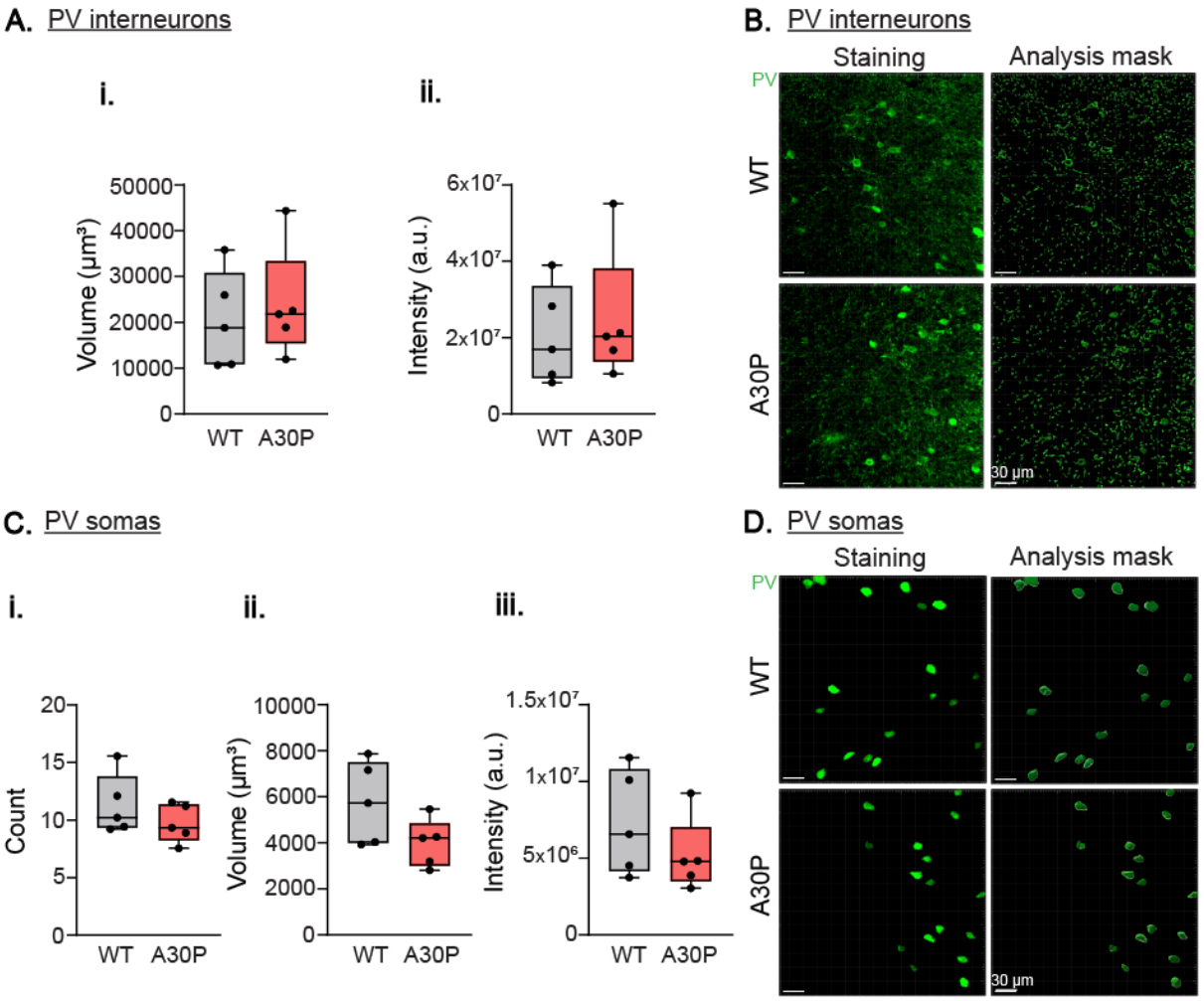

Figure 5.6. PV interneurons and PV somas only in the ACC of young A30P and WT mice. A - C. The median (**i**) volume (µm^3) and (**ii**) intensity (a.u.; arbitrary units) of (**A**) the PV interneurons and median (**i**) count, (**ii**) volume and (**iii**) intensity of (**C**) the PV somas are shown for the WT (grey) and A30P (red) mice. **B - D.** Staining and Imaris analysis mask example images for the (**B**) PV interneurons (including PV somas and processes) and (**D**) PV somas are shown for the WT and A30P mice. The images are taken from the deep layers of the ACC. Scale bars at 30 µm. Each data point represents the median values per animal.

Laminar distribution of PV interneurons in superficial and deep layers of the ACC in young A30P mice

To assess laminar differences in PV interneuron distribution within the ACC, we compared PV interneurons in young A30P and WT mice across superficial and deep layers. Log-transformed data for PV interneurons showed no statistically significant differences in mean volume and intensity between layers in young A30P mice compared to the WT (Fig. 5.7Ai and ii, $p > 0.05$, two-way ANOVA, N/n = 5/3). The two-way ANOVA results for the log-transformed mean count, volume, and intensity of PV somas revealed a statistically significant interaction effect between superficial and deep layers, with increased values in the deep layers (Fig. 5.7Bi, ii, and iii; count: $F(1,8) = 8.43$, $p < 0.05$; volume: $F(1,8) = 11.45$, $p < 0.05$; intensity: $F(1,8) = 9.04$, $p < 0.05$, two-way ANOVA, N/n = 5/3). Post hoc analysis indicated a significant increase in mean count, volume, and intensity of PV somas in the deep layers of A30P mice compared to superficial layers (Fig. 5.7Bi, ii, and iii, $p < 0.05$, Fisher's LSD, N/n = 5/3). Additionally, there was a significant decrease in the mean volume of PV somas in the superficial layers of A30P mice compared to WT (Fig. 5.7Bii, $p < 0.05$, Fisher's LSD, N/n = 5/3).

Overall, these findings indicate no significant differences in the total PV signal, including all PV somas and processes, between superficial and deep ACC layers or between the two genotypes. However, a statistically significant increase in the number, size, and PV expression specifically within PV somas was found in the deep ACC layers compared to superficial layers in young A30P mice. Additionally, while trends towards a reduced PV soma count, volume, and intensity in A30P mice were noted (Fig. 5.6C), these differences became statistically significant when examining the superficial layers separately.

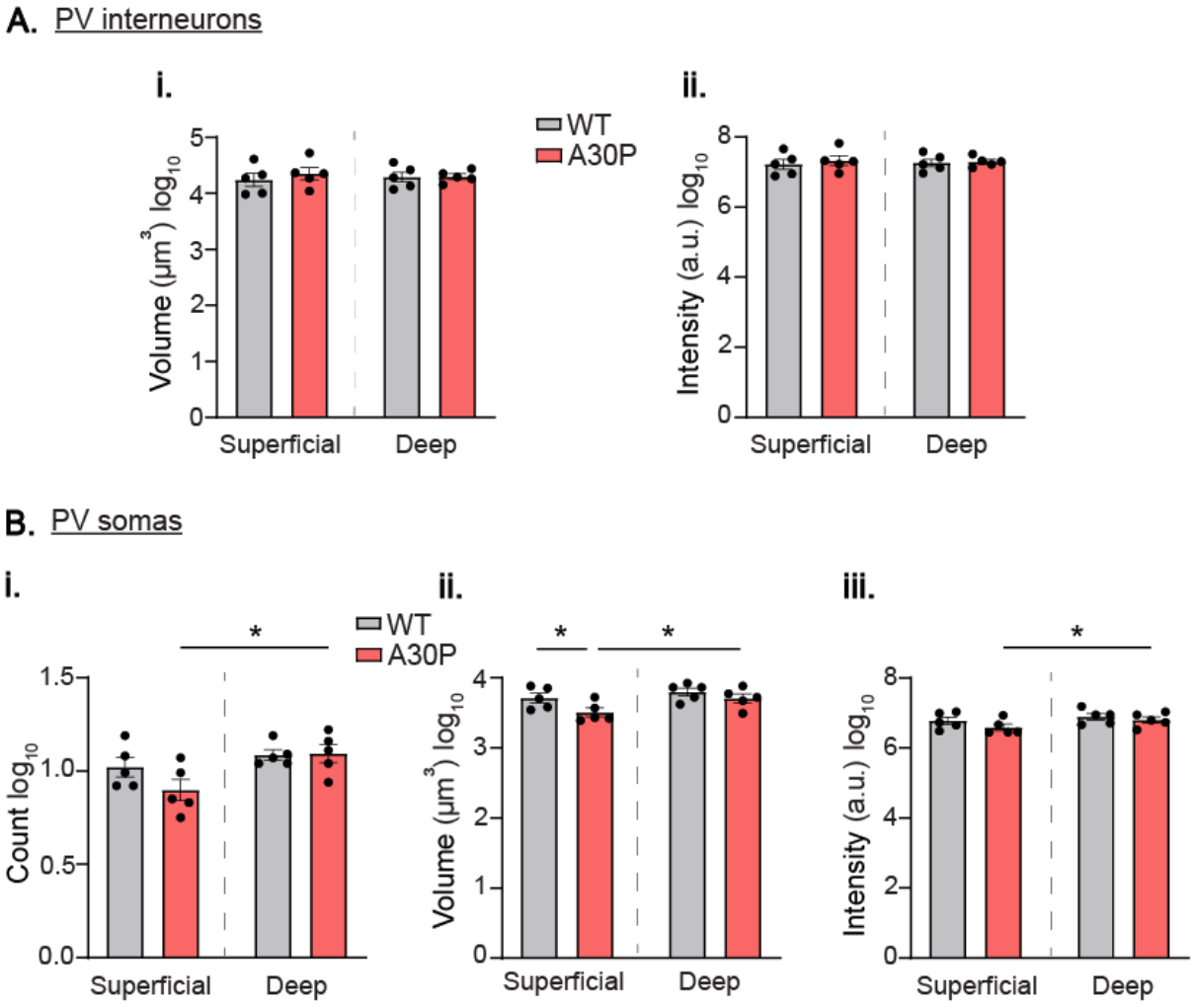

Figure 5.7. PV interneurons and PV somas only in the superficial and deep ACC of young A30P and WT mice. A - B. The log-transformed mean (**i**) volume (μm^3) and (**ii**) intensity (a.u.) of the (**A**) PV interneurons and log-transformed mean (**i**) count, (**ii**) volume and (**iii**) intensity of (**B**) PV somas are shown for the superficial and deep layers of the ACC in both young WT (grey) and A30P (red) mice. Each data point represents the mean values per animal.

5.4.2. *Association of PV interneurons with PNNs in the ACC of young A30P and WT mice.*

The WFA staining showed that there were numerous PNNs in the ACC of both A30P and WT mice, found scattered across all layers of the ACC (Fig. 5.8). The PNNs were evident as a clear mesh-like structure surrounding the cell somas and extending around the proximal dendrites in both genotypes.

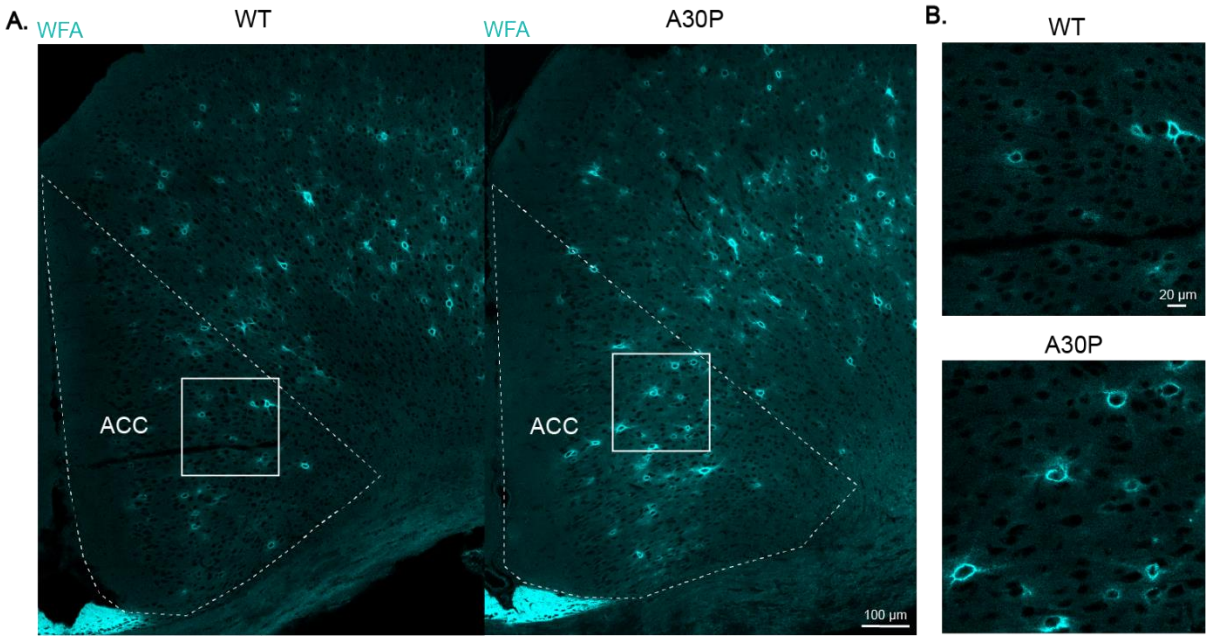

Figure 5.8. Expression of WFA+ PNNs in the ACC of young A30P and WT mice. **A.** Tile-scan (single z-plane) images showing the expression of PNNs labelled with biotinylated WFA lectin in the ACC of an example WT (left) and an A30P (right) mouse. **B.** Magnified single z-plane images of the squared areas demonstrating the WFA+ PNNs in the ACC of the WT and A30P mice. Scale bars at 100 µm and 20 µm.

The expression of PNNs around PV interneurons was confirmed in the ACC in both young A30P and WT mice (Fig. 5.9A and B, PNNs in cyan and PV interneurons in green). There were PNNs which surrounded PV interneurons, but also PNNs which surrounded non-PV neurons in the ACC in both A30P and WT mice. Also, some PV interneurons without PNNs were observed (Fig. 5.9B, white arrows = PV interneuron with a PNN; yellow arrows = PV interneuron without PNN; pink arrows = PNN surrounding non-PV neuron). In the ACC of the example A30P mouse, as shown in Figure 5.9 A, the PNNs were seen mostly in the superficial layers while the PV interneurons were mostly in the deep layers compared to the WT. Additionally, an increased WFA expression was observed in the middle area between the two

hemispheres above the corpus callosum, the indusium griseum (Allen mouse brain atlas) which might be defused ECM.

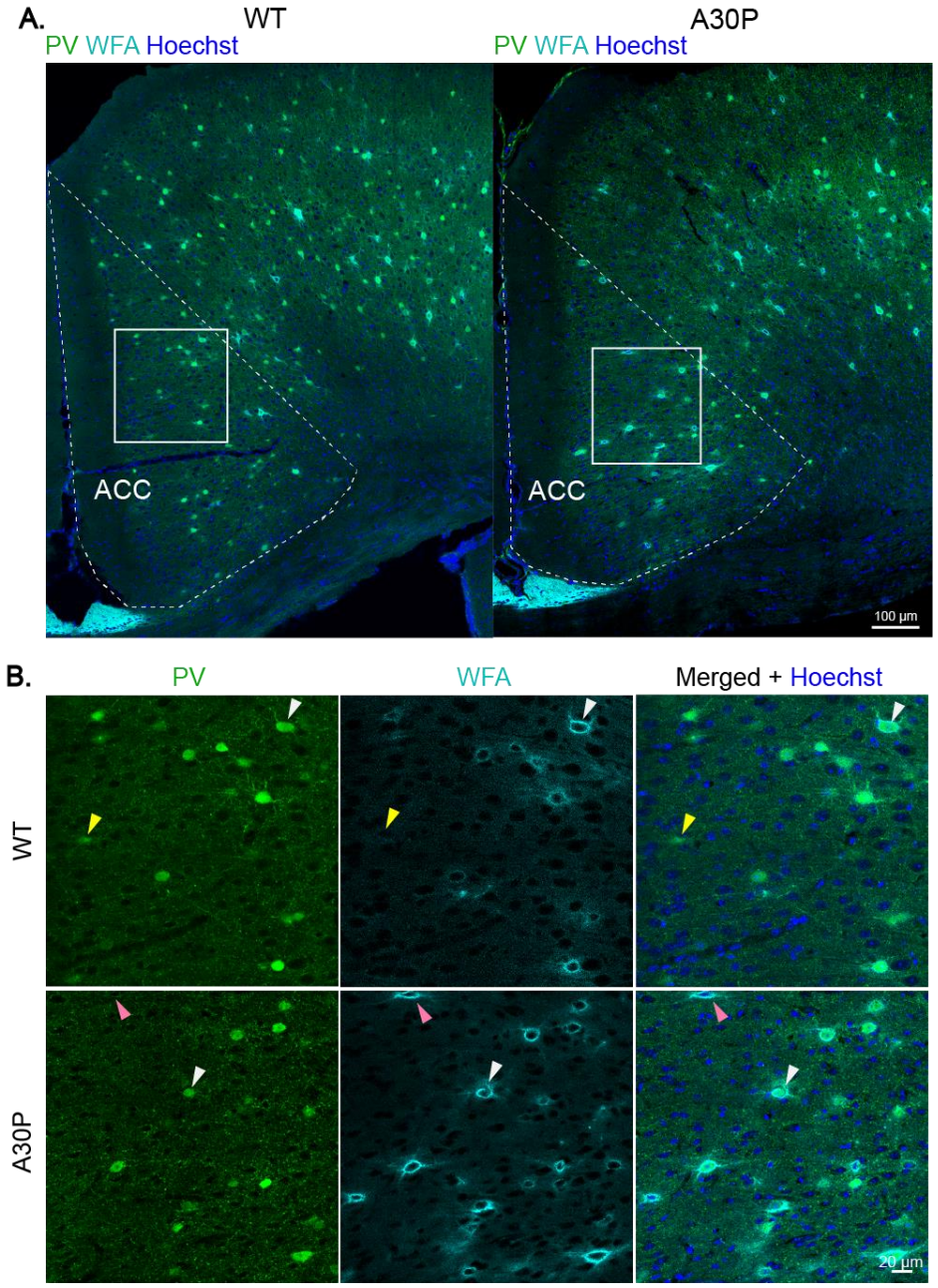

Figure 5.9. PNNs surrounded PV interneurons but also other types of neurons in the ACC of young A30P and WT mice. A. Tile-scan (single z-plane) ACC images for example WT (left) and A30P (right) mice showing the PV interneurons (green), WFA+ PNNs (cyan) and Hoechst+ nuclei (blue). **B.** Magnified single z-plane images of the squared areas showing the PV interneurons and PNNs in both genotypes. White arrows indicate PV interneurons surrounded by PNNs, yellow arrows highlight an example of a PV interneuron without a PNN, and pink arrows point to a PNN surrounding a non-PV neuron. Scale bars at 100 µm and 20 µm.

The co-localisation between the PV somas and PNNs was then investigated in the ACC of young A30P mice compared to the WT mice. In the A30P mice 86.5% of the number of PV somas from the total number of PV somas (n = 378/437) were surrounded by PNNs and 13.5% of PV somas did not have PNNs (n = 59/437). Similarly, in the WT mice, 84.5% of the total number of PV somas (n = 430/509) were surrounded by PNNs. Thus, 15.5% of the total number of PV somas (n = 79/509) were not surrounded by PNNs in the ACC of young WT mice. The proportion of PV somas with a PNN was not, therefore, different between young A30P and WT mice.

Expression of PV somas with and without a PNN in young mice

To further investigate PV interneurons, I then compared the PV expression levels of the PV somas surrounded and not surrounded by PNNs. The median count, volume and intensity of PV-expressing interneurons were calculated for the PV somas with PNNs (PV somas+ PNNs+) and the PV somas without PNNs (PV somas+ PNNs-) in young A30P and WT mice.

Interestingly, the results revealed a trend towards a decreased median count, volume, and intensity of PV somas with PNNs in the ACC of young A30P mice compared to WT, though this difference was not statistically significant (Fig. 5.10Ai, ii and iii, PV somas+ PNNs+, count: WT 8.33 (6.37, 12.74) vs A30P 8.67 (6.16, 10.64), volume: WT 4,982 μm^3 (2,893, 7,274) vs A30P 3,301 μm^3 (2,357, 4,762), intensity: WT 5,793,099 a.u. (2,272,442, 11,353,383) vs A30P 3,849,751 a.u. (1,818,851, 7,516,359), $p > 0.05$, Mann-Whitney, N/n = 5/3). A similar trend was observed in PV somas without PNNs, where A30P mice showed lower median count, volume, and intensity compared to WT (Fig. 5.7Ci, ii and iii, PV somas+ PNNs-, count: WT 1.78 (1.49, 2.02) vs A30P 1.22 (0.27, 2.35), volume: WT 668.9 μm^3 (580.6, 737.7) vs A30P 361.6 μm^3 (12.16, 843.1), intensity: WT 692,638 a.u. (536,103, 830,327) vs A30P 386,554 a.u. (21,442, 952,756), $p > 0.05$, Mann-Whitney, N/n = 5/3).

These findings suggest a trend toward fewer and smaller PV somas with reduced PV expression in both PV somas with and without PNNs in young A30P mice compared to WT, though these differences were not statistically significant. This trend aligns with the previously observed non-significant reduction in total PV soma count in

young A30P mice (Fig. 5.6). Moreover, the observed decrease in PV count and expression, regardless of PNN presence, suggested that PNNs may not directly impact PV soma properties.

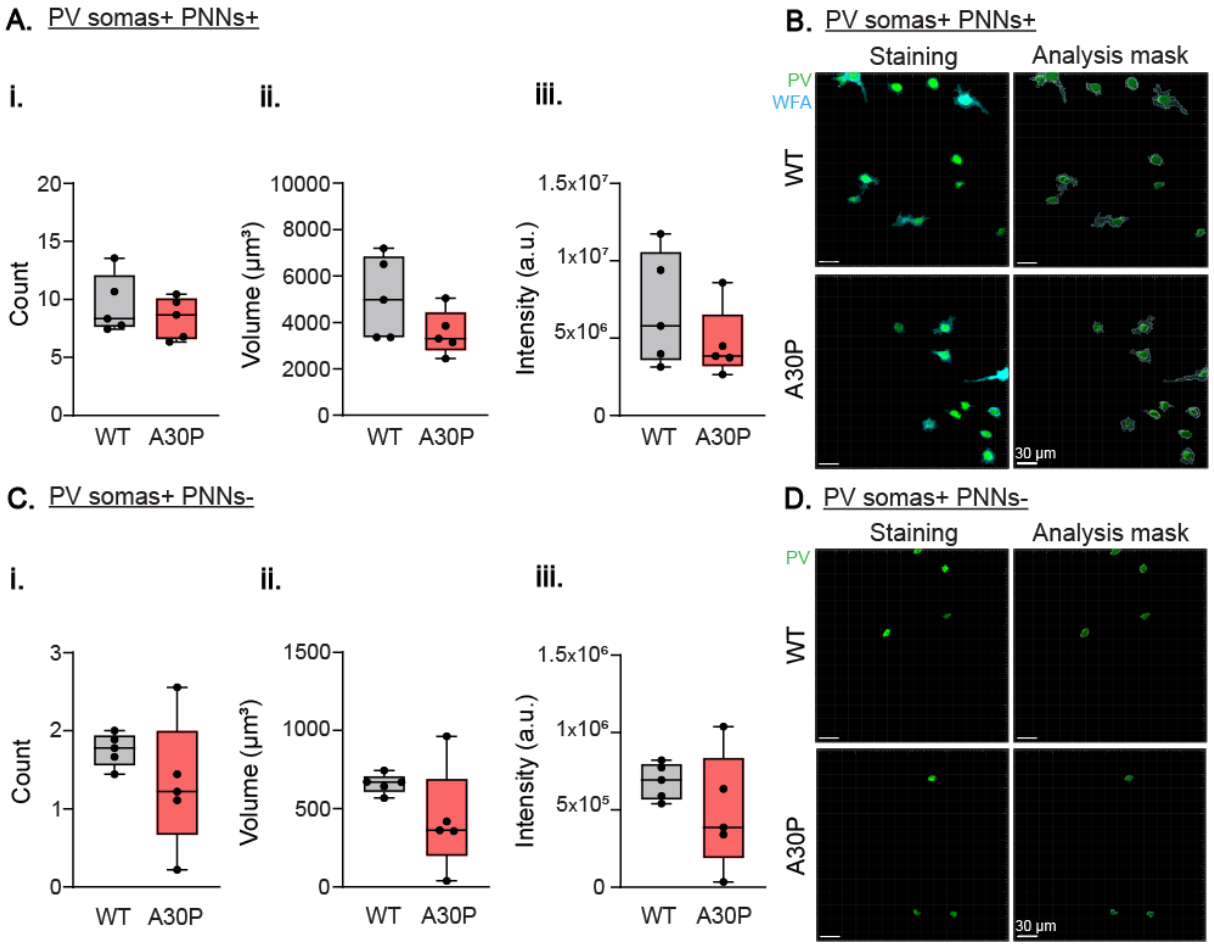

Figure 5.10. PV somas surrounded and not surrounded by PNNs in the ACC of young A30P and WT mice. A - C. The median (**i**) count, (**ii**) volume (µm^3) and (**iii**) intensity (a.u.) of the (**A**) PV somas with PNNs (PV somas+ PNNs+) and (**C**) PV somas without PNNs (PV somas+ PNNs-) are shown for the WT (grey) and A30P (red) mice. **B - D.** Staining and analysis mask example images for the (**B**) PV somas (green) with PNNs (cyan) and (**D**) PV somas without PNNs are shown for both WT and A30P mice. These images are taken from the deep layers of the ACC. Scale bars at 30 µm. Each data point represents the median values per animal.

PV somas with and without PNNs in the superficial and deep layers of the ACC in young A30P mice

I also analysed the distribution of PV somas with and without PNNs between the superficial and deep layers of the ACC. Starting with PV somas surrounded by PNNs, the two-way ANOVA results on the log-transformed data showed a statistically significant effect in the mean volume of PV somas with PNNs between the superficial and deep layers, with an increase in the deep layers (Fig. 5.11Aii, PV somas+ PNNs+, $F(1,8) = 7.56$, $p < 0.05$, two-way ANOVA, N/n = 5/3). Post hoc analyses further revealed a statistically significant increase in the mean count, volume, and intensity of PV somas with PNNs in the deep ACC layers of A30P mice compared to the superficial layers (Fig. 5.11Ai, ii, and iii, PV somas+ PNNs+, Fisher's LSD, $p < 0.05$, N/n = 5/3). However, no significant differences were found between young A30P and WT mice.

After log transformation, the count, volume, and intensity data of PV somas without PNNs were still not normally distributed, preventing the use of a two-way ANOVA to compare these variables between the superficial and deep ACC layers or between A30P and WT mice (Fig. 5.11Bi, ii and iii, PV somas+ PNNs-, N/n = 5/3).

Overall, we found PV expression was stronger in the deep layers of the ACC compared to the superficial layers with a statistically significant increase presented in the young A30P mice for the PV somas surrounded by PNNs.

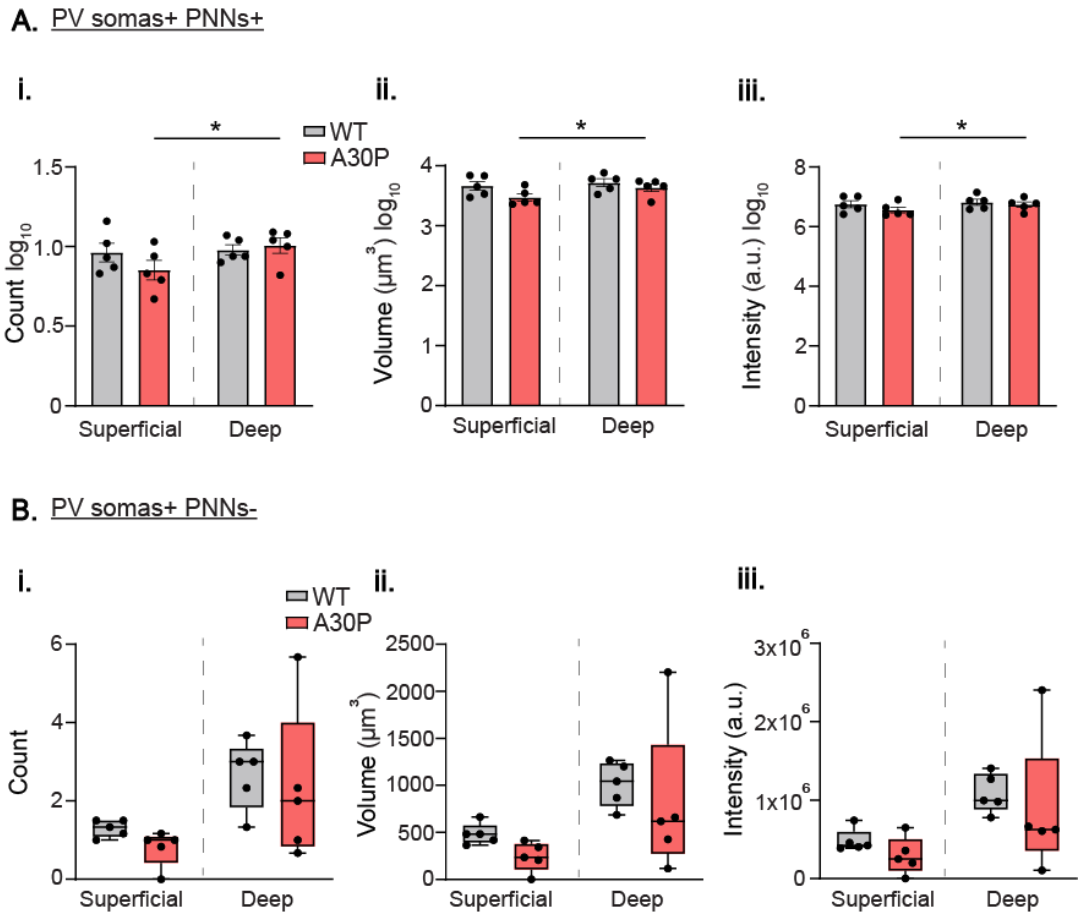

Figure 5.11. PV somas with and without a PNN in the superficial and deep ACC of young A30P and WT mice. A. The log-transformed mean (**i**) count, (**ii**) volume (μm^3) and (**iii**) intensity (a.u.) are demonstrated for the PV somas with PNNs (PV somas+ PNNs+) in the superficial and deep ACC layers in both WT (grey) and A30P (red) young mice. **B.** The median (**i**) count, (**ii**) volume and (**iii**) intensity are shown for the PV somas without PNNs (PV somas+ PNNs-) between the superficial and deep ACC layers in both WT and A30P mice. Each data point represents the mean or median values per animal.

Expression of PNNs surrounding PV interneurons and non-PV neurons in young A30P mice

I then investigated in more detail the PNN expression in the ACC. In the WT mice, 65.9% of the total number of PNNs were surrounding PV somas (n = 428/649) and 34.1% of PNNs were without PV somas (n = 221/649). In the A30P mice, however, only 49.6% of the total number of the PNNs were surrounding PV somas (n = 369/744) and 50.4% were without PV somas (n = 375/744). Interestingly, this suggests that in

the A30P mice, there is a trend for an increase in the PNNs around other non-PV neurons.

The median count, volume, and intensity of the PNNs regardless of neuron type was calculated between young A30P and WT mice to investigate possible differences between the genotypes. The A30P mice showed a slight non-significant increase in the median count and intensity but not the volume of all PNNs compared to the WT (Fig. 5.12Ai, ii and iii, count: WT 13.67 (10.21, 18.63) vs A30P 17.22 (12.89, 20.18), volume: WT 21,763 μm^3 (11,668, 30,132) vs A30P 22,585 μm^3 (16,092, 27,859), intensity: WT 100,977,691 a.u. (3,975,826, 15,526,573) vs A30P 12,500,234 a.u. (6765577, 14692601), $p > 0.05$, Mann-Whitney, N/n = 5/3).

For the PNNs with PV somas, there were no statistically significant differences in the median count, volume and intensity between the young A30P and WT mice (Fig. 5.8Bi, ii and iii, PNNs+ PV somas+, count: WT 8.33 (6.43, 12.59) vs A30P 8.44 (5.93, 10.47), volume: WT 13,606 μm^3 (8,026, 22,432) vs A30P 12,443 μm^3 (6,175, 17,503), intensity: WT 7,122,861 a.u. (2,783,772, 12,005,263) vs A30P 7,098,651 a.u. (2,709,842, 9,458,269), $p > 0.05$, Mann-Whitney, N/n = 5/3). On the other hand, for PNNs without PV somas, the A30P mice showed a statistically significant increase in the median count and volume, as well as a non-significant increase in median intensity, compared to WT mice (Fig. 5.8Ci and ii, PNNs+ PV somas-, count: WT 4.11 (3.32, 6.50) vs A30P 7.67 (4.35, 12.31), volume: WT 4127 μm^3 (2,580, 8,749) vs A30P 10141 μm^3 (6,888, 13,412), intensity: WT 1567266 a.u. (672,583, 4,033,232) vs A30P 5,401,595 a.u. (2,939,644, 6,361,311), $p < 0.05$, Mann-Whitney, N/n = 5/3).

Overall, while most PV interneurons were surrounded by PNNs in the ACC for both genotypes, a significantly higher number of PNNs were found surrounding non-PV neurons in A30P mice compared to WT mice.

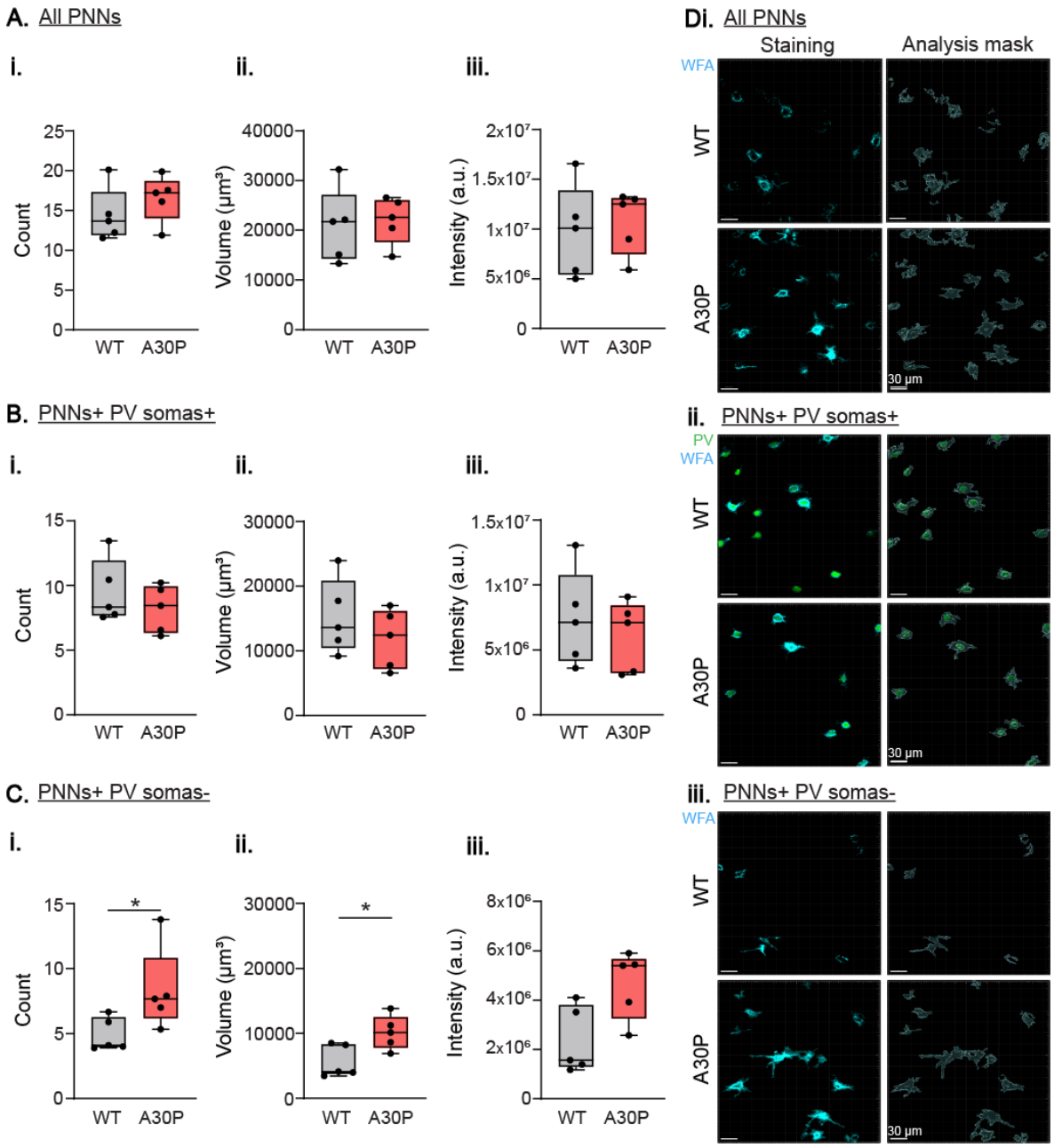

Figure 5.12. The PNNs in the ACC of young A30P and WT mice. A – C. The median (**i**) count, (**ii**) volume (µm^3) and (**iii**) intensity of (**A**) all PNNs, (**B**) PNNs with PV somas (PNNs+ PV somas+) and (**C**) PNNs without PV somas (PNNs+ PV somas-) are shown for the WT (grey) and A30P (red) mice. **D.** The staining and analysis mask example images for (**i**) all PNNs, (**ii**) PNNs with PV somas and (**iii**) PNNs without PV somas are demonstrated for both young WT and A30P mice. These images are taken from the superficial layers of the ACC. Each data point represents the median values per animal.

PNN distribution in the deep and superficial layers of the ACC in young A30P mice

I also quantified the total PNN expression in the deep and superficial layers of the ACC. The log-transformed mean count, volume, and intensity for the PNNs between superficial and deep layers were calculated in the young A30P and WT mice to examine potential density pattern differences. There were no statistically significant differences in the mean count, volume, and intensity of all PNNs between superficial and deep ACC in A30P mice compared to the WT (Fig. 5.13Ai, ii and iii, all PNNs, $p > 0.05$, two-way ANOVA, N/n = 5/3).

Following analysis of the PNNs regardless of the cell type, I next investigated the PNNs with PV somas. The two-way ANOVA results for the PNNs surrounding PV somas showed no significant differences in the mean count, volume, and intensity of these PNNs between superficial and deep layers and between A30P and WT. However, the post hoc examinations showed a marked increase in the count of PNNs surrounding PV somas in the deep layers of the ACC in the A30P mice compared to the superficial layers (Fig. 5.13Bi, PNNs+ PV somas+, $p < 0.05$, Fisher's LSD, N/n = 5/3).

For the PNNs without PV somas, the two-way ANOVA results showed a statistically significant effect between the superficial and deep layers of the ACC and between the A30P and WT animals (Fig. 5.13Cii, PNNs+ PV somas-, count: superficial vs deep $F(1,8) = 6.65$, $p < 0.05$, WT vs A30P $F(1,8) = 7.01$, $p < 0.05$, two-way ANOVA, N/n = 5/3). The post hoc examinations showed a marked increase in the mean count of PNNs without PV somas in the superficial and deep layers of the ACC in the A30P mice compared to the WT ($p < 0.05$, Fisher's LSD). Additionally, the two-way ANOVA revealed a statistically significant interaction between the two genotypes for the mean volume with a significant increase in the superficial layers in A30P mice compared to the WT (Fig. 5.13Cii, significant effect WT vs A30P $F(1,8) = 5.34$, $p < 0.05$, two-way ANOVA, Fisher's LSD, N/n = 5/3). Lastly, there were no statistically significant differences in the mean intensity of the PNNs without PV somas between the layers of the ACC and between the two genotypes.

Thus, the incidence of both PV+ and PV- neurons surrounded by PNNs was the same in the deep and superficial layers of the ACC. These data also show that the

increase in PNN count around non-PV neurons seen in the young A30P mice above (Fig. 5.12) occurred in both the superficial and deep layers of the ACC.

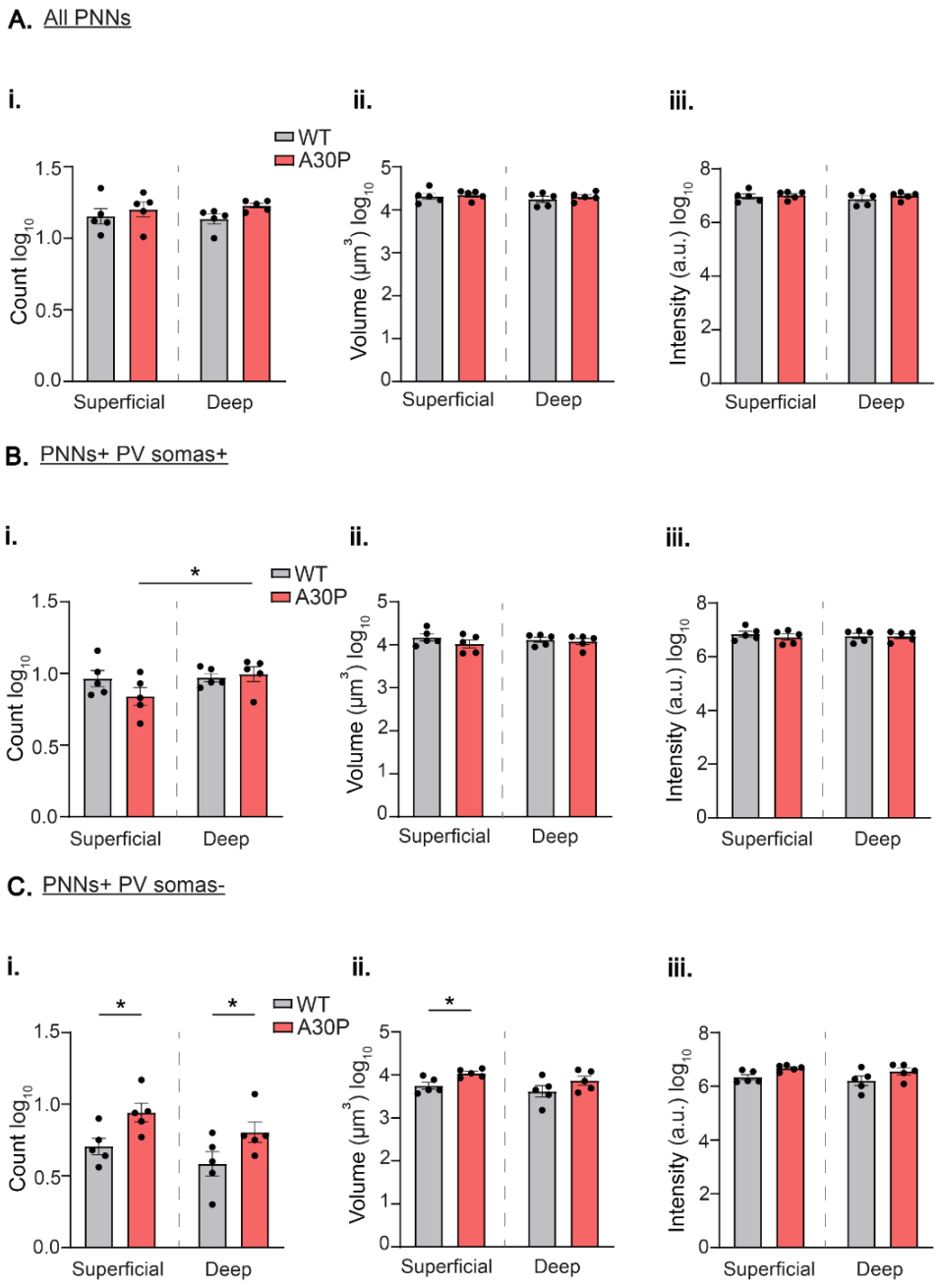

Figure 5.13. PNNs with and without PV somas in the superficial and deep ACC of young A30P and WT mice. A - C. The log-transformed mean (**i**) count, (**ii**) volume (μm^3) and (**iii**) intensity (a.u.) are shown for (**A**) all PNNs, (**B**) PNNs with PV somas (PNNs+ PV somas+) and (**C**) PNNs without PV somas (PNNs+ PV somas-) in the superficial and deep ACC layers in both WT (grey) and A30P (red) young mice. Each data point represents the mean values per animal.

5.4.3. *PV-expressing interneurons in the ACC of aged A30P and WT mice.*

The number of PV interneurons decreases with age but it has also been shown to be affected by α-syn pathology in DLB (Bernstein *et al.*, 2011; Ueno, Fujii, *et al.*, 2019). PV interneuron count, volume, and intensity were thus examined in the ACC of aged A30P and WT mice to assess the potential effects of hα-syn pathology and ageing on PV interneurons in A30P mice.

The median count, volume, and intensity values for PV interneurons (including somas and processes) and PV somas were determined for both genotypes. No statistically significant differences were found in the median volume and intensity of PV interneurons between aged A30P and WT mice (Fig. 5.14Ai and ii, volume: WT 31,201 μm³ (17,086, 51,329) vs A30P 39,549 μm³ (24,191, 50,100), intensity: WT 31,176,461 a.u. (11,648,043, 49,659,094) vs A30P 34,601,844 a.u. (18,650,316, 43,521,533), $p > 0.05$, Mann-Whitney, N/n = 5/3). For PV neuronal somas only, there was a trend toward decreased mean count and volume, but not median intensity, in A30P mice compared to WT, though this was not statistically significant (Fig. 5.14Ci, ii and iii, count: WT 14.27 vs A30P 11.82, volume: WT 8,820 μm³ vs A30P 6,045 μm³, $p > 0.05$, unpaired t-test, intensity: WT 8,322,470 a.u. (2,526,992, 22,834,905) vs A30P 9,735,773 a.u. (4,117,330, 12,431,594), $p > 0.05$, Mann-Whitney, N/n = 5/3).

These results, therefore, did not show any marked changes in PV expression in the ACC of aged A30P mice compared to aged WT. However, there was a trend towards an increase in PV expression in the processes, but a decrease in PV soma expression in A30P mice, similar to that seen in the young A30P mice (Fig. 5.6).

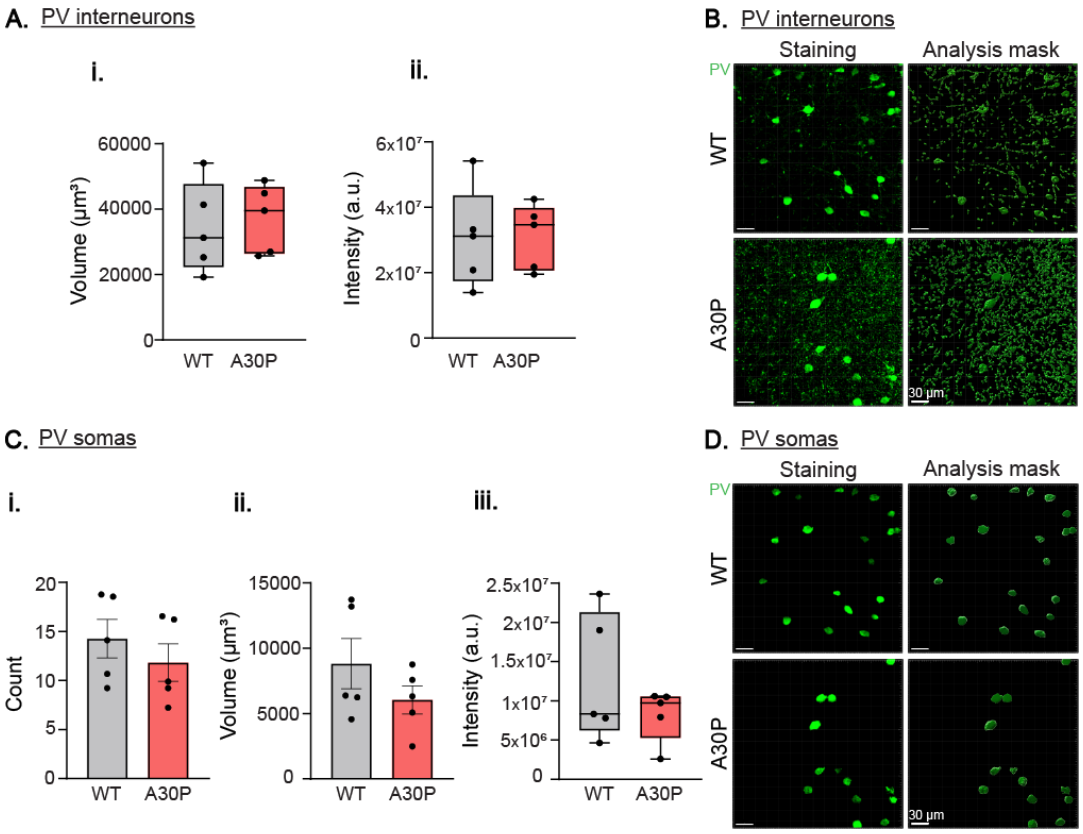

Figure 5.14. PV interneurons and PV somas only in the ACC of aged A30P and WT mice. A - C. The median (**i**) volume (µm^3) and (**ii**) intensity (a.u.) of (**A**) the PV interneurons and mean or median (**i**) count, (**ii**) volume and (**iii**) intensity of (**C**) the PV somas are shown for the WT (grey) and A30P (red) mice. **B - D.** Staining and Imaris analysis mask example images for the (**B**) PV interneurons (including PV somas and puncta) and (**D**) PV somas are shown for the WT and A30P aged mice. These images are taken from the deep layers of the ACC. Scale bars at 30 µm. Each data point represents the median or mean values per animal.

Laminar distribution of PV interneurons in the superficial and deep layers of the ACC in aged A30P mice

After analysing PV expression in the ACC of aged A30P and WT mice, I then compared PV expression between the superficial and deep ACC layers to investigate potential differences in PV soma properties across layers and between genotypes.

First, I examined PV expression in PV interneurons across these layers. Two-way ANOVA on log-transformed data revealed no significant differences in mean volume or intensity of PV expression between the superficial and deep layers or between aged A30P and WT mice (Fig. 5.15Ai and ii, $p > 0.05$, two-way ANOVA, N/n

= 5/3), consistent with Figure 5.14A, where no significant genotype differences were observed. Next, I compared PV somas between the superficial and deep ACC layers. No statistically significant differences were found in the log-transformed mean count, volume, or intensity of PV somas across layers or between the genotypes (Fig 5.15Bi, ii and iii, $p > 0.05$, two-way ANOVA, N/n = 5/3).

Thus, in contrast to the data seen in young A30P and WT mice where there was a greater expression of PV somas in the deep layers of the ACC (Fig. 5.7), in the aged animals this difference is no longer evident.

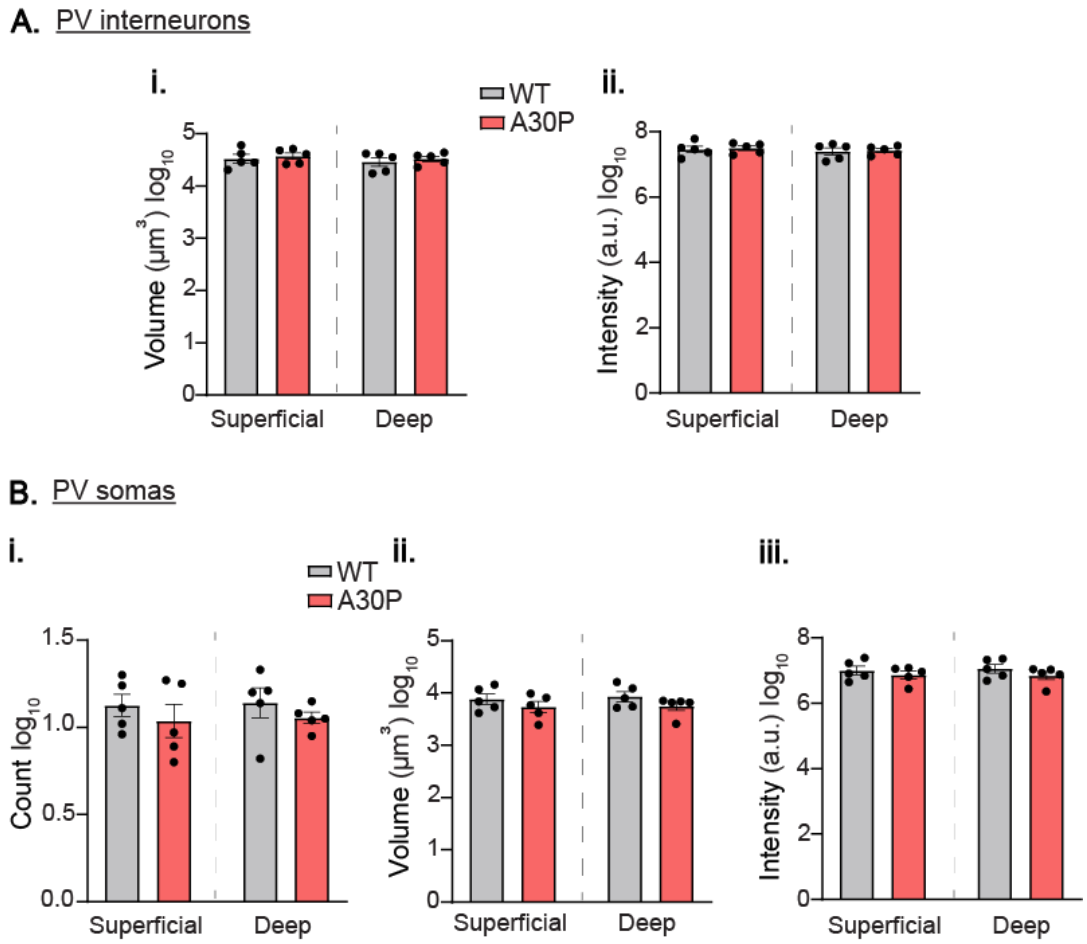

Figure 5.15. PV interneurons and PV somas only in the superficial and deep ACC layers of aged A30P and WT mice. A - B. The log-transformed mean (**i**) volume (μm^3) and (**ii**) intensity (a.u.) of the (**A**) PV interneurons and log-transformed mean (**i**) count, (**ii**) volume and (**iii**) intensity of (**B**) PV somas are shown for the superficial and deep layers of the ACC in both aged WT (grey) and A30P (red) mice. Each data point represents the mean values per animal.

5.4.4. *Association of PV interneurons with PNNs in the ACC of aged A30P and WT mice.*

PV interneurons and PNNs are influenced by ageing (Ueno *et al.*, 2018) and neurodegeneration (Reichelt, 2020) in mice. To explore this, PNNs and their co-localisation with PV interneurons were examined in the ACC of aged A30P and WT mice.

The expression of PNNs and their co-localisation with PV interneurons in the ACC was confirmed in both the aged A30P and WT mice (Fig. 5.16A and B, PNNs in cyan and PV interneurons in green). In both genotypes, there were PV interneurons surrounded and not surrounded by PNNs (Fig. 5.16C, white arrows = PV interneuron with a PNN; yellow arrows = PV interneurons without a PNN). Additionally, some PNNs surrounded non-PV neurons as previously seen in the young A30P and WT mice (Fig. 5.16C, pink arrows = PNNs with non-PV neurons).

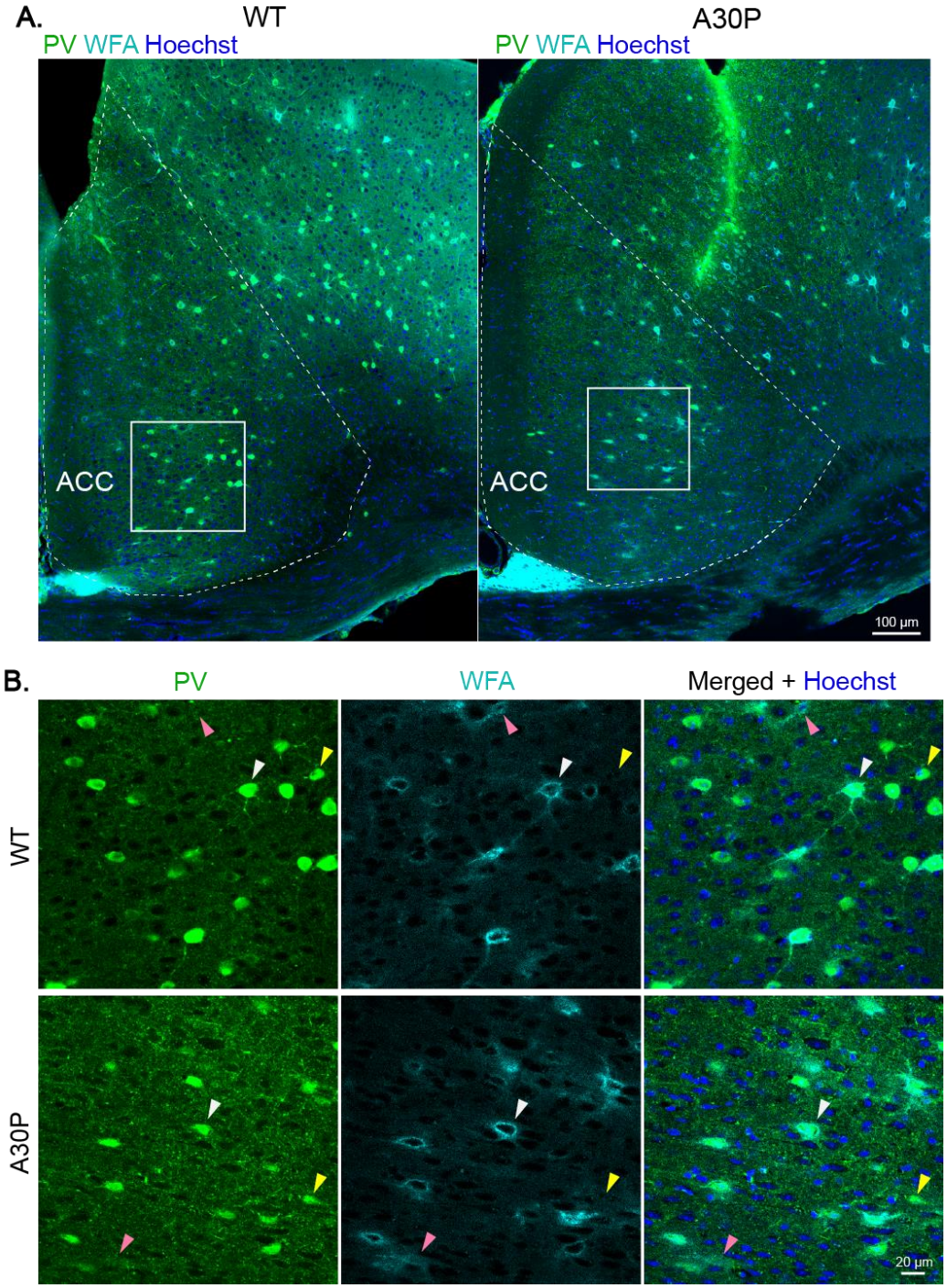

Figure 5.16. PNNs surrounded PV interneurons and non-PV neurons in the ACC of aged A30P and WT mice. A. Tile-scan (single z-plane) ACC images for example WT (left) and A30P (right) mice showing the PV interneurons (green), WFA+ PNNs (cyan) and Hoechst+ nuclei (blue). **B.** Magnified single z-plane images of the squared areas showing the PV interneurons and PNNs in both genotypes. White arrows indicate PV interneurons surrounded by PNNs, yellow arrows highlight an example of a PV interneuron without a PNN, and pink arrows point to a PNN surrounding a non-PV neuron. Scale bars at 100 µm and 20 µm.

Expression of PV in interneurons with and without a PNN in aged A30P mice

Following the observed expression of PNNs around PV interneurons and non-PV neurons in the ACC of aged mice, the interactions between PV somas and PNNs were further investigated in aged A30P and WT mice. In the aged A30P mice, 72.2% of PV somas from the total number of PV somas were surrounded by PNNs (n = 384/532), with 27.8% lacking PNNs (n = 148/532), compared to 86.5% and 13.5% in the young A30P group (Chapter 5.4.2). Similarly, in the aged WT mice, 69.2% of PV somas from the total number of PV somas were surrounded by PNNs (n = 444/642) and 30.8% lacked PNNs (n = 198/642), compared to 84.5% and 15.5% in the young WT group (Chapter 5.4.2). These findings indicate an age-related trend in both genotypes, with nearly twice as many PV somas lacking PNNs in aged animals compared to young animals.

Next, the interactions and PV expression levels in PV somas with and without PNNs were compared between aged A30P and WT mice. The average count, volume, and intensity of PV expression for A30P mice were calculated. First, I analysed PV somas with PNNs. No statistically significant differences were observed in the mean count, volume, or median intensity of PV somas with PNNs in aged A30P mice compared to aged WT (Fig. 5.17Ai, ii, and iii, PV somas+ PNNs+, count: WT 9.87 vs A30P 8.53, volume: WT 6,455 μm^3 vs A30P 4,751 μm^3, $p > 0.05$, unpaired t-test, intensity: WT 7,444,009 a.u. (2,759,478, 16,762,178) vs A30P 8,095,176 a.u. (3,204,200, 10,348,195), $p > 0.05$, Mann-Whitney, N/n = 5/3). However, a trend towards decreased PV expression in PV somas with PNNs was observed in aged A30P mice, consistent with findings in young A30P mice (Fig. 5.10).

The PV expression in the PV somas without PNNs was next investigated. No statistically significant differences in the median count, volume and intensity of these PV somas were shown between the aged A30P and WT mice (Fig. 5.17Ci, ii and iii, PV somas+ PNNs-, count: WT 2.56 (0.62, 8.18) vs A30P 3.67 (2.36, 4.21), volume: WT 1,380 μm^3 (132.3, 4,862) vs A30P 1,452 μm^3 (808.9, 1,777), intensity: WT 1,389,036 a.u. (463,271, 630,287) vs A30P 1,640,598 a.u. (824,864, 2,171,349), $p > 0.05$, Mann-Whitney, N/n = 5/3). We previously observed a trend towards decreased PV expression in the PV somas without PNNs in the young A30P mice which is not consistent with these findings (Fig. 5.10).

These findings showed that overall, there were no marked differences in the PV expression in the PV somas, regardless of PNN presence, between the two genotypes in the aged mice.

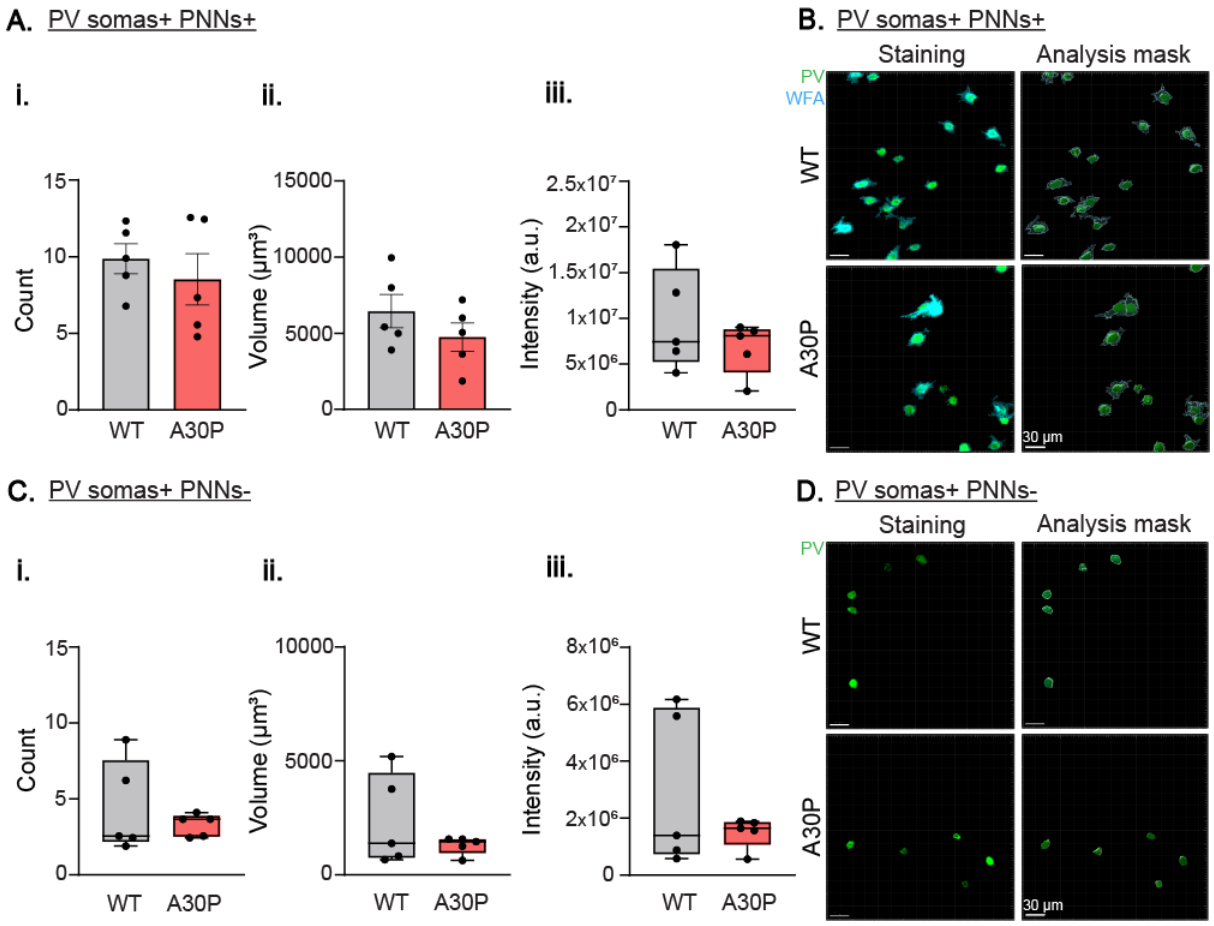

Figure 5.17. PV somas with and without a PNN in the ACC of aged A30P and WT mice. A - C. The mean or median (**i**) count, (**ii**) volume (µm^3) and (**iii**) intensity (a.u.) of the (**A**) PV somas with PNNs (PV somas+ PNNs+) and (**C**) PV somas without PNNs (PV somas+ PNNs-) are shown for the WT (grey) and A30P (red) mice. **B - D.** Staining and analysis mask example images for the (**B**) PV somas (green) with PNNs (cyan) and (**D**) PV somas without PNNs are shown for both WT and A30P aged mice. These images are taken from the deep layers of the ACC. Scale bars at 30 µm. Each data point represents the mean or median values per animal.

PV somas with and without PNNs in the superficial and deep layers of the ACC in aged A30P mice

The distribution of PV+ somas with and without a PNN was compared between the superficial and deep layers of the ACC in the aged mice. I first looked at PV somas surrounded by PNNs. The two-way ANOVA showed no statistically significant differences between the superficial and deep layers, nor between aged A30P and WT mice for the log-transformed mean count, volume and intensity of the PV expression in these PV somas (Fig. 5.18Ai, ii and iii, PV somas+ PNNs+, $p > 0.05$ two-way ANOVA, N/n = 5/3).

Next, PV somas without PNNs were examined. Two-way ANOVA on the log-transformed mean count, volume, and intensity revealed a statistically significant effect for the PV expression between the superficial and deep layers (Fig. 5.18Bi, ii and iii, PV somas+ PNNs-, count: $F(1,8) = 5.97$, volume: $F(1,8) = 9.88$, intensity: $F(1,8) = 9.62$, $p < 0.05$, two-way ANOVA, N/n = 5/3,). Post hoc analysis showed a significant increase in the mean count, volume, and intensity of PV somas without PNNs in the deep layers of the ACC in WT mice compared to the superficial layers ($p < 0.05$, Fisher's LSD). However, no significant differences were found between the genotypes.

Overall, these findings indicated no significant differences in the PV expression of PV somas with a PNN between the superficial and deep ACC layers, nor between the aged A30P and WT mice. In contrast, the young animals (Fig. 5.11) showed a significant increase in PV expression in PV somas with a PNN in the deep layers of the ACC in A30P mice compared to the superficial layers. However, in the aged mice, this trend reversed, with only WT mice showing a significant laminar difference, characterised by more PV interneurons in the deep layers, including PV somas without a PNN.

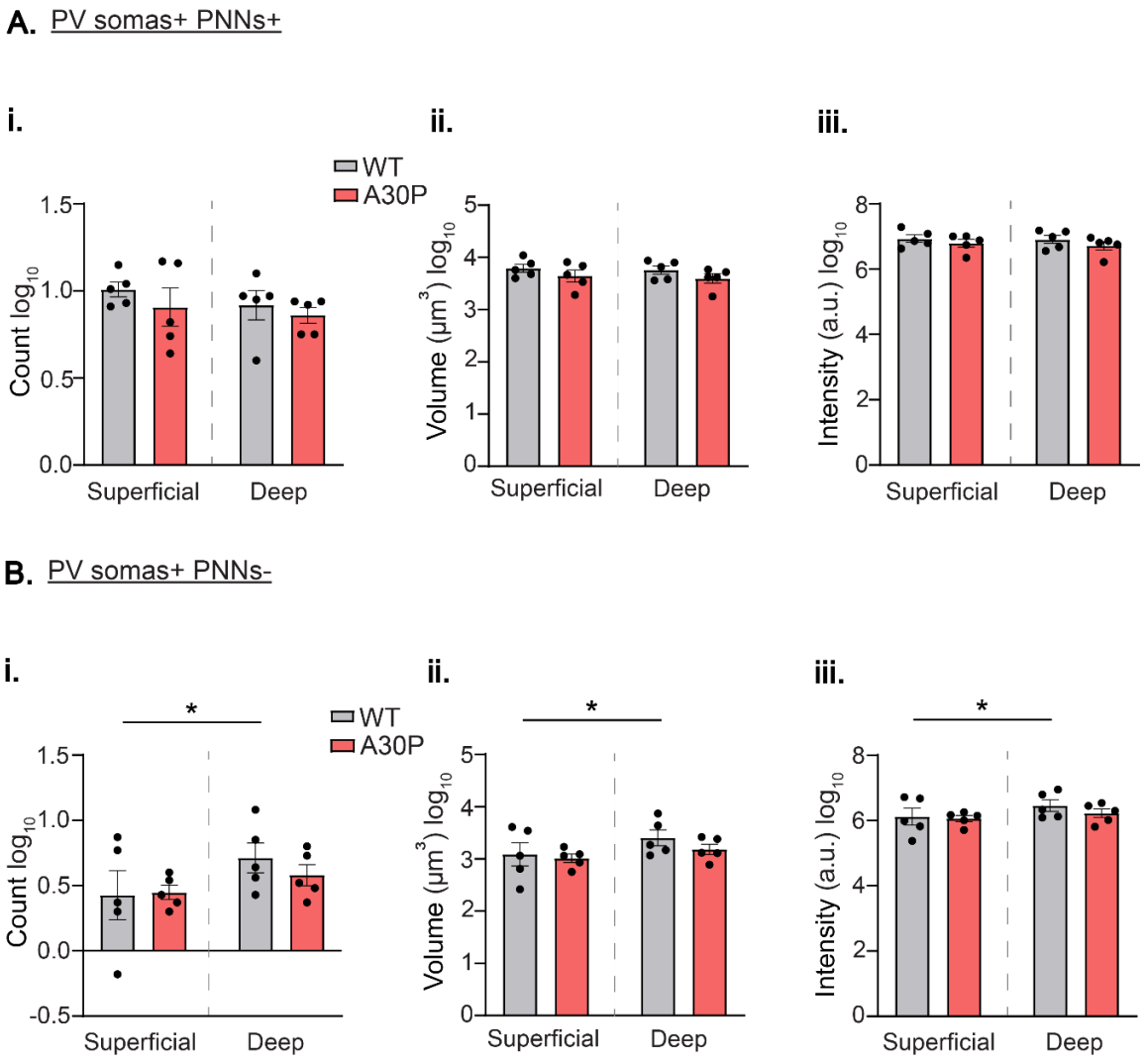

Figure 5.18. PV somas with and without a PNN in the superficial and deep ACC of aged A30P and WT mice. A - B. The log-transformed mean (**i**) count, (**ii**) volume (μm^3) and (**iii**) intensity (a.u.) are shown for the (**A**) PV somas with PNNs (PV somas+ PNNs+) and (**B**) PV somas without a PNN (PV somas+ PNNs-) in the superficial and deep ACC layers in both WT (grey) and A30P (red) aged mice. Each data point represents the mean values per animal.

Expression of PNNs surrounding PV interneurons and non-PV neurons in aged A30P mice

The PNN expression was analysed in the ACC of aged A30P and WT mice. Aged A30P mice had 55.5% PNNs surrounding PV interneurons from the total number of PNNs (n = 381/686) and 44.5% around non-PV neurons (n = 305/686). This differs from the young A30P mice showing a trend towards increased PNNs around non-PV neurons (50.4%). In contrast, aged WT mice had 65.2% PNNs around PV interneurons (n = 440/675) and 34.8% around non-PV neurons (n = 235/675) which is very similar to the 65.9% and 34.1% calculated in the young WT (Chapter 5.4.2). Aged A30P mice had a higher proportion of PNNs around non-PV neurons (44.5%) than the aged WT mice (34.8%), consistent with findings in young A30P mice.

The average count, volume and intensity of the PNN expression for all PNNs, regardless of the cell type, in the ACC was next analysed in the aged mice. No statistically significant differences were shown in the mean count, median volume and intensity between the aged A30P and WT mice (Fig. 5.19Ai, ii and iii, count: WT 15 vs A30P 15.24, $p > 0.05$, unpaired t-test, volume: WT 16,673 μm^3 (9,505, 19,848) vs A30P 15,298 μm^3 (11,675, 18,606), intensity: WT 8,097,658 a.u. (3,648,386, 10,365,601) vs A30P 6,872,697 a.u. (4,667,547, 9,401,646), $p > 0.05$, Mann-Whitney, N/n = 5/3).

I then investigated the PNNs surrounding PV somas. There were no statistically significant differences in the mean count, median volume and intensity of these PNNs between the two genotypes (Fig. 5.19Bi, ii and iii, PNNs+ PV somas+, count: WT 9.78 vs A30P 8.47, $p > 0.05$, unpaired t-test, volume: WT 10,145 μm^3 (6,497, 13,201) vs A30P 10,334 μm^3 (4,199, 14,170), intensity: WT 5,537,411 a.u. (2,384,603, 7,133,653) vs A30P 5,344,902 a.u. (19,98,262, 6,696,485), $p > 0.05$, Mann-Whitney, N/n = 5/3). For the PNNs without PV somas, the aged A30P mice showed a trend towards an increase in the median count, volume and intensity compared to the aged WT (Fig. 5.19Ci, ii and iii, PNNs+ PV somas-, count: WT 5.56 (1.07, 9.37) vs A30P 6.78 (2.97, 10.59), volume: WT 5,241 μm^3 (1,024, 8,630) vs A30P 7,213 μm^3 (1,697, 10,215), intensity: WT 2,432,312 a.u. (532,322, 3,961,802) vs A30P 2,982,140 a.u. (501,406, 4,869,934), $p > 0.05$, Mann-Whitney, N/n = 5/3).

Overall, no statistically significant differences were found in the total PNN expression in the ACC between aged A30P and WT mice, similar to the young mice (Fig. 5.12). While the aged A30P mice did not show a significant increase in PNNs without PV somas as observed in the young A30P mice, a trend toward an increase compared to the aged WT was evident.

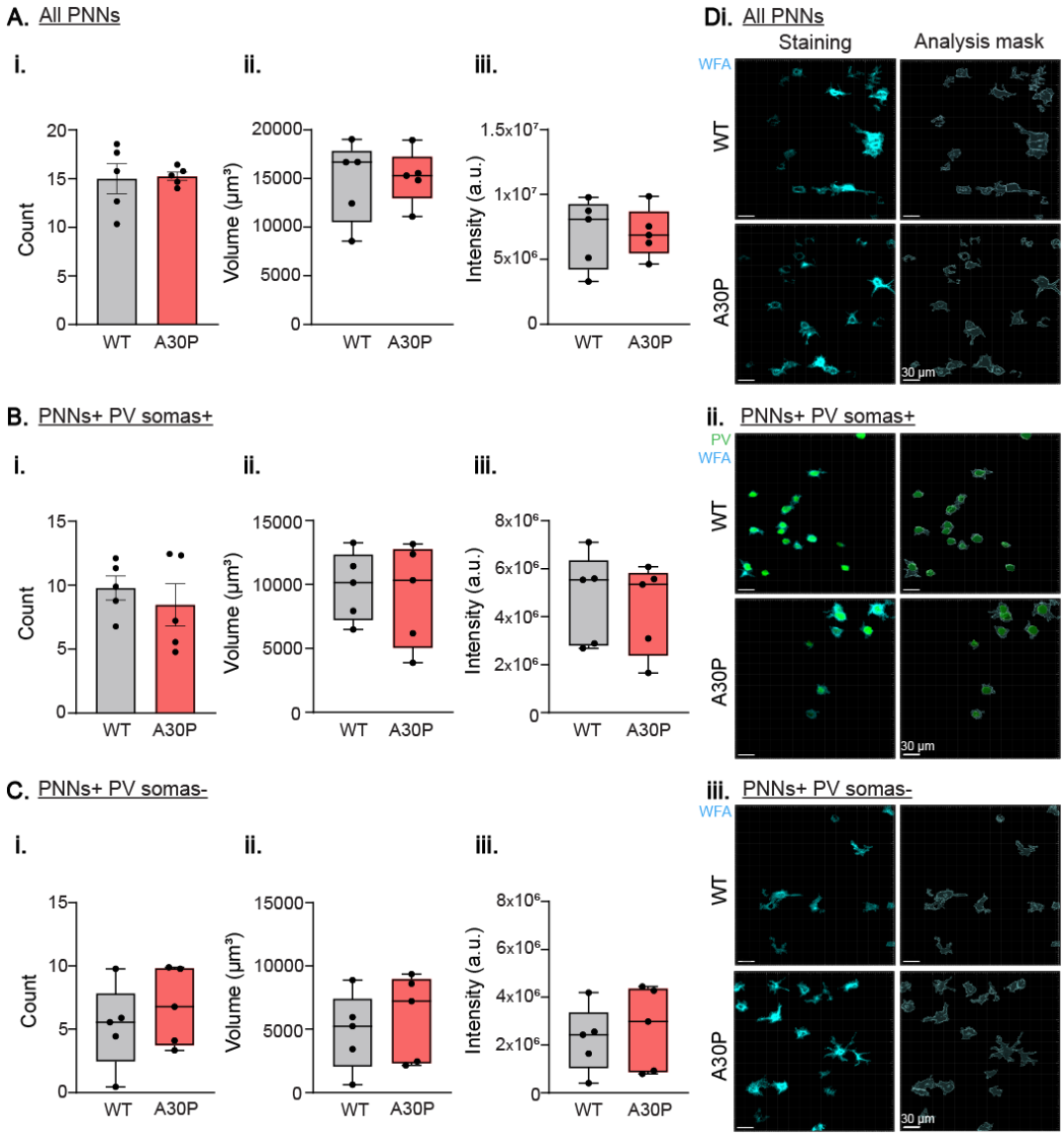

Figure 5.19. The PNNs in the ACC of aged A30P and WT mice. A – C. The median or mean (**i**) count, (**ii**) volume (µm^3) and (**iii**) intensity of (**A**) all PNNs, (**B**) PNNs with PV somas (PNNs+ PV somas+) and (**C**) PNNs without PV somas (PNNs+ PV somas-) are shown for the WT (grey) and A30P (red) mice. **D.** The staining and analysis mask example images for (**i**) all PNNs, (**ii**) PNNs with PV somas and (**iii**) PNNs without PV somas are demonstrated for both aged WT and A30P mice. These images are taken from the superficial ACC layers. Each data point represents the mean or median values per animal.

PNN expression in the deep and superficial layers of the ACC in aged A30P mice

As noted earlier, there were no differences in the count, volume, and intensity of all PNNs in the ACC between aged A30P and WT mice. Further analysis compared PNN expression between superficial and deep ACC layers in both genotypes. The two-way ANOVA on log-transformed data showed a significant effect between layers for both A30P and WT mice (Fig. 5.20Ai, ii, iii, count: $F(1,8) = 15.30$, volume: $F(1,8) = 15.28$, intensity: $F(1,8) = 17.32$, $p < 0.01$, two-way ANOVA, N/n = 5/3). Post hoc tests revealed significantly higher PNN mean count, volume, and intensity in superficial layers compared to deep layers for both aged A30P and WT mice ($p < 0.05$, Fisher's LSD), with no differences between genotypes.

PNNs around PV somas were also analysed in the superficial and deep ACC layers of aged mice. The two-way ANOVA on log-transformed data showed a significant effect between superficial and deep layers for both genotypes in the mean volume and intensity (Fig. 5.20Bi, ii, iii, PNNs+ PV somas+, volume: $F(1,8) = 5.32$, intensity: $F(1,8) = 6.66$, $p < 0.05$, two-way ANOVA, N/n = 5/3). Post hoc analysis revealed a significant increase in the mean intensity of PNNs around PV somas in the superficial ACC layers of WT mice compared to deep layers ($p < 0.05$, Fisher's LSD), though there was no significant difference in volume. Analysis of PNNs without PV somas (Fig. 5.20Ci, ii, iii, PNNs+ PV somas-) between layers and genotype was not possible, as the data remained not normally distributed despite log transformation, precluding the use of two-way ANOVA for these comparisons.

These findings suggest that total PNN expression, including PNNs around both PV and non-PV neurons, was higher in the superficial layers of the ACC in aged A30P and WT mice. This contrasts with the young mice, where total PNN expression showed no significant layer-specific differences. Notably, young A30P mice displayed a marked increase in PNNs around PV somas in the deep ACC layers compared to superficial layers which was not observed in the aged A30P group.

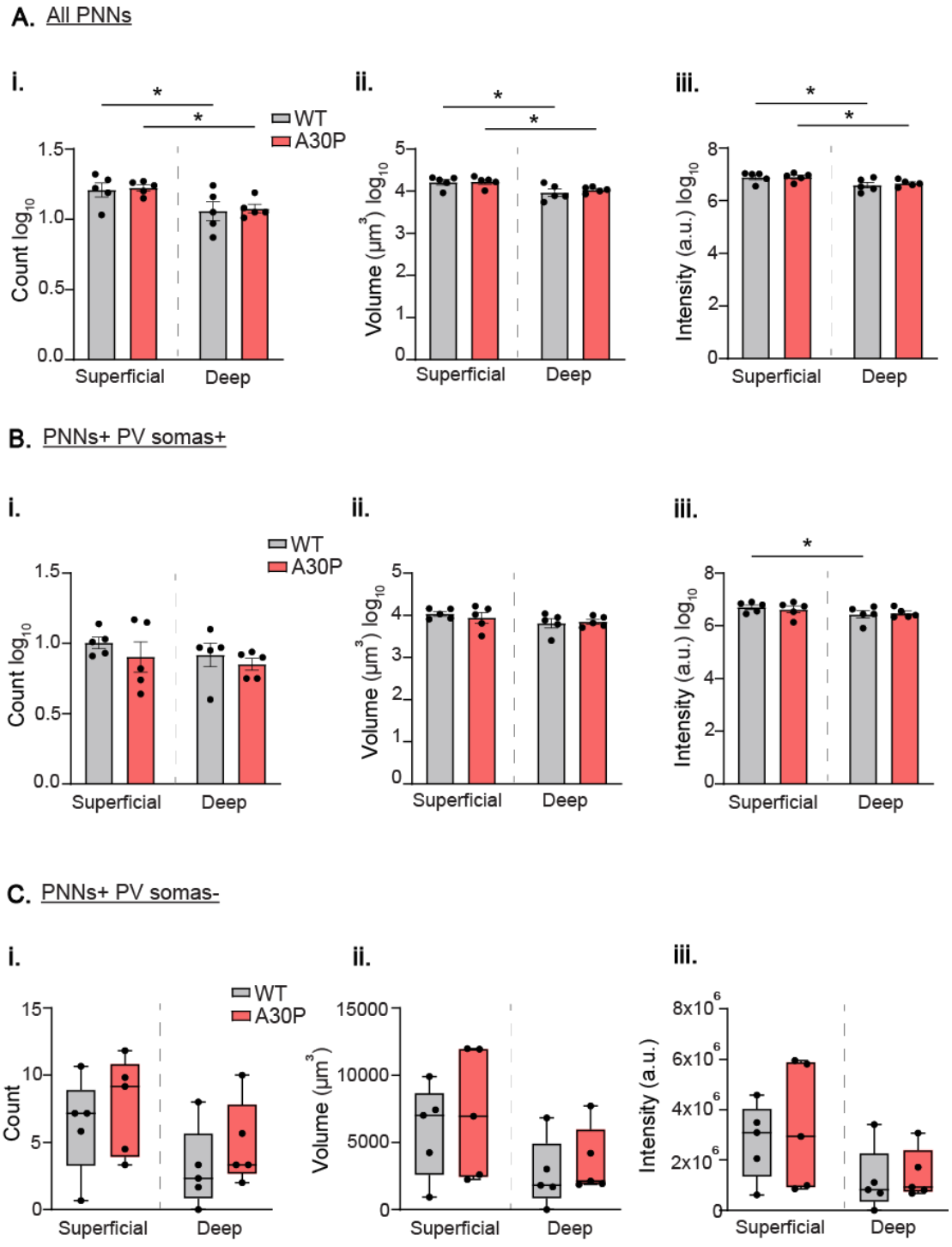

Figure 5.20. PNNs with PV somas and without PV somas in the superficial and deep ACC of aged A30P and WT mice. A - B. The log-transformed mean (**i**) count, (**ii**) volume (μm^3) and (**iii**) intensity (a.u.) are shown for (**A**) all PNNs and (**B**) PNNs with PV somas (PNNs+ PV somas+) in the superficial and deep ACC layers in both WT (grey) and A30P (red) aged mice. **C.** The median (**i**) count, (**ii**) volume and (**iii**) intensity for the PNNs without PV somas (PNNs+ PV somas-) are also shown in both the superficial and deep ACC layers in the WT and A30P aged mice. Each data point represents the mean or median values per animal.

5.4.5. *Effect of abnormal hα-syn on PV interneurons and PNNs in the ACC of young A30P transgenic mice.*

Research suggests that α-syn pathology, including its phosphorylation (pS129), worsens with age (Schell *et al.*, 2009). The A30P transgenic mouse model has shown network changes in PV interneurons potentially linked to age-related α-syn pathology (Schell *et al.*, 2009; Robson *et al.*, 2018; Gentzel *et al.*, 2021). Here, we assessed whether PNNs protect PV interneurons against hα-syn in the ACC across young and aged mice. First, hα-syn expression was examined in the superficial and deep ACC layers in young A30P mice to detect any expression differences. Next, hα-syn co-localisation with cell nuclei (Hoechst+ nuclei) was evaluated, with further analysis exploring hα-syn presence in PV somas and potential interactions with surrounding PNNs.

Laminar expression of hα-syn in the ACC in young A30P mice

Human α-syn was observed in neuronal somas as well as synaptic terminals in the ACC in the young A30P mice without any obvious expression patterns across the layers. The average volume and intensity of the hα-syn expression were analysed for the superficial and deep ACC layers (Fig. 5.21Ai and ii). No statistically significant differences were found for the mean volume or intensity of the hα-syn expression between the superficial and deep ACC layers (Fig 5.21Bi and ii, volume: Superficial 40,205 μm^3 vs Deep 22,891 μm^3, intensity: Superficial 68,961,083 a.u. vs Deep 31,663,027 a.u., $p > 0.05$, unpaired t-test, N/n = 5/3). However, a trend was observed suggesting slightly lower hα-syn expression in the deep layers compared to the superficial layers.

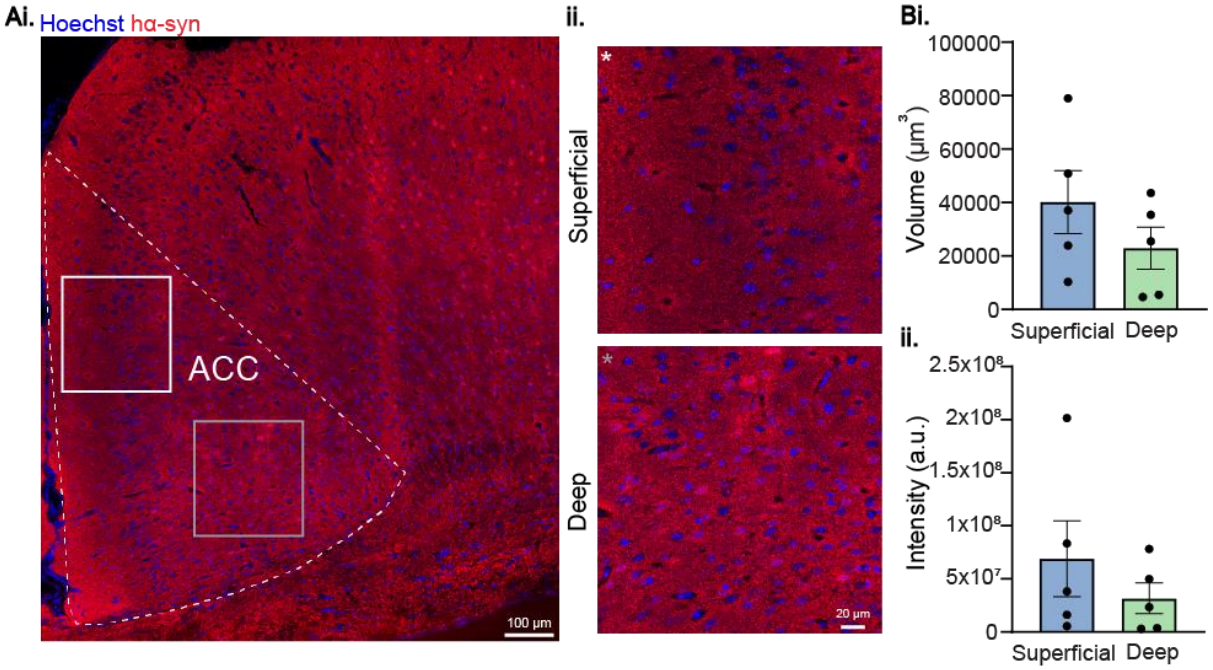

Figure 5.21. Expression of hα-syn in the superficial and deep layers of the ACC in young A30P mice. Ai. The overall expression of hα-syn (red) is demonstrated co-stained with all cell nuclei (Hoechst+ nuclei, blue) in an example young A30P mouse. **Aii**. Enlarged view of the squared areas showing the hα-syn expression in the superficial (white) and deep (grey) layers of the ACC. Scale bars at 100 µm and 20 µm. **B.** The mean (**i**) volume (µm^3) and (**ii**) intensity (a.u.) of the hα-syn expressed in the superficial and deep layers are shown for the young A30P mice. Each data point represents the mean values per animal.

Laminar localisation of hα-syn in cell nuclei

Evidence suggests that α-syn localises to the nuclei in transgenic animal models (Masliah *et al.*, 2000). However, whether hα-syn is present in the cell nuclei of A30P mice in the ACC remains unclear. To investigate, I examined hα-syn co-localisation with cell nuclei (Hoechst+) in the ACC of young A30P mice. The presence of hα-syn in some cell nuclei was confirmed (Fig. 5.22A, pink spots indicate hα-syn co-localising with Hoechst+ nuclei). I then measured the mean % volume and % intensity of hα-syn co-localising with Hoechst+ nuclei across the superficial and deep layers. Results showed no statistically significant differences in mean % volume or % intensity (Fig. 5.22Bi and ii, % volume: Superficial 2.79% vs Deep 2.65%, %intensity: Superficial 3.59% vs Deep 2.37%, $p > 0.05$, unpaired t-test, N/n = 5/3). However, there was a trend towards lower mean % intensity of hα-syn in Hoechst+ nuclei in the deep layers compared to the superficial layers.

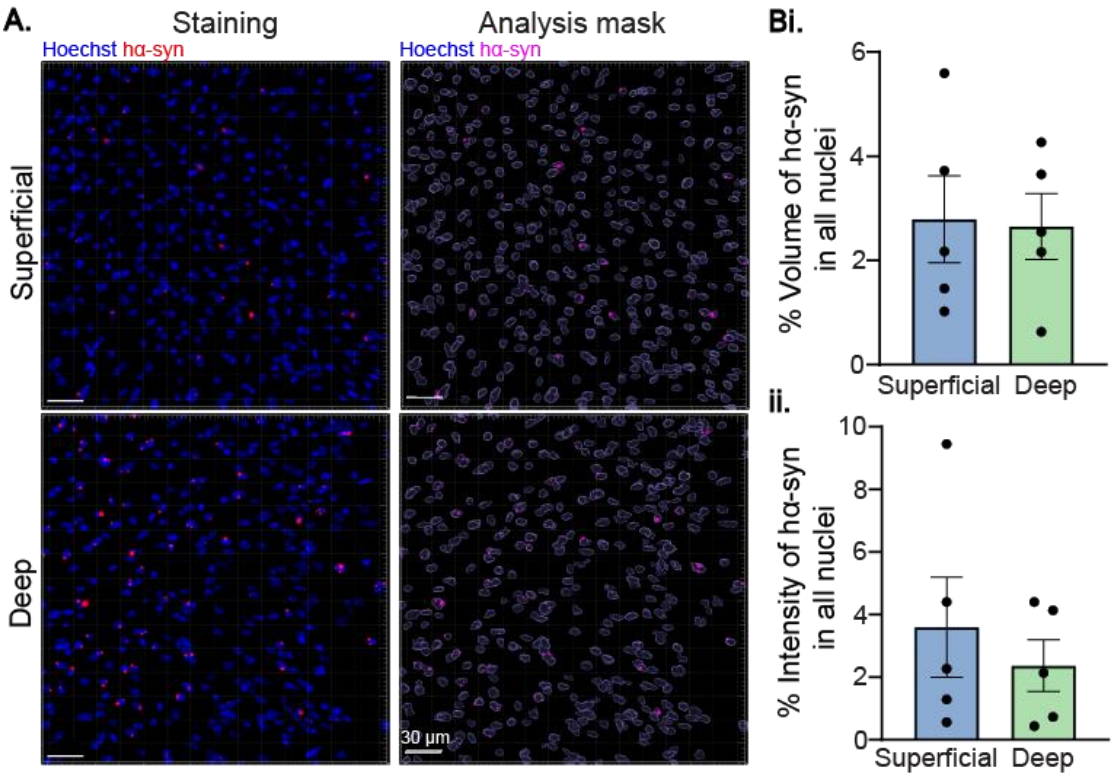

Figure 5.22. Nuclear localisation of hα-syn in the superficial and deep layers of the ACC in young A30P mice. A. The staining and analysis mask example images of hα-syn (red/pink) co-localising with cell nuclei (Hoechst+ nuclei, blue) in the superficial and deep ACC layers are shown. Scale bars at 30 µm. **B.** The mean (**i**) % volume and (**ii**) % intensity of hα-syn co-localising with the cell nuclei in the superficial and deep ACC layers are shown for the young A30P mice. Each data point represents the mean values per animal.

Expression of hα-syn in PV somas and PNNs in the ACC of young A30P mice

After confirming the cellular co-localisation of hα-syn, I examined its presence in PV somas and PNNs within the ACC of young A30P mice. PV somas co-localising with hα-syn were counted and categorised based on PNN presence and PNN co-localisation with hα-syn. Additionally, PV somas lacking hα-syn were measured (Fig. 5.23A). In young pre-symptomatic A30P mice, 64.8% of PV somas co-localised with hα-syn from the total number of PV somas (n = 251/437), while 35.2% did not (n = 154/437), indicating that hα-syn was present in about two-thirds of all PV neurons. Also, 57.4% of PV somas containing hα-syn were surrounded by PNNs (n = 251/437), while only 7.3% of PV somas containing hα-syn had no PNNs (n = 32/437). Of those

PV somas co-localising with both hα-syn and PNNs, 89.6% showed hα-syn within their PNNs (n = 225/251), while 10.4% had PNNs without hα-syn (n = 26/251).

The co-localisation of hα-syn within the PNNs was next quantified. Human α-syn was present in 77.7% of PNNs from the total number of PNNs (Fig. 5.23B, n = 578/744), regardless of cell type, while 22.3% of PNNs lacked hα-syn (n = 166/744). The 38.4% of PNNs contained hα-syn and surrounded PV somas (n = 286/744) while 39.2% of PNNs with hα-syn surrounded non-PV neurons (n = 292/744). Additionally, among PNNs co-localising with hα-syn, 74.8% surrounded PV somas that also contained hα-syn within the cell body (n = 214/286), while 25.2% surrounded PV somas without hα-syn (n = 72/286).

Overall, the data suggests that even in young pre-symptomatic A30P mice there is a considerable spread of hα-syn to the PV neuronal population. However, the amount of hα-syn present does not seem to depend upon the PNN presence.

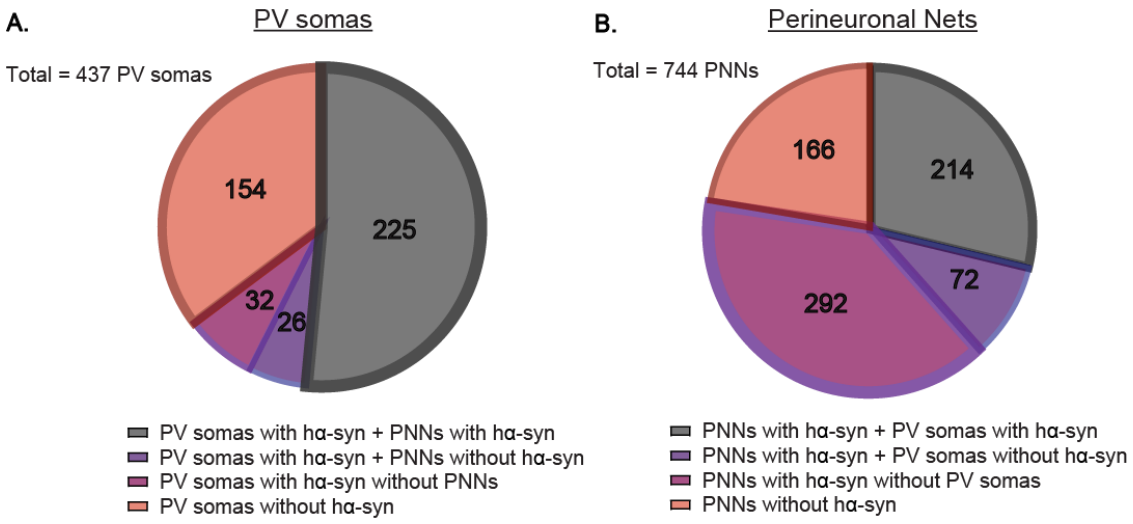

Figure 5.23. The proportion of PV somas and PNNs co-localising and not co-localising with hα-syn in the ACC of young A30P mice. A. Pie chart demonstrating the PV somas containing hα-syn surrounded by PNNs with hα-syn (grey, n = 225) and PNNs without hα-syn (purple, n = 26). Additionally, PV somas containing hα-syn but not surrounded by PNNs (magenta, n = 32) and PV somas not containing hα-syn (peach, n = 154) are shown. **B.** Pie chart showing the PNNs containing hα-syn around PV somas with hα-syn (grey, n = 214) and around PV somas without hα-syn (purple, n = 72). PNNs containing hα-syn but without PV somas (magenta, n = 292) and PNNs not containing hα-syn (peach, n = 166) are shown.

Impact of hα-syn on PV somas with and without PNNs in young A30P mice

I then investigated whether the presence of hα-syn in the PV somas affected PV expression. Specifically, I examined hα-syn levels in PV somas with and without PNNs in the ACC of young A30P mice (Fig. 5.24B, PV somas in green, PNNs in cyan, and hα-syn in red/pink) to determine if PNN presence influenced hα-syn presence within PV somas. The results showed no statistically significant differences in the mean % volume or % intensity of hα-syn between PV somas with PNNs (hα-syn in PV somas+ PNNs+) and those without PNNs (hα-syn in PV somas+ PNNs-) (Fig. 5.24Ci and ii, % volume of hα-syn in: PV somas+ PNNs+ 6.2% vs PV somas+ PNNs- 4.92%, % intensity of hα-syn in: PV somas+ PNNs+ 6.38% vs PV somas+ PNNs- 5.08%, $p > 0.05$, unpaired t-test, N/n = 5/3). This suggests that PNNs did not prevent hα-syn presence within PV somas.

Next, the hα-syn co-localisation with the PV somas with and without PNNs across ACC layers was examined in young A30P mice. Two-way ANOVA showed no statistically significant differences in mean % volume of hα-syn in PV somas with PNNs versus without PNNs, or between superficial and deep layers (Fig. 5.24Ciii, $p > 0.05$, N/n = 5/3). However, there was a trend towards reduced % volume of hα-syn in PV somas without PNNs in the deep layers compared to those with PNNs. For mean % intensity, a significant difference was observed between layers (Fig. 5.24Civ, $F(1,8) = 12.47$, $p < 0.01$, N/n = 5/3), with post hoc analysis indicating a marked decrease in hα-syn intensity in PV somas without PNNs in the deep layers versus superficial layers ($p < 0.01$, Fisher's LSD).

Overall, there were no differences between the expression of hα-syn in the PV somas with and without PNNs. However, there was a trend towards an increase in the co-localisation of hα-syn expression with the PV somas without PNNs in the superficial layers of the ACC.

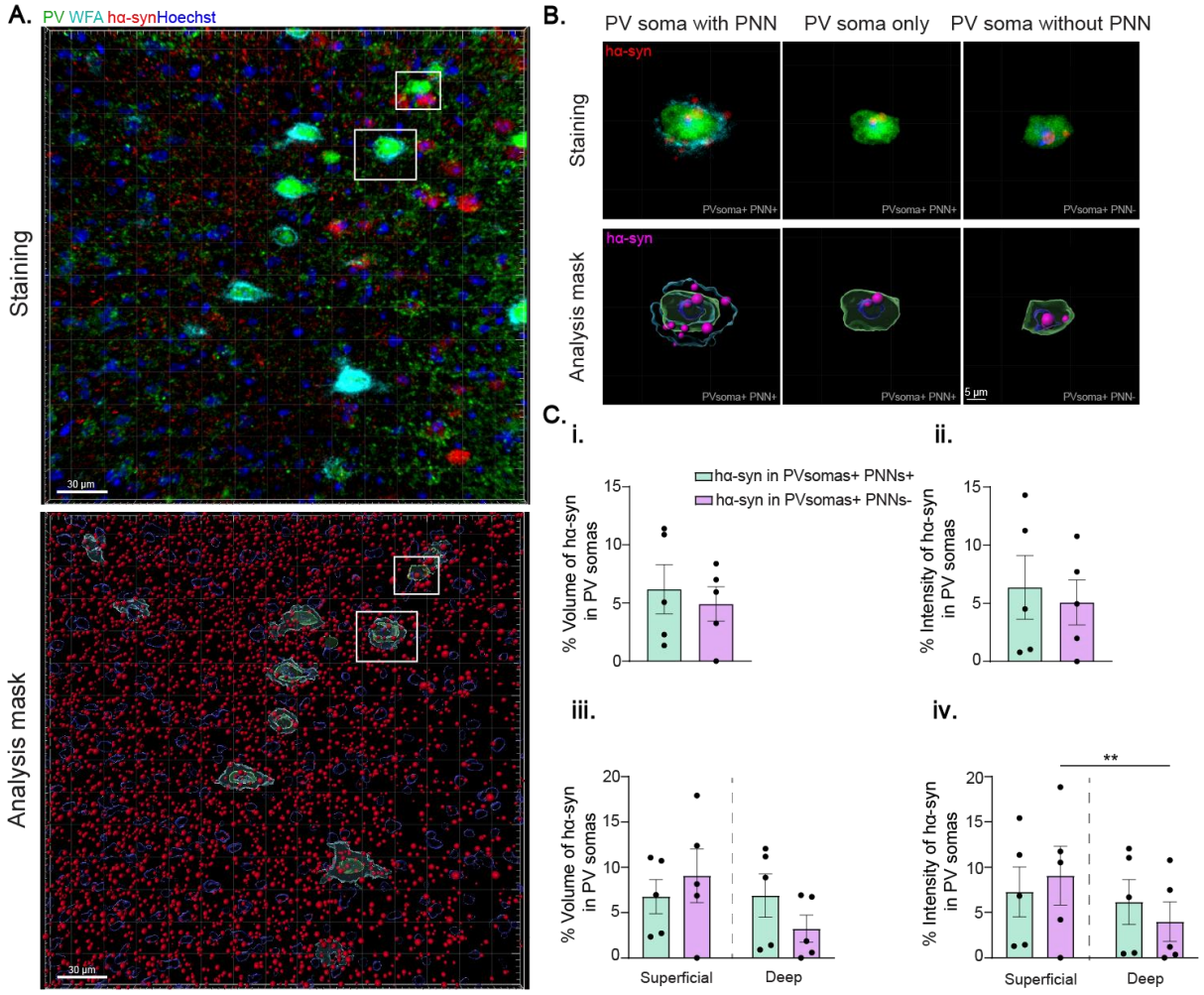

Figure 5.24. Co-localisation of hα-syn within PV somas with and without PNNs in the ACC of young A30P mice. A. Staining and analysis mask images showing PV somas (green), PNNs (cyan), hα-syn (red), and all nuclei (blue). **B.** Enlarged view of the squared areas showing the hα-syn (pink) co-localising with an example PV soma and its PNN and with another PV soma without a PNN. **C.** The mean (**i**) % volume and (**ii**) % intensity of the hα-syn in PV somas with PNN (green) and without a PNN (pink) in the ACC as well as the mean (**iii**) % volume and (**iv**) % intensity of hα-syn in PV somas with (green) and without PNNs (pink) across superficial and deep ACC layers in young A30P mice. Scale bars at 30 µm and 5 µm. Each data point represents the mean values per animal.

Co-localisation of hα-syn on PNNs with and without PV somas in young A30P mice

Human α-syn was detected in PNNs surrounding both PV somas and non-PV neurons in young A30P mice (Fig. 5.25B). To explore this further, the presence of hα-syn within PNNs surrounding PV somas versus non-PV neurons across the ACC was examined.

Results indicated no statistically significant differences in mean % volume or % intensity of hα-syn between PNNs with PV somas (hα-syn in PNNs+ PV somas+) and PNNs without PV somas (hα-syn in PNNs+ PV somas-) (Fig. 5.25Ci and ii, % volume of hα-syn in: PNNs+ PV somas+ 4.78% vs PNNs+ PV somas- 4.75%, % intensity of hα-syn in: PNNs+ PV somas+ 14.40% vs PNNs+ PV somas- 15.39%, $p > 0.05$, unpaired t-test, N/n = 5/3). Next, the hα-syn co-localisation with the PNNs with and without PV somas across ACC layers was examined in young A30P mice. The two-way ANOVA results showed no statistically significant differences in the mean % volume and % intensity of of hα-syn in PNNs with PV somas versus without PV somas, or between superficial and deep layers (Fig. 5.25Ciii and iv, $p > 0.05$, N/n = 5/3).

Thus, these findings showed the presence of hα-syn in those PNNs around PV somas and those around non-PV somas in the ACC of young pre-symptomatic A30P mice. Additionally, there were no differences in the presence of hα-syn in PNNs between the superficial and deep layers of the ACC.

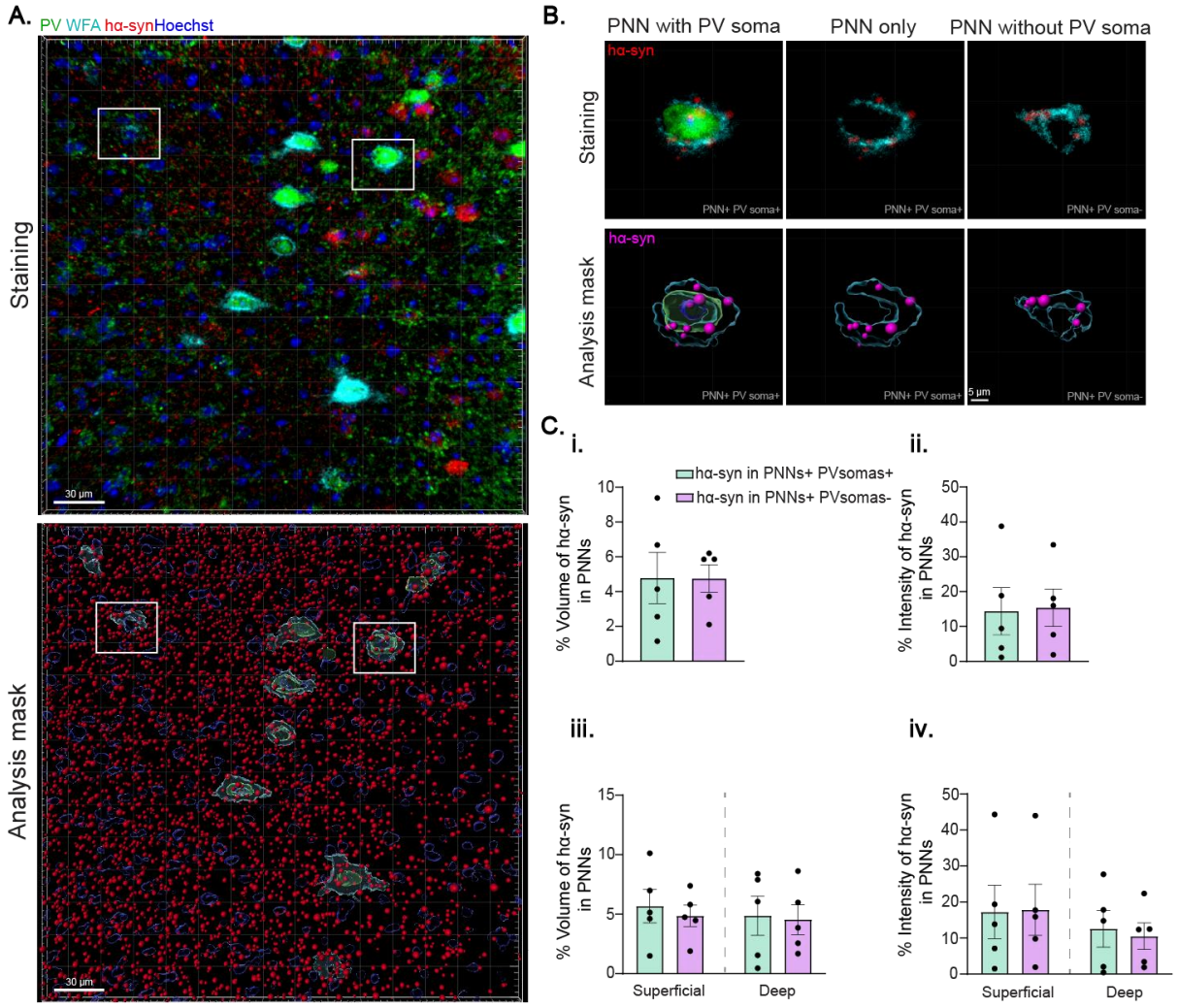

Figure 5.25. Co-localisation of hα-syn within PNNs with and without PV somas in the ACC of young A30P mice. A. Staining and analysis mask images showing PV somas (green), PNNs (cyan), hα-syn (red), and all nuclei (blue). **B.** Enlarged view of the squared areas showing the hα-syn (pink) co-localising with an example PNN and its PV soma and with another PNN without a PV soma. **C.** The mean (**i**) % volume and (**ii**) % intensity of the hα-syn in PNNs with PV somas (green) and without PV somas (pink) in the ACC as well as the mean (**iii**) % volume and (**iv**) % intensity of hα-syn in PNNs with (green) and without PV somas (pink) across superficial and deep ACC layers in young A30P mice. Scale bars at 30 µm and 5 µm. Each data point represents the mean values per animal.

5.4.6. *Effect of abnormal hα-syn on PV interneurons and PNNs in the ACC of aged A30P transgenic mice.*

Given that α-syn pathology is age-dependent, I investigated hα-syn expression in aged A30P mice (10 - 12 months). Specifically, I examined whether hα-syn was present in PV somas and PNNs.

Laminar expression of the hα-syn in the ACC in aged A30P mice

The mean volume and intensity of the hα-syn expression were analysed for the superficial and deep layers of the ACC in aged A30P mice (Fig. 5.26Ai and ii). No statistically significant differences were shown for the mean volume or intensity of the hα-syn expression between the superficial and deep layers of the ACC (Fig 5.26Bi and ii, volume: Superficial 41,084 μm^3 vs Deep 31,985 μm^3, intensity: Superficial 73,566,239 a.u. vs Deep 52,661,468 a.u., $p > 0.05$, unpaired t-test, N/n = 5/3). However, a trend towards a decrease in the hα-syn expression in the deep layers of the ACC compared to the superficial layers was observed which was also evident in the young A30P mice.

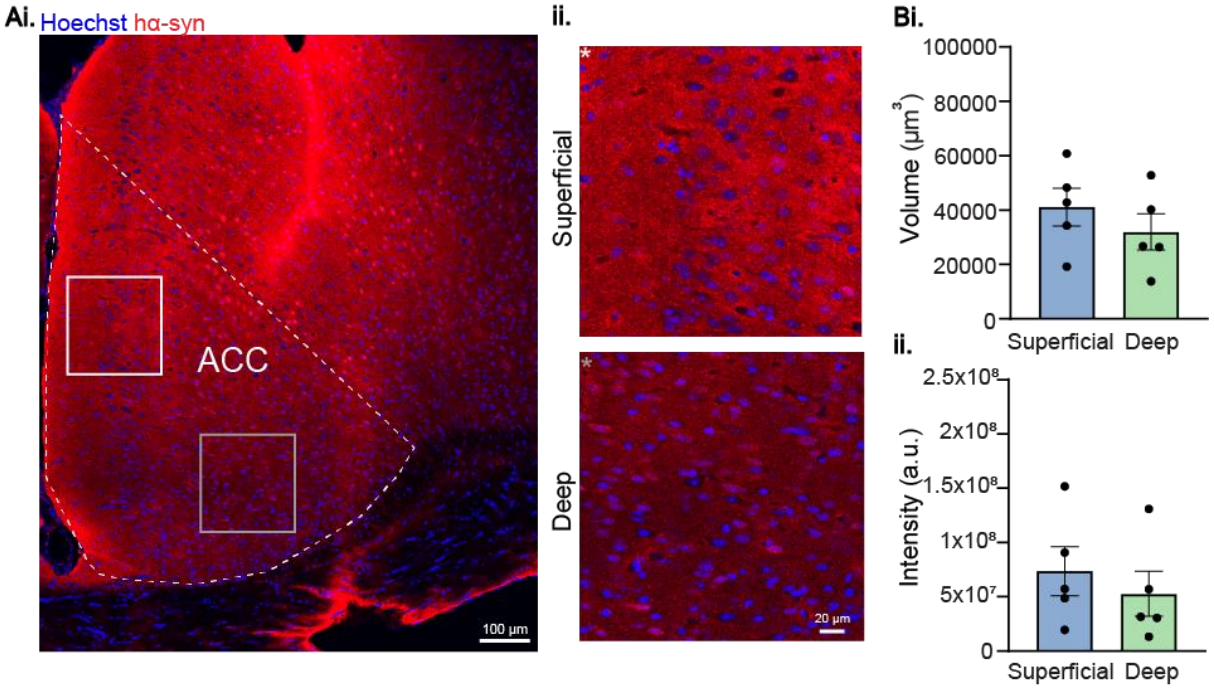

Figure 5.26. Expression of hα-syn in the superficial and deep layers of the ACC in aged A30P mice. Ai. The overall expression of hα-syn (red) is demonstrated co-stained with all cell nuclei (Hoechst+ nuclei, blue) in an example aged A30P mouse. **Aii.** Enlarged view of the squared areas showing the hα-syn expression in the superficial (white) and deep (grey) layers of the ACC. Scale bars at 100 µm and 20 µm. **B.** The mean (**i**) volume (μm^3) and (**ii**) intensity (a.u.) of the hα-syn expressed in the superficial and deep layers are shown for the aged A30P mice. Each data point represents the mean values per animal.

Laminar localisation of hα-syn in cell nuclei

After analysing overall hα-syn expression, I examined its co-localisation with cell nuclei (Hoechst+) in aged A30P mice. The presence of hα-syn in most cell nuclei was confirmed (Fig. 5.27A, with pink spots indicating hα-syn co-localising with Hoechst+ nuclei). Co-localisation was then assessed in the superficial and deep ACC layers, by measuring the median % volume and % intensity of hα-syn in Hoechst+ nuclei. No statistically significant differences were found in the median % volume or % intensity of hα-syn expression in Hoechst+ nuclei between superficial and deep ACC layers (Fig. 5.27Bi and ii, % volume: Superficial 5.13% (3.03, 6.50) vs Deep 3.64% (2.65, 5.99), %intensity: Superficial 4.85% (1.75, 9.65) vs Deep 3.19% (0.86, 9.32), $p > 0.05$, Mann-Whitney, N/n = 5/3). A trend towards reduced nuclear co-localisation in

the deep layers was though observed. Additionally, there was a noticeable increase in nuclear hα-syn co-localisation in aged A30P mice compared to young A30P mice.

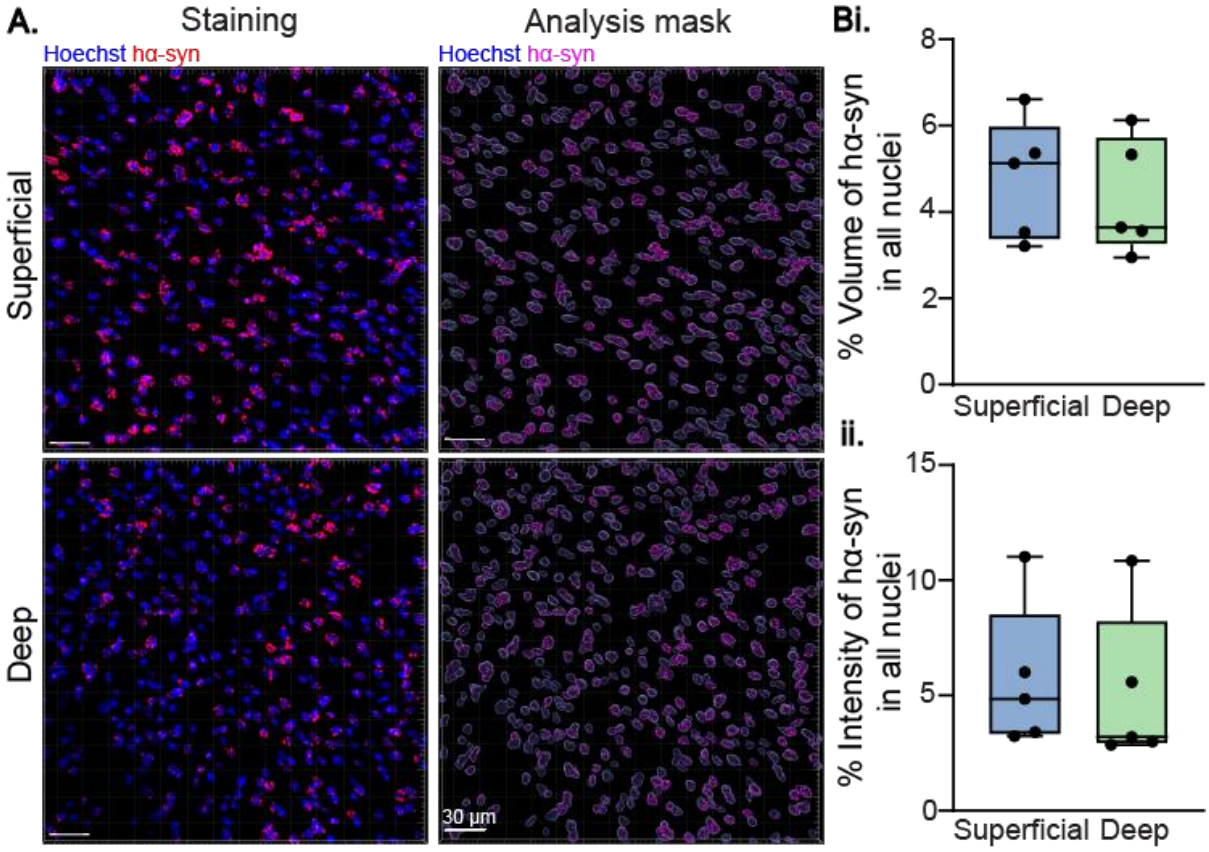

Figure 5.27. Nuclear localisation of hα-syn in the superficial and deep layers of the ACC in aged A30P mice. A. The staining and analysis mask example images of hα-syn (red/pink) co-localising with cell nuclei (Hoechst+ nuclei, blue) in the superficial and deep ACC layers are shown. Scale bars at 30 µm. **B.** The median (**i**) % volume and (**ii**) % intensity of the hα-syn co-localising with the cell nuclei in the superficial and deep ACC layers are shown for the aged A30P mice. Each data point represents the median values per animal.

Expression of hα-syn in PV somas and PNNs in the ACC of aged A30P mice

I next examined the presence of hα-syn in PV somas and PNNs in the ACC of aged A30P mice, as observed in younger mice (Fig. 5.24, 5.25). Counts of PV somas and PNNs co-localising with hα-syn were determined, with PV somas categorised based on whether they had a PNN, and whether that PNN also contained hα-syn. PV somas without hα-syn were also recorded (Fig. 5.28A). Of all PV somas, 99.4% co-localised with hα-syn (n = 529/532), a marked increase from the 64.8% seen in young A30P mice, indicating an age-dependent increase in hα-syn spread.

Of all PV somas, 72% co-localised with hα-syn and were surrounded by PNNs (n = 383/532), while 27.4% co-localised with hα-syn but lacked PNNs (n = 146/532). Only 0.6% of PV somas (n = 3/532) did not co-localise with hα-syn. Among the PV somas with hα-syn and surrounded by PNNs, 99.2% of them had PNNs which also contained hα-syn (n = 380/383), with just 0.8% having PNNs without hα-syn (n = 3/383).

The co-localisation of hα-syn within PNNs was examined in more detail (Fig. 5.28B). In aged A30P mice, 99.4% of all PNNs (n = 682/686) contained hα-syn, with only 0.6% not showing co-localisation (n = 4/686). Of all PNNs, 55.1% co-localised with hα-syn and surrounded PV somas that also contained hα-syn (n = 378/686), while 0.1% of PNNs with hα-syn surrounded PV somas without hα-syn (n = 1/686). Nearly half of the PNNs, 44.2%, co-localised with hα-syn and surrounded non-PV neurons (n = 303/686), suggesting a substantial presence of hα-syn in PNNs around non-PV neurons.

In the aged A30P mice, hα-syn co-localisation increased markedly in both PV somas and PNNs (99.4% for each) compared to young A30P mice, where only 64.8% of PV somas and 77.7% of PNNs showed co-localisation with hα-syn. Nearly all PV somas, with or without PNNs, and almost all PNNs, whether associated with PV somas or not, co-localised with hα-syn.

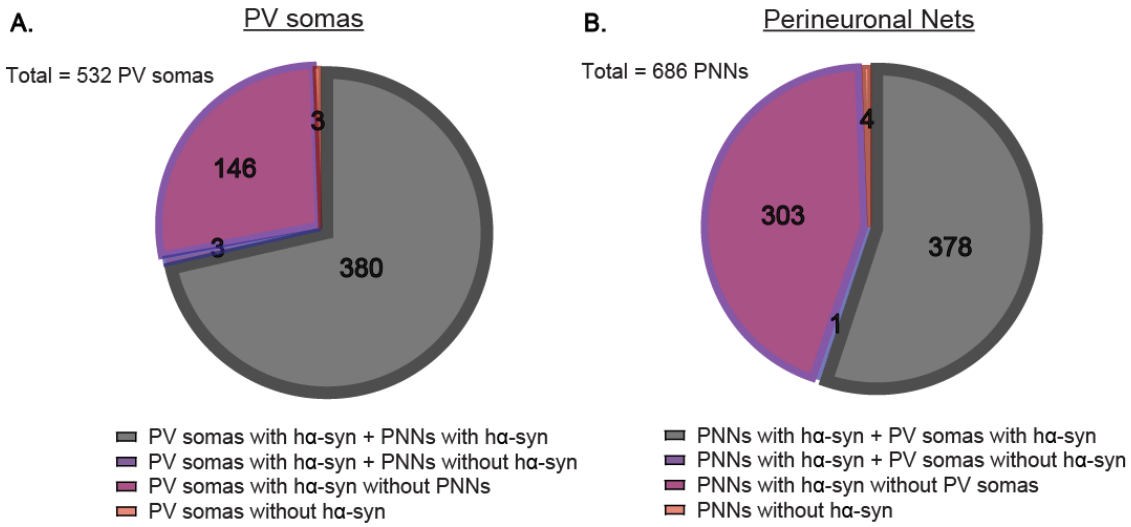

Figure 5.28. The proportion of PV somas and PNNs co-localising and not co-localising with hα-syn in the ACC of aged A30P mice. A. Pie chart demonstrating the PV somas containing hα-syn surrounded by PNNs with hα-syn (grey, n = 380) and PNNs without hα-syn (purple, n = 3). Additionally, PV somas containing hα-syn but not surrounded by PNNs (magenta, n = 146) and PV somas not containing hα-syn (peach, n = 3) are shown. **B.** Pie chart showing the PNNs containing hα-syn around PV somas with hα-syn (grey, n = 378) and around PV somas without hα-syn (purple, n = 1). PNNs containing hα-syn but without PV somas (magenta, n = 303) and PNNs not containing hα-syn (peach, n = 4) are shown.

Impact of hα-syn on PV somas with and without PNNs in aged A30P mice

The hα-syn co-localisation with PV somas was analysed in greater detail by examining its presence in PV somas with and without PNNs in the ACC of aged A30P mice (Fig. 5.29B, PV somas in green, PNNs in cyan, hα-syn in red/pink). No statistically significant differences were found in the mean % volume or median % intensity of hα-syn expression between PV somas with PNNs (hα-syn in PV somas+ PNNs+) and PV somas without PNNs (hα-syn in PV somas+ PNNs-) (Fig. 5.29Ci and ii, % volume of hα-syn in: PV somas+ PNNs+ 7.52% vs PV somas+ PNNs- 7.07%, $p > 0.05$, unpaired t-test, % intensity of hα-syn in: PV somas+ PNNs+ 7.27% (1.01, 17.33) vs PV somas+ PNNs- 8.57% (3.26, 18.86), $p > 0.05$, Mann-Whitney, N/n = 5/3). This suggests hα-syn co-localised consistently across PV somas in aged A30P mice, regardless of the presence of a surrounding PNN.

After assessing hα-syn co-localisation in PV somas in the ACC, I next examined its presence in PV somas between the superficial and deep layers. The two-way ANOVA revealed no statistically significant differences in the mean % volume of hα-syn co-localising with PV somas with PNNs versus without PNNs, nor between the superficial and deep ACC layers (Fig. 5.29Ciii, $p > 0.05$, two-way ANOVA, N/n = 5/3). Analysis of the average % intensity across layers could not be performed due to the non-normal distribution of data, even after log transformation (Fig. 5.29Civ).

Overall, these findings indicate that hα-syn was present in nearly all PV somas, regardless of PNN presence, with consistent expression across the superficial and deep ACC layers in aged A30P mice. Notably, the trend toward increased hα-syn co-localisation in PV somas without PNNs seen in the superficial layers of young A30P mice was absent in aged A30P mice (Fig. 5.24).

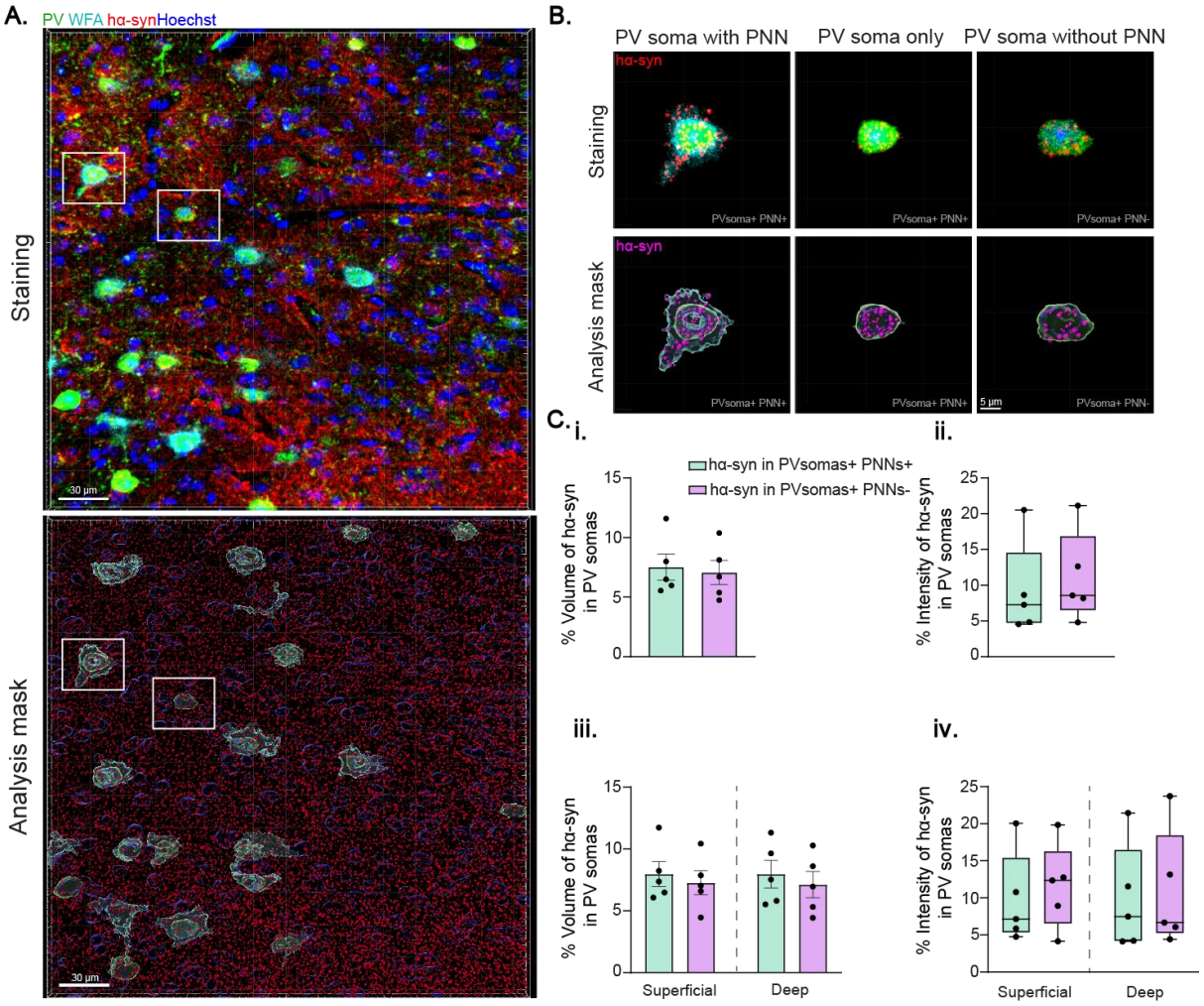

Figure 5.29. Co-localisation of hα-syn within PV somas with and without PNNs in the ACC of aged A30P mice. A. Staining and analysis mask images showing PV somas (green), PNNs (cyan), hα-syn (red), and all nuclei (blue). **B.** Enlarged view of the squared areas showing the hα-syn (pink) co-localising with an example PV soma and its PNN and with another PV soma without a PNN. **C.** The (**i**) mean % volume and (**ii**) median % intensity of the hα-syn in PV somas with PNN (green) and without a PNN (pink) in the ACC as well as the (**iii**) mean % volume and (**iv**) median % intensity of hα-syn in PV somas with (green) and without PNNs (pink) across superficial and deep ACC layers in aged A30P mice. Scale bars at 30 µm and 5 µm. Each data point represents the mean or median values per animal.

Co-localisation of hα-syn on PNNs with and without PV somas in aged A30P mice

Human α-syn was observed in both PNNs with PV somas and PNNs without PV somas in aged A30P mice (Fig. 5.30B). To investigate this further, I examined hα-syn co-localisation with PNNs in the ACC. Results showed no statistically significant differences in the mean % volume or % intensity of hα-syn expression between PNNs with PV somas (hα-syn in PNNs+ PV somas+) and PNNs without PV somas (hα-syn in PNNs+ PV somas-) (Fig. 5.30Ci and ii, % volume of hα-syn in: PNNs+ PV somas+ 6.89% vs PNNs+ PV somas- 6.29%, % intensity of hα-syn in: PNNs+ PV somas+ 27.83% vs PNNs+ PV somas- 23.97%, $p > 0.05$, unpaired t-test, N/n = 5/3). Similar results were found in young A30P mice (Fig. 5.25).

Further analysis of hα-syn expression in PNNs was conducted to explore potential differences between superficial and deep ACC layers. The mean % volume and % intensity of hα-syn were assessed. A significant interaction effect was observed between ACC layers for the mean % volume of hα-syn expression (Fig. 5.30Ciii, $F(1,8) = 14.15$, $p < 0.01$, two-way ANOVA, N/n = 5/3), with a marked increase in the superficial layers for both PNNs with and without PV somas compared to the deep layer, ($p < 0.05$, Fisher's LSD). No significant differences were found for the mean % intensity of hα-syn between layers (Fig. 5.30Civ, $p > 0.05$, two-way ANOVA, N/n = 5/3), though there was a trend for increased co-localisation in the superficial layer. This non-significant pattern was also observed in young A30P mice (Fig. 5.25).

Thus, hα-syn was detected in both PNNs with PV somas and those without PV somas in the ACC of aged (10-12-month-old) A30P mice. This co-localisation predominantly occurred in the superficial ACC layers, consistent with findings from young A30P mice (Chapter 5.4.5).

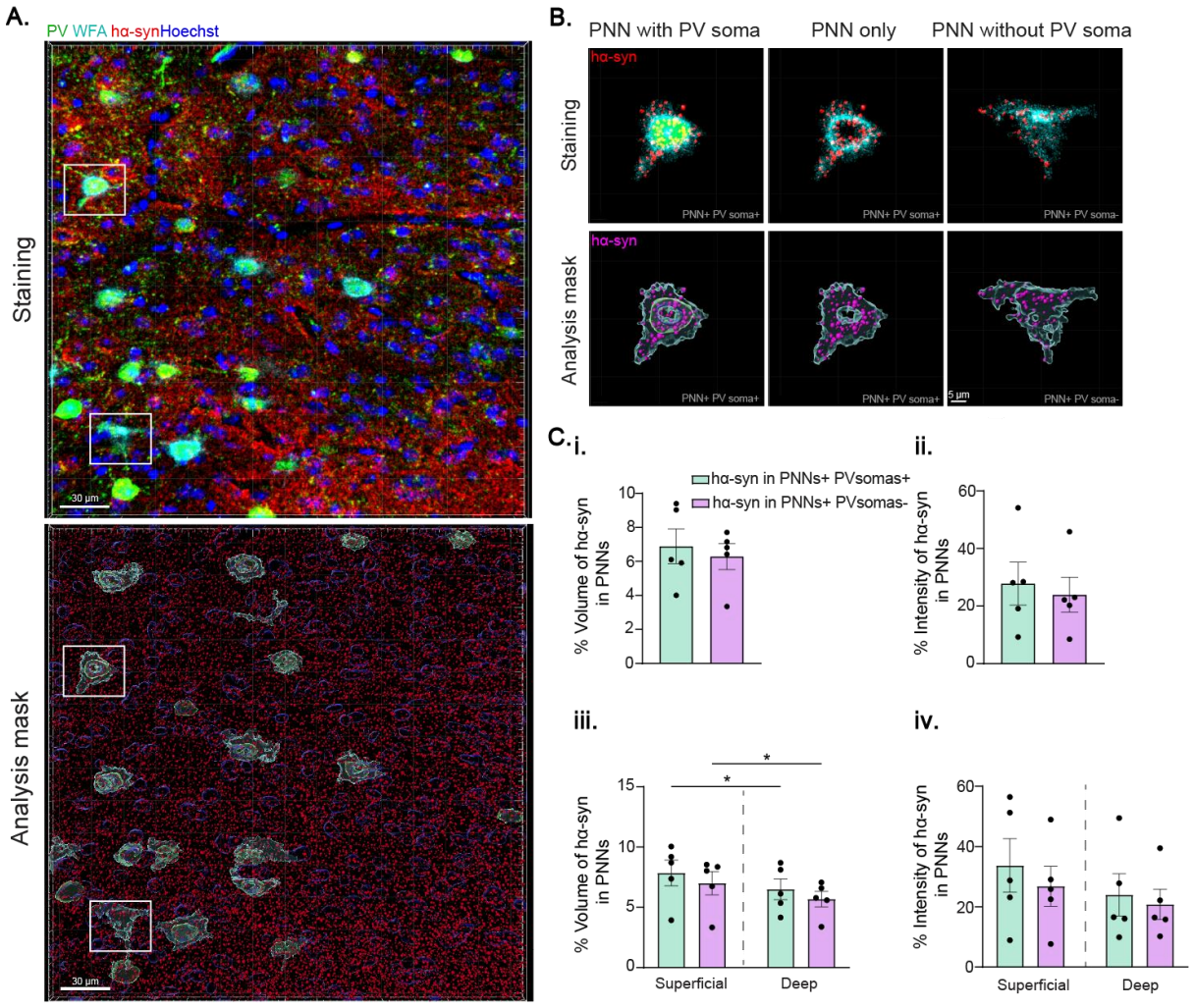

Figure 5.30. Co-localisation of hα-syn within PNNs with and without PV somas in the ACC of aged A30P mice. A. Staining and analysis mask images showing PV somas (green), PNNs (cyan), hα-syn (red), and all nuclei (blue). **B.** Enlarged view of the squared areas showing the hα-syn (pink) co-localising with an example PNN and its PV soma and with another PNN without a PV soma. **C.** The mean (**i**) % volume and (**ii**) % intensity of the hα-syn in PNNs with PV somas (green) and without PV somas (pink) in the ACC as well as the mean (**iii**) % volume and (**iv**) % intensity of hα-syn in PNNs with (green) and without PV somas (pink) across superficial and deep ACC layers in aged A30P mice. Scale bars at 30 µm and 5 µm. Each data point represents the mean values per animal.

5.5. Discussion

5.5.1. *Summary of the main findings in Chapter 5.*

Young 2-4-month-old mice

- PV soma number and intensity showed non-significant reductions in A30P mice, with a trend towards increased PV expression in PV+ processes.
- PV somas in the deep ACC layers of A30P mice were significantly larger and expressed higher PV levels compared to superficial layers. In WT mice, superficial PV somas were larger than those in A30P.
- A30P mice showed trends of reduced count, volume and intensity for PV somas with and without PNNs compared to WT, but deep ACC PV somas with PNNs in A30P mice were larger and expressed more PV than those in superficial layers.
- There were significantly more PNNs around non-PV neurons in A30P.
- Trend towards decreased expression of hα-syn in the deep layers of ACC in A30P mice compared to the superficial layers.
- Human α-syn was present in PV somas, PNNs, and some cell nuclei in the ACC of A30P mice.
- Most PV somas with hα-syn were surrounded by PNNs that also contained hα-syn.
-

Aged 10-12-month-old mice

- Trend towards decreased number and volume in all PV somas in A30P mice compared to the WT.
- PV expression in PV somas with and without PNNs did not differ significantly between superficial and deep ACC layers or between A30P and WT mice.
- PNN intensity and numbers were notably higher in the superficial ACC layers for both groups.
- A30P mice showed a trend towards an increase in PNNs without PV somas compared to WT.

- A trend towards decreased hα-syn expression in the deep ACC layers of aged A30P mice but higher in cell nuclei compared to young A30P mice.
- Presence of hα-syn in nearly all PV somas and PNNs.
- No layer-specific differences in hα-syn expression were observed in PV somas, but PNNs in superficial layers showed stronger hα-syn expression than those in deep layers.

5.5.2. *Age-dependent difference in hα-syn expression in the ACC of A30P mice.*

It is known that in the A30P mice, hα-syn is expressed under the Thy-1 promoter in the excitatory projection neurons (Feng *et al.*, 2000; Sugino *et al.*, 2005). However, there is limited understanding of the localisation of hα-syn and its impact on interneurons as well as PNNs in A30P mice. It is hypothesised that α-syn spread indirectly affects the interneurons through excitatory synaptic interactions (Ghiglieri *et al*., 2018; Calabresi *et al.*, 2023). A detailed co-localisation of hα-syn within the PV neuronal somas and PNNs was not studied before, particularly in the mouse ACC. Surprisingly, we found that hα-syn co-localised with most PV somas (64.8%) in the ACC of young pre-symptomatic 2-4-month-old A30P mice, including those surrounded and not surrounded by PNNs. Previous work in our lab showed the co-localisation of hα-syn in around 25% of PV neuronal somas in the hippocampus of young 2-5-month-old A30P mice (Tweedy *et al.*, 2021). However, no other study has revealed the presence of hα-syn in so many PV somas in the ACC of these mice at a young age.

From our observations, hα-syn was shown to be localised within the soma of some neurons with the typical morphology of pyramidal neurons, as well as in synaptic terminals around the cortex and ACC. Thus, it could be possible that hα-syn was spread through excitatory synaptic interactions via exocytosis from the neuronal soma and dendrites onto the surrounding PNNs and eventually to the PV neuronal somas (Lee *et al*., 2005; Emmanouilidou *et al.*, 2010; Alvarez-Erviti *et al.*, 2011; Fussi *et al.*, 2018; Minakaki *et al.*, 2018; Zhang *et al.*, 2018). This hypothesis could also apply to the PV interneurons without PNNs as we noticed that hα-syn was also present within their somas. However, hα-syn could also be expressed in the PV interneurons without being transferred from the excitatory synapses. Proskurina and Zaitsev (2021) found

that in mice expressing channelrhodopsin-2 (ChR2) under the Thy-1 promoter, apart from pyramidal cells expressing ChR2, there were also fast-spiking interneurons expressing ChR2 in the deep layers of the entorhinal cortex (Proskurina and Zaitsev, 2021). Thus, hα-syn protein might be synthesised in the somas of some PV interneurons in the ACC but also spread through the excitatory synaptic connections increasing its localisation in the interneurons and their PNNs. However, in this thesis, hα-syn expression in excitatory neurons in the ACC of A30P mice was not examined.

We also provided evidence for the presence of nuclear localisation of hα-syn (Hoechst+ nuclei) in the ACC of young A30P mice. The nuclear localisation of pathologic α-syn leads to physical and chemical property changes in the DNA (Vasudevaraju *et al.*, 2012; Milanese *et al.*, 2018). Also, nuclear localisation of α-syn has been found in other α-syn transgenic animals and cell models (McLean et al., 2000; Specht *et al.*, 2005; Yuan *et al.*, 2008; Gonçalves and Outeiro, 2013; Pinho *et al.*, 2019). However, to my knowledge, our results are the first to show the presence of hα-syn in the cell nuclei in the ACC of young A30P mice.

It is known that with increasing age, the α-syn pathology exacerbates and there is increased aggregation of α-syn into LBs and fibrils but also increased phosphorylation of α-syn (pS129) (Schell *et al.*, 2009; Gentzel *et al.*, 2021). In the aged A30P mice, there is increased hα-syn expression and aggregation into oligomers and fibrils while the animals exhibit cognitive impairments and motor dysfunction by 12 - 14 months of age (Kahle *et al*., 2000, 2001). In the ACC of aged 10-12-month-old A30P mice, there was significantly greater hα-syn expression in the cell somas, dendrites, axons, and synaptic terminals compared to the young A30P mice. Human α-syn was present in almost all PV neuronal somas (99.4%) and most of these PV interneurons were surrounded by PNNs in the ACC of aged A30P mice. Also, we found that hα-syn was present within nearly all cell nuclei in the ACC of aged A30P mice. Thus, the accumulation of hα-syn in PV somas and cell nuclei within the ACC increased with age in A30P transgenic mice. This age-related increase in hα-syn expression aligns with previous studies on these transgenic mice, which reported progressive hα-syn expression and aggregation over time (Kahle *et al*., 2000, 2001). However, we provided new findings for the A30P mouse model showing this increased pathology which also involved PV neurons in the ACC.

5.5.3. *No significant changes in PV expression in the ACC of young and aged A30P mice.*

To date, no studies have explored the effects of α-syn pathology on PV interneurons in any brain region of A30P mice at a pre-symptomatic stage. This study revealed that in the ACC of young pre-symptomatic A30P mice, there was a trend towards reduced PV soma number, size, and intensity compared to WT mice, accompanied by increased PV expression in neuronal processes. It is currently unclear why the PV soma size might be reduced in the A30P mice, while the expression of PV in the axonal plexus increased.

The A30P mice exhibited laminar differences, with fewer PV somas in the superficial layers of the ACC compared to the deep layers. The observed non-significant reduction in overall PV expression and PV cell number may contribute to altered neuronal network activity in the ACC, potentially linked to hα-syn pathology. Previous studies have demonstrated hyperexcitability in the hippocampus of young A30P transgenic mice, suggesting that hα-syn pathology may impair PV neuronal function (Tweedy *et al.*, 2021). As a higher cognitive region, the ACC plays a critical role in maintaining optimal neuronal network function. Subtle changes may emerge in the ACC of young pre-symptomatic A30P mice, potentially becoming more pronounced with age due to the progressive, age-dependent increase in hα-syn pathology (Schell *et al.*, 2009).

In the ACC of aged A30P mice, the non-significant decrease in the count, volume, and PV expression of all PV somas was also evident compared to the WT mice. On the other hand, the aged A30P mice did not show a trend towards an increased PV expression in the PV+ processes as seen in the young A30P mice. The observed trend of reduced PV expression in PV somas in both young and aged A30P mice may reflect subtle changes in PV activity and neuronal network function, potentially driven by early-stage hα-syn pathology. The 10-12-month-old A30P mice analysed in this study may not have been aged enough to exhibit severe hα-syn pathology, which could potentially lead to PV neuronal loss in older mice. However, due to the onset of severe motor dysfunction in A30P mice beyond 14 months of age, requiring euthanasia, investigating older animals is not feasible. Additionally,

interindividual variability has been reported in these α-syn transgenic mice (Fagerqvist *et al.*, 2013; Ekmark-Lewén *et al.*, 2018).

Evidence shows that in post-mortem brain tissue of DLB patients, there was a significant decrease in PV neuronal number in the hippocampus associated with the α-syn pathology (Bernstein *et al.*, 2011). However, most studies in neurodegeneration are focused on the hippocampus, thus knowledge about PV neuronal dysfunction in the mouse ACC is limited. A study demonstrated a significantly lower PV neuronal density in the deep layers of the cingulate cortex of 6-9-month-old 5xFAD mice, showing a 50% reduction compared to WT mice. This loss was associated with a marked cognitive decline and an increased Aβ plaque burden (Ali *et al.*, 2019). It has been shown that the ACC is a brain area affected early in AD as the accumulation of Aβ deposits was observed from an early stage in AD patients (Braak and Braak, 1991; Zhou *et al.*, 2012). The ACC is also affected at an early stage by α-syn pathology causing personality changes and cognitive decline in PD patients (Braak et al., 2000). However, there is no evidence showing neuronal network dysfunction associated with changes in PV interneurons in the ACC in DLB. Thus, our findings provide a first glimpse into potential neuronal network differences in a DLB transgenic mouse model.

For future research, it would be interesting to investigate brain areas that exhibit later α-syn pathology development in A30P transgenic mice, such as the motor cortex. While our study focused on ACC and other work in our lab investigated the hippocampus, which show early α-syn pathology (Kahle *et al.*, 2000, 2001; Kövari *et al.*, 2003; Outeiro *et al.*, 2019), examining a brain area with later pathology would provide a better understanding of α-syn progression and its impact on neuronal networks. Comparative analyses between the ACC, hippocampus, and motor cortex could help elucidate region-specific responses to α-syn pathology. It would be important to examine the localisation and interactions of hα-syn with PV interneurons and PNNs in both young and aged A30P mice. This could help determine whether the patterns observed in early affected areas apply or differ in regions affected later in disease progression.

5.5.4. *Increase in PNNs around non-PV neurons in the ACC of young and aged A30P mice.*

Previous research has shown that PV interneurons are surrounded by PNNs in the mPFC in young WT mice including the ACC (Ueno *et al.*, 2017; Ueno, Fujii, *et al.*, 2019). However, there are no studies examining the PNN expression in the ACC in animal models of neurodegeneration, specifically in α-synucleinopathies. We found that most of the PV interneurons in the ACC were surrounded by PNNs in both A30P and WT mice suggesting that hα-syn pathology at this early stage of disease did not affect the overall distribution of PNNs in the ACC.

In this study, PNNs around non-PV neurons were shown in the ACC in both genotypes. Interestingly, in the ACC of young A30P mice, significantly more PNNs were surrounding non-PV neurons compared to the young WT. Laminar differences were also observed in the young A30P mice. The PNNs around non-PV neurons were mainly located in the superficial layers compared to the deep layers which was not evident in the WT mice. This PNN population could have been around other types of inhibitory neurons or pyramidal cells. Studies showed that PNNs surrounded SST inhibitory interneurons, but this type of PNN expression was limited around the brain (McRae *et al.*, 2010; Berretta *et al.*, 2015; Chu *et al.*, 2018).

Literature suggests that PNNs surround excitatory neurons in some brain regions in rodents including the amygdaloid nuclei, pyriform cortex, dorsal tenia tecta and entorhinal cortex (Lensjø *et al.*, 2017; Morikawa *et al.*, 2017). PNNs have also been seen surrounding neurons with the typical morphology of pyramidal cells in the PFC in humans (Enwright *et al.*, 2016; Alcaide *et al.*, 2019). However, in this thesis, I did not specifically stain the pyramidal cell population thus I cannot confirm that the non-PV neurons with PNNs were pyramidal cells, but it is likely that a large proportion will be excitatory cells. This increase in PNNs around non-PV neurons in the A30P mice is interesting and might reflect a compensatory effect to alter the pyramidal cell intrinsic properties and reduce excitability.

Even though we did not find any differences in the overall PNN expression between aged A30P and WT mice, there was a significantly increased PNN number and expression in the superficial ACC layers in both genotypes. In aged A30P mice,

however, there were more PNNs with PV interneurons compared to PNNs with non-PV neurons but with a small difference of only 11%, while in the WT this difference was greater with 30.4%. This was inconsistent with the data in the young A30P mice which showed a trend towards an increased number of PNNs around non-PV neurons. On the other hand, the aged A30P mice had more PNNs around non-PV neurons (44.5%) compared to the aged WT (34.8%), also evident in young A30P mice.

A combination of PNNs around PV interneurons and PNNs around non-PV neurons, in the ACC of young and aged A30P mice might indicate a decrease in the plasticity of synaptic function. The increased amount of PNNs around non-PV neurons in the A30P mice might also contribute to different network structures and the development of different neuronal circuits as well as synaptic activity compared to the WT. Evidence shows that PNNs surrounded excitatory pyramidal neurons in the CA2 of mouse hippocampus including their excitatory synapses. Additionally, the PNNs were critical in restricting the plasticity of the synaptic function of these neurons (Carstens *et al.*, 2016). The expression of PNNs has not been investigated in DLB transgenic mice or patients before. Therefore, this shift in PNN localisation around non-PV neurons in the A30P mice could suggest a protective role of the PNNs for other types of neurons in the ACC against the hα-syn pathology.

5.5.5. *Were the PNNs protective against the hα-syn pathology in the ACC of A30P mice?*

In our findings, we have shown that the majority of PNNs (77.7%) in the ACC contained hα-syn in the young A30P mice. Human α-syn was present in both PNNs surrounding PV interneurons and PNNs around non-PV neurons. Importantly, most PNNs with hα-syn surrounded PV somas that also co-localised with hα-syn. Thus, we provided evidence that PNNs also take up hα-syn, possibly through synaptic interactions that contain hα-syn and/or the surrounded neuronal somas. This is the first study to show the presence of hα-syn in the PNNs at a young age in the A30P mice. By 12 months of age, almost all PNNs (99.4%) co-localised with hα-syn in the ACC of A30P mice. More than half of the PNNs with hα-syn surrounded PV somas which also contained hα-syn while the rest of the PNNs with hα-syn surrounded non-

PV neurons. Therefore, these findings suggest an increased concentration of hα-syn in both the PV somas and the PNNs with increasing age in the ACC in the A30P mice.

The hα-syn inside the PNNs might contribute to the dysfunction of ECM molecules and thus could cause changes in neuronal activity. However, we did not see any differences in the PV expression within the PV neuronal somas between PV neurons surrounded by PNNs, and PV neurons not surrounded by PNNs, in the young and aged A30P mice. Additionally, there were no differences in the hα-syn content between cells with and without a PNN. Therefore, our findings suggest that the PNNs might not be as protective as initially hypothesised against the hα-syn spread. Particularly, the PNNs might not be protecting the PV interneurons against the hα-syn pathology without, however, excluding the possibility of being protective for other neuronal types they surround. There might be hα-syn in excitatory neurons in the ACC in young and aged A30P mice and the surrounding PNNs might be protecting the excitatory neurons by maintaining their balanced neuronal activity. Future studies are necessary to address the role of PNNs around excitatory neurons in the α-syn pathology in the A30P mice.

In the ACC of our aged A30P mice, we did not find a decrease in the number of PV interneurons and PNNs as previously shown in AD transgenic mice following the breakdown of PNNs by increased neuroinflammation (Takahashi *et al.*, 2010; Mahar *et al.*, 2016; Crapser, Ochaba, *et al.*, 2020; Kudo *et al.*, 2023). Thus, it could be possible that α-syn pathology in DLB does not trigger the breakdown of ECM around neurons as the Aβ and tau pathology does in AD. However, we have only examined PNN expression in the ACC of the A30P mice and not in other brain areas with an increased pathology.

5.6. Conclusions

We have shown that the hα-syn protein was highly expressed in the ACC of A30P mice and this expression increased with age. PV interneurons contained hα-syn in their somas, despite supposedly not expressing the Thy-1 promoter and by 12 months of age, nearly all PV interneurons contained hα-syn. This suggests that either some or all PV interneurons express Thy1 and/or hα-syn spreads to PV interneurons transynaptically or via a more generalised release into the extracellular space from other hα-syn-expressing neurons. We also demonstrated that PNNs have the capacity to sequester hα-syn. PNNs are rich in negatively charged glycosaminoglycans, particularly chondroitin sulphate, which are known to interact electrostatically with positively charged regions of proteins like hα-syn. This interaction could lead to the sequestration of hα-syn in the ECM surrounding neurons, potentially preventing its spread or accumulation in surrounding tissues. However, despite the presence of PNNs around PV interneurons, they did not prevent the uptake of hα-syn by these cells. This suggests that while PNNs can sequester hα-syn, they may not fully protect neurons from its pathological effects, particularly if the protein is released into the extracellular space in large quantities. The effects of hα-syn on the phenotype and survival of PV interneurons were small and not statistically significant. There was a trend towards reduced PV expression and numbers of PV+ interneurons in the A30P mice at both ages studied compared to the WT, regardless of whether they co-localised with a PNN. The most striking difference was an increase in the number of neurons not expressing PV surrounded by a PNN in aged A30P mice, especially in the superficial layers. This may represent a protective response to pathology in the A30P transgenic mouse model.

Chapter 6. Microglial and astrocytic activation in the ACC of young and aged A30P and WT mice.

6.1. Introduction

The action of glial cells, including microglia and astrocytes, is normally a protective immune response for repairing damaged tissue in the CNS (Wyss-Coray and Mucke, 2002). Under pathological conditions such as protein aggregation, however, there is increased and persistent microglial and astrocytic activation which contributes to neurodegeneration (Glass *et al.*, 2010; Kempuraj *et al.*, 2016; Russo and McGavern, 2016; Stephenson *et al.*, 2018). The protective anti-inflammatory microglia and astrocytes shift to a neurotoxic pro-inflammatory phenotype (Jimenez *et al.*, 2008; Tang and Le, 2016; Liddelow and Barres, 2017; Liddelow *et al.*, 2017). Increased levels of pro-inflammatory cytokines are then released which diminish the phagocytic activity of both activated microglia and astrocytes and contribute to neurotoxicity (González-Reyes *et al.*, 2017; Liddelow *et al.*, 2017; Kwon and Koh, 2020).

Post-mortem examinations of PD patients have revealed an increased microglial activation in the hippocampus and substantia nigra (Rocha *et al*., 2015). Research indicates an early increase in microglial and astrocytic activation prior to disease progression and this was shown in AD, PD and DLB (Tarkowski *et al.*, 2003; Glass *et al.*, 2010; Craig-Schapiro *et al.*, 2010; Brosseron *et al.*, 2014; Wennström *et al.*, 2015; Stokholm *et al.*, 2017; Morenas-Rodríguez *et al.*, 2019; Oksanen *et al.*, 2019; Amin *et al.*, 2022; Gao *et al.*, 2023). However, there is a lack of evidence about early neuroinflammation in the ACC in DLB, even though it is a brain area affected early in α-syn pathology and has a high LB density (Kövari *et al.*, 2003).

One of the pro-inflammatory mediators released by the activated microglia is nitric oxide (NO) (Garden and Möller, 2006; Hanisch and Kettenmann, 2007; Colton, 2009; Lull and Block, 2010; Saijo and Glass, 2011). NO is a highly lipophilic radical gas molecule involved in cellular signalling, which moves across cell membranes without specific binding to membrane receptors (Govers and Oess, 2004; Pacher *et al*., 2007). NO plays a key role in different processes such as immune responses, neurotransmission and neuromodulation, as well as platelet aggregation (Benjamin *et al.*, 1994; Lundberg *et al.*, 1994; Zweier *et al.*, 1995; Cosby *et al.*, 2003; Schlossmann *et al*., 2003; Lundberg, Weitzberg and Gladwin, 2008; Knott and Bossy-Wetzel, 2009).

However, increased NO production together with nitrosative/oxidative stress contributes to neuroinflammation and neurodegeneration (Caruso *et al.*, 2017). Post-mortem examinations of patients with LBs and AD demonstrated cortex-wide nitration of LBs and LNs (Duda *et al.*, 2000).

NO production occurs from the catalysation of L-arginine and molecular oxygen by the NO synthase (NOS) (Kang *et al.*, 2004; Pacher *et al*., 2007; Förstermann and Sessa, 2012). There are three isotypes of NOS including the endothelial NOS (eNOS), neuronal NOS (nNOS) and inducible NOS (iNOS) which is expressed in macrophages, microglia, astrocytes and other cell types following LPS and cytokine release (Govers and Oess, 2004; Pacher, Beckman and Liaudet, 2007; Brown and Neher, 2010). However, iNOS is mostly expressed in activated microglia in response to the inflammatory mediators IL-1, interferon-γ and NK-κB (Lüth *et al.*, 2001; Guix *et al.*, 2005; Garden and Möller, 2006; Saha and Pahan, 2006; Harooni *et al.*, 2009; Brown and Neher, 2010). During inflammation under pathological conditions, iNOS is upregulated causing nitration leading to protein structural disruption and dysfunction in neurodegeneration (Kummer *et al.*, 2011; Guivernau *et al.*, 2016; Bandookwala and Sengupta, 2020; Bourgognon *et al.*, 2021). Overexpression of iNOS has been shown in the amygdala, hippocampus, entorhinal cortex and insular cortex in post-mortem brains of DLB patients (Katsuse *et al*., 2003). However, iNOS expression by activated microglia has not been investigated in the ACC in DLB.

In this chapter, the expression of all microglia and reactive astrocytes will be assessed in the ACC of young 2-4-month-old and aged 10-12-month-old A30P transgenic mice compared to age-matched WT. There is no evidence of neuroinflammation occurring early specifically in the ACC in DLB but early neuroinflammation is a feature of DLB (Iannaccone *et al.*, 2013; King *et al.*, 2018; Surendranathan *et al.*, 2018). Thus, by using the A30P mice we will be able to provide a further understanding of neuroinflammatory markers in the ACC during a pre-symptomatic stage and an advanced stage of hα-syn pathology. The microglia expressing iNOS, as well as the overall iNOS expression will also be examined in the ACC of young and aged A30P mice compared to the WT to examine the microglial activation.

6.2. Aims

- To address differences in the expression of Iba-1+ microglia and GFAP+ astrocytes in the ACC between young and aged A30P mice compared to the WT.

- Investigation of the activated microglia expressing iNOS in the ACC between young and aged A30P and WT mice.

6.3. Methods

6.3.1. *Free-floating IHC-Immunofluorescence*

Fixed mouse brains were sectioned into 40 µm slices, with ACC plates 21 - 30 selected based on the Paxinos and Franklin mouse brain atlas (2001, Fig. 2.1). For these experiments, 5 A30P and 5 age-matched WT male mice were used from two age groups: 2 - 4 months (young) and 10 - 12 months (aged). The IHC protocol was carried out as described in Chapter 2.3.2, using primary-secondary antibody combinations outlined in Table 6.1. One set of ACC sections was immunolabeled with combination 1, and another set with combination 2. Not all sections were from the same animals. For analysis, one ACC section and one hemisphere per animal were examined (N = 5 mice per WT/ A30P group, n = 1 section per animal). Sections were imaged with the Zeiss Axio Imager apotome 2 fluorescence microscope at 40x magnification using the 3-z-stack-box method (Fig. 2.4). Densitometric analysis was performed using FIJI software (Chapter 2.3.4), excluding GFAP+ astrocytes around blood vessels. One aged WT mouse was excluded from staining combination 1 due to excessive background staining.

Staining Combination 1	
Primary Antibody	**Secondary Antibody**
Goat anti-Iba-1	Donkey anti-goat Alexa Fluor 488
Rabbit anti-GFAP	Donkey anti-rabbit Alexa Fluor 568
Staining Combination 2	
Goat anti-Iba-1	Donkey anti-goat Alexa Fluor 488
Rabbit anti-iNOS	Donkey anti-rabbit Alexa Fluor 568

Table 6.1. IHC staining combinations used for the ACC sections of young and aged A30P and WT mice.

6.3.2. *Statistical analysis*

For normally distributed data, parametric tests were applied including unpaired t-tests or two-way ANOVA. On the other hand, for not normally distributed data, non-parametric tests were applied including Mann-Whitney. Additionally, some of the non-parametric data in this chapter were transformed into logarithmic $\log_{10}x$ and/or $\log_{10}(x+1)$ if data were closed to 0, which allowed for normal distribution and a two-way ANOVA test was performed with uncorrected Fisher's LSD test for the post hoc examinations (Chapter 2.4).

6.4. Results

6.4.1. *Microglia and astrocyte changes in the ACC between young and aged A30P and WT mice.*

This study aimed to determine whether microglial and astrocytic activation occurs early in the ACC of A30P mice and whether neuroinflammation is age-dependent. To address this, we examined Iba-1+ microglia and GFAP+ astrocytes in the ACC, a region not previously investigated in this context. Comparisons were made between young and aged A30P and WT mice to evaluate potential differences across distinct stages of hα-syn pathology.

Iba-1+ microglia and GFAP+ astrocytes were observed in the ACC of all young (2 - 4 months) and aged (10 - 12 months) A30P and WT mice (Fig. 6.1). No notable differences in the distribution patterns of Iba-1+ microglia were found between age groups or genotypes, with microglia present across all ACC layers. GFAP+ astrocytes were predominantly located near the tissue edges, meninges, and corpus callosum, indicating their prevalence in white matter. Somas of both Iba-1+ microglia and GFAP+ astrocytes co-localised with Hoechst-stained nuclei. Notably, beaded structures in Iba-1 and GFAP expression were visible in some ACC sections, particularly more pronounced in aged mice of both genotypes, with aged A30P and WT mice showing increased GFAP beading compared to younger mice.

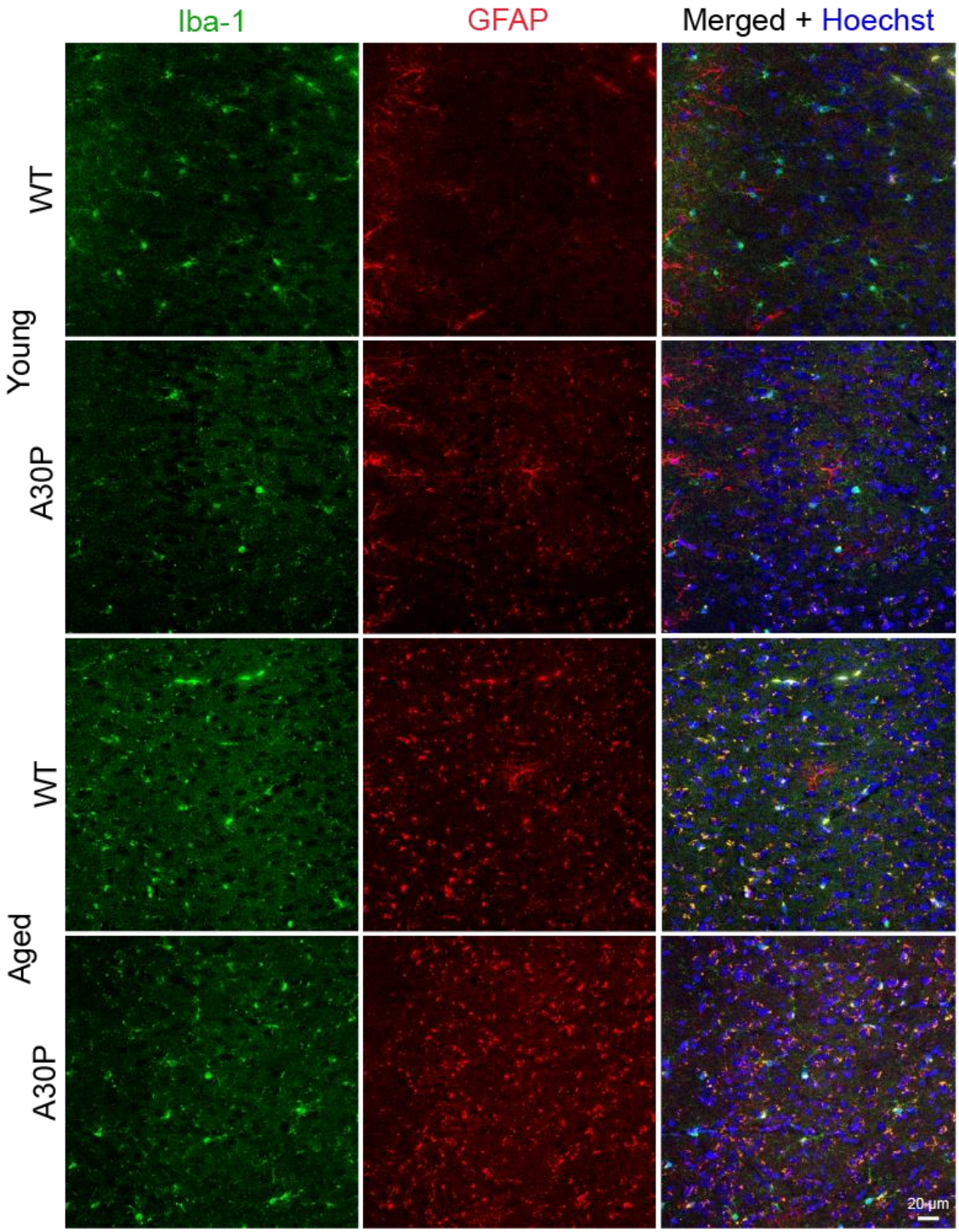

Figure 6.1. Iba-1+ microglia and GFAP+ astrocytes in the ACC of young and aged A30P and WT mice. The expression of all microglia (Iba-1, green), reactive astrocytes (GFAP, red), all nuclei (Hoechst, blue) and a composite of the staining is shown in the ACC of young and aged A30P and WT mice. These images are collapsed z-stacks with maximum intensity taken from the superficial layers. Scale bar at 20 µm.

The mean % area and intensity of Iba-1+ microglia expression across the ACC layers were quantified in young and aged A30P and WT mice. No significant differences were observed between age groups or genotypes for either measure (Fig. 6.2A and B, $p > 0.05$, two-way ANOVA, young WT/A30P: N = 5 mice/n = 1 section, aged WT: N = 4 mice/n = 1 section, aged A30P: N = 5 mice/n = 1 section). However, there was a trend towards an increased mean % area of Iba-1 expression in the aged A30P mice compared to both young A30P and aged WT mice. It should be noted that the denser appearance of the Iba-1+ signal in aged mice images is partly due to increased beading patterns, potentially associated with microglial activation and ageing, which may not be fully captured by the thresholding method used in the quantification.

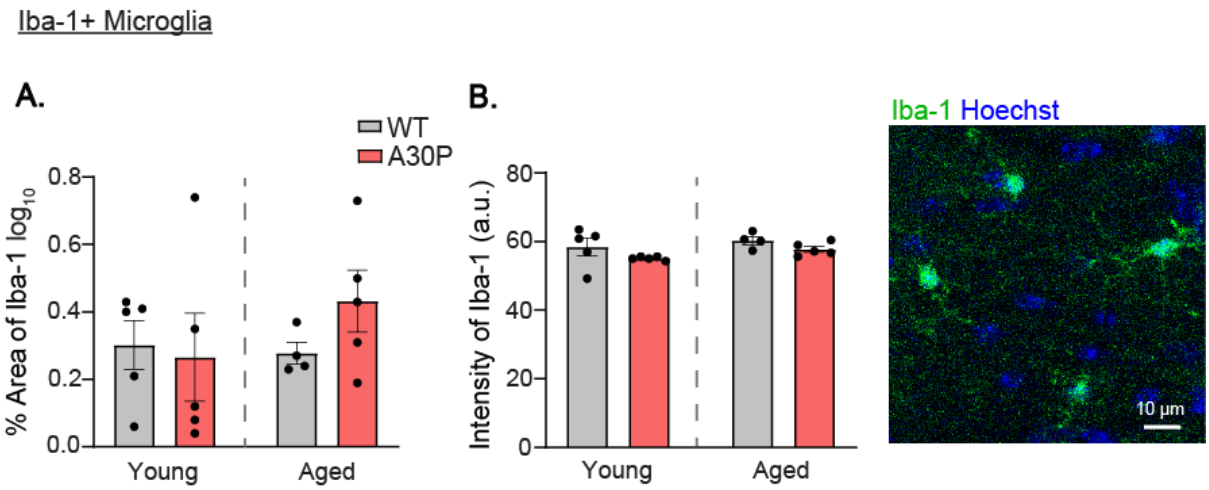

Figure 6.2. Iba-1 expression in the ACC between young and aged A30P and WT mice. The mean (**A**) % area of the log-transformed (x+1) data and (**B**) intensity (a.u.) of the Iba-1+ microglial expression are shown between the young and aged WT (grey) and A30P (red) mice. On the right side, an enlarged view of Iba-1+ microglia co-stained with Hoechst are shown. Each data point represents the average value across superficial and deep ACC layers per animal.

The mean % area and intensity of GFAP expression were analysed in the ACC to assess changes in reactive astrocytes in young and aged A30P and WT mice. A significant increase in GFAP % area was observed in aged animals of both genotypes compared to young animals (Fig. 6.3A, $p < 0.001$, $F(1,15) = 23.56$, two-way ANOVA, young WT/A30P: N = 5 mice/n = 1 section, aged WT: N = 4 mice/n = 1 section, aged A30P: N = 5 mice/n = 1 section). Post hoc analysis confirmed a significant increase in GFAP % area in aged A30P and WT mice versus young A30P and WT mice ($p < 0.01$, Fisher's LSD). Similarly, GFAP intensity levels were significantly higher in aged animals of both genotypes compared to young animals (Fig. 6.3B, $p < 0.001$, $F(1,15) = 22.35$, two-way ANOVA, young WT/A30P: N = 5 mice/n = 1 section, aged WT: N = 4 mice/n = 1 section, aged A30P: N = 5 mice/n = 1 section). Post hoc tests confirmed increased GFAP intensity in aged A30P and WT mice the younger animals ($p < 0.01$, Fisher's LSD).

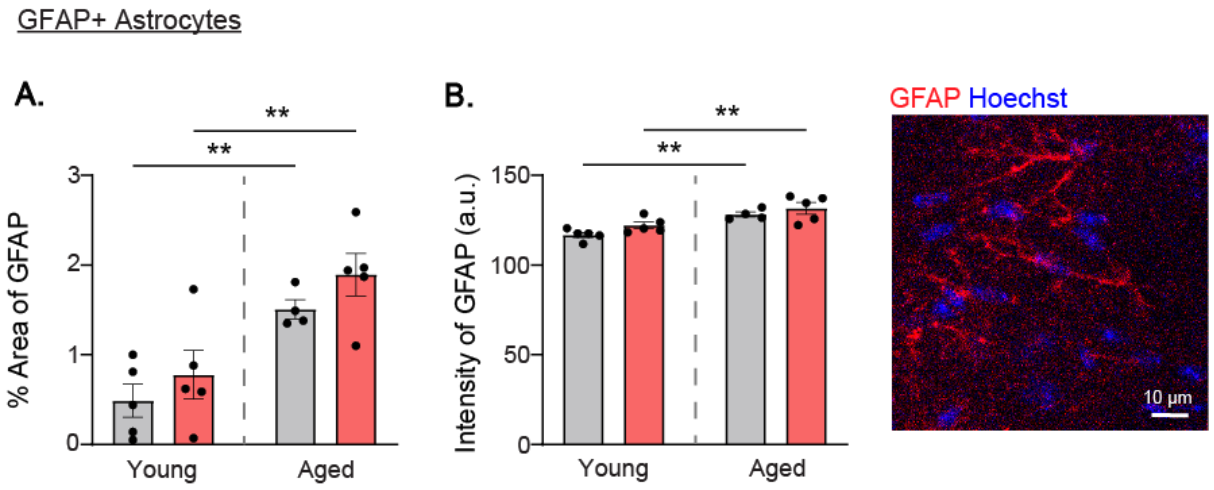

Figure 6.3. GFAP expression in the ACC between young and aged A30P and WT mice. The mean (**A**) % area and (**B**) intensity (a.u.) of the GFAP+ astrocytic expression are shown between the young and aged WT (grey) and A30P (red) mice. On the right side, an enlarged view of GFAP+ astrocytes co-stained with Hoechst are shown. Each data point represents the mean values across superficial and deep ACC layers per animal.

These findings suggest a trend towards increased Iba-1+ microglial expression in the ACC of aged A30P mice compared to young A30P and aged WT mice. Notably, GFAP expression was significantly higher in reactive astrocytes of aged A30P and WT mice compared to the young mice. A non-significant increase in the % area of GFAP+ astrocytes was also observed in young and aged A30P mice relative to WT mice. However, no statistically significant differences in glial cell expression were detected between the two genotypes.

Correlation between GFAP and Iba-1 expression in young and aged mice

To assess the relationship between glial cell expression in the ACC of A30P and WT mice, a correlation between the mean % area of GFAP and Iba-1 expression was analysed. In young A30P and WT mice, a simple linear regression revealed a significant positive correlation between GFAP and Iba-1 expression (Fig. 6.4Bi, R^2 = 0.66, F (1,8) = 15.63, $p < 0.01$, $y = 0.32*x + 0.26$, young WT/A30P: N = 5 mice/n = 1 section), indicating that increased GFAP+ astrocytic expression was associated with increased Iba-1+ microglial expression.

Similarly, in aged A30P and WT mice, a positive relationship was observed, with an even stronger correlation compared to the young animals (Fig. 6.4Bii, R^2 = 0.73, F (1,7) = 18.78, $p < 0.01$, $y = 0.31*x + 1.25$, aged WT: N = 4 mice/n = 1 section, aged A30P: N = 5 mice/n = 1 section). This suggests that in aged animals, a higher mean % area of GFAP expression correlated with a higher mean % area of Iba-1 expression per mouse, consistent with findings in young animals.

These correlation analysis results thus, showed a statistically significant positive relationship between the expression of microglia and reactive astrocytes in the ACC of young and aged A30P and WT mice.

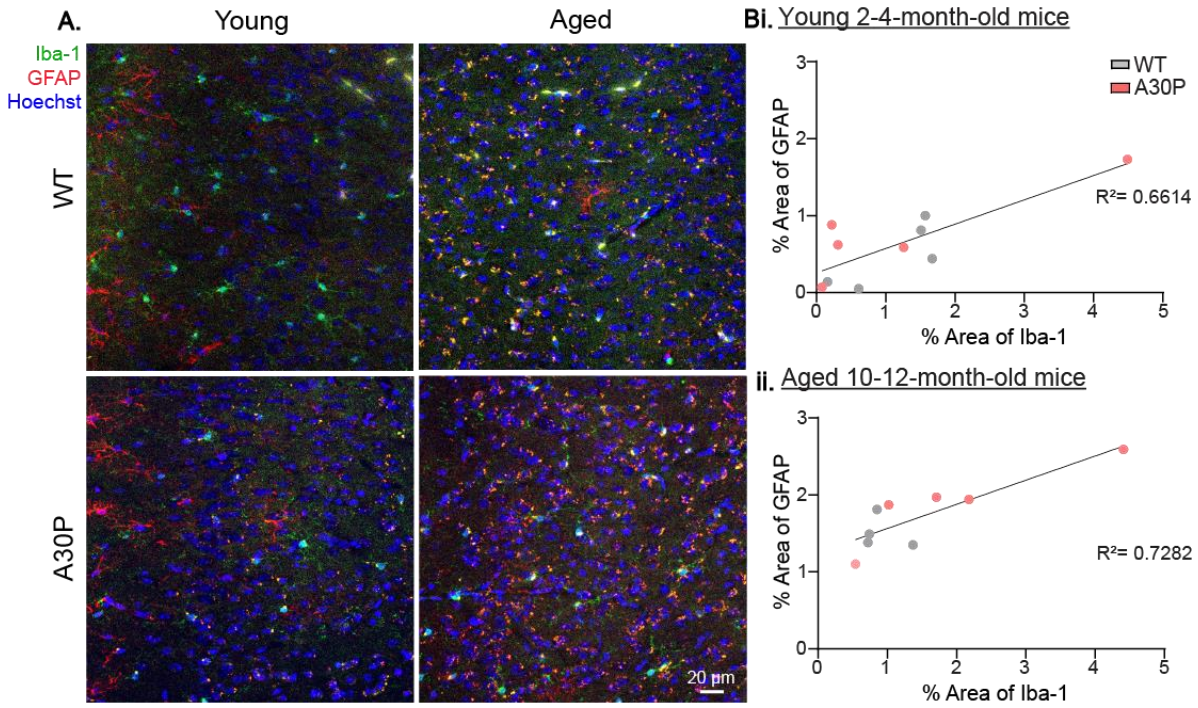

Figure 6.4. Positive relationship between Iba-1 and GFAP expression in the ACC of young and aged A30P and WT mice. A. Merged example images showing the expression of Iba-1+ microglia (green), GFAP+ astrocytes (red) and all Hoechst+ cell nuclei (blue) in the young and aged A30P and WT mice. Scale bar at 20 µm. **B.** The correlation analysis between the mean % area of GFAP and Iba-1 expression in the ACC is demonstrated for both (**i**) young and (**ii**) aged WT (grey) and A30P (red) mice. Each data point represents the mean values across superficial and deep ACC layers per animal.

6.4.2. *Differences in the expression of reactive microglia expressing iNOS in the ACC between young and aged A30P and WT mice.*

The upregulation of the microglia-derived pro-inflammatory enzyme iNOS has been seen in post-mortem brains of patients with PD and DLB (Hunot *et al.*, 1996; Knott *et al*., 2000; Katsuse *et al*., 2003). In PD, increased iNOS expression has been linked to elevated microglial activation (Gerhard *et al.*, 2006). Pro-inflammatory microglial activation in the ACC has not been previously studied in DLB. To address this, we examined reactive microglia expressing iNOS in the ACC of young and aged A30P mice and compared them to WT controls.

The expression of Iba-1+ microglia and iNOS was confirmed in the ACC of all young (2 – 4 months) and aged (10 - 12 months) A30P and WT mice (Fig. 6.5). The Iba-1+ microglia were observed across the different layers of the ACC with obvious somas and ramified processes. The somas also co-localised with the Hoechst+ cell nuclei. The expression of iNOS appeared in a clustered, punctate form again found across the whole of the ACC. Additionally, some Iba-1+ microglia were observed to co-localise with iNOS in both young A30P and WT mice (Fig. 6.5).

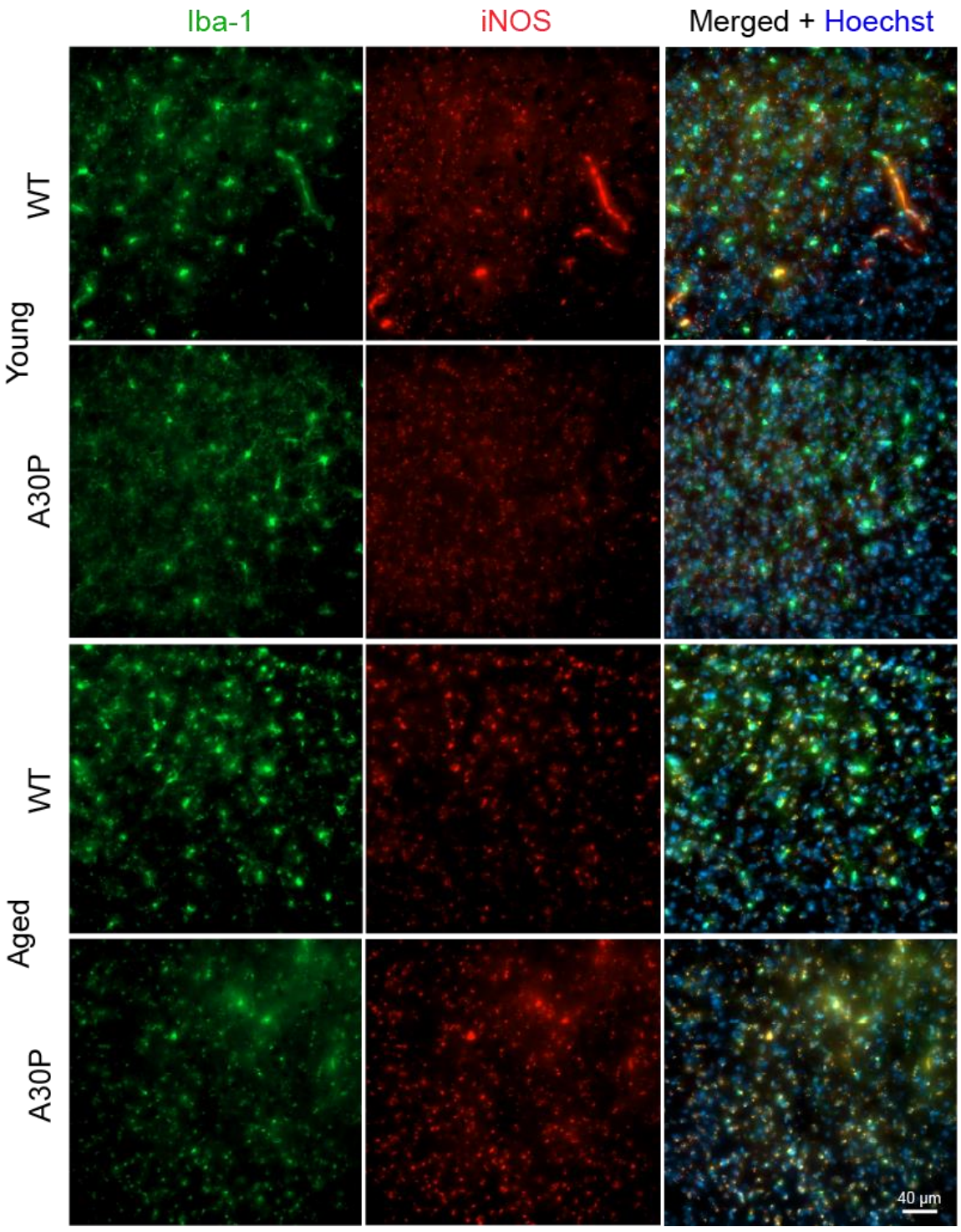

Figure 6.5. Microglia and iNOS expression in the ACC of young and aged A30P and WT mice. The expression of all microglia (Iba-1, green), iNOS enzyme (iNOS, red), all nuclei (Hoechst, blue) and a composite of the staining is shown in the ACC of young and aged A30P and WT mice. These images are collapsed z-stacks with maximum intensity taken from the deep ACC layers. Scale bar at 40 µm.

Some Iba-1+ microglia co-localising with iNOS were observed in the ACC of both genotypes and age groups and we wanted to investigate this further. Firstly, all Iba-1+ microglia with a clear Hoechst+ cell nucleus were manually counted. A two-way ANOVA revealed significant interaction effects between age groups and genotypes (Fig. 6.6Bi, young vs aged: $F(1,16) = 10.73$, $p < 0.01$, WT vs A30P: $F(1,16) = 8.02$, $p < 0.05$, two-way ANOVA, young/aged WT/A30P: N = 5 mice/n = 1 section). Post hoc analysis showed a significant decrease in the mean Iba-1+ microglia count in aged A30P mice (mean = 16.53) compared to both young A30P mice (mean = 24.73, $p < 0.05$, Fisher's LSD) and aged WT mice (mean = 23.80, Fisher's LSD, $p < 0.05$). Overall, the results indicated a trend toward a reduced Iba-1+ microglia count in aged mice compared to young mice, with a more pronounced decrease in A30P mice across both age groups.

The count of Iba-1+ microglia co-localised with iNOS expression in the ACC was analysed across age groups and genotypes. The percentage of Iba-1+ microglia expressing iNOS from the total count of Iba-1+ microglia previously counted was calculated. A notably high percentage of Iba-1+ microglia expressed iNOS in both A30P and WT mice. A two-way ANOVA revealed a significant interaction effect with age, showing an increased mean count of reactive microglia in aged animals compared to young ones (Fig. 6.6Bii, $F(1,16) = 15.27$, $p < 0.01$, two-way ANOVA, young/aged WT/A30P: N = 5 mice/n = 1 section). Post hoc tests confirmed a statistically significant increase in the mean count of reactive microglia in the ACC of aged A30P and WT mice compared to the young mice ($p < 0.05$, Fisher's LSD). The percentage of Iba-1+ microglia expressing iNOS was 84.04% in young A30P mice, 80.24% in young WT mice, 92.17% in aged A30P mice and 89.26% in aged WT mice. Despite these increases with age, there were no significant differences between the A30P and WT mice.

These results indicate a reduction in the overall count of Iba-1+ microglia in the ACC of aged A30P and WT mice, with a significant decrease observed in aged A30P mice compared to the aged WT. However, microglial activation was significantly increased in aged A30P and WT mice compared to the young mice.

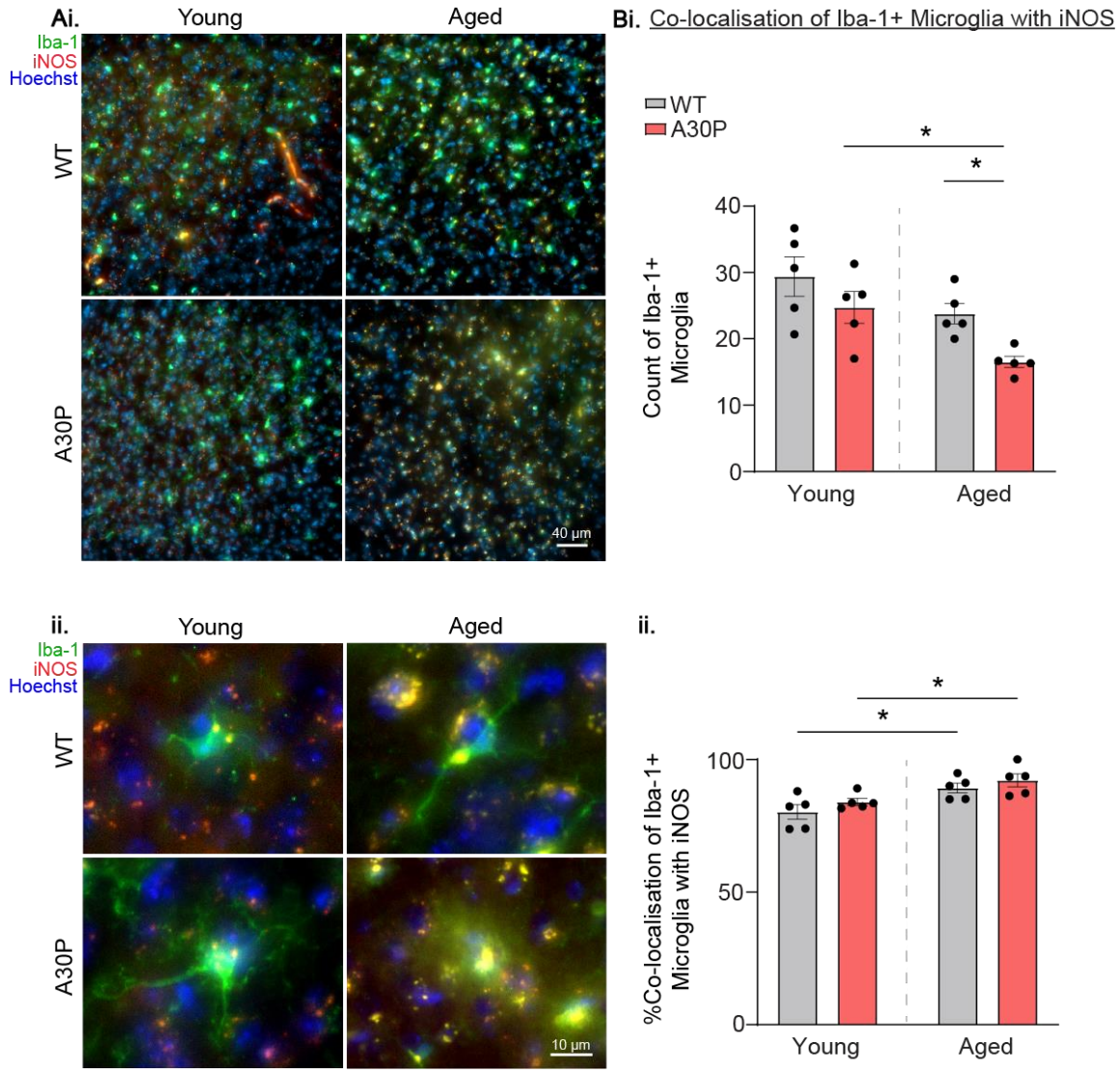

Figure 6.6. Iba-1+ microglia and reactive microglia expressing iNOS in the ACC of young and aged A30P and WT mice. Ai. Merged example images showing the expression of Iba-1+ microglia (green), iNOS (red) and all Hoechst+ cell nuclei (blue) in the young and aged A30P and WT mice. **Aii.** Enlarged views of example Iba-1+ microglia expressing iNOS in both ages and genotypes. **B.** The mean count of (**i**) all Iba-1+ microglia and (**ii**) Iba-1+ microglia expressing iNOS in the ACC of young and aged WT (grey) and A30P (red) mice are demonstrated. Scale bars at 40 µm and 10 µm. Each data point represents the mean values across superficial and deep ACC layers per animal.

6.5. Discussion

6.5.1. *Summary of the main findings in Chapter 6.*

- No significant changes in the Iba-1+ microglial expression but significantly higher GFAP+ astrocytic expression in the ACC of aged mice in both genotypes.
- Positive correlation between the % area of GFAP+ astrocytic and Iba-1+ microglial expression in the ACC in young and aged mice.
- A trend towards fewer Iba-1+ microglia in aged mice compared to young mice and a statistically significant decrease in aged A30P mice compared to the aged WT and young A30P mice.
- The number of reactive Iba-1+ microglia expressing iNOS was significantly increased with age.

6.5.2. *A significant increase in GFAP expression highlighting increased astrogliosis in the ACC of aged mice.*

Sustained and persistent glial cell activation, including microglia and astrocytes, is involved in the development of neuronal degeneration (Kempuraj *et al.*, 2016; Russo and McGavern, 2016). We examined the expression of Iba-1+ microglia and GFAP+ astrocytes during different stages of the hα-syn pathology to elucidate changes in neuroinflammatory responses with progressive disease pathology as the phosphorylation of α-syn (pS129) increases with age. There were no marked changes in the Iba-1 expression but a gradual increase in the mean % area of Iba-1 from young WT to aged A30P mice was shown. Thus, there was a potential increase in the Iba-1+ microglial expression with increasing age, which was greater with the presence of hα-syn pathology. Our findings represent preliminary evidence for Iba-1+ microglia expression in the ACC in the young and aged A30P transgenic mice. Increased microglial neuroinflammation has previously been reported from early stages in AD, PD and DLB patients and animal models (Tarkowski *et al.*, 2003; Glass *et al.*, 2010; Craig-Schapiro *et al.*, 2010; Brosseron *et al.*, 2014; Wennström *et al.*, 2015; Stokholm *et al.*, 2017; Morenas-Rodríguez *et al.*, 2019; Oksanen *et al.*, 2019; Amin *et al.*, 2022;

Gao *et al.*, 2023). However, no other studies have reported a potential age-related increase in Iba-1 expression in the ACC in α-syn transgenic mice.

Importantly, we found a significant increase in the GFAP expression in the ACC of aged animals compared to the young mice, but no differences between the two genotypes. However, a trend towards an increase in the GFAP expression was observed in both the young and aged A30P mice compared to the WT. The potential increase in reactive astrocytes, highlighting astrogliosis, at a young age in the A30P mice might have been related to the hα-syn overexpression. Recent work in our lab has shown a significantly increased GFAP expression in the hippocampus of 2-4-month-old A30P mice (Al-Musawi *et al.*, 2024). This could suggest that there are brain area differences in neuroinflammatory responses in the A30P mice during the early stages of pathology. Higher cognitive brain areas such as the ACC might then show increased neuroinflammation with increasing age, and at later stages of hα-syn pathology compared to the hippocampus.

Other studies have also shown an age-dependent increase in neuroinflammation in other brain areas in α-syn transgenic mice. Increased expression of GFAP+ astrocytes, associated with dopaminergic neurodegeneration, was found in the substantia nigra of 16-17-month-old A30P/A53T double mutated α-syn transgenic mice compared to their age-matched WT and young 2-3-month-old transgenic mice (Rauschenberger *et al.*, 2022). Another study demonstrated astrogliosis, microgliosis and increased release of pro-inflammatory cytokines in the neocortex, hippocampus, and striatum of 10-11-month-old Thy-1 α-syn transgenic mice (Iba *et al.*, 2020). Our study is the first to show an age-dependent increase in neuroinflammatory markers in the ACC in the A30P transgenic mouse model of DLB.

There is generally a lack of evidence showing astrocytic activation with normal ageing. Importantly, studies showed the increased levels of GFAP and vimentin cytoskeletal proteins in ageing, which are associated with astrocytic activation, in rodents and humans (Nichols *et al.*, 1993; Porchet *et al.*, 2003). Clarke et al. (2018) demonstrated region-specific transcriptional changes in reactive astrocyte genes, with higher upregulation observed in brain regions prone to cognitive decline, such as the hippocampus and striatum, compared to the cortex in mice. Furthermore, the age-related upregulation of reactive astrocyte genes was associated with the pro-

inflammatory genes including IL-1α, TNF, and C1q expressed by activated microglia suggesting potential crosstalk in the activation of the two glial cell types (Clarke *et al.*, 2018). Our findings here provided evidence for increased astrogliosis with increasing age in the ACC of A30P and WT mice.

6.5.3. *Beading GFAP expression in aged mice could be related to astrocytic clasmatodendrosis.*

Interestingly, beading of GFAP expression was evident even in the young animals, specifically the young A30P mice, but not as strong as in the aged mice. However, this beading GFAP expression was also observed in the ACC of aged WT mice, suggesting age-dependent changes in reactive astrocytes. The beading GFAP expression observed in the ACC of young and aged mice might be related to a phenomenon called clasmatodendrosis which was first described by Ramon y Cajal in 1913 (Balaban *et al.*, 2021). Clasmatodendrosis refers to the fragmentation of distal astrocytic cell processes and the fragmentation or beading of the astrocytic proximal processes close to the soma. Damage in astrocytes may be caused by the cleavage of membrane and cytoskeletal proteins, including GFAP (Balaban *et al.*, 2021). Astrocytes undergoing clasmatodendrosis lose their spatial alignment and show decreased synapse coverage contributing to impaired synaptic connectivity and homeostasis in neurons (Rodríguez *et al.*, 2008; Verkhratsky *et al.*, 2010).

This astrocytic programmed death (apoptosis) has been reported with ageing under pathological conditions in ischemia, acidosis, dementia, head trauma, infection and demyelination disease (Tomimoto *et al.*, 1997; Hulse *et al.*, 2001; Sahlas *et al.*, 2002; Sakai *et al*., 2013; Mercatelli *et al.*, 2016; Bouchat *et al.*, 2019; Tachibana *et al.*, 2019). Research has shown that the apoptotic astrocytes can be detected with immunohistochemical staining for the cleaving enzyme caspase-3, involved in the apoptotic pathway, and TUNEL (terminal deoxynucleotidyl transferase dUTP nick end labelling) staining for DNA fragmentation (Umpierre *et al*., 2001; Wu *et al.*, 2021).

However, it is still unclear whether clasmatodendrosis occurs because of normal ageing. Evidence shows that there is metabolic remodelling and increased oxidative metabolism in astrocytes with ageing leading to decreased metabolic

substrate supply to neurons (Jiang and Cadenas, 2014; Yin *et al*., 2014). Also, with ageing, there are deficits in energy metabolism and redox homeostasis which play a critical role in age-induced neurodegeneration and cognitive impairment (Biessels and Kappelle, 2005; Boveris and Navarro, 2008). However, in neurodegenerative disorders, these neuronal network changes occur at an early stage (Yin *et al*., 2014). We found GFAP beading expression even in the young A30P mice, possibly implying an early dysfunction in reactive astrocytes under pathological conditions contributing to ACC neurodegeneration. In future studies, it would be interesting to quantify these beading phenomena in more detail.

6.5.4. *Increased GFAP expression correlated with increased Iba-1 expression in young and aged animals.*

Reciprocal communication between microglia and astrocytes has been previously shown (Liddelow and Barres, 2017; Jha *et al*., 2019). Activated microglia control the activation of astrocytes and can influence their shift either towards the neurotoxic A1 phenotype or the neuroprotective A2 phenotype (Burda and Sofroniew, 2017). Therefore, increased microglia activation might also lead to increased astrocytic activation and exacerbate pathology (Liddelow and Barres, 2017; Liddelow *et al*., 2017). We then assessed the relationship between the GFAP and Iba-1 expression in the ACC in A30P and WT mice at different pathology stages. Our findings showed a significant positive correlation between the GFAP and Iba-1 expression in young A30P and WT mice as both increased together. This positive relationship between the GFAP and Iba-1 expression was also shown in the aged mice, however, with an increase in the overall glial cell expression. Therefore, there might be crosstalk between GFAP+ astrocytes and Iba-1+ microglia in the ACC occurring at an early age in both genotypes.

Reactive astrocytes and microglia communicate with neurons through extracellular vesicle release (Matejuk and Ransohoff, 2020). However, in disease, this glial cell crosstalk contributes to the cell-to-cell spread of pathology. The accumulation of α-syn and Aβ aggregates has been seen in cultured astrocytes suggesting the take-up of protein aggregates by glial cells (Söllvander *et al*., 2016; Rostami *et al*., 2017).

This is consistent with evidence showing that reactive astrocytes contribute to protein aggregate removal including α-syn (Giusti *et al.*, 2024). The synergistic interplay between astrocytes and microglia has also been shown. Microglia and astrocytes can exchange α-syn and Aβ protein aggregates, with microglia playing a role in their degradation. This can be an important immune response to the clearance of protein accumulation in PD and AD, however, it could also facilitate its spread within the neuronal networks (Rostami *et al.*, 2021).

6.5.5. *Reactive microglia were significantly increased in the ACC of aged mice.*

Under pathological conditions, there is an upregulation of iNOS expression by reactive microglia demonstrated in the amygdala, hippocampus and entorhinal and insular cortices in DLB patients (Katsuse *et al*., 2003; Kummer *et al.*, 2011; Guivernau *et al.*, 2016; Bandookwala and Sengupta, 2020; Bourgognon *et al.*, 2021). However, whether an iNOS upregulation by pro-inflammatory microglia occurs in the ACC in DLB, is unknown. We found an increased number of reactive Iba-1+ microglia expressing iNOS in the ACC with increasing age but no differences between the A30P and WT genotypes. Disruption in the CNS homeostasis during ageing results in glial cell activation including an increase in reactive microglia (Helmut *et al.*, 2011). PET scans *in vivo* showed an age-dependent increase in neuroinflammation in the frontal, cingulate, temporal, entorhinal, parietal and occipital areas and the hippocampus, thalamus and cerebellum in healthy humans (Schuitemaker *et al.*, 2012). In 20-month-old WT mice, a raised microglial count in the primary visual cortex and auditory cortex has been shown compared to the young 3-month-old mice (Tremblay *et al.*, 2012). However, some studies did not find any activated microglia in the mouse CA1 and dentate gyrus in aged mice while other studies showed a decrease in microglial density in the substantia nigra and striatum, but not in the neocortex (Long *et al.*, 1998; Sharaf, Krieglstein and Spittau, 2013). Therefore, research suggests region-dependent as well as species-dependent changes in microglial activation with ageing. Here, we showed increased microglial activation in the ACC in aged A30P transgenic and control mice, a region which has not previously been examined.

During ageing, there is also an increased production of ROS leading to chronic oxidative stress and age-induced impairments in brain function (Jung *et al*., 2012). Increased levels of long-term oxidative stress contribute to NO generation (Peinado, 1998). NO is critical in ageing under normal conditions and neurodegeneration (Zhuo and Hawkins, 1995; Law *et al*., 2001). Studies have demonstrated an increased NO concentration during ageing (McCann *et al*., 1998; Calabrese *et al*., 2000; Law *et al*., 2001). Increased NO levels could also suggest an increase in NOS activity, including iNOS expressed in microglia, responsible for NO production (Coleman, 2001). Overall, increased iNOS activity triggered by reactive microglia and thus, NO production during neuroinflammation increases neurotoxicity leading to neuronal damage (Olivera *et al.*, 2016). In our findings, we showed an age-dependent increase in reactive microglia expressing iNOS which could imply upregulated NO production in the ACC in both genotypes. Surprisingly, we also saw a lot of Iba-1+ microglia co-localising with iNOS in the ACC of young WT mice. Increased iNOS expression is not usually observed under physiological conditions and other work in our lab has shown <10% of Iba-1+ cells co-expressing iNOS in the hippocampus of young WT mice (Al-Musawi *et al.*, 2024). The high expression of iNOS, indicative of reactive microglia, is intriguing and requires further investigation. Future studies should explore iNOS expression in other cortical areas to determine if this is a characteristic unique to the ACC. Certain stimuli including stress can upregulate the iNOS activity (Fernandes *et al.*, 2021) but the young A30P mice are all housed in the CBC under the same conditions and similar animals were used for the hippocampus and ACC studies.

6.5.6. *Ageing-related changes in the ACC include decreased microglia number but beading of Iba-1 expression possibly due to structure dysmorphism.*

In our findings, we have shown a decreased number of Iba-1+ microglia in the ACC of aged mice but a decrease in the overall Iba-1 expression of % area was not observed. Interestingly, we also saw beading of the Iba-1 expression in presumed microglial processes similar to that seen with GFAP expression. During ageing, microglia demonstrate morphological changes characterised by a decreased number and shorter processes and are thus described as dystrophic microglia (Streit *et al.*, 2004; Conde and Streit, 2006a, 2006b; Streit, 2006; Flanary *et al.*, 2007). There are

also cytoplasmic structure changes in senescent microglia including cytoplasmic inclusions as well as de-ramification of processes and membrane blebbing (Sheng *et al*., 1998; Streit *et al.*, 2008). Age-induced altered microglia morphology related to a reactive phenotype has been observed in humans and rats (Vaughan and Peters, 1974; Samorajski, 1976; Schuitemaker *et al.*, 2012). Dystrophic, senescent microglia in humans exhibit de-ramification and thinning or fragmentation of their processes, along with the formation of spheroids and gnarled processes (Streit *et al.*, 2004).

During the morphological changes of reactive microglia, as well as during microglial locomotion and phagocytosis, there is remodelling of their actin cytoskeleton (Kanazawa *et al.*, 2002). The Iba-1 calcium-binding protein, specific to macrophages and microglia, is implicated in membrane ruffling, a process associated with active cell membrane movement during the reactive state, as well as the motility of both macrophages and microglia (Allen *et al.*, 1997; Kanazawa *et al.*, 2002). An early study by Ohsawa et al. (2000) showed the role of the Iba-1 protein in both the membrane ruffling and phagocytotic abilities of macrophages and microglia (Ohsawa *et al.*, 2000). Importantly, calcium controls the actin cytoskeleton by regulating the Iba-1 protein activity and by activating protein kinases and phosphatases implicated in actin remodelling (Hartwig and Yin, 1988; Stossel, 1993; Janmey, 1994). However, in ageing, the dystrophic microglia exhibit decreased actin dynamics which contribute to their morphological changes (Galatro *et al.*, 2017).

We, therefore, hypothesise that in our experiments there were some Iba-1+ microglia in the ACC in aged animals that maintained their structure but had enlarged soma and shorter processes. On the other hand, other Iba-1+ microglia exhibited morphological changes adopting a dystrophic shape. Future work would involve a more detailed morphological analysis of astrocyte and microglia shapes. This hypothesis would then support our findings of decreased microglial number, but no decrease in the overall Iba-1 expression, with ageing in the ACC. Additionally, the decreased count of microglia in the ACC of aged A30P mice compared to the aged WT could suggest severe morphological changes of microglia which might be related to both ageing but also the hα-syn pathology.

6.6. Conclusions

In this chapter, we showed age-related changes in neuroinflammatory markers including microglia and reactive astrocytes in the ACC. We found a significant increase in GFAP expression in the ACC with increasing age but no changes between the A30P and WT genotypes. A beading GFAP signal was observed which might be related to clasmatodendrosis suggesting structural disruption of astrocytes induced by ageing. We also saw a decrease in the Iba-1+ microglia count but an increase in the count of reactive microglia expressing iNOS in the aged mice compared to the young. Our results, therefore, suggest an age-induced increase in microglial activation in the ACC. Furthermore, the decreased number of microglia shown might be associated with morphological changes of microglia adopting a dystrophic shape due to potentially altered metabolism during ageing.

Chapter 7. General Discussion.

7.1. Overview of the main findings.

In this study, we first investigated the neuronal network activity in the deep layers of the ACC in young WT mice *in vitro* under induced epileptic conditions with 4-AP. We found increased IID and seizure-like activity in the deep layers of ACC leading to increased PV expression. These data suggest that the ACC in WT mice generates hyperexcitability driven by 4-AP in which the PV interneurons are known to be also involved. Network activity under induced epileptic conditions was also examined in the ACC *in vitro* in the young A30P mice compared to the WT. Gabazine induced a shift from simple IIDs to complex IIDs in the A30P mice, suggesting a potential increase in network hyperexcitability at a pre-symptomatic disease state. Additionally, 4-AP induced seizure-like activity without, however, any differences between A30P and WT mice. Importantly, we showed increased GFAP expression following 4-AP in the A30P mice indicating increased astrocytic activity but no changes in the PV expression compared to the WT.

We were also interested in exploring possible differences in the fast network oscillatory activity evoked with KA in the deep layers of the ACC between young A30P and WT mice. We found fast gamma oscillations with no differences, however, in the area power, peak amplitude, and frequency between the two genotypes.

The PV neuronal and PNN interactions were also assessed in the young 2-4-month-old and aged 10-12-month-old A30P and WT mice. There was a non-significant reduction in the PV expression in the ACC of young and aged A30P mice. Even though most PV interneurons were surrounded by PNNs, more PNNs were surrounding non-PV neurons in the ACC of young and aged A30P mice compared to the WT. Importantly, in young A30P mice, hα-syn was present in most PV somas and PNNs in the ACC and by 12 months of age it was present in almost all of them. These findings may suggest the spread of α-syn pathology to interneurons and PNNs with increasing age. This spread of hα-syn could possibly occur through excitatory synapses, or the expression of hα-syn in PV interneurons starting from a young pre-symptomatic age in the A30P mice. We also found an age-dependent increase in the expression of reactive astrocytes as well as in reactive microglia expressing iNOS in the ACC in both genotypes. Thus, we did not see marked changes in neuroinflammatory markers in

the early stages of α-syn pathology in the ACC but neuroinflammation increased with age.

7.2. Network hyperexcitability and oscillatory activity in the ACC of young A30P mice.

There is generally a lack of evidence on the different types of neuronal network activity that can be observed in the ACC, especially in mice. We, therefore, started investigating the activity of ACC neuronal networks in the young 2-4-month-old WT mice before examining this in the A30P mice. Following the 4-AP application in the ACC, epileptic-like conditions including frequent IIDs were observed which then developed into seizure-like activity. This induced abnormal hyperexcitable state led to rapid changes in the ACC including an upregulation of PV expression and a trend towards an increase in c-Fos expression but no changes in PNNs. The increased PV activity we found in the ACC is consistent with other studies showing enhanced levels of intraneuronal activity, including PV neurons, before the onset of seizure-like activity following 4-AP in the mouse entorhinal cortex *in vitro* (Yekhlef *et al.*, 2015; Librizzi *et al.*, 2017). However, even though studies suggest microglia and astrocytes contribute to seizure activity (Verhoog *et al.*, 2020; Sano *et al.*, 2021; Li *et al.*, 2023), we did not see any changes in the Iba-1 and GFAP expression in the ACC following 4-AP.

We then addressed potential differences during gabazine-induced and 4-AP-induced hyperexcitability between young A30P and WT mice. A shift from simple IIDs to complex IIDs was revealed in the deep layers of ACC in young A30P mice over the increasing gabazine concentrations which was not evident in the WT. We showed similar increased IID activity following gabazine as previously reported in the hippocampus of young A30P mice (Tweedy *et al.*, 2021). However, this is the first study to show an increase in network excitability, in the ACC of young A30P mice which might be related to the overexpression of α-syn. Following incremental 4-AP concentrations, seizure-like activity was seen in the ACC in both genotypes. The 4-AP-induced hyperexcitability in the ACC of A30P mice led to a significant increase in GFAP expression and a potential increase in Iba-1 expression compared to the WT. This increase in glial cell expression in the A30P mice could be related to the overexpression of hα-syn which might also contribute to hyperexcitability seen in the

ACC. Studies have previously shown that proteins involved in familial forms of PD, including α-syn, control the activation of both microglia and astrocytes (Glass *et al.*, 2010; Oksanen *et al.*, 2019). Following 4-AP in the ACC, we also observed a trend towards a decrease in PV expression in the A30P mice and towards an increase in c-Fos expression compared to the WT but no changes in the PNNs.

These data might suggest an overall increase in the ACC neuronal networks of A30P mice and a potential involvement of α-syn pathology in the PV neuronal activity. Additionally, PNNs might need a longer 4-AP incubation time or higher concentrations to observe changes in the ECM structure.

The network oscillatory activity in the ACC in A30P mice has not been investigated before. There is also a limited number of studies showing KA-evoked oscillations in the mouse ACC. We saw fast-frequency oscillatory activity evoked by KA, in the beta and gamma frequency band (15 – 90 Hz), in the deep layers of the ACC in young 2-4-month-old A30P and WT mice. However, there were no differences in the oscillation area power, peak amplitude, and frequency between the two genotypes. Beta and gamma frequency oscillations have also been shown in the ACC in young adult rats evoked by KA but this was not previously shown in the mouse ACC (Dennis *et al.*, 2023). Previous work in our lab found KA-evoked fast gamma frequency oscillations in the hippocampus of young A30P mice consisting of a big area power compared to our ACC oscillations (Robson *et al.*, 2018; Tweedy *et al.*, 2021). However, the hippocampus consists of different network dynamics compared to the ACC. Thus, this highlights neuronal network differences between the hippocampus and ACC in the A30P transgenic mice.

7.3. The impact of α-syn pathology on PV interneurons and PNNs in the ACC neuronal networks of young and aged A30P mice.

Studies by Ueno et al. (2017, 2019) have shown PV neuronal and PNN interactions in the mouse ACC at different ages (Ueno *et al.*, 2017; Ueno, Fujii, *et al.*, 2019). However, there are no studies demonstrating interactions of PNNs with PV interneurons in the ACC in DLB transgenic mice. Thus, we investigated PV interneurons and PNNs in the ACC of young 2-4-month-old and aged 10-12-month-

old A30P and WT mice. In both the young and aged A30P mice, we found a non-significant reduction in PV expression in the PV somas and number compared to the WT.

Interestingly, even though most PV interneurons were surrounded by PNNs, in the young and aged A30P mice more PNNs surrounded other types of neurons compared to the WT. Additionally, in the aged WT animals, we noticed an increase in PV interneurons without PNNs compared to the young mice suggesting potential age-related upregulation in PV expression. The non-significant decrease in PV expression in the PV somas of A30P mice, and thus a decrease in calcium activity, might indicate changes in the firing activity of PV interneurons possibly associated with α-syn pathology. Also, the increase in PNNs around non-PV neurons in the ACC of A30P mice highlights a shift to the localisation of PNNs around other types of interneurons or excitatory neurons. Studies have shown that in other brain areas, PNNs surrounded SST interneurons as well as excitatory neurons (McRae *et al.*, 2010; Berretta *et al.*, 2015; Lensjø *et al.*, 2017; Morikawa *et al.*, 2017). Importantly, the PNNs around non-PV cells may regulate their firing properties and potentially lead to different network structures and synaptic activity in the ACC of A30P mice compared to the WT.

There is limited knowledge about the impact of α-syn pathology on interneurons. A previous study in our lab demonstrated the co-localisation of hα-syn with around 25% of PV interneurons in the hippocampus of young A30P mice (Tweedy *et al.*, 2021). We found that hα-syn was present in 64.8% of PV neuronal somas and in 77.7% of PNNs in the ACC of young A30P mice. Most PV interneurons with hα-syn were surrounded by PNNs which also contained hα-syn. Importantly, by 12 months of age, hα-syn was present in 99.4% of PV somas and PNNs in the ACC of A30P mice. The general increase of hα-syn observed in the ACC was expected as evidence shows elevated hα-syn expression and aggregation in aged A30P mice (Kahle et al., 2000, 2001). However, to our knowledge, we are the first to show hα-syn expression in PV somas and PNNs in the ACC of A30P mice from a young pre-symptomatic state. The expression of hα-syn in the A30P mice is driven by the Thy-1 promoter in the excitatory neurons (Feng *et al.*, 2000; Sugino *et al.*, 2005). Therefore, the hα-syn localisation revealed in the somas and nuclei of PV interneurons in the ACC of A30P mice might be due to its spread through excitatory synaptic interactions. On the other hand, the PV interneurons might also express hα-syn as a study recently revealed the Thy-1

expression in interneurons and potentially fast-spiking PV interneurons (Proskurina and Zaitsev, 2021). Our findings could also suggest that the PNNs may not be protecting the PV interneurons from α-syn pathology, potentially affecting the neuronal network dynamics in the ACC of A30P mice, even from a young age. However, the PNNs in the A30P mice might be protecting excitatory pyramidal neurons against hα-syn overexpression considering their increased localisation around non-PV neurons observed.

Interestingly, the early α-syn pathology observed in the ACC, an area associated with early stages of LB pathology (Kövari *et al.*, 2003), contrasts with the later development of pathology in areas such as the motor cortex (Outeiro *et al.*, 2019). This raises the question whether the protective role of PNNs diminishes in later disease stages or in different brain areas as α-syn aggregates progress and ultimately contribute to neuronal death. Our findings, therefore, highlight the importance of studying region-specific differences in α-syn localisation and PNN function at distinct stages of disease progression. The observed α-syn pathology in the aged A30P mice may also align with the eventual emergence of symptoms, offering insights into how PNNs affect the optimal neuronal function throughout this process.

7.4. Age-related increase in astrocytic and microglial activation in the ACC.

Neuroinflammation in neurodegenerative disorders has been investigated in brain areas such as the hippocampus, striatum, substantia nigra, amygdala and entorhinal cortex but not in the ACC (Katsuse *et al*., 2003; Rocha *et al*., 2015; Lai *et al.*, 2024). In this study, the Iba-1 and GFAP expression was examined in the ACC in young 2-4-month-old and aged 10-12-month-old A30P mice compared to the WT. We found a trend towards an increase in the Iba-1 expression and a significant increase in GFAP expression in the aged animals compared to the young animals, without however any differences between the genotypes. Therefore, an increase in astrocytic activation was revealed in the ACC with increased ageing which has not been investigated before in both A30P and WT mice.

In neurodegeneration, there is upregulated iNOS expression by reactive microglia leading to increased NO production and contributing to neurotoxicity

(Kummer et al., 2011; Guivernau et al., 2016; Bandookwala and Sengupta, 2020; Bourgognon et al., 2021). We thus examined Iba-1+ microglia and reactive microglia co-expressing Iba-1 and iNOS in the ACC in young and aged A30P mice compared to the WT. Even though we found a decrease in Iba-1+ microglia, there were no marked changes in the overall Iba-1 expression. Additionally, significantly fewer Iba-1+ microglia were observed in the aged A30P mice compared to the aged WT mice which could be associated with the α-syn pathology. Therefore, we suggest that microglia in the ACC of aged mice underwent age-induced morphological changes adopting a dystrophic shape which could explain the beading Iba-1 expression and the decreased microglial number observed (Sheng et al., 1998; Streit et al., 2004, 2008; Conde and Streit, 2006a, 2006b; Streit, 2006; Flanary et al., 2007). However, in the aged A30P mice, these dystrophic changes might have been more severe compared to the WT due to increased hα-syn expression. On the other hand, we found an increased number of reactive microglia expressing iNOS in the ACC of aged A30P and WT mice compared to the young mice. These data thus indicate an increase in iNOS activity in the ACC of aged mice, implying an increased NO production induced by ageing as previously observed in other brain regions (McCann et al., 1998; Calabrese et al., 2000; Coleman, 2001; Law et al., 2001).

Ageing causes increased microglial activation due to changes in CNS homeostasis and this has been shown in different brain regions in both humans and rodents (Ogura et al., 1994; Morgan et al., 1999; Helmut et al., 2011; Schuitemaker et al., 2012; Tremblay et al., 2012; Yegla et al., 2021). However, there is a lack of evidence for reactive microglia in the ACC in mice related to neurodegeneration in DLB. In this study, we provided an understanding of neuroinflammatory markers associated with both the astrocytic and microglial activation in the ACC under both ageing and α-syn pathological conditions in A30P mice.

7.5. Limitations and future work

7.5.1. *Network hyperexcitability in the ACC of A30P mice*

There were some limitations in this study which need to be addressed. The *in vitro* electrophysiology experiments were completed during refreshment of the A30P mouse breeding line and problems in the CBC facility led to a limited number of A30P mice available for experiments and insufficient male and female mice. However, we did not see any obvious differences in activity between the genders. For future investigations, it would be interesting to examine gender differences in the ACC network activity between young A30P and WT mice.

Following the assessment of 4-AP-induced hyperexcitability in the ACC of WT and A30P mice, we saw no statistically significant differences in the WFA+ PNN expression between A30P and WT mice. However, ECM component alterations might have been revealed with more detailed experimental methods such as proteomics or RNA sequencing as well as maybe other ECM markers. Also, an important experimental study to understand the role of PNNs in the ACC neuronal networks would be to pharmacologically induce the breakdown of the PNN component hyaluronan using the enzyme hyase. The neuronal network activity could then be assessed following hyase incubation in the ACC slices between young A30P and WT mice.

7.5.2. *The expression of PV neurons, PNNs and glial cells in the ACC of young and aged A30P mice*

In our study, we showed PV neuronal and PNN interactions in the ACC of young and aged A30P mice and the presence of hα-syn both within the PNN and within the PV neuronal soma and nuclei. It would be interesting to examine the pathological spread of pS129 on PV interneurons and PNNs. An increased expression of PNNs around non-PV neurons, potentially excitatory pyramidal cells, was also revealed in the ACC of A30P mice in this study. Future studies would involve specific labelling of

other neuronal types e.g., pyramidal neurons and SST interneurons to assess PNN localisation around other neuronal types in both A30P and WT mice.

We also made a preliminary investigation of changes in neuroinflammatory markers involving astrocytic and microglial activation in the ACC between young and aged A30P mice compared to the WT. However, we only analysed one ACC slice and hemisphere per animal due to limited time. Thus, our next steps will involve the analysis of more ACC slices per animal in each age group to increase the statistical power. It would also be interesting to investigate the pathological spread of pS129 on Iba-1+ microglia and GFAP+ astrocytes.

The mice used in these experiments were categorised between two age groups including 2-4-months-old and 10-12-months-old. The investigation of differences in PV, PNN and glial cell expression would be important to be conducted in the ACC of older 12-14-month-old A30P mice compared to age-matched WT. We saw changes in the ACC neuronal networks in the A30P mice occurring from a young age, but it would be essential to examine changes related to the α-syn pathology during the later symptomatic stages in the A30P mice. During this study, we also attempted to investigate the PV, PNN and glial cell expression in AD, DLB and control human cases. However, given the time limitations, we could not perform all the IHC experiments and finish the different antibody calibrations in the human post-mortem tissue.

References

Aarsland, Dag *et al.* (2001) ‘A comparative study of psychiatric symptoms in dementia with Lewy bodies and Parkinson’s disease with and without dementia’, *International journal of geriatric psychiatry*, 16(5), pp. 528–536. doi: 10.1002/GPS.389.

Aarsland, D. *et al.* (2001) ‘Comparison of extrapyramidal signs in dementia with Lewy bodies and Parkinson’s disease’, *The Journal of neuropsychiatry and clinical neurosciences*, 13(3), pp. 374–379. doi: 10.1176/JNP.13.3.374.

Abbott, N. J., Rönnbäck, L. and Hansson, E. (2006) ‘Astrocyte-endothelial interactions at the blood-brain barrier’, *Nature reviews. Neuroscience*, 7(1), pp. 41–53. doi: 10.1038/NRN1824.

Acosta, C., Anderson, H. D. and Anderson, C. M. (2017) ‘Astrocyte dysfunction in Alzheimer disease’, *Journal of Neuroscience Research*, 95(12), pp. 2430–2447. doi: 10.1002/JNR.24075.

Adams, I. *et al.* (2001) ‘Perineuronal nets in the rhesus monkey and human basal forebrain including basal ganglia’, *Neuroscience*, 108(2), pp. 285–298. doi: 10.1016/S0306-4522(01)00419-5.

Adams, N. E. *et al.* (2017) ‘Hetereogeneity in Neuronal Intrinsic Properties: A Possible Mechanism for Hub-Like Properties of the Rat Anterior Cingulate Cortex during Network Activity’, *eNeuro*, 4(1), pp. 313–329. doi: 10.1523/ENEURO.0313-16.2017.

Adler, C. H. and Beach, T. G. (2016) ‘Neuropathological basis of nonmotor manifestations of Parkinson’s disease’, *Movement Disorders*, 31(8), pp. 1114–1119. doi: 10.1002/MDS.26605.

Akdağ, M. Z. *et al.* (2023) ‘The increase in c-fos expression in epileptic seizures is inhibited by magnetic field application, but not KCa1.1 channel expression’, *Electromagnetic biology and medicine*, 42(2), pp. 81–97. doi: 10.1080/15368378.2023.2247027.

Akiyama, H. *et al.* (1993) ‘Morphological diversities of CD44 positive astrocytes in the cerebral cortex of normal subjects and patients with Alzheimer’s disease’, *Brain*

research, 632(1–2), pp. 249–259. doi: 10.1016/0006-8993(93)91160-T.

Akiyama, H. *et al.* (2000) 'Inflammation and Alzheimer's disease', *Neurobiology of aging*, 21(3), p. 383. doi: 10.1016/S0197-4580(00)00124-X.

Al-Musawi, I. *et al.* (2024) 'Evidence for prodromal changes in neuronal excitability and neuroinflammation in the hippocampus in young alpha-synuclein (A30P) transgenic mice', *Frontiers in Dementia*, 3, p. 1404841. doi: 10.3389/FRDEM.2024.1404841.

Al'Qteishat, A. *et al.* (2006) 'Changes in hyaluronan production and metabolism following ischaemic stroke in man', *Brain*, 129(8), pp. 2158–2176. doi: 10.1093/BRAIN/AWL139.

Alcaide, J. *et al.* (2019) 'Alterations of perineuronal nets in the dorsolateral prefrontal cortex of neuropsychiatric patients', *International Journal of Bipolar Disorders*, 7(1), pp. 1–9. doi: 10.1186/S40345-019-0161-0/FIGURES/2.

Ali, A. B. *et al.* (2001) 'Kainate Receptors Regulate Unitary IPSCs Elicited in Pyramidal Cells by Fast-Spiking Interneurons in the Neocortex', *The Journal of Neuroscience*, 21(9), p. 2992. doi: 10.1523/JNEUROSCI.21-09-02992.2001.

Ali, F. *et al.* (2019) 'Parvalbumin-positive neuron loss and amyloid-beta deposits in the frontal cortex of Alzheimer's disease-related mice', *Journal of Alzheimer's disease : JAD*, 72(4), p. 1323. doi: 10.3233/JAD-181190.

Allen, W. E. *et al.* (1997) 'Rho, Rac and Cdc42 regulate actin organization and cell adhesion in macrophages', *Journal of Cell Science*, 110(6), pp. 707–720. doi: 10.1242/JCS.110.6.707.

Alliot, F., Godin, I. and Pessac, B. (1999) 'Microglia derive from progenitors, originating from the yolk sac, and which proliferate in the brain', *Developmental Brain Research*, 117(2), pp. 145–152. doi: 10.1016/S0165-3806(99)00113-3.

Alpár, A. *et al.* (2006) 'Distribution of pyramidal cells associated with perineuronal nets in the neocortex of rat', *Brain research*, 1120(1), pp. 13–22. doi: 10.1016/J.BRAINRES.2006.08.069.

Alvarez-Erviti, L. *et al.* (2011) 'Lysosomal dysfunction increases exosome-mediated alpha-synuclein release and transmission', *Neurobiology of Disease*, 42(3), p. 360.

doi: 10.1016/J.NBD.2011.01.029.

Amin, J. *et al.* (2020) ‘Neuroinflammation in dementia with Lewy bodies: a human post-mortem study’, *Translational psychiatry*, 10(1). doi: 10.1038/S41398-020-00954-8.

Amin, J. *et al.* (2022) ‘Inflammation in dementia with Lewy bodies’, *Neurobiology of Disease*, 168, p. 105698. doi: 10.1016/J.NBD.2022.105698.

Anastasiades, P. G., Collins, D. P. and Carter, A. G. (2020) ‘Mediodorsal and ventromedial thalamus engage distinct L1 circuits in the prefrontal cortex’, *bioRxiv*. bioRxiv, p. 2020.01.08.898817. doi: 10.1101/2020.01.08.898817.

Anderson, M. A., Ao, Y. and Sofroniew, M. V. (2014) ‘Heterogeneity of reactive astrocytes’, *Neuroscience letters*, 0, p. 23. doi: 10.1016/J.NEULET.2013.12.030.

Anderson, M. D. *et al.* (2020) ‘ChABC infusions into medial prefrontal cortex, but not posterior parietal cortex, improve the performance of rats tested on a novel, challenging delay in the touchscreen TUNL task’, *Learning & memory (Cold Spring Harbor, N.Y.)*, 27(6), pp. 222–235. doi: 10.1101/LM.050245.119.

Andersson, M. *et al.* (2008) ‘Electroencephalogram variability in dementia with lewy bodies, Alzheimer’s disease and controls’, *Dementia and geriatric cognitive disorders*, 26(3), pp. 284–290. doi: 10.1159/000160962.

Angelova, P. R. *et al.* (2016) ‘Ca2+ is a key factor in α-synuclein-induced neurotoxicity’, *Journal of Cell Science*, 129(9), p. 1792. doi: 10.1242/JCS.180737.

Angulo, M. C. *et al.* (2004) ‘Glutamate Released from Glial Cells Synchronizes Neuronal Activity in the Hippocampus’, *The Journal of Neuroscience*, 24(31), p. 6920. doi: 10.1523/JNEUROSCI.0473-04.2004.

Appel, S. H. *et al.* (2011) ‘The Microglial-Motoneuron dialogue in ALS’, *Acta Myologica*, 30(1), p. 4. Available at: /pmc/articles/PMC3185827/ (Accessed: 12 March 2024).

Araque, A. *et al.* (1999) ‘Tripartite synapses: Glia, the unacknowledged partner’, *Trends in Neurosciences*, 22(5), pp. 208–215. doi: 10.1016/S0166-2236(98)01349-6.

Archibald, N. K. *et al.* (2009) ‘The retina in Parkinson’s disease’, *Brain : a journal of*

neurology, 132(Pt 5), pp. 1128–1145. doi: 10.1093/BRAIN/AWP068.

Armstrong, C. M. and Loboda, A. (2001) 'A Model for 4-Aminopyridine Action on K Channels: Similarities to Tetraethylammonium Ion Action', *Biophysical Journal*, 81(2), pp. 895–904. doi: 10.1016/S0006-3495(01)75749-9.

Arranz, A. M. *et al.* (2014) 'Hyaluronan Deficiency Due to Has3 Knock-Out Causes Altered Neuronal Activity and Seizures via Reduction in Brain Extracellular Space', *Journal of Neuroscience*, 34(18), pp. 6164–6176. doi: 10.1523/JNEUROSCI.3458-13.2014.

Asai, H. *et al.* (2015) 'Depletion of microglia and inhibition of exosome synthesis halt tau propagation', *Nature neuroscience*, 18(11), pp. 1584–1593. doi: 10.1038/NN.4132.

Atallah, B. V. and Scanziani, M. (2009) 'Instantaneous Modulation of Gamma Oscillation Frequency by Balancing Excitation with Inhibition', *Neuron*, 62(4), pp. 566–577. doi: 10.1016/j.neuron.2009.04.027.

Avermann, M. *et al.* (2012) 'Microcircuits of excitatory and inhibitory neurons in layer 2/3 of mouse barrel cortex', *Journal of Neurophysiology*, 107(11), pp. 3116–3134. doi: 10.1152/JN.00917.2011/ASSET/IMAGES/LARGE/Z9K0111213530008.JPEG.

Avoli, M. *et al.* (1996) 'Synchronous GABA-Mediated Potentials and Epileptiform Discharges in the Rat Limbic System In Vitro', *Journal of Neuroscience*, 16(12), pp. 3912–3924. doi: 10.1523/JNEUROSCI.16-12-03912.1996.

Avoli, M. *et al.* (2002) 'Network and pharmacological mechanisms leading to epileptiform synchronization in the limbic system in vitro', *Progress in Neurobiology*, 68(3), pp. 167–207. doi: 10.1016/S0301-0082(02)00077-1.

Avoli, M. *et al.* (2016) 'Specific imbalance of excitatory/inhibitory signaling establishes seizure onset pattern in temporal lobe epilepsy', *Journal of Neurophysiology*, 115(6), pp. 3229–3237. doi: 10.1152/JN.01128.2015/ASSET/IMAGES/LARGE/Z9K0071636960005.JPEG.

Baba, Y. *et al.* (2009) 'Timp-3 deficiency impairs cognitive function in mice', *Laboratory Investigation*, 89(12), pp. 1340–1347. doi: 10.1038/LABINVEST.2009.101.

Babiloni, C. *et al.* (2004) ‘Abnormal fronto-parietal coupling of brain rhythms in mild Alzheimer’s disease: a multicentric EEG study’, *The European journal of neuroscience*, 19(9), pp. 2583–2590. doi: 10.1111/J.0953-816X.2004.03333.X.

Bachstetter, A. D. *et al.* (2015) ‘Disease-related microglia heterogeneity in the hippocampus of Alzheimer’s disease, dementia with Lewy bodies, and hippocampal sclerosis of aging’, *Acta neuropathologica communications*, 3(1), p. 32. doi: 10.1186/S40478-015-0209-Z/FIGURES/10.

Badin, A. S., Fermani, F. and Greenfield, S. A. (2017) ‘The features and functions of neuronal assemblies: Possible dependency on mechanisms beyond synaptic transmission’, *Frontiers in Neural Circuits*, 10, p. 223604. doi: 10.3389/FNCIR.2016.00114/BIBTEX.

Baeg, E. H. *et al.* (2003) ‘Dynamics of population code for working memory in the prefrontal cortex’, *Neuron*, 40(1), pp. 177–188. doi: 10.1016/S0896-6273(03)00597-X.

Baig, S., Wilcock, G. K. and Love, S. (2005a) ‘Loss of perineuronal net N-acetylgalactosamine in Alzheimer’s disease’, *Acta neuropathologica*, 110(4), pp. 393–401. doi: 10.1007/S00401-005-1060-2.

Baig, S., Wilcock, G. K. and Love, S. (2005b) ‘Loss of perineuronal net N-acetylgalactosamine in Alzheimer’s disease’, *Acta neuropathologica*, 110(4), pp. 393–401. doi: 10.1007/S00401-005-1060-2.

Bak, L. K., Schousboe, A. and Waagepetersen, H. S. (2006) ‘The glutamate/GABA-glutamine cycle: aspects of transport, neurotransmitter homeostasis and ammonia transfer’, *Journal of neurochemistry*, 98(3), pp. 641–653. doi: 10.1111/J.1471-4159.2006.03913.X.

Balaban, D. *et al.* (2021) ‘The phenomenon of clasmatodendrosis’, *Heliyon*, 7(7). doi: 10.1016/J.HELIYON.2021.E07605.

Balashova, A. *et al.* (2019) ‘Enzymatic Digestion of Hyaluronan-Based Brain Extracellular Matrix in vivo Can Induce Seizures in Neonatal Mice’, *Frontiers in Neuroscience*, 13(SEP). doi: 10.3389/FNINS.2019.01033.

Balmer, T. S. (2016) ‘Perineuronal Nets Enhance the Excitability of Fast-Spiking

Neurons', *eNeuro*, 3(4), pp. 745–751. doi: 10.1523/ENEURO.0112-16.2016.

Bancaud, J. and Talairach, J. (1992) 'Clinical semiology of frontal lobe seizures.', *Advances in neurology*.

Bandookwala, M. and Sengupta, P. (2020) '3-Nitrotyrosine: a versatile oxidative stress biomarker for major neurodegenerative diseases', *The International journal of neuroscience*, 130(10), pp. 1047–1062. doi: 10.1080/00207454.2020.1713776.

Banerjee, S. B. *et al.* (2017a) 'Perineuronal Nets in the Adult Sensory Cortex Are Necessary for Fear Learning', *Neuron*, 95(1), pp. 169-179.e3. doi: 10.1016/J.NEURON.2017.06.007.

Banerjee, S. B. *et al.* (2017b) 'Perineuronal Nets in the Adult Sensory Cortex Are Necessary for Fear Learning', *Neuron*, 95(1), pp. 169-179.e3. doi: 10.1016/J.NEURON.2017.06.007.

Barakat, L. and Bordey, A. (2002) 'GAT-1 and reversible GABA transport in Bergmann glia in slices', *Journal of neurophysiology*, 88(3), pp. 1407–1419. doi: 10.1152/JN.2002.88.3.1407.

Bardóczi, Z. *et al.* (2017) 'Glycinergic Input to the Mouse Basal Forebrain Cholinergic Neurons', *The Journal of Neuroscience*, 37(39), p. 9534. doi: 10.1523/JNEUROSCI.3348-16.2017.

Barkholt, P. *et al.* (2012) 'LONG-TERM POLARIZATION OF MICROGLIA UPON-SYNUCLEIN OVEREXPRESSION IN NONHUMAN PRIMATES'. doi: 10.1016/j.neuroscience.2012.02.004.

Baroncelli, L. *et al.* (2016) 'Experience Affects Critical Period Plasticity in the Visual Cortex through an Epigenetic Regulation of Histone Post-Translational Modifications', *The Journal of Neuroscience*, 36(12), p. 3430. doi: 10.1523/JNEUROSCI.1787-15.2016.

von Bartheld, C. S., Bahney, J. and Herculano-Houzel, S. (2016) 'The Search for True Numbers of Neurons and Glial Cells in the Human Brain: A Review of 150 Years of Cell Counting', *The Journal of comparative neurology*, 524(18), p. 3865. doi: 10.1002/CNE.24040.

Bartos, M., Vida, I. and Jonas, P. (2007) 'Synaptic mechanisms of synchronized

gamma oscillations in inhibitory interneuron networks', *Nature Reviews Neuroscience 2007 8:1*, 8(1), pp. 45–56. doi: 10.1038/nrn2044.

Başar, E. *et al.* (2016) 'Delay of cognitive gamma responses in Alzheimer's disease', *NeuroImage: Clinical*, 11, pp. 106–115. doi: 10.1016/J.NICL.2016.01.015.

Batiuk, M. Y. *et al.* (2020) 'Identification of region-specific astrocyte subtypes at single cell resolution', *Nature Communications 2020 11:1*, 11(1), pp. 1–15. doi: 10.1038/s41467-019-14198-8.

Baulac, M. *et al.* (2015) 'Epilepsy priorities in Europe: A report of the ILAE-IBE Epilepsy Advocacy Europe Task Force', *Epilepsia*, 56(11), p. 1687. doi: 10.1111/EPI.13201.

Beagle, A. J. *et al.* (2017) 'Relative Incidence of Seizures and Myoclonus in Alzheimer's Disease, Dementia with Lewy Bodies, and Frontotemporal Dementia', *Journal of Alzheimer's disease : JAD*, 60(1), p. 211. doi: 10.3233/JAD-170031.

Becker, L. J. *et al.* (2023) 'The basolateral amygdala-anterior cingulate pathway contributes to depression-like behaviors and comorbidity with chronic pain behaviors in male mice', *Nature Communications 2023 14:1*, 14(1), pp. 1–23. doi: 10.1038/s41467-023-37878-y.

Bellucci, A. *et al.* (2016) 'Review: Parkinson's disease: from synaptic loss to connectome dysfunction', *Neuropathology and Applied Neurobiology*, 42(1), pp. 77–94. doi: 10.1111/NAN.12297.

Beltrán-Castillo, S. *et al.* (2017) 'D-serine released by astrocytes in brainstem regulates breathing response to CO2 levels', *Nature Communications*, 8(1). doi: 10.1038/S41467-017-00960-3.

Benjamin, N. *et al.* (1994) 'Stomach NO synthesis', *Nature*, 368(6471), p. 502. doi: 10.1038/368502A0.

Béraud, Dawn *et al.* (2012) 'Microglial Activation and Antioxidant Responses Induced by the Parkinson's Disease Protein α-Synuclein', *Journal of Neuroimmune Pharmacology 2012 8:1*, 8(1), pp. 94–117. doi: 10.1007/S11481-012-9401-0.

Bernstein, H. G. *et al.* (2011) 'Partial loss of parvalbumin-containing hippocampal interneurons in dementia with Lewy bodies', *Neuropathology*, 31(1), pp. 1–10. doi:

10.1111/J.1440-1789.2010.01117.X.

Berretta, S. *et al.* (2015) 'LOSING THE SUGAR COATING: POTENTIAL IMPACT OF PERINEURONAL NET ABNORMALITIES ON INTERNEURONS IN SCHIZOPHRENIA', *Schizophrenia research*, 167(0), p. 18. doi: 10.1016/J.SCHRES.2014.12.040.

Biessels, G. J. and Kappelle, L. J. (2005) 'Increased risk of Alzheimer's disease in Type II diabetes: insulin resistance of the brain or insulin-induced amyloid pathology?', *Biochemical Society transactions*, 33(Pt 5), pp. 1041–1044. doi: 10.1042/BST0331041.

Bisaglia, M., Mammi, S. and Bubacco, L. (2009) 'Structural insights on physiological functions and pathological effects of ±-synuclein', *The FASEB Journal*, 23(2), pp. 329–340. doi: 10.1096/FJ.08-119784.

Bitanihirwe, B. K. Y. and Woo, T. U. W. (2014) 'Perineuronal Nets and Schizophrenia: The Importance of Neuronal Coatings', *Neuroscience and biobehavioral reviews*, 45, p. 85. doi: 10.1016/J.NEUBIOREV.2014.03.018.

Blanc, F. *et al.* (2016) 'Grey matter atrophy in prodromal stage of dementia with Lewy bodies and Alzheimer's disease', *Alzheimer's Research and Therapy*, 8(1), pp. 1–11. doi: 10.1186/S13195-016-0198-6/FIGURES/3.

Bohnen, N. I. *et al.* (2003) 'Cortical Cholinergic Function Is More Severely Affected in Parkinsonian Dementia Than in Alzheimer Disease: An In Vivo Positron Emission Tomographic Study', *Archives of Neurology*, 60(12), pp. 1745–1748. doi: 10.1001/ARCHNEUR.60.12.1745.

Boison, D. and Steinhäuser, C. (2018) 'Epilepsy and astrocyte energy metabolism', *Glia*, 66(6), p. 1235. doi: 10.1002/GLIA.23247.

Boldog, E. *et al.* (2018) 'Transcriptomic and morphophysiological evidence for a specialized human cortical GABAergic cell type', *Nature neuroscience*, 21(9), p. 1185. doi: 10.1038/S41593-018-0205-2.

Bonanni, L. *et al.* (2008) 'EEG comparisons in early Alzheimer's disease, dementia with Lewy bodies and Parkinson's disease with dementia patients with a 2-year follow-up', *Brain : a journal of neurology*, 131(Pt 3), pp. 690–705. doi:

10.1093/BRAIN/AWM322.

Bonanni, L. *et al.* (2016) ‘EEG Markers of Dementia with Lewy Bodies: A Multicenter Cohort Study’, *Journal of Alzheimer’s disease : JAD*, 54(4), pp. 1649–1657. doi: 10.3233/JAD-160435.

Bonnans, C., Chou, J. and Werb, Z. (2014) ‘Remodelling the extracellular matrix in development and disease’, *Nature reviews. Molecular cell biology*, 15(12), pp. 786–801. doi: 10.1038/NRM3904.

den Boon, F. S. *et al.* (2015) ‘Activation of type-1 cannabinoid receptor shifts the balance between excitation and inhibition towards excitation in layer II/III pyramidal neurons of the rat prelimbic cortex’, *Pflugers Archiv European Journal of Physiology*, 467(7), pp. 1551–1564. doi: 10.1007/S00424-014-1586-Z/FIGURES/6.

Booth, H. D. E., Hirst, W. D. and Wade-Martins, R. (2017) ‘The Role of Astrocyte Dysfunction in Parkinson’s Disease Pathogenesis’, *Trends in neurosciences*, 40(6), pp. 358–370. doi: 10.1016/J.TINS.2017.04.001.

Bouchat, J. *et al.* (2019) ‘Ultrastructural Analysis of Thalamus Damages in a Mouse Model of Osmotic-Induced Demyelination’, *Neurotoxicity research*, 36(1), pp. 144–162. doi: 10.1007/S12640-019-00041-X.

Bourgognon, J. M. *et al.* (2021) ‘Inhibition of neuroinflammatory nitric oxide signaling suppresses glycation and prevents neuronal dysfunction in mouse prion disease’, *Proceedings of the National Academy of Sciences of the United States of America*, 118(10). doi: 10.1073/PNAS.2009579118/-/DCSUPPLEMENTAL.

Bourguignon, L. Y. W. *et al.* (2007) ‘Hyaluronan-CD44 interaction stimulates Rac1 signaling and PKN gamma kinase activation leading to cytoskeleton function and cell migration in astrocytes’, *Journal of neurochemistry*, 101(4), pp. 1002–1017. doi: 10.1111/J.1471-4159.2007.04485.X.

Bouvier, D. S. *et al.* (2016) ‘High Resolution Dissection of Reactive Glial Nets in Alzheimer’s Disease’, *Scientific Reports 2016 6:1*, 6(1), pp. 1–15. doi: 10.1038/srep24544.

Boveris, A. and Navarro, A. (2008) ‘Brain mitochondrial dysfunction in aging’, *IUBMB Life*, 60(5), pp. 308–314. doi: 10.1002/IUB.46.

Braak, H. *et al.* (1994) ‘Amygdala pathology in Parkinson’s disease’, *Acta Neuropathologica 1994 88:6*, 88(6), pp. 493–500. doi: 10.1007/BF00296485.

Braak, H. *et al.* (2000) ‘Pathological changes in the parahippocampal region in select non-Alzheimer’s dementias’, *Annals of the New York Academy of Sciences*, 911, pp. 221–239. doi: 10.1111/J.1749-6632.2000.TB06729.X.

Braak, H. *et al.* (2003) ‘Idiopathic Parkinson’s disease: Possible routes by which vulnerable neuronal types may be subject to neuroinvasion by an unknown pathogen’, *Journal of Neural Transmission*, 110(5), pp. 517–536. doi: 10.1007/S00702-002-0808-2/METRICS.

Braak, Heiko *et al.* (2003) ‘Staging of brain pathology related to sporadic Parkinson’s disease’, *Neurobiology of Aging*, 24(2), pp. 197–211. doi: 10.1016/S0197-4580(02)00065-9.

Braak, H. and Braak, E. (1991) ‘Neuropathological stageing of Alzheimer-related changes’, *Acta neuropathologica*, 82(4), pp. 239–259. doi: 10.1007/BF00308809.

Braak, H., Sastre, M. and Del Tredici, K. (2007) ‘Development of alpha-synuclein immunoreactive astrocytes in the forebrain parallels stages of intraneuronal pathology in sporadic Parkinson’s disease’, *Acta neuropathologica*, 114(3), pp. 231–241. doi: 10.1007/S00401-007-0244-3.

Brady, D. R. and Mufson, E. J. (1997) ‘Parvalbumin-immunoreactive neurons in the hippocampal formation of Alzheimer’s diseased brain’, *Neuroscience*, 80(4), pp. 1113–1125. doi: 10.1016/S0306-4522(97)00068-7.

Braidy, N. *et al.* (2013) ‘Uptake and mitochondrial dysfunction of alpha-synuclein in human astrocytes, cortical neurons and fibroblasts’, *Translational Neurodegeneration*, 2(1), p. 20. doi: 10.1186/2047-9158-2-20.

Bronner-Fraser, M. (1986) ‘An antibody to a receptor for fibronectin and laminin perturbs cranial neural crest development in vivo’, *Developmental Biology*, 117(2), pp. 528–536. doi: 10.1016/0012-1606(86)90320-9.

Brosseron, F. *et al.* (2014) ‘Body fluid cytokine levels in mild cognitive impairment and Alzheimer’s disease: a comparative overview’, *Molecular neurobiology*, 50(2), pp. 534–544. doi: 10.1007/S12035-014-8657-1.

Brown, G. C. and Neher, J. J. (2010) ‘Inflammatory neurodegeneration and mechanisms of microglial killing of neurons’, *Molecular neurobiology*, 41(2–3), pp. 242–247. doi: 10.1007/S12035-010-8105-9.

Brozzi, F. *et al.* (2009) ‘S100B Protein Regulates Astrocyte Shape and Migration via Interaction with Src Kinase: IMPLICATIONS FOR ASTROCYTE DEVELOPMENT, ACTIVATION, AND TUMOR GROWTH*S’, *The Journal of Biological Chemistry*, 284(13), p. 8797. doi: 10.1074/JBC.M805897200.

Bucher, E. A. *et al.* (2021) ‘Coherence and cognition in the cortex: the fundamental role of parvalbumin, myelin, and the perineuronal net’, *Brain Structure and Function 2021 226:7*, 226(7), pp. 2041–2055. doi: 10.1007/S00429-021-02327-3.

Bullitt, E. (1990) ‘Expression of c-fos-like protein as a marker for neuronal activity following noxious stimulation in the rat’, *The Journal of comparative neurology*, 296(4), pp. 517–530. doi: 10.1002/CNE.902960402.

Burda, J. E. and Sofroniew, M. V. (2017) ‘Seducing astrocytes to the dark side’, *Cell Research*, 27(6), p. 726. doi: 10.1038/CR.2017.37.

Burré, J. (2015) ‘The Synaptic Function of α-Synuclein’, *Journal of Parkinson’s Disease*, 5(4), p. 699. doi: 10.3233/JPD-150642.

Busche, M. A. *et al.* (2015) ‘Rescue of long-range circuit dysfunction in Alzheimer’s disease models’, *Nature Neuroscience 2015 18:11*, 18(11), pp. 1623–1630. doi: 10.1038/nn.4137.

Busche, M. A. and Konnerth, A. (2016) ‘Impairments of neural circuit function in Alzheimer’s disease’, *Philosophical Transactions of the Royal Society B: Biological Sciences*, 371(1700). doi: 10.1098/RSTB.2015.0429.

Buzsáki, G. and Draguhn, A. (2004) ‘Neuronal olscillations in cortical networks’, *Science*. Science, pp. 1926–1929. doi: 10.1126/science.1099745.

Buzśaki, G. and Wang, X. J. (2012) ‘Mechanisms of Gamma Oscillations’, *Annual review of neuroscience*, 35, p. 203. doi: 10.1146/ANNUREV-NEURO-062111-150444.

Cabral-Pacheco, G. A. *et al.* (2020) ‘The Roles of Matrix Metalloproteinases and Their Inhibitors in Human Diseases’, *International Journal of Molecular Sciences*

2020, Vol. 21, Page 9739, 21(24), p. 9739. doi: 10.3390/IJMS21249739.

Cabungcal, J. H. *et al.* (2013) 'Perineuronal nets protect fast-spiking interneurons against oxidative stress', *Proceedings of the National Academy of Sciences of the United States of America*, 110(22), pp. 9130–9135. doi: 10.1073/PNAS.1300454110/SUPPL_FILE/PNAS.201300454SI.PDF.

Calabrese, V., Bates, T. E. and Giuffrida Stella, A. M. (2000) 'NO synthase and NO-dependent signal pathways in brain aging and neurodegenerative disorders: the role of oxidant/antioxidant balance', *Neurochemical research*, 25(9–10), pp. 1315–1341. doi: 10.1023/A:1007604414773.

Calabresi, P. *et al.* (2023) 'Alpha-synuclein in Parkinson's disease and other synucleinopathies: from overt neurodegeneration back to early synaptic dysfunction', *Cell Death & Disease 2023 14:3*, 14(3), pp. 1–16. doi: 10.1038/s41419-023-05672-9.

Campanac, E. *et al.* (2013) 'Enhanced Intrinsic Excitability in Basket Cells Maintains Excitatory-Inhibitory Balance in Hippocampal Circuits', *Neuron*, 77(4), pp. 712–722. doi: 10.1016/J.NEURON.2012.12.020.

Cancedda, L. *et al.* (2004) 'Acceleration of Visual System Development by Environmental Enrichment', *The Journal of Neuroscience*, 24(20), p. 4840. doi: 10.1523/JNEUROSCI.0845-04.2004.

Cano, A. *et al.* (2021) 'Epilepsy in Neurodegenerative Diseases: Related Drugs and Molecular Pathways', *Pharmaceuticals*, 14(10), p. 1057. doi: 10.3390/PH14101057.

Carceller, H. *et al.* (2020) 'Perineuronal Nets Regulate the Inhibitory Perisomatic Input onto Parvalbumin Interneurons and γ Activity in the Prefrontal Cortex', *Journal of Neuroscience*, 40(26), pp. 5008–5018. doi: 10.1523/JNEUROSCI.0291-20.2020.

Carceller, H. *et al.* (2022) 'Perineuronal Nets: Subtle Structures with Large Implications', *Neuroscientist*. doi: 10.1177/10738584221106346/ASSET/IMAGES/LARGE/10.1177_10738584221106346-FIG7.JPEG.

Cargill, R. *et al.* (2012) 'Astrocytes in aged nonhuman primate brain gray matter synthesize excess hyaluronan', *Neurobiology of Aging*, 33(4), pp. 830.e13-830.e24. doi: 10.1016/J.NEUROBIOLAGING.2011.07.006.

Carlén, M. (2017) ‘What constitutes the prefrontal cortex?’, *Science*. American Association for the Advancement of Science, pp. 478–482. doi: 10.1126/science.aan8868.

Carrillo, M. *et al.* (2019) ‘Emotional Mirror Neurons in the Rat’s Anterior Cingulate Cortex’, *Current Biology*, 29(8), pp. 1301-1312.e6. doi: 10.1016/J.CUB.2019.03.024.

Carstens, K. E. *et al.* (2016) ‘Perineuronal Nets Suppress Plasticity of Excitatory Synapses on CA2 Pyramidal Neurons’, *The Journal of Neuroscience*, 36(23), p. 6312. doi: 10.1523/JNEUROSCI.0245-16.2016.

Carulli, D. *et al.* (2010) ‘Animals lacking link protein have attenuated perineuronal nets and persistent plasticity’, *Brain : a journal of neurology*, 133(Pt 8), pp. 2331–2347. doi: 10.1093/BRAIN/AWQ145.

Caruso, G. *et al.* (2017) ‘Carnosine modulates nitric oxide in stimulated murine RAW 264.7 macrophages’, *Molecular and cellular biochemistry*, 431(1–2), p. 197. doi: 10.1007/S11010-017-2991-3.

Cattaud, V. *et al.* (2018) ‘Early disruption of parvalbumin expression and perineuronal nets in the hippocampus of the Tg2576 mouse model of Alzheimer’s disease can be rescued by enriched environment’, *Neurobiology of Aging*, 72, pp. 147–158. doi: 10.1016/J.NEUROBIOLAGING.2018.08.024.

Caviness, J. N. *et al.* (2002) ‘Small-amplitude cortical myoclonus in Parkinson’s disease: physiology and clinical observations’, *Movement disorders : official journal of the Movement Disorder Society*, 17(4), pp. 657–662. doi: 10.1002/MDS.10177.

Caviness, J. N. *et al.* (2003) ‘Electrophysiology of the myoclonus in dementia with Lewy bodies’, *Neurology*, 60(3), pp. 523–524. doi: 10.1212/WNL.60.3.523.

Caviness, J. N. *et al.* (2011) ‘Parkinson’s Disease, Cortical Dysfunction, and Alpha-Synuclein’, *Movement disorders : official journal of the Movement Disorder Society*, 26(8), p. 1436. doi: 10.1002/MDS.23697.

Celio, M. R. *et al.* (1998) ‘Perineuronal nets: past and present’, *Trends in neurosciences*, 21(12), pp. 510–515. doi: 10.1016/S0166-2236(98)01298-3.

Cera, N. *et al.* (2019) ‘Altered Cingulate Cortex Functional Connectivity in Normal Aging and Mild Cognitive Impairment’, *Frontiers in Neuroscience*, 13, p. 463174. doi:

10.3389/FNINS.2019.00857/BIBTEX.

Chałupnik, P. and Szymańska, E. (2023) ‘Kainate Receptor Antagonists: Recent Advances and Therapeutic Perspective’, *International Journal of Molecular Sciences*, 24(3). doi: 10.3390/IJMS24031908.

Chang, M. *et al.* (2018) ‘Brief activation of GABAergic interneurons initiates the transition to ictal events through post-inhibitory rebound excitation’, *Neurobiology of disease*, 109(Pt A), pp. 102–116. doi: 10.1016/J.NBD.2017.10.007.

Chaunsali, L., Tewari, B. P. and Sontheimer, H. (2021) ‘Perineuronal Net Dynamics in the Pathophysiology of Epilepsy’, *Epilepsy Currents*, 21(4), p. 273. doi: 10.1177/15357597211018688.

Chelini, G. *et al.* (2018) ‘The tetrapartite synapse: a key concept in the pathophysiology of schizophrenia’, *European psychiatry : the journal of the Association of European Psychiatrists*, 50, pp. 60–69. doi: 10.1016/J.EURPSY.2018.02.003.

Chen, Y. *et al.* (2020) ‘The role of astrocytes in oxidative stress of central nervous system: A mixed blessing’, *Cell Proliferation*, 53(3). doi: 10.1111/CPR.12781.

Chertkow, H. *et al.* (2013) ‘Definitions of dementia and predementia states in Alzheimer’s disease and vascular cognitive impairment: consensus from the Canadian conference on diagnosis of dementia’, *Alzheimer’s research & therapy*, 5(Suppl 1), p. S2. doi: 10.1186/ALZRT198.

Chesselet, M. F. *et al.* (2012) ‘A Progressive Mouse Model of Parkinson’s Disease: The Thy1-aSyn (“Line 61”) Mice’, *Neurotherapeutics*, 9(2), p. 297. doi: 10.1007/S13311-012-0104-2.

Cho, K. K. A. *et al.* (2015) ‘Gamma rhythms link prefrontal interneuron dysfunction with cognitive inflexibility in Dlx5/6+/− mice’, *Neuron*, 85(6), p. 1332. doi: 10.1016/J.NEURON.2015.02.019.

Choi, I. *et al.* (2020) ‘Microglia clear neuron-released α-synuclein via selective autophagy and prevent neurodegeneration’, *Nature Communications 2020 11:1*, 11(1), pp. 1–14. doi: 10.1038/s41467-020-15119-w.

Choi, S. *et al.* (2018) ‘Pathology of nNOS-Expressing GABAergic Neurons in Mouse

Model of Alzheimer's Disease', *Neuroscience*, 384, pp. 41–53. doi: 10.1016/J.NEUROSCIENCE.2018.05.013.

Christensen, A. C. *et al.* (2021) 'Perineuronal nets stabilize the grid cell network', *Nature Communications 2021 12:1*, 12(1), pp. 1–17. doi: 10.1038/s41467-020-20241-w.

Christensen, J. K. *et al.* (2004) 'A Mosaic of Functional Kainate Receptors in Hippocampal Interneurons', *The Journal of Neuroscience*, 24(41), p. 8986. doi: 10.1523/JNEUROSCI.2156-04.2004.

Chu, P. *et al.* (2018) 'The Impact of Perineuronal Net Digestion Using Chondroitinase ABC on the Intrinsic Physiology of Cortical Neurons', *Neuroscience*, 388, p. 23. doi: 10.1016/J.NEUROSCIENCE.2018.07.004.

Cisneros-Franco, J. M. and De Villers-Sidani, É. (2019) 'Reactivation of critical period plasticity in adult auditory cortex through chemogenetic silencing of parvalbumin-positive interneurons', *Proceedings of the National Academy of Sciences of the United States of America*, 116(52), pp. 26329–26331. doi: 10.1073/PNAS.1913227117/SUPPL_FILE/PNAS.1913227117.SD01.XLSX.

Clarke, L. E. *et al.* (2018) 'Normal aging induces A1-like astrocyte reactivity', *Proceedings of the National Academy of Sciences of the United States of America*, 115(8), pp. E1896–E1905. doi: 10.1073/PNAS.1800165115/-/DCSUPPLEMENTAL.

Clayton, M. S., Yeung, N. and Cohen Kadosh, R. (2015) 'The roles of cortical oscillations in sustained attention', *Trends in Cognitive Sciences*, 19(4), pp. 188–195. doi: 10.1016/J.TICS.2015.02.004.

Clements-Cortes, A. *et al.* (2016) 'Short-Term Effects of Rhythmic Sensory Stimulation in Alzheimer's Disease: An Exploratory Pilot Study', *Journal of Alzheimer's disease : JAD*, 52(2), pp. 651–660. doi: 10.3233/JAD-160081.

Codadu, N. K. *et al.* (2019) 'Divergent paths to seizure-like events', *Physiological Reports*, 7(19), p. e14226. doi: 10.14814/PHY2.14226.

Codadu, N. K., Parrish, R. R. and Trevelyan, A. J. (2019) 'Region-specific differences and areal interactions underlying transitions in epileptiform activity', *The Journal of Physiology*, 597(7), pp. 2079–2096. doi: 10.1113/JP277267.

Coetzee, W. A. *et al.* (1999) ‘Molecular diversity of K+ channels’, *Annals of the New York Academy of Sciences*, 868, pp. 233–255. doi: 10.1111/J.1749-6632.1999.TB11293.X.

Cole, S. R. and Voytek, B. (2017) ‘Brain Oscillations and the Importance of Waveform Shape’, *Trends in Cognitive Sciences*, 21(2), pp. 137–149. doi: 10.1016/J.TICS.2016.12.008.

Coleman, J. W. (2001) ‘Nitric oxide in immunity and inflammation’, *International immunopharmacology*, 1(8), pp. 1397–1406. doi: 10.1016/S1567-5769(01)00086-8.

Colombo, E. and Farina, C. (2016) ‘Astrocytes: Key Regulators of Neuroinflammation’, *Trends in immunology*, 37(9), pp. 608–620. doi: 10.1016/J.IT.2016.06.006.

Colonna, M. and Butovsky, O. (2017) ‘Microglia Function in the Central Nervous System During Health and Neurodegeneration’, *Annual review of immunology*, 35, p. 441. doi: 10.1146/ANNUREV-IMMUNOL-051116-052358.

Colton, C. A. (2009) ‘Heterogeneity of Microglial Activation in the Innate Immune Response in the Brain’, *Journal of Neuroimmune Pharmacology*, 4(4), p. 399. doi: 10.1007/S11481-009-9164-4.

Conde, J. R. and Streit, W. J. (2006a) ‘Effect of aging on the microglial response to peripheral nerve injury’, *Neurobiology of Aging*, 27(10), pp. 1451–1461. doi: 10.1016/J.NEUROBIOLAGING.2005.07.012.

Conde, J. R. and Streit, W. J. (2006b) ‘Microglia in the Aging Brain’, *Journal of Neuropathology & Experimental Neurology*, 65(3), pp. 199–203. doi: 10.1097/01.JNEN.0000202887.22082.63.

Cosby, K. *et al.* (2003) ‘Nitrite reduction to nitric oxide by deoxyhemoglobin vasodilates the human circulation’, *Nature medicine*, 9(12), pp. 1498–1505. doi: 10.1038/NM954.

Cossart, R. *et al.* (2001) ‘Presynaptic kainate receptors that enhance the release of GABA on CA1 hippocampal interneurons’, *Neuron*, 29(2), pp. 497–508. doi: 10.1016/S0896-6273(01)00221-5.

Cotter, D. *et al.* (2001) ‘Reduced Glial Cell Density and Neuronal Size in the Anterior

Cingulate Cortex in Major Depressive Disorder', *Archives of General Psychiatry*, 58(6), pp. 545–553. doi: 10.1001/ARCHPSYC.58.6.545.

Craig-Schapiro, R. *et al.* (2010) 'YKL-40: a novel prognostic fluid biomarker for preclinical Alzheimer's disease', *Biological psychiatry*, 68(10), pp. 903–912. doi: 10.1016/J.BIOPSYCH.2010.08.025.

Crapser, J. D., Spangenberg, E. E., *et al.* (2020) 'Microglia facilitate loss of perineuronal nets in the Alzheimer's disease brain', *EBioMedicine*, 58. doi: 10.1016/J.EBIOM.2020.102919/ATTACHMENT/35CC2133-FA06-4498-B0C5-CFCFB8C22B41/MMC2.MP4.

Crapser, J. D., Ochaba, J., *et al.* (2020) 'Microglial depletion prevents extracellular matrix changes and striatal volume reduction in a model of Huntington's disease', *Brain : a journal of neurology*, 143(1), pp. 266–288. doi: 10.1093/BRAIN/AWZ363.

Crespo-García, M. *et al.* (2022) 'Anterior Cingulate Cortex Signals the Need to Control Intrusive Thoughts during Motivated Forgetting', *Journal of Neuroscience*, 42(21), pp. 4342–4359. doi: 10.1523/JNEUROSCI.1711-21.2022.

Cunningham, E. *et al.* (2015) 'Dementia', *The Ulster Medical Journal*, 84(2), p. 79. doi: 10.1007/978-3-319-93215-6_6.

de Curtis, M. *et al.* (2019) 'GABAA receptor-mediated networks during focal seizure onset and progression in vitro', *Neurobiology of disease*, 125, pp. 190–197. doi: 10.1016/J.NBD.2019.02.007.

Custod, J. T. and Young, I. J. (1968) 'CAT BRAIN MUCOPOLYSACCHARIDES AND THEIR IN VIVO HYALURONIDASE DIGESTION', *Journal of Neurochemistry*, 15(8), pp. 809–813. doi: 10.1111/J.1471-4159.1968.TB10326.X.

Członkowska, A. and Kurkowska-Jastrzebska, I. (2011) 'Inflammation and gliosis in neurological diseases--clinical implications', *Journal of neuroimmunology*, 231(1–2), pp. 78–85. doi: 10.1016/J.JNEUROIM.2010.09.020.

D'Agostino, A. *et al.* (2017) 'Is molecular size a discriminating factor in hyaluronan interaction with human cells?', *Carbohydrate polymers*, 157, pp. 21–30. doi: 10.1016/J.CARBPOL.2016.07.125.

Dal Bianco, A. *et al.* (2008) 'Multiple sclerosis and Alzheimer's disease', *Annals of*

neurology, 63(2), pp. 174–183. doi: 10.1002/ANA.21240.

Dalley, J. W., Cardinal, R. N. and Robbins, T. W. (2004) 'Prefrontal executive and cognitive functions in rodents: Neural and neurochemical substrates', *Neuroscience and Biobehavioral Reviews*, 28(7), pp. 771–784. doi: 10.1016/j.neubiorev.2004.09.006.

Davalos, D. *et al.* (2005) 'ATP mediates rapid microglial response to local brain injury in vivo', *Nature neuroscience*, 8(6), pp. 752–758. doi: 10.1038/NN1472.

Deepa, S. S. *et al.* (2006) 'Composition of perineuronal net extracellular matrix in rat brain: a different disaccharide composition for the net-associated proteoglycans', *The Journal of biological chemistry*, 281(26), pp. 17789–17800. doi: 10.1074/JBC.M600544200.

Dennis, B. H. *et al.* (2023) 'Modulation of circuit oscillations in the rat anterior cingulate cortex (ACC) in vitro by mGlu2 metabotropic glutamate receptors and alleviation of the effects of phencyclidine-induced NMDA-receptor hypofunction', *Pharmacology Biochemistry and Behavior*, 223, p. 173532. doi: 10.1016/J.PBB.2023.173532.

Desai, N. S., Rutherford, L. C. and Turrigiano, G. G. (1999) 'BDNF Regulates the Intrinsic Excitability of Cortical Neurons', *Learning & Memory*, 6(3), p. 284. doi: 10.1101/lm.6.3.284.

Deture, M. A. and Dickson, D. W. (2019) 'The neuropathological diagnosis of Alzheimer's disease', *Molecular Neurodegeneration 2019 14:1*, 14(1), pp. 1–18. doi: 10.1186/S13024-019-0333-5.

Devinsky, O. *et al.* (2013a) 'Glia and epilepsy: excitability and inflammation', *Trends in Neurosciences*, 36(3), pp. 174–184. doi: 10.1016/J.TINS.2012.11.008.

Devinsky, O. *et al.* (2013b) 'Glia and epilepsy: excitability and inflammation', *Trends in neurosciences*, 36(3), pp. 174–184. doi: 10.1016/J.TINS.2012.11.008.

Dichter, M. A. and Ayala, G. F. (1987) 'Cellular Mechanisms of Epilepsy: A Status Report', *Science*, 237(4811), pp. 157–164. doi: 10.1126/SCIENCE.3037700.

Dickinson, R. *et al.* (2003) 'The effects of general anaesthetics on carbachol-evoked gamma oscillations in the rat hippocampus in vitro', *Neuropharmacology*, 44(7), pp.

864–872. doi: 10.1016/S0028-3908(03)00083-2.

DiNuzzo, M. (2016) ‘Astrocyte-Neuron Interactions during Learning May Occur by Lactate Signaling Rather than Metabolism’, *Frontiers in Integrative Neuroscience*, 10(JAN). doi: 10.3389/FNINT.2016.00002.

Dityatev, A. *et al.* (2007) ‘Activity-dependent formation and functions of chondroitin sulfate-rich extracellular matrix of perineuronal nets’, *Developmental neurobiology*, 67(5), pp. 570–588. doi: 10.1002/DNEU.20361.

Dityatev, A. *et al.* (2009) ‘Extracellular Matrix Molecules: Synaptic Plasticity and Learning’, *Encyclopedia of Neuroscience*, pp. 149–156. doi: 10.1016/B978-008045046-9.00793-2.

Do, K. Q. *et al.* (1997) ‘beta-Adrenergic stimulation promotes homocysteic acid release from astrocyte cultures: evidence for a role of astrocytes in the modulation of synaptic transmission’, *Journal of neurochemistry*, 68(6), pp. 2386–2394. doi: 10.1046/J.1471-4159.1997.68062386.X.

Doorn, K. J. *et al.* (2014) ‘Microglial phenotypes and toll-like receptor 2 in the substantia nigra and hippocampus of incidental Lewy body disease cases and Parkinson’s disease patients’, *Acta neuropathologica communications*, 2(1). doi: 10.1186/S40478-014-0090-1.

Doty, R. L. (2012) ‘Olfactory dysfunction in Parkinson disease’, *Nature Reviews Neurology 2012 8:6*, 8(6), pp. 329–339. doi: 10.1038/nrneurol.2012.80.

Dougherty, S. E. *et al.* (2014) ‘Hyperactivity and cortical disinhibition in mice with restricted expression of mutant huntingtin to parvalbumin-positive cells’, *Neurobiology of Disease*, 62, pp. 160–171. doi: 10.1016/J.NBD.2013.10.002.

Dubey, D. *et al.* (2017) ‘Increased metalloproteinase activity in the hippocampus following status epilepticus’, *Epilepsy research*, 132, pp. 50–58. doi: 10.1016/J.EPLEPSYRES.2017.02.021.

Duda, J. E. *et al.* (2000) ‘Widespread Nitration of Pathological Inclusions in Neurodegenerative Synucleinopathies’, *The American Journal of Pathology*, 157(5), p. 1439. doi: 10.1016/S0002-9440(10)64781-5.

Duong, S., Patel, T. and Chang, F. (2017) ‘Dementia: What pharmacists need to

know', *Canadian Pharmacists Journal : CPJ*, 150(2), p. 118. doi: 10.1177/1715163517690745.

Ekmark-Lewén, S. *et al.* (2018) 'Early fine motor impairment and behavioral dysfunction in (Thy-1)-h[A30P] alpha-synuclein mice', *Brain and Behavior*, 8(3). doi: 10.1002/BRB3.915.

Ellender, T. J. *et al.* (2014) 'Excitatory Effects of Parvalbumin-Expressing Interneurons Maintain Hippocampal Epileptiform Activity via Synchronous Afterdischarges', *The Journal of Neuroscience*, 34(46), p. 15208. doi: 10.1523/JNEUROSCI.1747-14.2014.

Ellison, D. W. *et al.* (1986) 'A postmortem study of amino acid neurotransmitters in Alzheimer's disease', *Annals of Neurology*, 20(5), pp. 616–621. doi: 10.1002/ANA.410200510.

Elston, G. N. *et al.* (2011) 'Pyramidal cells in prefrontal cortex of primates: Marked differences in neuronal structure among species', *Frontiers in Neuroanatomy*, 0(FEB), pp. 1–17. doi: 10.3389/FNANA.2011.00002/BIBTEX.

Emmanouilidou, E. *et al.* (2010) 'Cell-Produced α-Synuclein Is Secreted in a Calcium-Dependent Manner by Exosomes and Impacts Neuronal Survival', *The Journal of Neuroscience*, 30(20), p. 6838. doi: 10.1523/JNEUROSCI.5699-09.2010.

Eng, L. F., Ghirnikar, R. S. and Lee, Y. L. (2000) 'Glial fibrillary acidic protein: GFAP-thirty-one years (1969-2000)', *Neurochemical research*, 25(9–10), pp. 1439–1451. doi: 10.1023/A:1007677003387.

Enwright, J. F. *et al.* (2016) 'Reduced Labeling of Parvalbumin Neurons and Perineuronal Nets in the Dorsolateral Prefrontal Cortex of Subjects with Schizophrenia', *Neuropsychopharmacology 2016 41:9*, 41(9), pp. 2206–2214. doi: 10.1038/npp.2016.24.

Erö, C. *et al.* (2018) 'A Cell Atlas for the Mouse Brain', *Frontiers in Neuroinformatics*, 12, p. 84. doi: 10.3389/fninf.2018.00084.

Erskine, D. *et al.* (2018) 'Molecular changes in the absence of severe pathology in the pulvinar in dementia with Lewy bodies', *Movement Disorders*, 33(6), pp. 982–991. doi: 10.1002/MDS.27333.

Escartin, C., Guillemaud, O. and Carrillo-de Sauvage, M. A. (2019) ‘Questions and (some) answers on reactive astrocytes’, *Glia*, 67(12), pp. 2221–2247. doi: 10.1002/GLIA.23687.

Esiri, M. M., Al Izzi, M. S. and Reading, M. C. (1991) ‘Macrophages, microglial cells, and HLA-DR antigens in fetal and infant brain.’, *Journal of Clinical Pathology*, 44(2), pp. 102–106. doi: 10.1136/JCP.44.2.102.

Espinoza, C. *et al.* (2018) ‘Parvalbumin+ interneurons obey unique connectivity rules and establish a powerful lateral-inhibition microcircuit in dentate gyrus’, *Nature Communications 2018 9:1*, 9(1), pp. 1–10. doi: 10.1038/s41467-018-06899-3.

Estrada-Sánchez, A. M., Levine, M. S. and Cepeda, C. (2017) ‘Epilepsy in Other Neurodegenerative Disorders: Huntington’s and Parkinson’s Diseases’, *Models of Seizures and Epilepsy: Second Edition*, pp. 1043–1058. doi: 10.1016/B978-0-12-804066-9.00073-0.

Etkin, A., Egner, T. and Kalisch, R. (2011) ‘Emotional processing in anterior cingulate and medial prefrontal cortex’, *Trends in cognitive sciences*, 15(2), p. 85. doi: 10.1016/J.TICS.2010.11.004.

Eulenburg, V. and Gomeza, J. (2010) ‘Neurotransmitter transporters expressed in glial cells as regulators of synapse function’, *Brain research reviews*, 63(1–2), pp. 103–112. doi: 10.1016/J.BRAINRESREV.2010.01.003.

Fagerqvist, T. *et al.* (2013) ‘Monoclonal antibodies selective for α-synuclein oligomers/protofibrils recognize brain pathology in Lewy body disorders and α-synuclein transgenic mice with the disease-causing A30P mutation’, *Journal of neurochemistry*, 126(1), pp. 131–144. doi: 10.1111/JNC.12175.

Falcón-Moya, R., Sihra, T. S. and Rodríguez-Moreno, A. (2018) ‘Kainate receptors: Role in epilepsy’, *Frontiers in Molecular Neuroscience*, 11, p. 375886. doi: 10.3389/FNMOL.2018.00217/BIBTEX.

Falkowska, A. *et al.* (2015) ‘Energy Metabolism of the Brain, Including the Cooperation between Astrocytes and Neurons, Especially in the Context of Glycogen Metabolism’, *International Journal of Molecular Sciences*, 16(11), p. 25959. doi: 10.3390/IJMS161125939.

Fanne, R. A. *et al.* (2010) ‘Blood-brain barrier permeability and tPA-mediated neurotoxicity’, *Neuropharmacology*, 58(7), pp. 972–980. doi: 10.1016/J.NEUROPHARM.2009.12.017.

Fanselow, M. S. and Dong, H. W. (2010) ‘Are The Dorsal and Ventral Hippocampus functionally distinct structures?’, *Neuron*, 65(1), p. 7. doi: 10.1016/J.NEURON.2009.11.031.

Favuzzi, E. *et al.* (2017) ‘Activity-Dependent Gating of Parvalbumin Interneuron Function by the Perineuronal Net Protein Brevican’, *Neuron*, 95(3), pp. 639-655.e10. doi: 10.1016/J.NEURON.2017.06.028.

Favuzzi, E. *et al.* (2019) ‘Distinct molecular programs regulate synapse specificity in cortical inhibitory circuits’, *Science (New York, N.Y.)*, 363(6425), pp. 413–417. doi: 10.1126/SCIENCE.AAU8977.

Fawcett, J. W. *et al.* (2022) ‘The extracellular matrix and perineuronal nets in memory’, *Molecular Psychiatry 2022 27:8*, 27(8), pp. 3192–3203. doi: 10.1038/s41380-022-01634-3.

Fawcett, J. W., Oohashi, T. and Pizzorusso, T. (2019) ‘The roles of perineuronal nets and the perinodal extracellular matrix in neuronal function’, *Nature Reviews Neuroscience 2019 20:8*, 20(8), pp. 451–465. doi: 10.1038/s41583-019-0196-3.

Fellin, T. and Carmignoto, G. (2004) ‘Neurone-to-astrocyte signalling in the brain represents a distinct multifunctional unit’, *The Journal of Physiology*, 559(Pt 1), p. 3. doi: 10.1113/JPHYSIOL.2004.063214.

Fellner, L. *et al.* (2013) ‘Toll-like receptor 4 is required for α-synuclein dependent activation of microglia and astroglia’, *Glia*, 61(3), p. 349. doi: 10.1002/GLIA.22437.

Feng, G. *et al.* (2000) ‘Imaging neuronal subsets in transgenic mice expressing multiple spectral variants of GFP’, *Neuron*. 2000/11/22, 28(1), pp. 41–51. Available at: http://www.ncbi.nlm.nih.gov/pubmed/11086982.

Fernandes, G. G. *et al.* (2021) ‘Genetic Ablation of the Inducible Form of Nitric Oxide in Male Mice Disrupts Immature Neuron Survival in the Adult Dentate Gyrus’, *Frontiers in Immunology*, 12. doi: 10.3389/FIMMU.2021.782831/FULL.

Fiser, A. *et al.* (2016) ‘Experience-dependent spatial expectations in mouse visual

cortex', *Nature Neuroscience 2016 19:12*, 19(12), pp. 1658–1664. doi: 10.1038/nn.4385.

Flanary, B. E. *et al.* (2007) 'Evidence That Aging And Amyloid Promote Microglial Cell Senescence', *https://home.liebertpub.com/rej*, 10(1), pp. 61–74. doi: 10.1089/REJ.2006.9096.

Forno, L. S. and Norville, R. L. (1976) 'Ultrastructure of Lewy bodies in the stellate ganglion', *Acta neuropathologica*, 34(3), pp. 183–197. doi: 10.1007/BF00688674.

Förstermann, U. and Sessa, W. C. (2012) 'Nitric oxide synthases: regulation and function', *European Heart Journal*, 33(7), p. 829. doi: 10.1093/EURHEARTJ/EHR304.

Foscarin, S. *et al.* (2017) 'Brain ageing changes proteoglycan sulfation, rendering perineuronal nets more inhibitory', *Aging*, 9(6), pp. 1607–1622. doi: 10.18632/AGING.101256.

Fowke, T. M. *et al.* (2018) 'Loss of interneurons and disruption of perineuronal nets in the cerebral cortex following hypoxia-ischaemia in near-term fetal sheep', *Scientific reports*, 8(1). doi: 10.1038/S41598-018-36083-Y.

Freichel, C. *et al.* (2007) 'Age-dependent cognitive decline and amygdala pathology in alpha-synuclein transgenic mice', *Neurobiology of aging*, 28(9), pp. 1421–1435. doi: 10.1016/J.NEUROBIOLAGING.2006.06.013.

Frerking, M., Petersen, C. C. H. and Nicoll, R. A. (1999) 'Mechanisms underlying kainate receptor-mediated disinhibition in the hippocampus', *Proceedings of the National Academy of Sciences of the United States of America*, 96(22), p. 12917. doi: 10.1073/PNAS.96.22.12917.

Frischknecht, R. *et al.* (2009) 'Brain extracellular matrix affects AMPA receptor lateral mobility and short-term synaptic plasticity', *Nature neuroscience*, 12(7), pp. 897–904. doi: 10.1038/NN.2338.

Fröhlich, F. *et al.* (2008) 'Potassium Dynamics in the Epileptic Cortex: New Insights on an Old Topic', *The Neuroscientist : a review journal bringing neurobiology, neurology and psychiatry*, 14(5), p. 422. doi: 10.1177/1073858408317955.

Froula, J. M. *et al.* (2019) 'Defining α-synuclein species responsible for Parkinson's

disease phenotypes in mice', *The Journal of Biological Chemistry*, 294(27), p. 10392. doi: 10.1074/JBC.RA119.007743.

Fu, A. K. and Ip, N. Y. (2017) 'Regulation of postsynaptic signaling in structural synaptic plasticity', *Current opinion in neurobiology*, 45, pp. 148–155. doi: 10.1016/J.CONB.2017.05.016.

Fujiwara, H. *et al.* (2002) 'alpha-Synuclein is phosphorylated in synucleinopathy lesions', *Nature cell biology*, 4(2), pp. 160–164. doi: 10.1038/NCB748.

Fusco, G. *et al.* (2017) 'Structural basis of membrane disruption and cellular toxicity by α-synuclein oligomers', *Science (New York, N.Y.)*, 358(6369), pp. 1440–1443. doi: 10.1126/SCIENCE.AAN6160.

Fussi, N. *et al.* (2018) 'Exosomal secretion of α-synuclein as protective mechanism after upstream blockage of macroautophagy', *Cell Death & Disease*, 9(7). doi: 10.1038/S41419-018-0816-2.

Fuster, J. M. and Alexander, G. E. (1971) 'Neuron activity related to short-term memory', *Science (New York, N.Y.)*, 173(3997), pp. 652–654. doi: 10.1126/SCIENCE.173.3997.652.

Gabbott, P. L. A. *et al.* (2005) 'Prefrontal cortex in the rat: Projections to subcortical autonomic, motor, and limbic centers', *Journal of Comparative Neurology*, 492(2), pp. 145–177. doi: 10.1002/cne.20738.

Gai, W. P. *et al.* (2000) 'In situ and in vitro study of colocalization and segregation of alpha-synuclein, ubiquitin, and lipids in Lewy bodies', *Experimental neurology*, 166(2), pp. 324–333. doi: 10.1006/EXNR.2000.7527.

Galarreta, M. and Hestrin, S. (1998) 'Frequency-dependent synaptic depression and the balance of excitation and inhibition in the neocortex', *Nature Neuroscience 1998 1:7*, 1(7), pp. 587–594. doi: 10.1038/2822.

Galatro, T. F. *et al.* (2017) 'Transcriptomic analysis of purified human cortical microglia reveals age-associated changes', *Nature neuroscience*, 20(8), pp. 1162–1171. doi: 10.1038/NN.4597.

Galtrey, C. M. *et al.* (2008) 'Distribution and synthesis of extracellular matrix proteoglycans, hyaluronan, link proteins and tenascin-R in the rat spinal cord', *The*

European journal of neuroscience, 27(6), pp. 1373–1390. doi: 10.1111/J.1460-9568.2008.06108.X.

Galvin, J. E., Lee, V. M. Y. and Trojanowski, J. Q. (2001) 'Synucleinopathies: Clinical and Pathological Implications', *Archives of Neurology*, 58(2), pp. 186–190. doi: 10.1001/ARCHNEUR.58.2.186.

Gao, C. *et al.* (2023) 'Microglia in neurodegenerative diseases: mechanism and potential therapeutic targets', *Signal Transduction and Targeted Therapy 2023 8:1*, 8(1), pp. 1–37. doi: 10.1038/s41392-023-01588-0.

Garden, G. A. and Möller, T. (2006) 'Microglia biology in health and disease', *Journal of neuroimmune pharmacology : the official journal of the Society on NeuroImmune Pharmacology*, 1(2), pp. 127–137. doi: 10.1007/S11481-006-9015-5.

Gentzel, R. C. *et al.* (2021) 'Intracranial administration of alpha-synuclein fibrils in A30P-synuclein transgenic mice causes robust synucleinopathy and microglial induction', *Neurobiology of Aging*, 106, pp. 12–25. doi: 10.1016/J.NEUROBIOLAGING.2021.05.012.

George, N. and Geller, H. M. (2018) 'Extracellular matrix and traumatic brain injury', *Journal of Neuroscience Research*, 96(4), pp. 573–588. doi: 10.1002/JNR.24151.

George, S. *et al.* (2019) 'Microglia affect α-synuclein cell-to-cell transfer in a mouse model of Parkinson's disease', *Molecular Neurodegeneration*, 14(1), pp. 1–22. doi: 10.1186/S13024-019-0335-3/FIGURES/7.

Gerhard, A. *et al.* (2006) 'In vivo imaging of microglial activation with [11C](R)-PK11195 PET in idiopathic Parkinson's disease', *Neurobiology of disease*, 21(2), pp. 404–412. doi: 10.1016/J.NBD.2005.08.002.

Ghanem, S. S. *et al.* (2022) 'α-Synuclein phosphorylation at serine 129 occurs after initial protein deposition and inhibits seeded fibril formation and toxicity', *Proceedings of the National Academy of Sciences of the United States of America*, 119(15). doi: 10.1073/PNAS.2109617119/-/DCSUPPLEMENTAL.

Ghiglieri, V., Calabrese, V. and Calabresi, P. (2018) 'Alpha-Synuclein: From Early Synaptic Dysfunction to Neurodegeneration', *Frontiers in Neurology*, 9(MAY), p. 1. doi: 10.3389/FNEUR.2018.00295.

Giasson, B. I. *et al.* (2002) ‘Neuronal α-synucleinopathy with severe movement disorder in mice expressing A53T human α-synuclein’, *Neuron*, 34(4), pp. 521–533. doi: 10.1016/S0896-6273(02)00682-7.

Ginhoux, F. *et al.* (2013) ‘Origin and differentiation of microglia’, *Frontiers in Cellular Neuroscience*, 7(MAR). doi: 10.3389/FNCEL.2013.00045.

Giusti, V. *et al.* (2024) ‘Brain clearance of protein aggregates: a close-up on astrocytes’, *Molecular Neurodegeneration 2024 19:1*, 19(1), pp. 1–18. doi: 10.1186/S13024-024-00703-1.

Glass, Christopher K. *et al.* (2010) ‘Mechanisms underlying inflammation in neurodegeneration’, *Cell*, 140(6), pp. 918–934. doi: 10.1016/J.CELL.2010.02.016.

Glass, C K *et al.* (2010) ‘Mechanisms underlying inflammation in neurodegeneration’, *Cell*. 2010/03/23, 140(6), pp. 918–934. doi: 10.1016/j.cell.2010.02.016.

Glykys, J. *et al.* (2014) ‘Local impermeant anions establish the neuronal chloride concentration’, *Science (New York, N.Y.)*, 343(6171), pp. 670–675. doi: 10.1126/SCIENCE.1245423.

Goedert, M. *et al.* (1996) ‘Assembly of microtubule-associated protein tau into Alzheimer-like filaments induced by sulphated glycosaminoglycans’, *Nature*, 383(6600), pp. 550–553. doi: 10.1038/383550A0.

Gogolla, N. *et al.* (2009) ‘Common circuit defect of excitatory-inhibitory balance in mouse models of autism’, *J Neurodev Disord*. 2010/07/29, 1(2), pp. 172–181. doi: 10.1007/s11689-009-9023-x.

Goldberg, E. M. *et al.* (2005) ‘Specific Functions of Synaptically Localized Potassium Channels in Synaptic Transmission at the Neocortical GABAergic Fast-Spiking Cell Synapse’, *Journal of Neuroscience*, 25(21), pp. 5230–5235. doi: 10.1523/JNEUROSCI.0722-05.2005.

Goldberg, E. M. *et al.* (2008) ‘K+ Channels at the Axon Initial Segment Dampen Near-Threshold Excitability of Neocortical Fast-Spiking GABAergic Interneurons’, *Neuron*, 58(3), pp. 387–400. doi: 10.1016/J.NEURON.2008.03.003.

Goldman-Rakic, P. S. (1995) ‘Cellular basis of working memory’, *Neuron*, 14(3), pp. 477–485. doi: 10.1016/0896-6273(95)90304-6.

Gomez-Arboledas, A. *et al.* (2018) ‘Phagocytic clearance of presynaptic dystrophies by reactive astrocytes in Alzheimer’s disease’, *Glia*, 66(3), p. 637. doi: 10.1002/GLIA.23270.

Gonçalves, S. and Outeiro, T. F. (2013) ‘Assessing the subcellular dynamics of alpha-synuclein using photoactivation microscopy’, *Molecular neurobiology*, 47(3), pp. 1081–1092. doi: 10.1007/S12035-013-8406-X.

Gonzalez-Burgos, G. and Lewis, D. A. (2008) ‘GABA Neurons and the Mechanisms of Network Oscillations: Implications for Understanding Cortical Dysfunction in Schizophrenia’, *Schizophrenia Bulletin*, 34(5), p. 944. doi: 10.1093/SCHBUL/SBN070.

González-Reyes, R. E. *et al.* (2017) ‘Involvement of astrocytes in Alzheimer’s disease from a neuroinflammatory and oxidative stress perspective’, *Frontiers in Molecular Neuroscience*, 10, p. 314479. doi: 10.3389/FNMOL.2017.00427/BIBTEX.

Gonzalez-Sulser, A. *et al.* (2011) ‘THE 4-AMINOPYRIDINE IN VITRO EPILEPSY MODEL ANALYZED WITH A PERFORATED MULTI-ELECTRODE ARRAY’, *Neuropharmacology*, 60(7–8), p. 1142. doi: 10.1016/J.NEUROPHARM.2010.10.007.

González, O. C. *et al.* (2015) ‘Modeling of Age-Dependent Epileptogenesis by Differential Homeostatic Synaptic Scaling’, *The Journal of neuroscience : the official journal of the Society for Neuroscience*, 35(39), pp. 13448–13462. doi: 10.1523/JNEUROSCI.5038-14.2015.

González, O. C. *et al.* (2018) ‘Role of KCC2-dependent potassium efflux in 4-Aminopyridine-induced Epileptiform synchronization’, *Neurobiology of Disease*, 109, pp. 137–147. doi: 10.1016/J.NBD.2017.10.011.

Gordon, G. R. J. *et al.* (2005) ‘Norepinephrine triggers release of glial ATP to increase postsynaptic efficacy’, *Nature neuroscience*, 8(8), pp. 1078–1086. doi: 10.1038/NN1498.

Gordon, G. R. J., Mulligan, S. J. and MacVicar, B. A. (2007) ‘Astrocyte control of the cerebrovasculature’, *Glia*, 55(12), pp. 1214–1221. doi: 10.1002/GLIA.20543.

Govers, R. and Oess, S. (2004) ‘To NO or not to NO: “where?” is the question’, *Histology and histopathology*, 19(2), pp. 585–605. doi: 10.14670/HH-19.585.

Gray, D. T. *et al.* (2023) ‘Retrosplenial cortex microglia and perineuronal net densities are associated with memory impairment in aged rhesus macaques’, *Cerebral Cortex*, 33(8), pp. 4626–4644. doi: 10.1093/CERCOR/BHAC366.

Griguoli, M. and Cherubini, E. (2017) ‘Early Correlated Network Activity in the Hippocampus: Its Putative Role in Shaping Neuronal Circuits’, *Frontiers in cellular neuroscience*, 11. doi: 10.3389/FNCEL.2017.00255.

Guarnieri, R. *et al.* (2005) ‘Suppression of obsessive-compulsive symptoms after epilepsy surgery’, *Epilepsy & behavior : E&B*, 7(2), pp. 316–319. doi: 10.1016/J.YEBEH.2005.05.024.

Guivernau, B. *et al.* (2016) ‘Amyloid-β Peptide Nitrotyrosination Stabilizes Oligomers and Enhances NMDAR-Mediated Toxicity’, *The Journal of Neuroscience*, 36(46), p. 11693. doi: 10.1523/JNEUROSCI.1081-16.2016.

Guix, F. X. *et al.* (2005) ‘The physiology and pathophysiology of nitric oxide in the brain’, *Progress in neurobiology*, 76(2), pp. 126–152. doi: 10.1016/J.PNEUROBIO.2005.06.001.

Gutman, G. A. *et al.* (2005) ‘International Union of Pharmacology. LIII. Nomenclature and molecular relationships of voltage-gated potassium channels’, *Pharmacological reviews*, 57(4), pp. 473–508. doi: 10.1124/PR.57.4.10.

Haber, S. N. and Knutson, B. (2009) ‘The Reward Circuit: Linking Primate Anatomy and Human Imaging’, *Neuropsychopharmacology 2010 35:1*, 35(1), pp. 4–26. doi: 10.1038/npp.2009.129.

Haberman, R. P., Branch, A. and Gallagher, M. (2017) ‘Targeting Neural Hyperactivity as a Treatment to Stem Progression of Late-Onset Alzheimer’s Disease’, *Neurotherapeutics*, 14(3), pp. 662–676. doi: 10.1007/S13311-017-0541-Z.

Haj-Yasein, N. N. *et al.* (2012) ‘Aquaporin-4 regulates extracellular space volume dynamics during high-frequency synaptic stimulation: a gene deletion study in mouse hippocampus’, *Glia*, 60(6), pp. 867–874. doi: 10.1002/GLIA.22319.

Halassa, M. M. *et al.* (2007) ‘Synaptic islands defined by the territory of a single astrocyte’, *The Journal of neuroscience : the official journal of the Society for Neuroscience*, 27(24), pp. 6473–6477. doi: 10.1523/JNEUROSCI.1419-07.2007.

Hamidi, S. and Avoli, M. (2015) ‘KCC2 function modulates in vitro ictogenesis’, *Neurobiology of Disease*, 79, pp. 51–58. doi: 10.1016/J.NBD.2015.04.006.

Hanisch, U. K. and Kettenmann, H. (2007) ‘Microglia: active sensor and versatile effector cells in the normal and pathologic brain’, *Nature neuroscience*, 10(11), pp. 1387–1394. doi: 10.1038/NN1997.

Happel, M. F. K. *et al.* (2014) ‘Enhanced cognitive flexibility in reversal learning induced by removal of the extracellular matrix in auditory cortex’, *Proceedings of the National Academy of Sciences of the United States of America*, 111(7), pp. 2800–2805. doi: 10.1073/PNAS.1310272111/-/DCSUPPLEMENTAL/PNAS.201310272SI.PDF.

Harooni, H. E. *et al.* (2009) ‘The role of hippocampal nitric oxide (NO) on learning and immediate, short- and long-term memory retrieval in inhibitory avoidance task in male adult rats’, *Behavioural brain research*, 201(1), pp. 166–172. doi: 10.1016/J.BBR.2009.02.011.

Härtig, W. *et al.* (2017) ‘Damaged Neocortical Perineuronal Nets Due to Experimental Focal Cerebral Ischemia in Mice, Rats and Sheep’, *Frontiers in Integrative Neuroscience*, 11. doi: 10.3389/FNINT.2017.00015.

Den Hartog Jager, W. A. (1969) ‘Sphingomyelin in Lewy inclusion bodies in Parkinson’s disease’, *Archives of neurology*, 21(6), pp. 615–619. doi: 10.1001/ARCHNEUR.1969.00480180071006.

Hartwig, J. H. and Yin, H. L. (1988) ‘The organization and regulation of the macrophage actin skeleton’, *Cell Motility and the Cytoskeleton*, 10(1–2), pp. 117–125. doi: 10.1002/CM.970100116.

Haunsø, A. *et al.* (1999) ‘Phosphacan immunoreactivity is associated with perineuronal nets around parvalbumin-expressing neurones’, *Brain research*, 834(1–2), pp. 219–222. doi: 10.1016/S0006-8993(99)01596-6.

Hayani, H., Song, I. and Dityatev, A. (2018) ‘Increased excitability and reduced excitatory synaptic input into fast-spiking CA2 interneurons after enzymatic attenuation of extracellular matrix’, *Frontiers in Cellular Neuroscience*, 12, p. 339094. doi: 10.3389/FNCEL.2018.00149/BIBTEX.

Hayashida, K. *et al.* (1993) ‘An early cytoplasmic change before Lewy body maturation: an ultrastructural study of the substantia nigra from an autopsy case of juvenile parkinsonism’, *Acta neuropathologica*, 85(4), pp. 445–448. doi: 10.1007/BF00334457.

Helmich, R. C. *et al.* (2012) ‘Cerebral causes and consequences of parkinsonian resting tremor: a tale of two circuits?’, *Brain : a journal of neurology*, 135(Pt 11), pp. 3206–3226. doi: 10.1093/BRAIN/AWS023.

Helmut, K. *et al.* (2011) ‘Physiology of microglia’, *Physiological reviews*, 91(2), pp. 461–553. doi: 10.1152/PHYSREV.00011.2010.

Henderson, M. X. *et al.* (2019) ‘α-Synuclein pathology spread through the brain connectome is modulated by selective vulnerability and predicted by network analysis’, *Nature neuroscience*, 22(8), p. 1248. doi: 10.1038/S41593-019-0457-5.

Heneka, M. T. *et al.* (2015) ‘Neuroinflammation in Alzheimer’s disease’, *The Lancet. Neurology*, 14(4), pp. 388–405. doi: 10.1016/S1474-4422(15)70016-5.

Herculano-Houzel, S. (2014) ‘The glia/neuron ratio: how it varies uniformly across brain structures and species and what that means for brain physiology and evolution’, *Glia*, 62(9), pp. 1377–1391. doi: 10.1002/GLIA.22683.

Hernandez-Lallement, J. *et al.* (2020) ‘Harm to Others Acts as a Negative Reinforcer in Rats’, *Current Biology*, 30(6), pp. 949-961.e7. doi: 10.1016/J.CUB.2020.01.017.

Herrmann, C. S. *et al.* (2016) ‘EEG oscillations: From correlation to causality’, *International Journal of Psychophysiology*, 103, pp. 12–21. doi: 10.1016/J.IJPSYCHO.2015.02.003.

Herrmann, C. S. and Demiralp, T. (2005) ‘Human EEG gamma oscillations in neuropsychiatric disorders’, *Clinical Neurophysiology*, 116(12), pp. 2719–2733. doi: 10.1016/J.CLINPH.2005.07.007.

Herrmann, C. S., Munk, M. H. J. and Engel, A. K. (2004) ‘Cognitive functions of gamma-band activity: memory match and utilization’, *Trends in Cognitive Sciences*, 8(8), pp. 347–355. doi: 10.1016/J.TICS.2004.06.006.

Hesdorffer, D. C. *et al.* (2011) ‘Estimating risk for developing epilepsy: A population-based study in Rochester, Minnesota’, *Neurology*, 76(1), p. 23. doi:

10.1212/WNL.0B013E318204A36A.

Hickman, S. *et al.* (2018) ‘Microglia in neurodegeneration’, *Nature neuroscience*, 21(10), pp. 1359–1369. doi: 10.1038/S41593-018-0242-X.

Hirsch, E. C. and Hunot, S. (2009) ‘Neuroinflammation in Parkinson’s disease: a target for neuroprotection?’, *The Lancet. Neurology*, 8(4), pp. 382–397. doi: 10.1016/S1474-4422(09)70062-6.

Hishikawa, N. *et al.* (2001) ‘Widespread occurrence of argyrophilic glial inclusions in Parkinson’s disease’, *Neuropathology and applied neurobiology*, 27(5), pp. 362–372. doi: 10.1046/J.1365-2990.2001.00345.X.

Hockfield, S. *et al.* (1990) ‘Expression of neural proteoglycans correlates with the acquisition of mature neuronal properties in the mammalian brain’, *Cold Spring Harbor symposia on quantitative biology*, 55, pp. 505–514. doi: 10.1101/SQB.1990.055.01.049.

Holmes, B. B. *et al.* (2013) ‘Heparan sulfate proteoglycans mediate internalization and propagation of specific proteopathic seeds’, *Proceedings of the National Academy of Sciences of the United States of America*, 110(33). doi: 10.1073/PNAS.1301440110.

Holroyd, C. B. and McClure, S. M. (2015) ‘Hierarchical control over effortful behavior by rodent medial frontal cortex: A computational model’, *Psychological review*, 122(1), pp. 54–83. doi: 10.1037/A0038339.

Holroyd, C. B. and Yeung, N. (2012) ‘Motivation of extended behaviors by anterior cingulate cortex’, *Trends in cognitive sciences*, 16(2), pp. 122–128. doi: 10.1016/J.TICS.2011.12.008.

Hoogland, T. M. *et al.* (2009) ‘Radially expanding transglial calcium waves in the intact cerebellum’, *Proceedings of the National Academy of Sciences of the United States of America*, 106(9), p. 3496. doi: 10.1073/PNAS.0809269106.

Hoover, W. B. and Vertes, R. P. (2007) ‘Anatomical analysis of afferent projections to the medial prefrontal cortex in the rat’, *Brain Structure and Function*, 212(2), pp. 149–179. doi: 10.1007/s00429-007-0150-4.

Howell, M. D. and Gottschall, P. E. (2012) ‘Lectican proteoglycans, their cleaving

metalloproteinases, and plasticity in the central nervous system extracellular microenvironment', *Neuroscience*, 217, p. 6. doi: 10.1016/J.NEUROSCIENCE.2012.05.034.

Hu, H., Gan, J. and Jonas, P. (2014) 'Fast-spiking, parvalbumin+ GABAergic interneurons: From cellular design to microcircuit function', *Science*, 345(6196). doi: 10.1126/SCIENCE.1255263.

Huang, S. H. *et al.* (2015) 'Cortical metabolic and nigrostriatal abnormalities associated with clinical stage-specific dementia with Lewy bodies', *Clinical nuclear medicine*, 40(1), pp. 26–31. doi: 10.1097/RLU.0000000000000620.

Huh, S. *et al.* (2016) 'The reemergence of long-term potentiation in aged Alzheimer's disease mouse model', *Scientific reports*, 6. doi: 10.1038/SREP29152.

Hulse, R. E. *et al.* (2001) 'Astrocytic Clasmatodendrosis in Hippocampal Organ Culture', *Glia*, 33(2), p. 169. doi: 10.1002/1098-1136(200102)33:2<169::aid-glia1016>3.0.co;2-b.

Hunot, S. *et al.* (1996) 'Nitric oxide synthase and neuronal vulnerability in Parkinson's disease', *Neuroscience*, 72(2), pp. 355–363. doi: 10.1016/0306-4522(95)00578-1.

Hussaini, S. M. Q. and Jang, M. H. (2018) 'New Roles for Old Glue: Astrocyte Function in Synaptic Plasticity and Neurological Disorders', *International Neurourology Journal*, 22(Suppl 3), p. S106. doi: 10.5213/INJ.1836214.107.

Hutchins, K. D. *et al.* (1990) 'Localization of morphologically distinct microglial populations in the developing human fetal brain: implications for ontogeny', *Developmental Brain Research*, 55(1), pp. 95–102. doi: 10.1016/0165-3806(90)90109-C.

Huynh, M. B. *et al.* (2019) 'Glycosaminoglycans from Alzheimer's disease hippocampus have altered capacities to bind and regulate growth factors activities and to bind tau', *PloS one*, 14(1). doi: 10.1371/JOURNAL.PONE.0209573.

Iadecola, C. and Nedergaard, M. (2007) 'Glial regulation of the cerebral microvasculature', *Nature neuroscience*, 10(11), pp. 1369–1376. doi: 10.1038/NN2003.

Iannaccone, S. *et al.* (2013) ‘In vivo microglia activation in very early dementia with Lewy bodies, comparison with Parkinson’s disease’, *Parkinsonism & related disorders*, 19(1), pp. 47–52. doi: 10.1016/J.PARKRELDIS.2012.07.002.

Iba, M. *et al.* (2020) ‘Neuroinflammation is associated with infiltration of T cells in Lewy body disease and α-synuclein transgenic models’, *Journal of Neuroinflammation*, 17(1), pp. 1–14. doi: 10.1186/S12974-020-01888-0/FIGURES/8.

Imamura, K. *et al.* (2003) ‘Distribution of major histocompatibility complex class II-positive microglia and cytokine profile of Parkinson’s disease brains’, *Acta neuropathologica*, 106(6), pp. 518–526. doi: 10.1007/S00401-003-0766-2.

Iqbal, Z. *et al.* (2023a) ‘Adrenergic signalling to astrocytes in anterior cingulate cortex contributes to pain-related aversive memory in rats’, *Communications Biology 2023 6:1*, 6(1), pp. 1–19. doi: 10.1038/s42003-022-04405-6.

Iqbal, Z. *et al.* (2023b) ‘Adrenergic signalling to astrocytes in anterior cingulate cortex contributes to pain-related aversive memory in rats’, *Communications Biology 2023 6:1*, 6(1), pp. 1–19. doi: 10.1038/s42003-022-04405-6.

Ishii, R. *et al.* (2018) ‘Healthy and Pathological Brain Aging: From the Perspective of Oscillations, Functional Connectivity, and Signal Complexity’, *Neuropsychobiology*, 75(4), pp. 151–161. doi: 10.1159/000486870.

Jafari, Z., Kolb, B. E. and Mohajerani, M. H. (2020) ‘Neural oscillations and brain stimulation in Alzheimer’s disease’, *Progress in Neurobiology*, 194, p. 101878. doi: 10.1016/J.PNEUROBIO.2020.101878.

Jäkel, S. and Dimou, L. (2017) ‘Glial Cells and Their Function in the Adult Brain: A Journey through the History of Their Ablation’, *Frontiers in Cellular Neuroscience*, 11. doi: 10.3389/FNCEL.2017.00024.

Janmey, P. A. (1994) ‘Phosphoinositides and calcium as regulators of cellular actin assembly and disassembly’, *Annual Review of Physiology*, 56(Volume 56,), pp. 169–191. doi: 10.1146/ANNUREV.PH.56.030194.001125/CITE/REFWORKS.

Jean, Y. Y., Lercher, L. D. and Dreyfus, C. F. (2008) ‘Glutamate elicits release of BDNF from basal forebrain astrocytes in a process dependent on metabotropic receptors and the PLC pathway’, *Neuron glia biology*, 4(1), pp. 35–42. doi:

10.1017/S1740925X09000052.

Jellinger, K. A. and Attems, J. (2011) ‘Prevalence and pathology of dementia with Lewy bodies in the oldest old: a comparison with other dementing disorders’, *Dementia and geriatric cognitive disorders*, 31(4), pp. 309–316. doi: 10.1159/000327360.

Jenkins, H. G. and Bachelard, H. S. (1988) ‘Developmental and age-related changes in rat brain glycosaminoglycans’, *Journal of neurochemistry*, 51(5), pp. 1634–1640. doi: 10.1111/J.1471-4159.1988.TB01134.X.

Jha, M. K. *et al.* (2019) ‘Microglia-Astrocyte Crosstalk: An Intimate Molecular Conversation’, *The Neuroscientist : a review journal bringing neurobiology, neurology and psychiatry*, 25(3), pp. 227–240. doi: 10.1177/1073858418783959.

Jiang, T. and Cadenas, E. (2014) ‘Astrocytic metabolic and inflammatory changes as a function of age’, *Aging cell*, 13(6), pp. 1059–1067. doi: 10.1111/ACEL.12268.

Jiménez-González, C. *et al.* (2011) ‘Non-neuronal, slow GABA signalling in the ventrobasal thalamus targets δ-subunit-containing GABAA receptors’, *The European Journal of Neuroscience*, 33(8), p. 1471. doi: 10.1111/J.1460-9568.2011.07645.X.

Jimenez, S. *et al.* (2008) ‘Inflammatory Response in the Hippocampus of PS1M146L/APP751SL Mouse Model of Alzheimer’s Disease: Age-Dependent Switch in the Microglial Phenotype from Alternative to Classic’, *The Journal of Neuroscience*, 28(45), p. 11650. doi: 10.1523/JNEUROSCI.3024-08.2008.

Jin, X. T. and Smith, Y. (2011) ‘Localization and Functions of Kainate Receptors in the Basal Ganglia’, *Advances in experimental medicine and biology*, 717, p. 27. doi: 10.1007/978-1-4419-9557-5_3.

Jobson, D. D. *et al.* (2021) ‘The role of the medial prefrontal cortex in cognition, ageing and dementia’, *Brain Communications*, 3(3). doi: 10.1093/BRAINCOMMS/FCAB125.

Johnson, C. *et al.* (2020) ‘Distinct VIP interneurons in the cingulate cortex encode anxiogenic and social stimuli’, *bioRxiv*, p. 2020.12.22.424056. doi: 10.1101/2020.12.22.424056.

Johnston, G. A. R. (1996) ‘GABAA receptor pharmacology’, *Pharmacology and*

Therapeutics, 69(3), pp. 173–198. doi: 10.1016/0163-7258(95)02043-8.

Jukkola, P. *et al.* (2013) 'Astrocytes differentially respond to inflammatory autoimmune insults and imbalances of neural activity', *Acta Neuropathologica Communications*, 1(1), pp. 1–19. doi: 10.1186/2051-5960-1-70/FIGURES/8.

Jung, J., Na, C. and Huh, Y. (2012) 'Alterations in Nitric Oxide Synthase in the Aged CNS', *Oxidative Medicine and Cellular Longevity*, 2012. doi: 10.1155/2012/718976.

Jung, M. W. *et al.* (1998) 'Firing characteristics of deep layer neurons in prefrontal cortex in rats performing spatial working memory tasks', *Cerebral cortex (New York, N.Y. : 1991)*, 8(5), pp. 437–450. doi: 10.1093/CERCOR/8.5.437.

Jung, Y. J. and Chung, W. S. (2018) 'Phagocytic Roles of Glial Cells in Healthy and Diseased Brains', *Biomolecules & Therapeutics*, 26(4), p. 350. doi: 10.4062/BIOMOLTHER.2017.133.

Kahle, P. J. *et al.* (2000) 'Subcellular Localization of Wild-Type and Parkinson's Disease-Associated Mutant α-Synuclein in Human and Transgenic Mouse Brain', *The Journal of Neuroscience*, 20(17), p. 6365. doi: 10.1523/JNEUROSCI.20-17-06365.2000.

Kahle, P. J. *et al.* (2001) 'Selective Insolubility of α-Synuclein in Human Lewy Body Diseases Is Recapitulated in a Transgenic Mouse Model', *The American Journal of Pathology*, 159(6), pp. 2215–2225. doi: 10.1016/S0002-9440(10)63072-6.

Kamigaki, T. (2019) 'Prefrontal circuit organization for executive control', *Neuroscience Research*. Elsevier Ireland Ltd, pp. 23–36. doi: 10.1016/j.neures.2018.08.017.

Kamphuis, W. *et al.* (2012) 'GFAP Isoforms in Adult Mouse Brain with a Focus on Neurogenic Astrocytes and Reactive Astrogliosis in Mouse Models of Alzheimer Disease', *PLoS ONE*, 7(8), p. 42823. doi: 10.1371/JOURNAL.PONE.0042823.

Kanazawa, H. *et al.* (2002) 'Macrophage/Microglia-specific Protein Iba1 Enhances Membrane Ruffling and Rac Activation via Phospholipase C-γ-dependent Pathway', *Journal of Biological Chemistry*, 277(22), pp. 20026–20032. doi: 10.1074/JBC.M109218200.

Kane, J. P. M. *et al.* (2018) 'Clinical prevalence of Lewy body dementia', *Alzheimer's*

Research & Therapy, 10(1). doi: 10.1186/S13195-018-0350-6.

Kang, Y. C. *et al.* (2004) 'Regulation of Programmed Cell Death in Neuronal Cells by Nitric Oxide', *In Vivo*, 18(3), pp. 367–376. Available at: https://iv.iiarjournals.org/content/18/3/367 (Accessed: 9 April 2024).

Kasatkina, L. A. (2016) '4-Aminopyridine sequesters intracellular Ca2+ which triggers exocytosis in excitable and non-excitable cells', *Scientific Reports*, 6. doi: 10.1038/SREP34749.

Katarzyna Greda, A. and Nowicka, D. (2021) 'Hyaluronidase inhibition accelerates functional recovery from stroke in the mouse brain', *Journal of Neurochemistry*, 157(3), pp. 781–801. doi: 10.1111/JNC.15279.

Katsuse, O., Iseki, E. and Kosaka, K. (2003) 'Immunohistochemical study of the expression of cytokines and nitric oxide synthases in brains of patients with dementia with Lewy bodies', *Neuropathology : official journal of the Japanese Society of Neuropathology*, 23(1), pp. 9–15. doi: 10.1046/J.1440-1789.2003.00483.X.

Kaushik, R. *et al.* (2021) 'Fine structure analysis of perineuronal nets in the ketamine model of schizophrenia', *The European journal of neuroscience*, 53(12), pp. 3988–4004. doi: 10.1111/EJN.14853.

Kellie, J. F. *et al.* (2014) 'Quantitative Measurement of Intact Alpha-Synuclein Proteoforms from Post-Mortem Control and Parkinson's Disease Brain Tissue by Intact Protein Mass Spectrometry', *Scientific Reports*, 4. doi: 10.1038/SREP05797.

Kempuraj, D. *et al.* (2016) 'Neuroinflammation Induces Neurodegeneration', *Journal of neurology, neurosurgery and spine*, 1(1). Available at: /pmc/articles/PMC5260818/ (Accessed: 12 March 2024).

Kettenmann, H., Kirchhoff, F. and Verkhratsky, A. (2013) 'Microglia: New Roles for the Synaptic Stripper', *Neuron*, 77(1), pp. 10–18. doi: 10.1016/J.NEURON.2012.12.023.

Khundakar, A. A. *et al.* (2016) 'Analysis of primary visual cortex in dementia with Lewy bodies indicates GABAergic involvement associated with recurrent complex visual hallucinations', *Acta neuropathologica communications*, 4(1). doi: 10.1186/S40478-016-0334-3.

Kilavik, B. E. *et al.* (2013) ‘The ups and downs of beta oscillations in sensorimotor cortex’, *Experimental Neurology*, 245, pp. 15–26. doi: 10.1016/J.EXPNEUROL.2012.09.014.

Kilpeläinen, T. *et al.* (2019) ‘Behavioural and dopaminergic changes in double mutated human A30P*A53T alpha-synuclein transgenic mouse model of Parkinson´s disease’, *Scientific Reports 2019 9:1*, 9(1), pp. 1–13. doi: 10.1038/s41598-019-54034-z.

Kim, H. *et al.* (2016a) ‘Prefrontal Parvalbumin Neurons in Control of Attention’, *Cell*, 164(1–2), p. 208. doi: 10.1016/J.CELL.2015.11.038.

Kim, H. *et al.* (2016b) ‘Prefrontal Parvalbumin Neurons in Control of Attention’, *Cell*, 164(1–2), pp. 208–218. doi: 10.1016/j.cell.2015.11.038.

Kim, H. Y. *et al.* (2009) ‘Structural properties of pore-forming oligomers of alpha-synuclein’, *Journal of the American Chemical Society*, 131(47), pp. 17482–17489. doi: 10.1021/JA9077599.

Kim, S. Y. *et al.* (2017) ‘TGFβ signaling is associated with changes in inflammatory gene expression and perineuronal net degradation around inhibitory neurons following various neurological insults’, *Scientific Reports*, 7(1). doi: 10.1038/S41598-017-07394-3.

Kim, Y., Park, J. and Choi, Y. K. (2019) ‘The Role of Astrocytes in the Central Nervous System Focused on BK Channel and Heme Oxygenase Metabolites: A Review’, *Antioxidants*, 8(5). doi: 10.3390/ANTIOX8050121.

Kimelberg, H. K. *et al.* (1990) ‘Swelling-induced release of glutamate, aspartate, and taurine from astrocyte cultures’, *The Journal of Neuroscience*, 10(5), p. 1583. doi: 10.1523/JNEUROSCI.10-05-01583.1990.

Kimelberg, H. K. and Nedergaard, M. (2010) ‘Functions of astrocytes and their potential as therapeutic targets’, *Neurotherapeutics*, 7(4), p. 338. doi: 10.1016/J.NURT.2010.07.006.

King, E. *et al.* (2018) ‘Peripheral inflammation in prodromal Alzheimer’s and Lewy body dementias’, *Journal of neurology, neurosurgery, and psychiatry*, 89(4), pp. 339–345. doi: 10.1136/JNNP-2017-317134.

Kinney, G. A. and Spain, W. J. (2002) ‘Synaptically evoked GABA transporter currents in neocortical glia’, *Journal of Neurophysiology*, 88(6), pp. 2899–2908. doi: 10.1152/JN.00037.2002/ASSET/IMAGES/LARGE/9K1222765006.JPEG.

Kjellén, L. and Lindahl, U. (1991) ‘Proteoglycans: Structures and interactions’, *Annual Review of Biochemistry*, 60(Volume 60, 1991), pp. 443–475. doi: 10.1146/ANNUREV.BI.60.070191.002303/CITE/REFWORKS.

Klueva, J. *et al.* (2003) ‘Synaptic and non-synaptic mechanisms of amygdala recruitment into temporolimbic epileptiform activities’, *European Journal of Neuroscience*, 18(10), pp. 2779–2791. doi: 10.1111/J.1460-9568.2003.02984.X.

Knott, A. B. and Bossy-Wetzel, E. (2009) ‘Nitric Oxide in Health and Disease of the Nervous System’, *Antioxidants & Redox Signaling*, 11(3), p. 541. doi: 10.1089/ARS.2008.2234.

Knott, C., Stern, G. and Wilkin, G. P. (2000) ‘Inflammatory regulators in Parkinson’s disease: iNOS, lipocortin-1, and cyclooxygenases-1 and -2’, *Molecular and cellular neurosciences*, 16(6), pp. 724–739. doi: 10.1006/MCNE.2000.0914.

Kochlamazashvili, G. *et al.* (2010) ‘The Extracellular Matrix Molecule Hyaluronic Acid Regulates Hippocampal Synaptic Plasticity by Modulating Postsynaptic L-Type Ca2+ Channels’, *Neuron*, 67(1), p. 116. doi: 10.1016/J.NEURON.2010.05.030.

Kolling, N. *et al.* (2016) ‘Multiple signals in anterior cingulate cortex’, *Current Opinion in Neurobiology*, 37, p. 36. doi: 10.1016/J.CONB.2015.12.007.

Kövari, E. *et al.* (2003) ‘Lewy body densities in the entorhinal and anterior cingulate cortex predict cognitive deficits in Parkinson’s disease’, *Acta Neuropathologica*, 106(1), pp. 83–88. doi: 10.1007/S00401-003-0705-2/TABLES/4.

Krantic, S. *et al.* (2012) ‘Hippocampal GABAergic neurons are susceptible to amyloid-β toxicity in vitro and are decreased in number in the Alzheimer’s disease TgCRND8 mouse model’, *Journal of Alzheimer’s disease : JAD*, 29(2), pp. 293–308. doi: 10.3233/JAD-2011-110830.

Krishnan, G. P. and Bazhenov, M. (2011) ‘Ionic Dynamics Mediate Spontaneous Termination of Seizures and Postictal Depression State’, *The Journal of Neuroscience*, 31(24), p. 8870. doi: 10.1523/JNEUROSCI.6200-10.2011.

Krüger, R. *et al.* (1998) ‘AlaSOPro mutation in the gene encoding α-synuclein in Parkinson’s disease’, *Nature Genetics 1998 18:2*, 18(2), pp. 106–108. doi: 10.1038/ng0298-106.

Krzan, M. *et al.* (2003) ‘Calcium-Dependent Exocytosis of Atrial Natriuretic Peptide from Astrocytes’, *The Journal of Neuroscience*, 23(5), p. 1580. doi: 10.1523/JNEUROSCI.23-05-01580.2003.

Kudo, T. *et al.* (2023) ‘Selective dysfunction of fast-spiking inhibitory interneurons and disruption of perineuronal nets in a tauopathy mouse model’, *iScience*, 26(4), p. 106342. doi: 10.1016/J.ISCI.2023.106342.

Kuga, N. *et al.* (2011) ‘Large-Scale Calcium Waves Traveling through Astrocytic Networks In Vivo’, *The Journal of Neuroscience*, 31(7), p. 2607. doi: 10.1523/JNEUROSCI.5319-10.2011.

Kummer, M. P. *et al.* (2011) ‘Nitration of tyrosine 10 critically enhances amyloid β aggregation and plaque formation’, *Neuron*, 71(5), pp. 833–844. doi: 10.1016/J.NEURON.2011.07.001.

Künze, G., Huster, D. and Samsonov, S. A. (2021) ‘Investigation of the structure of regulatory proteins interacting with glycosaminoglycans by combining NMR spectroscopy and molecular modeling - The beginning of a wonderful friendship’, *Biological Chemistry*, 402(11), pp. 1337–1355. doi: 10.1515/HSZ-2021-0119/ASSET/GRAPHIC/J_HSZ-2021-0119_FIG_003.JPG.

Kwok, C. *et al.* (2008) ‘Proteoglycans in the central nervous system: plasticity, regeneration and their stimulation with chondroitinase ABC’.

Kwok, J. C. F. *et al.* (2011) ‘Extracellular matrix and perineuronal nets in CNS repair’, *Developmental Neurobiology*, 71(11), pp. 1073–1089. doi: 10.1002/DNEU.20974.

Kwon, H. S. and Koh, S. H. (2020) ‘Neuroinflammation in neurodegenerative disorders: the roles of microglia and astrocytes’, *Translational Neurodegeneration 2020 9:1*, 9(1), pp. 1–12. doi: 10.1186/S40035-020-00221-2.

Lagler, M. *et al.* (2016) ‘Divisions of Identified Parvalbumin-Expressing Basket Cells during Working Memory-Guided Decision Making’, *Neuron*, 91(6), pp. 1390–1401. doi: 10.1016/J.NEURON.2016.08.010.

Lai, T. T. *et al.* (2024) ‘Microglial inhibition alleviates alpha-synuclein propagation and neurodegeneration in Parkinson’s disease mouse model’, *npj Parkinson’s Disease 2024 10:1*, 10(1), pp. 1–10. doi: 10.1038/s41531-024-00640-2.

Laricchiuta, D. *et al.* (2024) ‘The role of glial cells in mental illness: a systematic review on astroglia and microglia as potential players in schizophrenia and its cognitive and emotional aspects’, *Frontiers in Cellular Neuroscience*, 18, p. 1358450. doi: 10.3389/FNCEL.2024.1358450/BIBTEX.

Lastres-Becker, I. *et al.* (2014) ‘Fractalkine activates NRF2/NFE2L2 and heme oxygenase 1 to restrain tauopathy-induced microgliosis’, *Brain : a journal of neurology*, 137(Pt 1), pp. 78–91. doi: 10.1093/BRAIN/AWT323.

Laubach, M. *et al.* (2018) ‘Cognition and Behavior What, If Anything, Is Rodent Prefrontal Cortex?’, *eNeuro*, 5(5), pp. 315–333. doi: 10.1523/ENEURO.0315-18.2018.

Laubach, M., Caetano, M. S. and Narayanan, N. S. (2015) ‘Mistakes were made: Neural mechanisms for the adaptive control of action initiation by the medial prefrontal cortex’, *Journal of physiology, Paris*, 109(1–3), p. 104. doi: 10.1016/J.JPHYSPARIS.2014.12.001.

Lauri, S. E. *et al.* (2006) ‘Functional Maturation of CA1 Synapses Involves Activity-Dependent Loss of Tonic Kainate Receptor-Mediated Inhibition of Glutamate Release’, *Neuron*, 50(3), pp. 415–429. doi: 10.1016/J.NEURON.2006.03.020/ATTACHMENT/4F960145-0AD7-44B8-A7AE-E086E0B840C0/MMC1.PDF.

Lauri, S. E. *et al.* (2021) ‘Kainate receptors in the developing neuronal networks’, *Neuropharmacology*, 195, p. 108585. doi: 10.1016/J.NEUROPHARM.2021.108585.

Law, A., Gauthier, S. and Quirion, R. (2001) ‘Say NO to Alzheimer’s disease: The putative links between nitric oxide and dementia of the Alzheimer’s type’, *Brain Research Reviews*, 35(1), pp. 73–96. doi: 10.1016/S0165-0173(00)00051-5.

Lee, A. T. *et al.* (2014) ‘Pyramidal neurons in prefrontal cortex receive subtype-specific forms of excitation and inhibition’, *Neuron*. 2013/12/24, 81(1), pp. 61–68. doi: 10.1016/j.neuron.2013.10.031.

Lee, D. C. *et al.* (2010) ‘LPS- induced inflammation exacerbates phospho-tau pathology in rTg4510 mice’, *Journal of neuroinflammation*, 7. doi: 10.1186/1742-2094-7-56.

Lee, H. J. *et al.* (2010) ‘Direct transfer of alpha-synuclein from neuron to astroglia causes inflammatory responses in synucleinopathies’, *The Journal of biological chemistry*, 285(12), pp. 9262–9272. doi: 10.1074/JBC.M109.081125.

Lee, H. J., Patel, S. and Lee, S. J. (2005) ‘Intravesicular Localization and Exocytosis of α-Synuclein and its Aggregates’, *The Journal of Neuroscience*, 25(25), p. 6016. doi: 10.1523/JNEUROSCI.0692-05.2005.

Lee, M. K. *et al.* (2002) ‘Human α-synuclein-harboring familial Parkinson’s disease-linked Ala-53 → Thr mutation causes neurodegenerative disease with α-synuclein aggregation in transgenic mice’, *Proceedings of the National Academy of Sciences of the United States of America*, 99(13), p. 8968. doi: 10.1073/PNAS.132197599.

Lee, M., Schwab, C. and Mcgeer, P. L. (2011) ‘Astrocytes are GABAergic cells that modulate microglial activity’, *Glia*, 59(1), pp. 152–165. doi: 10.1002/GLIA.21087.

Lee, Y. *et al.* (2019) ‘Significant roles of neuroinflammation in Parkinson’s disease: therapeutic targets for PD prevention’, *Archives of pharmacal research*, 42(5), pp. 416–425. doi: 10.1007/S12272-019-01133-0.

Leinweber, M. *et al.* (2017) ‘A Sensorimotor Circuit in Mouse Cortex for Visual Flow Predictions’, *Neuron*, 95(6), pp. 1420-1432.e5. doi: 10.1016/J.NEURON.2017.08.036.

Lensjø, K. K. *et al.* (2017) ‘Differential Expression and Cell-Type Specificity of Perineuronal Nets in Hippocampus, Medial Entorhinal Cortex, and Visual Cortex Examined in the Rat and Mouse’, *eNeuro*, 4(3). doi: 10.1523/ENEURO.0379-16.2017.

Leow, Y. N. *et al.* (2022) ‘Brain-wide mapping of inputs to the mouse lateral posterior (LP/Pulvinar) thalamus–anterior cingulate cortex network’, *The Journal of Comparative Neurology*, 530(11), p. 1992. doi: 10.1002/CNE.25317.

Levenga, J. *et al.* (2014) ‘Tau pathology induces loss of GABAergic interneurons leading to altered synaptic plasticity and behavioral impairments’, *Acta*

Neuropathologica Communications, 2(1), pp. 1–14. doi: 10.1186/2051-5960-1-34/FIGURES/5.

Lévesque, M. *et al.* (2013) 'Temporal lobe epileptiform activity following systemic administration of 4-aminopyridine in rats', *Epilepsia*, 54(4), p. 596. doi: 10.1111/EPI.12041.

Levin, B. and Duchowny, M. (1991) 'Childhood obsessive-compulsive disorder and cingulate epilepsy', *Biological psychiatry*, 30(10), pp. 1049–1055. doi: 10.1016/0006-3223(91)90124-5.

Li, P. *et al.* (2018) 'Electrophysiological measures reveal the role of anterior cingulate cortex in learning from unreliable feedback', *Cognitive, Affective and Behavioral Neuroscience*, 18(5), pp. 949–963. doi: 10.3758/S13415-018-0615-3/FIGURES/9.

Li, Q. Y. *et al.* (2022) 'Neuroinflammation in the anterior cingulate cortex: the potential supraspinal mechanism underlying the mirror-image pain following motor fiber injury', *Journal of Neuroinflammation*, 19(1), p. 162. doi: 10.1186/S12974-022-02525-8.

Li, W. *et al.* (2023) 'Neuroinflammation in epileptogenesis: from pathophysiology to therapeutic strategies', *Frontiers in Immunology*, 14. doi: 10.3389/FIMMU.2023.1269241.

Li, Y. *et al.* (2017) 'Tau Pathology Promotes the Reorganization of the Extracellular Matrix and Inhibits the Formation of Perineuronal Nets by Regulating the Expression and the Distribution of Hyaluronic Acid Synthases', *Journal of Alzheimer's Disease*, 57(2), p. 395. doi: 10.3233/JAD-160804.

Librizzi, L. *et al.* (2017) 'Interneuronal Network Activity at the Onset of Seizure-Like Events in Entorhinal Cortex Slices', *The Journal of Neuroscience*, 37(43), p. 10398. doi: 10.1523/JNEUROSCI.3906-16.2017.

Liddelow, S. A. *et al.* (2017) 'Neurotoxic reactive astrocytes are induced by activated microglia', *Nature*, 541(7638), pp. 481–487. doi: 10.1038/NATURE21029.

Liddelow, S. A. and Barres, B. A. (2017) 'Reactive Astrocytes: Production, Function, and Therapeutic Potential', *Immunity*, 46(6), pp. 957–967. doi: 10.1016/J.IMMUNI.2017.06.006.

Lillis, K. P. *et al.* (2012) ‘Pyramidal cells accumulate chloride at seizure onset’, *Neurobiology of Disease*, 47(3), p. 358. doi: 10.1016/J.NBD.2012.05.016.

Lin, R. *et al.* (2011) ‘6-Sulphated chondroitins have a positive influence on axonal regeneration’, *PloS one*, 6(7). doi: 10.1371/JOURNAL.PONE.0021499.

Lindström, V. *et al.* (2014) ‘Immunotherapy targeting α-synuclein protofibrils reduced pathology in (Thy-1)-h[A30P] α-synuclein mice’, *Neurobiology of disease*, 69, pp. 134–143. doi: 10.1016/J.NBD.2014.05.009.

Ling, E. A. (1976) ‘Some aspects of amoeboid microglia in the corpus callosum and neighbouring regions of neonatal rats.’, *Journal of Anatomy*, 121(Pt 1), p. 29. Available at: /pmc/articles/PMC1231817/?report=abstract (Accessed: 26 February 2024).

Liu, B. and Hong, J. S. (2003) ‘Role of Microglia in Inflammation-Mediated Neurodegenerative Diseases: Mechanisms and Strategies for Therapeutic Intervention’, *Journal of Pharmacology and Experimental Therapeutics*, 304(1), pp. 1–7. doi: 10.1124/JPET.102.035048.

Liu, C. C. *et al.* (2016) ‘Neuronal heparan sulfates promote amyloid pathology by modulating brain amyloid-β clearance and aggregation in Alzheimer’s disease’, *Science Translational Medicine*, 8(332). doi: 10.1126/SCITRANSLMED.AAD3650/SUPPL_FILE/8-332RA44_SM.PDF.

Liu, I. H. *et al.* (2005) ‘Agrin binds alpha-synuclein and modulates alpha-synuclein fibrillation’, *Glycobiology*, 15(12), pp. 1320–1331. doi: 10.1093/GLYCOB/CWJ014.

Lobsiger, C. S. and Cleveland, D. W. (2007) ‘Glial cells as intrinsic components of non-cell-autonomous neurodegenerative disease’, *Nature neuroscience*, 10(11), pp. 1355–1360. doi: 10.1038/NN1988.

Long, J. M. *et al.* (1998) ‘Stereological analysis of astrocyte and microglia in aging mouse hippocampus’, *Neurobiology of aging*, 19(5), pp. 497–503. doi: 10.1016/S0197-4580(98)00088-8.

Lopategui Cabezas, I., Herrera Batista, A. and Pentón Rol, G. (2014) ‘The role of glial cells in Alzheimer disease: potential therapeutic implications’, *Neurologia (Barcelona, Spain)*, 29(5), pp. 305–309. doi: 10.1016/J.NRL.2012.10.006.

Lorenzen, N. *et al.* (2014) ‘The N-terminus of α-synuclein is essential for both monomeric and oligomeric interactions with membranes’, *FEBS letters*, 588(3), pp. 497–502. doi: 10.1016/J.FEBSLET.2013.12.015.

Lorenzl, S. *et al.* (2003) ‘Tissue inhibitors of matrix metalloproteinases are elevated in cerebrospinal fluid of neurodegenerative diseases’, *Journal of the Neurological Sciences*, 207(1–2), pp. 71–76. doi: 10.1016/S0022-510X(02)00398-2.

Louis, E. D. *et al.* (1997) ‘Comparison of extrapyramidal features in 31 pathologically confirmed cases of diffuse Lewy body disease and 34 pathologically confirmed cases of Parkinson’s disease’, *Neurology*, 48(2), pp. 376–380. doi: 10.1212/WNL.48.2.376/ASSET/65ADFE90-7924-4C2E-823D-8F3964114B11/ASSETS/GRAPHIC/16TT1.JPEG.

Lozano, A. M. *et al.* (2016) ‘A Phase II Study of Fornix Deep Brain Stimulation in Mild Alzheimer’s Disease’, *Journal of Alzheimer’s disease : JAD*, 54(2), pp. 777–787. doi: 10.3233/JAD-160017.

LS, F. (1986) ‘Lewy bodies’, *The New England journal of medicine*, 314(2), pp. 122–123. doi: 10.1056/NEJM198601093140219.

Ludtmann, M. H. R. *et al.* (2018) ‘α-synuclein oligomers interact with ATP synthase and open the permeability transition pore in Parkinson’s disease’, *Nature Communications 2018 9:1*, 9(1), pp. 1–16. doi: 10.1038/s41467-018-04422-2.

Lue, L. F. *et al.* (2015) ‘TREM2 Protein Expression Changes Correlate with Alzheimer’s Disease Neurodegenerative Pathologies in Post-Mortem Temporal Cortices’, *Brain Pathology*, 25(4), p. 469. doi: 10.1111/BPA.12190.

Lull, M. E. and Block, M. L. (2010) ‘Microglial activation and chronic neurodegeneration’, *Neurotherapeutics*, 7(4), p. 354. doi: 10.1016/J.NURT.2010.05.014.

Lundberg, J. O. N. *et al.* (1994) ‘Intragastric nitric oxide production in humans: measurements in expelled air’, *Gut*, 35(11), pp. 1543–1546. doi: 10.1136/GUT.35.11.1543.

Lundberg, J. O., Weitzberg, E. and Gladwin, M. T. (2008) ‘The nitrate-nitrite-nitric oxide pathway in physiology and therapeutics’, *Nature reviews. Drug discovery*, 7(2),

pp. 156–167. doi: 10.1038/NRD2466.

Lüth, H. J. *et al.* (2001) ‘Expression of endothelial and inducible NOS-isoforms is increased in Alzheimer’s disease, in APP23 transgenic mice and after experimental brain lesion in rat: evidence for an induction by amyloid pathology’, *Brain research*, 913(1), pp. 57–67. doi: 10.1016/S0006-8993(01)02758-5.

Magen, I. *et al.* (2012) ‘Cognitive deficits in a mouse model of pre-manifest Parkinson’s disease’, *The European journal of neuroscience*, 35(6), p. 870. doi: 10.1111/J.1460-9568.2012.08012.X.

Magen, I. *et al.* (2015) ‘Social Cognition Impairments in Mice Overexpressing Alpha-Synuclein Under the Thy1 Promoter, a Model of Pre-manifest Parkinson’s Disease’, *Journal of Parkinson’s Disease*, 5(3), p. 669. doi: 10.3233/JPD-140503.

Mahar, I. *et al.* (2016) ‘Phenotypic Alterations in Hippocampal NPY- and PV-Expressing Interneurons in a Presymptomatic Transgenic Mouse Model of Alzheimer’s Disease’, *Frontiers in Aging Neuroscience*, 8(JAN). doi: 10.3389/FNAGI.2016.00327.

Marín-padilla, M. (1995) ‘Prenatal development of fibrous (white matter), protoplasmic (gray matter), and layer I astrocytes in the human cerebral cortex: a Golgi study’, *The Journal of comparative neurology*, 357(4), pp. 554–572. doi: 10.1002/CNE.903570407.

Maroteaux, L., Campanelli, J. T. and Scheller, R. H. (1988) ‘Synuclein: a neuron-specific protein localized to the nucleus and presynaptic nerve terminal’, *Journal of Neuroscience*, 8(8), pp. 2804–2815. doi: 10.1523/JNEUROSCI.08-08-02804.1988.

Martin, L. J. *et al.* (2006) ‘Parkinson’s Disease α-Synuclein Transgenic Mice Develop Neuronal Mitochondrial Degeneration and Cell Death’, *The Journal of Neuroscience*, 26(1), p. 41. doi: 10.1523/JNEUROSCI.4308-05.2006.

Masliah, E. *et al.* (2000) ‘Dopaminergic Loss and Inclusion Body Formation in α-Synuclein Mice: Implications for Neurodegenerative Disorders’, *Science*, 287(5456), pp. 1265–1269. doi: 10.1126/SCIENCE.287.5456.1265.

Matejuk, A. and Ransohoff, R. M. (2020) ‘Crosstalk Between Astrocytes and Microglia: An Overview’, *Frontiers in Immunology*, 11, p. 1416. doi:

10.3389/FIMMU.2020.01416.

Mathew, S. S., Pozzo-Miller, L. and Hablitz, J. J. (2008) ‘Kainate Modulates Presynaptic GABA Release from Two Vesicle Pools’, *The Journal of Neuroscience*, 28(3), p. 725. doi: 10.1523/JNEUROSCI.3625-07.2008.

Mauney, S. A. *et al.* (2013a) ‘Developmental pattern of perineuronal nets in the human prefrontal cortex and their deficit in schizophrenia’, *Biological psychiatry*, 74(6), pp. 427–435. doi: 10.1016/J.BIOPSYCH.2013.05.007.

Mauney, S. A. *et al.* (2013b) ‘Developmental pattern of perineuronal nets in the human prefrontal cortex and their deficit in schizophrenia’, *Biological psychiatry*, 74(6), pp. 427–435. doi: 10.1016/J.BIOPSYCH.2013.05.007.

McCann, S. M. *et al.* (1998) ‘The nitric oxide hypothesis of aging’, *Experimental gerontology*, 33(7–8), pp. 813–826. doi: 10.1016/S0531-5565(98)00050-3.

McCarthy, G. *et al.* (1994) ‘Functional magnetic resonance imaging of human prefrontal cortex activation during a spatial working memory task’, *Proceedings of the National Academy of Sciences of the United States of America*, 91(18), pp. 8690–8694. doi: 10.1073/PNAS.91.18.8690.

McKeith, I. (2017) *Dementia with Lewy bodies: A clinical overview | 75 | 5 Dementia | Ian*. Available at: https://www.taylorfrancis.com/chapters/edit/10.1201/9781315381572-75/dementia-lewy-bodies-clinical-overview-ian-mckeith (Accessed: 19 July 2022).

Mckeith, I. G. *et al.* (2017) ‘Diagnosis and management of dementia with Lewy bodies Fourth consensus report of the DLB Consortium’.

McKeith, I. G. *et al.* (2020) ‘Research criteria for the diagnosis of prodromal dementia with Lewy bodies’, *Neurology*, 94(17), pp. 743–755. doi: 10.1212/WNL.0000000000009323/ASSET/9D505976-0B14-4F1B-8306-0A8334F14282/ASSETS/GRAPHIC/16TTU1B.JPEG.

McKeon, R. J., Jurynec, M. J. and Buck, C. R. (1999) ‘The Chondroitin Sulfate Proteoglycans Neurocan and Phosphacan Are Expressed by Reactive Astrocytes in the Chronic CNS Glial Scar’, *Journal of Neuroscience*, 19(24), pp. 10778–10788. doi: 10.1523/JNEUROSCI.19-24-10778.1999.

McLean, P. J., Ribich, S. and Hyman, B. T. (2000) ‘Subcellular localization of alpha-synuclein in primary neuronal cultures: effect of missense mutations’, *Journal of neural transmission. Supplementum*, (58), pp. 53–63. doi: 10.1007/978-3-7091-6284-2_5.

Mcrae, P. A. *et al.* (2012) ‘Persistent decrease in multiple components of the perineuronal net following status epilepticus’, *The European journal of neuroscience*, 36(11), p. 3471. doi: 10.1111/J.1460-9568.2012.08268.X.

McRae, P. A. *et al.* (2010) ‘Aggrecan expression, a component of the inhibitory interneuron perineuronal net, is altered following an early life seizure’, *Neurobiology of disease*, 39(3), p. 439. doi: 10.1016/J.NBD.2010.05.015.

McRae, P. A. and Porter, B. E. (2012) ‘The Perineuronal Net Component of the Extracellular Matrix in Plasticity and Epilepsy’, *Neurochemistry international*, 61(7), p. 963. doi: 10.1016/J.NEUINT.2012.08.007.

Mehra, S. *et al.* (2018) ‘Glycosaminoglycans have variable effects on α-synuclein aggregation and differentially affect the activities of the resulting amyloid fibrils’, *The Journal of Biological Chemistry*, 293(34), p. 12975. doi: 10.1074/JBC.RA118.004267.

Mercatelli, R. *et al.* (2016) ‘Clasmatodendrosis and β-amyloidosis in aging hippocampus’, *FASEB journal : official publication of the Federation of American Societies for Experimental Biology*, 30(4), pp. 1480–1491. doi: 10.1096/FJ.15-275503.

Le Merre, P., Ährlund-Richter, S. and Carlén, M. (2021) ‘The mouse prefrontal cortex: Unity in diversity’, *Neuron*, 109(12), pp. 1925–1944. doi: 10.1016/J.NEURON.2021.03.035.

Miklossy, J. *et al.* (2006) ‘Role of ICAM-1 in persisting inflammation in Parkinson disease and MPTP monkeys’, *Experimental Neurology*, 197(2), pp. 275–283. doi: 10.1016/J.EXPNEUROL.2005.10.034.

Milanese, C. *et al.* (2018) ‘Activation of the DNA damage response in vivo in synucleinopathy models of Parkinson’s disease’, *Cell Death & Disease*, 9(8). doi: 10.1038/S41419-018-0848-7.

Miller, E. K. and Cohen, J. D. (2001) ‘An integrative theory of prefrontal cortex function’, *Annual review of neuroscience*, 24, pp. 167–202. doi: 10.1146/ANNUREV.NEURO.24.1.167.

Minakaki, G. *et al.* (2018) ‘Autophagy inhibition promotes SNCA/alpha-synuclein release and transfer via extracellular vesicles with a hybrid autophagosome-exosome-like phenotype’, *Autophagy*, 14(1), p. 98. doi: 10.1080/15548627.2017.1395992.

Miyata, S. *et al.* (2012) ‘Persistent cortical plasticity by upregulation of chondroitin 6-sulfation’, *Nature neuroscience*, 15(3), pp. 414–422. doi: 10.1038/NN.3023.

Miyata, S., Nishimura, Y. and Nakashima, T. (2007) ‘Perineuronal nets protect against amyloid β-protein neurotoxicity in cultured cortical neurons’, *Brain Research*, 1150(1), pp. 200–206. doi: 10.1016/J.BRAINRES.2007.02.066.

Mohamedi, Y. *et al.* (2020) ‘New Insights into ADAMTS Metalloproteases in the Central Nervous System’, *Biomolecules 2020, Vol. 10, Page 403*, 10(3), p. 403. doi: 10.3390/BIOM10030403.

Molofsky, A. V. and Deneen, B. (2015) ‘Astrocyte development: A Guide for the Perplexed’, *Glia*, 63(8), pp. 1320–1329. doi: 10.1002/GLIA.22836.

Morales, B., Choi, S. Y. and Kirkwood, A. (2002) ‘Dark Rearing Alters the Development of GABAergic Transmission in Visual Cortex’, *The Journal of Neuroscience*, 22(18), p. 8084. doi: 10.1523/JNEUROSCI.22-18-08084.2002.

Morawski, M. *et al.* (2004) ‘Perineuronal nets potentially protect against oxidative stress’, *Experimental Neurology*, 188(2), pp. 309–315. doi: 10.1016/j.expneurol.2004.04.017.

Morawski, M. *et al.* (2005) ‘The Binding of Iron to Perineuronal Nets: A Combined Nuclear Microscopy and Mössbauer Study’, *HFI/NQI 2004*, pp. 719–725. doi: 10.1007/3-540-30924-1_116.

Morawski, M. *et al.* (2009) ‘Chondroitin sulfate proteoglycan-based extracellular matrix in chicken (Gallus domesticus) brain’, *Brain research*, 1275, pp. 10–23. doi: 10.1016/J.BRAINRES.2009.02.046.

Morawski, M. *et al.* (2012) ‘Involvement of perineuronal and perisynaptic extracellular

matrix in Alzheimer's disease neuropathology', *Brain pathology (Zurich, Switzerland)*, 22(4), pp. 547–561. doi: 10.1111/J.1750-3639.2011.00557.X.

Morellini, F. *et al.* (2010) 'Improved reversal learning and working memory and enhanced reactivity to novelty in mice with enhanced GABAergic innervation in the dentate gyrus', *Cerebral cortex (New York, N.Y. : 1991)*, 20(11), pp. 2712–2727. doi: 10.1093/CERCOR/BHQ017.

Morenas-Rodríguez, E. *et al.* (2019) 'Different pattern of CSF glial markers between dementia with Lewy bodies and Alzheimer's disease', *Scientific reports*, 9(1). doi: 10.1038/S41598-019-44173-8.

Morgan, J. I. *et al.* (1987) 'Mapping patterns of c-fos expression in the central nervous system after seizure', *Science (New York, N.Y.)*, 237(4811), pp. 192–197. doi: 10.1126/SCIENCE.3037702.

Morikawa, S. *et al.* (2017) 'Activation of perineuronal net-expressing excitatory neurons during associative memory encoding and retrieval', *Scientific reports*, 7. doi: 10.1038/SREP46024.

Morris, M. *et al.* (2015) 'Network dysfunction in α-synuclein transgenic mice and human Lewy body dementia', *Annals of Clinical and Translational Neurology*, 2(11), p. 1012. doi: 10.1002/ACN3.257.

Mouri, A. *et al.* (2007) 'Phencyclidine animal models of schizophrenia: approaches from abnormality of glutamatergic neurotransmission and neurodevelopment', *Neurochemistry international*, 51(2–4), pp. 173–184. doi: 10.1016/J.NEUINT.2007.06.019.

Mueller, A. L. *et al.* (2016) 'Distribution of N-Acetylgalactosamine-Positive Perineuronal Nets in the Macaque Brain: Anatomy and Implications', *Neural Plasticity*, 2016. doi: 10.1155/2016/6021428.

Mulle, C. *et al.* (2000) 'Subunit composition of kainate receptors in hippocampal interneurons', *Neuron*, 28(2), pp. 475–484. doi: 10.1016/S0896-6273(00)00126-4.

Myers, T. L. *et al.* (2018) 'Characterizing Concentration-Dependent Neural Dynamics of 4-Aminopyridine-Induced Epileptiform Activity', *Epilepsy journal*, 4(2). doi: 10.4172/2472-0895.1000128.

Naffah-Mazzacoratti, M. G. *et al.* (1999) ‘Selective alterations of glycosaminoglycans synthesis and proteoglycan expression in rat cortex and hippocampus in pilocarpine-induced epilepsy’, *Brain Research Bulletin*, 50(4), pp. 229–239. doi: 10.1016/S0361-9230(99)00195-1.

Nagano, N., Aoyagi, M. and Hirakawa, K. (1993) ‘Extracellular matrix modulates the proliferation of rat astrocytes in serum-free culture’, *Glia*, 8(2), pp. 71–76. doi: 10.1002/GLIA.440080202.

Najm, R., Jones, E. A. and Huang, Y. (2019) ‘Apolipoprotein E4, inhibitory network dysfunction, and Alzheimer’s disease’, *Molecular Neurodegeneration 2019 14:1*, 14(1), pp. 1–13. doi: 10.1186/S13024-019-0324-6.

Narayanan, N. S. and Laubach, M. (2006) ‘TOP-DOWN CONTROL OF MOTOR CORTEX ENSEMBLES BY DORSOMEDIAL PREFRONTAL CORTEX’, *Neuron*, 52(5), p. 921. doi: 10.1016/J.NEURON.2006.10.021.

Nelson, S. B. and Turrigiano, G. G. (1998) ‘Synaptic depression: a key player in the cortical balancing act’, *Nature Neuroscience 1998 1:7*, 1(7), pp. 539–541. doi: 10.1038/2775.

Neuper, C. and Pfurtscheller, G. (2001) ‘Event-related dynamics of cortical rhythms: frequency-specific features and functional correlates’, *International Journal of Psychophysiology*, 43(1), pp. 41–58. doi: 10.1016/S0167-8760(01)00178-7.

Newman, E. A. (2003) ‘Glial Cell Inhibition of Neurons by Release of ATP’, *The Journal of Neuroscience*, 23(5), p. 1659. doi: 10.1523/JNEUROSCI.23-05-01659.2003.

Nichols, N. R. *et al.* (1993) ‘GFAP mRNA increases with age in rat and human brain’, *Neurobiology of aging*, 14(5), pp. 421–429. doi: 10.1016/0197-4580(93)90100-P.

Nielsen, H. M. *et al.* (2013) ‘NG2 cells, a new trail for Alzheimer’s disease mechanisms?’, *Acta Neuropathologica Communications*, 1(1). doi: 10.1186/2051-5960-1-7.

Nikolenko, V. N. *et al.* (2020) ‘Amygdala: Neuroanatomical and Morphophysiological Features in Terms of Neurological and Neurodegenerative Diseases’, *Brain Sciences*, 10(8), pp. 1–18. doi: 10.3390/BRAINSCI10080502.

Nimmerjahn, A. *et al.* (2004) ‘Sulforhodamine 101 as a specific marker of astroglia in the neocortex in vivo’, *Nature methods*, 1(1), pp. 31–37. doi: 10.1038/NMETH706.

Nimmerjahn, A., Kirchhoff, F. and Helmchen, F. (2005) ‘Neuroscience: Resting microglial cells are highly dynamic surveillants of brain parenchyma in vivo’, *Science*, 308(5726), pp. 1314–1318. doi: 10.1126/SCIENCE.1110647/SUPPL_FILE/1110647S9.MOV.

Nowicka, D. *et al.* (2009) ‘Parvalbumin-containing neurons, perineuronal nets and experience-dependent plasticity in murine barrel cortex’, *The European journal of neuroscience*, 30(11), pp. 2053–2063. doi: 10.1111/J.1460-9568.2009.06996.X.

Nunnari, J. and Suomalainen, A. (2012) ‘Mitochondria: In sickness and in health’, *Cell*, 148(6), pp. 1145–1159. doi: 10.1016/J.CELL.2012.02.035/ASSET/2F18342E-AC01-4501-8CC2-236EEE4152AE/MAIN.ASSETS/GR2.JPG.

Ohsawa, K. *et al.* (2000) ‘Involvement of Iba1 in membrane ruffling and phagocytosis of macrophages/microglia’, *Journal of Cell Science*, 113(17), pp. 3073–3084. doi: 10.1242/JCS.113.17.3073.

Okamoto, M., Mori, S. and Endo, H. (1994) ‘A protective action of chondroitin sulfate proteoglycans against neuronal cell death induced by glutamate’, *Brain research*, 637(1–2), pp. 57–67. doi: 10.1016/0006-8993(94)91217-3.

Oksanen, M. *et al.* (2019) ‘Astrocyte alterations in neurodegenerative pathologies and their modeling in human induced pluripotent stem cell platforms’, *Cellular and molecular life sciences : CMLS*, 76(14), pp. 2739–2760. doi: 10.1007/S00018-019-03111-7.

Olivera, G. C. *et al.* (2016) ‘Nitric Oxide Protects against Infection-Induced Neuroinflammation by Preserving the Stability of the Blood-Brain Barrier’, *PLoS Pathogens*, 12(2). doi: 10.1371/JOURNAL.PPAT.1005442.

Ongali, B. *et al.* (2018) ‘Transforming growth factor-β1 induces cerebrovascular dysfunction and astrogliosis through angiotensin II type 1 receptor-mediated signaling pathways’, *Canadian journal of physiology and pharmacology*, 96(5), pp. 527–534. doi: 10.1139/CJPP-2017-0640.

Öngür, D. and Price, J. L. (2000) ‘The organization of networks within the orbital and

medial prefrontal cortex of rats, monkeys and humans', *Cerebral cortex (New York, N.Y. : 1991)*, 10(3), pp. 206–219. doi: 10.1093/CERCOR/10.3.206.

Outeiro, T. F. *et al.* (2019) 'Dementia with Lewy bodies: an update and outlook', *Molecular Neurodegeneration 2019 14:1*, 14(1), pp. 1–18. doi: 10.1186/S13024-019-0306-8.

Pacher, P., Beckman, J. S. and Liaudet, L. (2007) 'Nitric Oxide and Peroxynitrite in Health and Disease', *Physiological reviews*, 87(1), p. 315. doi: 10.1152/PHYSREV.00029.2006.

Packer, A. M. and Yuste, R. (2011) 'Dense, unspecific connectivity of neocortical parvalbumin-positive interneurons: A canonical microcircuit for inhibition?', *Journal of Neuroscience*, 31(37), pp. 13260–13271. doi: 10.1523/JNEUROSCI.3131-11.2011.

Page, C. E. *et al.* (2019) 'Prefrontal parvalbumin cells are sensitive to stress and mediate anxiety-related behaviors in female mice', *Scientific Reports*, 9(1). doi: 10.1038/S41598-019-56424-9.

Pala, A. and Petersen, C. C. H. (2015) 'InVivo Measurement of Cell-Type-Specific Synaptic Connectivity and Synaptic Transmission in Layer 2/3 Mouse Barrel Cortex', *Neuron*, 85(1), pp. 68–75. doi: 10.1016/j.neuron.2014.11.025.

Palop, J. J. and Mucke, L. (2009) 'Epilepsy and cognitive impairments in Alzheimer disease', *Archives of neurology*, 66(4), pp. 435–440. doi: 10.1001/ARCHNEUROL.2009.15.

Palop, J. J. and Mucke, L. (2010) 'Amyloid-β–induced neuronal dysfunction in Alzheimer's disease: from synapses toward neural networks', *Nature Neuroscience 2010 13:7*, 13(7), pp. 812–818. doi: 10.1038/nn.2583.

Palop, J. J. and Mucke, L. (2016) 'Network abnormalities and interneuron dysfunction in Alzheimer disease', *Nature Reviews Neuroscience 2016 17:12*, 17(12), pp. 777–792. doi: 10.1038/nrn.2016.141.

Pan, G. *et al.* (2016) 'Postnatal development of the electrophysiological properties of somatostatin interneurons in the anterior cingulate cortex of mice', *Scientific Reports 2016 6:1*, 6(1), pp. 1–12. doi: 10.1038/srep28137.

Panuccio, G. *et al.* (2009) 'Epileptiform synchronization in the cingulate cortex',

Epilepsia, 50(3), p. 521. doi: 10.1111/J.1528-1167.2008.01779.X.

Pardo, J. V., Fox, P. T. and Raichle, M. E. (1991) 'Localization of a human system for sustained attention by positron emission tomography', *Nature*, 349(6304), pp. 61–64. doi: 10.1038/349061A0.

Park, K. W. *et al.* (2005) 'Neuroprotective role of microglia expressing interleukin-4', *Journal of neuroscience research*, 81(3), pp. 397–402. doi: 10.1002/JNR.20483.

Parker, K. L. *et al.* (2013) 'Executive dysfunction in Parkinson's disease and timing deficits', *Frontiers in Integrative Neuroscience*, 7(OCT), p. 75. doi: 10.3389/FNINT.2013.00075/BIBTEX.

Parpura, V. *et al.* (1994) 'Glutamate-mediated astrocyte-neuron signalling', *Nature*, 369(6483), pp. 744–747. doi: 10.1038/369744A0.

Patel, D. C. *et al.* (2023) 'Infection-induced epilepsy is caused by increased expression of chondroitin sulfate proteoglycans in hippocampus and amygdala', *bioRxiv*. doi: 10.1101/2023.05.16.541066.

Pathak, D., Guan, D. and Foehring, R. C. (2016) 'Roles of specific Kv channel types in repolarization of the action potential in genetically identified subclasses of pyramidal neurons in mouse neocortex', *Journal of Neurophysiology*, 115(5), p. 2317. doi: 10.1152/JN.01028.2015.

Paulson, O. B. and Newman, E. A. (1987) 'Does the Release of Potassium from Astrocyte Endfeet Regulate Cerebral Blood Flow?', *Science (New York, N.Y.)*, 237(4817), p. 896. doi: 10.1126/SCIENCE.3616619.

Pavlov, I. *et al.* (2009) 'Outwardly rectifying tonically active GABAA receptors in pyramidal cells modulate neuronal offset, not gain', *The Journal of neuroscience : the official journal of the Society for Neuroscience*, 29(48), pp. 15341–15350. doi: 10.1523/JNEUROSCI.2747-09.2009.

Peinado, M. A. (1998) 'Histology and Histochemistry of the Aging Cerebral Cortex: An Overview', *Microsc. Res. Tech*, 43, pp. 1–7. doi: 10.1002/(SICI)1097-0029(19981001)43:1.

Pellerin, L. *et al.* (2007) 'Activity-dependent regulation of energy metabolism by astrocytes: an update', *Glia*, 55(12), pp. 1251–1262. doi: 10.1002/GLIA.20528.

Pellerin, L. and Magistretti, P. J. (1994) ‘Glutamate uptake into astrocytes stimulates aerobic glycolysis: a mechanism coupling neuronal activity to glucose utilization.’, *Proceedings of the National Academy of Sciences of the United States of America*, 91(22), p. 10625. doi: 10.1073/PNAS.91.22.10625.

Peng, C., Trojanowski, J. Q. and Lee, V. M. Y. (2020) ‘Protein transmission in neurodegenerative disease’, *Nature Reviews Neurology 2020 16:4*, 16(4), pp. 199–212. doi: 10.1038/s41582-020-0333-7.

Perea, G., Navarrete, M. and Araque, A. (2009) ‘Tripartite synapses: astrocytes process and control synaptic information’, *Trends in neurosciences*, 32(8), pp. 421–431. doi: 10.1016/J.TINS.2009.05.001.

Perez-Nievas, B. G. and Serrano-Pozo, A. (2018) ‘Deciphering the Astrocyte Reaction in Alzheimer’s Disease’, *Frontiers in aging neuroscience*, 10(APR). doi: 10.3389/FNAGI.2018.00114.

Perosa, S. R. *et al.* (2002) ‘Extracellular matrix components are altered in the hippocampus, cortex, and cerebrospinal fluid of patients with mesial temporal lobe epilepsy’, *Epilepsia*, 43 Suppl 5(SUPPL. 5), pp. 159–161. doi: 10.1046/J.1528-1157.43.S.5.30.X.

Perry, E. K. *et al.* (1994) ‘Neocortical cholinergic activities differentiate Lewy body dementia from classical Alzheimer’s disease’, *Neuroreport*, 5(7), pp. 747–749. doi: 10.1097/00001756-199403000-00002.

Perry, T. L. *et al.* (1987) ‘Amino acids, glutathione, and glutathione transferase activity in the brains of patients with Alzheimer’s disease’, *Annals of Neurology*, 21(4), pp. 331–336. doi: 10.1002/ANA.410210403.

Perry, V. H., Hume, D. A. and Gordon, S. (1985) ‘Immunohistochemical localization of macrophages and microglia in the adult and developing mouse brain’, *Neuroscience*, 15(2), pp. 313–326. doi: 10.1016/0306-4522(85)90215-5.

Peters, S. T. *et al.* (2020) ‘Ablating Tau Reduces Hyperexcitability and Moderates Electroencephalographic Slowing in Transgenic Mice Expressing A53T Human α-Synuclein’, *Frontiers in Neurology*, 11, p. 563. doi: 10.3389/FNEUR.2020.00563/BIBTEX.

Petrache, A. L. *et al.* (2019) ‘Aberrant Excitatory-Inhibitory Synaptic Mechanisms in Entorhinal Cortex Microcircuits During the Pathogenesis of Alzheimer’s Disease’, *Cerebral cortex (New York, N.Y. : 1991)*, 29(4), pp. 1834–1850. doi: 10.1093/CERCOR/BHZ016.

Piez, K. A. (1997) ‘History of extracellular matrix: a personal view’, *Matrix biology : journal of the International Society for Matrix Biology*, 16(3), pp. 85–92. doi: 10.1016/S0945-053X(97)90037-8.

Pillai, J. and Sperling, M. R. (2006) ‘Interictal EEG and the Diagnosis of Epilepsy’, *Epilepsia*, 47(SUPPL. 1), pp. 14–22. doi: 10.1111/J.1528-1167.2006.00654.X.

Pinho, R. *et al.* (2019) ‘Nuclear localization and phosphorylation modulate pathological effects of alpha-synuclein’, *Human molecular genetics*, 28(1), pp. 31–50. doi: 10.1093/HMG/DDY326.

Pintér, A. *et al.* (2020) ‘Chondroitin sulfate proteoglycan-5 forms perisynaptic matrix assemblies in the adult rat cortex’, *Cellular Signalling*, 74, p. 109710. doi: 10.1016/J.CELLSIG.2020.109710.

Pintér, P. and Alpár, A. (2022) ‘The Role of Extracellular Matrix in Human Neurodegenerative Diseases’, *International Journal of Molecular Sciences*, 23(19). doi: 10.3390/IJMS231911085.

Pirbhoy, P. S. *et al.* (2020) ‘Acute pharmacological inhibition of matrix metalloproteinase-9 activity during development restores perineuronal net formation and normalizes auditory processing in Fmr1 KO mice’, *Journal of neurochemistry*, 155(5), p. 538. doi: 10.1111/JNC.15037.

De Pittà, M., Brunel, N. and Volterra, A. (2016) ‘Astrocytes: Orchestrating synaptic plasticity?’, *Neuroscience*, 323, pp. 43–61. doi: 10.1016/J.NEUROSCIENCE.2015.04.001.

Pizzorusso, Tommaso *et al.* (2002) ‘Reactivation of ocular dominance plasticity in the adult visual cortex’, *Science (New York, N.Y.)*, 298(5596), pp. 1248–1251. doi: 10.1126/SCIENCE.1072699.

Pizzorusso, T *et al.* (2002) ‘Reactivation of ocular dominance plasticity in the adult visual cortex’, *Science*. 2002/11/09, 298(5596), pp. 1248–1251. doi:

10.1126/science.1072699.

Pollock, E. *et al.* (2014) ‘Metalloproteinase inhibition prevents inhibitory synapse reorganization and seizure genesis’, *Neurobiology of disease*, 70, pp. 21–31. doi: 10.1016/J.NBD.2014.06.003.

Polymeropoulos, M. H. *et al.* (1997) ‘Mutation in the α-Synuclein Gene Identified in Families with Parkinson’s Disease’, *Science*, 276(5321), pp. 2045–2047. doi: 10.1126/SCIENCE.276.5321.2045.

Porchet, R. *et al.* (2003) ‘Analysis of glial acidic fibrillary protein in the human entorhinal cortex during aging and in Alzheimer’s disease’, *Proteomics*, 3(8), pp. 1476–1485. doi: 10.1002/PMIC.200300456.

Posporelis, S. *et al.* (2018) ‘Deep Brain Stimulation of the Memory Circuit: Improving Cognition in Alzheimer’s Disease’, *Journal of Alzheimer’s Disease*, 64(2), pp. 337–347. doi: 10.3233/JAD-180212.

Pouille, F. *et al.* (2009) ‘Input normalization by global feedforward inhibition expands cortical dynamic range’, *Nat Neurosci*. 2009/11/03, 12(12), pp. 1577–1585. doi: 10.1038/nn.2441.

Pouille, F. and Scanziani, M. (2001) ‘Enforcement of Temporal Fidelity in Pyramidal Cells by Somatic Feed-Forward Inhibition’, *Science*, 293(5532), pp. 1159–1163. doi: 10.1126/SCIENCE.1060342.

Pracucci, E. *et al.* (2021) ‘Neuroinflammation: A Signature or a Cause of Epilepsy?’, *International Journal of Molecular Sciences 2021, Vol. 22, Page 6981*, 22(13), p. 6981. doi: 10.3390/IJMS22136981.

Proskurina, E. Y. and Zaitsev, A. V. (2021) ‘Photostimulation activates fast-spiking interneurons and pyramidal cells in the entorhinal cortex of Thy1-ChR2-YFP line 18 mice’, *Biochemical and Biophysical Research Communications*, 580, pp. 87–92. doi: 10.1016/J.BBRC.2021.10.002.

Van Der Putten, H. *et al.* (2000) ‘Neuropathology in Mice Expressing Human α-Synuclein’, *The Journal of Neuroscience*, 20(16), p. 6021. doi: 10.1523/JNEUROSCI.20-16-06021.2000.

Quist, A. *et al.* (2005) ‘Amyloid ion channels: A common structural link for protein-

misfolding disease', *Proceedings of the National Academy of Sciences of the United States of America*, 102(30), p. 10427. doi: 10.1073/PNAS.0502066102.

Rabinowicz, A. L. *et al.* (2000) 'Transient epileptic amnesia in dementia: a treatable unrecognized cause of episodic amnestic wandering', *Alzheimer disease and associated disorders*, 14(4), pp. 231–233. doi: 10.1097/00002093-200010000-00008.

Rajkumar, A. P. *et al.* (2020) 'Postmortem Cortical Transcriptomics of Lewy Body Dementia Reveal Mitochondrial Dysfunction and Lack of Neuroinflammation', *The American Journal of Geriatric Psychiatry*, 28(1), pp. 75–86. doi: 10.1016/J.JAGP.2019.06.007.

Ramachandran, G. and Udgaonkar, J. B. (2011) 'Understanding the Kinetic Roles of the Inducer Heparin and of Rod-like Protofibrils during Amyloid Fibril Formation by Tau Protein', *The Journal of Biological Chemistry*, 286(45), p. 38948. doi: 10.1074/JBC.M111.271874.

Ramos, B. *et al.* (2006) 'Early neuropathology of somatostatin/NPY GABAergic cells in the hippocampus of a PS1 × APP transgenic model of Alzheimer's disease', *Neurobiology of Aging*, 27(11), pp. 1658–1672. doi: 10.1016/j.neurobiolaging.2005.09.022.

Rangaraju, S. *et al.* (2015) 'Potassium Channel Kv1.3 Is Highly Expressed by Microglia in Human Alzheimer's Disease', *Journal of Alzheimer's disease : JAD*, 44(3), p. 797. doi: 10.3233/JAD-141704.

Rankin-Gee, E. K. *et al.* (2015) 'Perineuronal net degradation in epilepsy', *Epilepsia*, 56(7), pp. 1124–1133. doi: 10.1111/EPI.13026.

Rannikko, E. H., Weber, S. S. and Kahle, P. J. (2015) 'Exogenous α-synuclein induces toll-like receptor 4 dependent inflammatory responses in astrocytes', *BMC Neuroscience*, 16(1), p. 57. doi: 10.1186/S12868-015-0192-0.

Rao, Y. L. *et al.* (2022) 'Hippocampus and its involvement in Alzheimer's disease: a review', *3 Biotech*, 12(2), p. 55. doi: 10.1007/S13205-022-03123-4.

Rauschenberger, L. *et al.* (2022) 'Age-dependent neurodegeneration and neuroinflammation in a genetic A30P/A53T double-mutated α-synuclein mouse

model of Parkinson's disease', *Neurobiology of Disease*, 171, p. 105798. doi: 10.1016/J.NBD.2022.105798.

Reed, M. J. *et al.* (2019) 'Increased Hyaluronan and TSG-6 in Association with Neuropathologic Changes of Alzheimer's Disease', *Journal of Alzheimer's disease : JAD*, 67(1), p. 91. doi: 10.3233/JAD-180797.

Reemst, K. *et al.* (2016) 'The Indispensable Roles of Microglia and Astrocytes during Brain Development', *Frontiers in Human Neuroscience*, 10(NOV2016). doi: 10.3389/FNHUM.2016.00566.

Reichelt, A. C. *et al.* (2019) 'Perineuronal Nets: Plasticity, Protection, and Therapeutic Potential', *Trends in Neurosciences*, 42(7), pp. 458–470. doi: 10.1016/J.TINS.2019.04.003.

Reichelt, A. C. (2020) 'Is loss of perineuronal nets a critical pathological event in Alzheimer's disease?', *EBioMedicine*, 59. doi: 10.1016/J.EBIOM.2020.102946.

Reish, H. E. A. and Standaert, D. G. (2015) 'Role of α-synuclein in inducing innate and adaptive immunity in Parkinson disease', *Journal of Parkinson's disease*, 5(1), p. 1. doi: 10.3233/JPD-140491.

Ren, M. *et al.* (2007) 'Specialized inhibitory synaptic actions between nearby neocortical pyramidal neurons', *Science (New York, N.Y.)*, 316(5825), pp. 758–761. doi: 10.1126/SCIENCE.1135468.

Ren, S. Q. *et al.* (2018) 'Amyloid β causes excitation/inhibition imbalance through dopamine receptor 1-dependent disruption of fast-spiking GABAergic input in anterior cingulate cortex', *Scientific Reports*, 8(1). doi: 10.1038/S41598-017-18729-5.

Reynolds, A. D. *et al.* (2009) 'Nitrated α-Synuclein-Induced Alterations in Microglial Immunity Are Regulated by CD4+ T Cell Subsets', *The Journal of Immunology*, 182(7), pp. 4137–4149. doi: 10.4049/JIMMUNOL.0803982.

Rezaie, P. *et al.* (2005) 'Microglia in the Cerebral Wall of the Human Telencephalon at Second Trimester', *Cerebral Cortex*, 15(7), pp. 938–949. doi: 10.1093/CERCOR/BHH194.

Rezaie, P. and Male, D. (1999) 'Colonisation of the Developing Human Brain and

Spinal Cord by Microglia: A Review', *Microsc. Res. Tech*, 45, pp. 359–382. doi: 10.1002/(SICI)1097-0029(19990615)45:6.

Richardson, A. *et al.* (2022) 'Kv3.3 subunits control presynaptic action potential waveform and neurotransmitter release at a central excitatory synapse', *eLife*, 11. doi: 10.7554/ELIFE.75219.

Ridderinkhof, K. R. *et al.* (2004) 'The role of the medial frontal cortex in cognitive control', *Science (New York, N.Y.)*, 306(5695), pp. 443–447. doi: 10.1126/SCIENCE.1100301.

Rivera, E. J. *et al.* (2005) 'Insulin and insulin-like growth factor expression and function deteriorate with progression of Alzheimer's disease: link to brain reductions in acetylcholine', *Journal of Alzheimer's disease : JAD*, 8(3), pp. 247–268. doi: 10.3233/JAD-2005-8304.

Robel, S. (2017) 'Astroglial Scarring and Seizures: A Cell Biological Perspective on Epilepsy', *The Neuroscientist : a review journal bringing neurobiology, neurology and psychiatry*, 23(2), pp. 152–168. doi: 10.1177/1073858416645498.

Robson, E. *et al.* (2018) 'Impaired Fast Network Oscillations and Mitochondrial Dysfunction in a Mouse Model of Alpha-synucleinopathy (A30P)', *Neuroscience*, 377, pp. 161–173. doi: 10.1016/J.NEUROSCIENCE.2018.02.032.

Rocha, N. P., De Miranda, A. S. and Teixeira, A. L. (2015a) 'Insights into Neuroinflammation in Parkinson's Disease: From Biomarkers to Anti-Inflammatory Based Therapies', *BioMed Research International*, 2015. doi: 10.1155/2015/628192.

Rocha, N. P., De Miranda, A. S. and Teixeira, A. L. (2015b) 'Insights into Neuroinflammation in Parkinson's Disease: From Biomarkers to Anti-Inflammatory Based Therapies', *BioMed Research International*, 2015. doi: 10.1155/2015/628192.

Rodríguez-Moreno, A., Herreras, O. and Lerma, J. (1997) 'Kainate receptors presynaptically downregulate GABAergic inhibition in the rat hippocampus', *Neuron*, 19(4), pp. 893–901. doi: 10.1016/S0896-6273(00)80970-8.

Rodriguez-Moreno, A., López-Garcia, J. C. and Lerma, J. (2000) 'Two populations of kainate receptors with separate signaling mechanisms in hippocampal interneurons', *Proceedings of the National Academy of Sciences of the United States of America*,

97(3), p. 1293. doi: 10.1073/PNAS.97.3.1293.

Rodriguez-Oroz, M. C. *et al.* (2009) ‘Initial clinical manifestations of Parkinson’s disease: features and pathophysiological mechanisms’, *The Lancet. Neurology*, 8(12), pp. 1128–1139. doi: 10.1016/S1474-4422(09)70293-5.

Rodríguez, J. J. *et al.* (2008) ‘Astroglia in dementia and Alzheimer’s disease’, *Cell Death & Differentiation 2009 16:3*, 16(3), pp. 378–385. doi: 10.1038/cdd.2008.172.

Rogers, S. L. *et al.* (2018) ‘Normal development of the Perineuronal net in humans; in patients with and without epilepsy’, *Neuroscience*, 384, p. 350. doi: 10.1016/J.NEUROSCIENCE.2018.05.039.

Rojanathammanee, L., Murphy, E. J. and Combs, C. K. (2011) ‘Expression of mutant alpha-synuclein modulates microglial phenotype in vitro’, *Journal of neuroinflammation*, 8. doi: 10.1186/1742-2094-8-44.

Romberg, C. *et al.* (2013) ‘Depletion of perineuronal nets enhances recognition memory and long-term depression in the perirhinal cortex’, *The Journal of neuroscience : the official journal of the Society for Neuroscience*, 33(16), pp. 7057–7065. doi: 10.1523/JNEUROSCI.6267-11.2013.

Rose, J. and Woolsey, C. (1948) ‘The orbitofrontal cortex and its connections with the mediodorsal nucleus in rabbit, sheep and cat.’, *Research publications - Association for Research in Nervous and Mental Disease*.

Rossini, P. M. *et al.* (2006) ‘Conversion from mild cognitive impairment to Alzheimer’s disease is predicted by sources and coherence of brain electroencephalography rhythms’, *Neuroscience*, 143(3), pp. 793–803. doi: 10.1016/J.NEUROSCIENCE.2006.08.049.

Rossini, P. M. *et al.* (2007) ‘Clinical neurophysiology of aging brain: From normal aging to neurodegeneration’, *Progress in Neurobiology*, 83(6), pp. 375–400. doi: 10.1016/J.PNEUROBIO.2007.07.010.

Rossiter, H. E. *et al.* (2014) ‘Beta oscillations reflect changes in motor cortex inhibition in healthy ageing’, *NeuroImage*, 91, pp. 360–365. doi: 10.1016/J.NEUROIMAGE.2014.01.012.

Rossor, M. N. *et al.* (1982) ‘A POST-MORTEM STUDY OF THE CHOLINERGIC

AND GABA SYSTEMS IN SENILE DEMENTIA', *Brain*, 105(2), pp. 313–330. doi: 10.1093/BRAIN/105.2.313.

Rostami, J. *et al.* (2017) 'Human Astrocytes Transfer Aggregated Alpha-Synuclein via Tunneling Nanotubes', *The Journal of neuroscience : the official journal of the Society for Neuroscience*, 37(49), pp. 11835–11853. doi: 10.1523/JNEUROSCI.0983-17.2017.

Rostami, J. *et al.* (2021) 'Crosstalk between astrocytes and microglia results in increased degradation of α-synuclein and amyloid-β aggregates', *Journal of Neuroinflammation*, 18(1), pp. 1–20. doi: 10.1186/S12974-021-02158-3/FIGURES/9.

Rothé, M. *et al.* (2011) 'Coordination of High Gamma Activity in Anterior Cingulate and Lateral Prefrontal Cortical Areas during Adaptation', *The Journal of Neuroscience*, 31(31), p. 11110. doi: 10.1523/JNEUROSCI.1016-11.2011.

Le Roux, N. *et al.* (2008) 'Impaired GABAergic transmission disrupts normal homeostatic plasticity in rat cortical networks', *European Journal of Neuroscience*, 27(12), pp. 3244–3256. doi: 10.1111/J.1460-9568.2008.06288.X.

Rowlands, D. *et al.* (2018) 'Aggrecan Directs Extracellular Matrix-Mediated Neuronal Plasticity', *The Journal of Neuroscience*, 38(47), p. 10102. doi: 10.1523/JNEUROSCI.1122-18.2018.

Rudy, B. and McBain, C. J. (2001) 'Kv3 channels: voltage-gated K+ channels designed for high-frequency repetitive firing', *Trends in Neurosciences*, 24(9), pp. 517–526. doi: 10.1016/S0166-2236(00)01892-0.

Rupert, D. D. and Shea, S. D. (2022) 'Parvalbumin-Positive Interneurons Regulate Cortical Sensory Plasticity in Adulthood and Development Through Shared Mechanisms', *Frontiers in Neural Circuits*, 16, p. 886629. doi: 10.3389/FNCIR.2022.886629/BIBTEX.

Rushworth, M. F. S. *et al.* (2012) 'Valuation and decision-making in frontal cortex: one or many serial or parallel systems?', *Current opinion in neurobiology*, 22(6), pp. 946–955. doi: 10.1016/J.CONB.2012.04.011.

Russo, M. V. and McGavern, D. B. (2016) 'Inflammatory neuroprotection following traumatic brain injury', *Science (New York, N.Y.)*, 353(6301), pp. 783–785. doi:

10.1126/SCIENCE.AAF6260.

Saha, R. N. and Pahan, K. (2006) ‘Regulation of Inducible Nitric Oxide Synthase Gene in Glial Cells’, *Antioxidants & redox signaling*, 8(5–6), p. 929. doi: 10.1089/ARS.2006.8.929.

Sahlas, D. J. *et al.* (2002) ‘Clasmatodendrosis correlating with periventricular hyperintensity in mixed dementia’, *Annals of neurology*, 52(3), pp. 378–381. doi: 10.1002/ANA.10310.

Saijo, K., Crotti, A. and Glass, C. K. (2013) ‘Regulation of microglia activation and deactivation by nuclear receptors’, *Glia*, 61(1), pp. 104–111. doi: 10.1002/GLIA.22423.

Saijo, K. and Glass, C. K. (2011) ‘Microglial cell origin and phenotypes in health and disease’, *Nature reviews. Immunology*, 11(11), pp. 775–787. doi: 10.1038/NRI3086.

Sakai, K., Fukuda, T. and Iwadate, K. (2013) ‘Beading of the astrocytic processes (clasmatodendrosis) following head trauma is associated with protein degradation pathways’, *Brain injury*, 27(13–14), pp. 1692–1697. doi: 10.3109/02699052.2013.837198.

Saksela, O. and Laiho, M. (1997) ‘Growth factors in the extracellular matrix’, *FASEB journal : official publication of the Federation of American Societies for Experimental Biology*, 11(1), pp. 297–306. doi: 10.1096/FASEBJ.11.1.9034166.

Sale, A. *et al.* (2004) ‘Enriched environment and acceleration of visual system development’, *Neuropharmacology*, 47(5), pp. 649–660. doi: 10.1016/j.neuropharm.2004.07.008.

SAMORAJSKI, T. (1976) ‘How the human brain responds to aging’, *Journal of the American Geriatrics Society*, 24(1), pp. 4–11. doi: 10.1111/J.1532-5415.1976.TB03246.X.

Sancandi, M. *et al.* (2018) ‘Structural changes observed in the piriform cortex in a rat model of pre-motor Parkinson’s disease’, *Frontiers in Cellular Neuroscience*, 12, p. 423621. doi: 10.3389/FNCEL.2018.00479/BIBTEX.

Sano, F. *et al.* (2021) ‘Reactive astrocyte-driven epileptogenesis is induced by microglia initially activated following status epilepticus’, *JCI Insight*, 6(9). doi:

10.1172/JCI.INSIGHT.135391.

Sasaki, H. *et al.* (1986) 'Regional distribution of amino acid transmitters in postmortem brains of presenile and senile dementia of Alzheimer type', *Annals of Neurology*, 19(3), pp. 263–269. doi: 10.1002/ANA.410190307.

Satoh, J. ichi *et al.* (2016) 'TMEM119 marks a subset of microglia in the human brain', *Neuropathology : official journal of the Japanese Society of Neuropathology*, 36(1), pp. 39–49. doi: 10.1111/NEUP.12235.

Saur, L. *et al.* (2014) 'Physical exercise increases GFAP expression and induces morphological changes in hippocampal astrocytes', *Brain structure & function*, 219(1), pp. 293–302. doi: 10.1007/S00429-012-0500-8.

Savage, J. C., Carrier, M. and Tremblay, M. È. (2019) 'Morphology of Microglia Across Contexts of Health and Disease', *Methods in molecular biology (Clifton, N.J.)*, 2034, pp. 13–26. doi: 10.1007/978-1-4939-9658-2_2.

Scheiblich, H. *et al.* (2021) 'Microglia jointly degrade fibrillar alpha-synuclein cargo by distribution through tunneling nanotubes', *Cell*, 184(20), p. 5089. doi: 10.1016/J.CELL.2021.09.007.

Schell, H. *et al.* (2009) 'Nuclear and neuritic distribution of serine-129 phosphorylated α-synuclein in transgenic mice', *Neuroscience*, 160(4), pp. 796–804. doi: 10.1016/J.NEUROSCIENCE.2009.03.002.

Schell, M. J. *et al.* (1997) 'd-Serine as a Neuromodulator: Regional and Developmental Localizations in Rat Brain Glia Resemble NMDA Receptors', *The Journal of Neuroscience*, 17(5), p. 1604. doi: 10.1523/JNEUROSCI.17-05-01604.1997.

Schevon, C. A. *et al.* (2012) 'Evidence of an inhibitory restraint of seizure activity in humans', *Nature communications*, 3. doi: 10.1038/NCOMMS2056.

Schlossmann, J., Feil, R. and Hofmann, F. (2003) 'Signaling through NO and cGMP-dependent protein kinases', *Annals of medicine*, 35(1), pp. 21–27. doi: 10.1080/07853890310004093.

Schnitzler, A. and Gross, J. (2005) 'Normal and pathological oscillatory communication in the brain', *Nature Reviews Neuroscience 2005 6:4*, 6(4), pp. 285–

296. doi: 10.1038/nrn1650.

Scholefield, Z. *et al.* (2003) ‘Heparan sulfate regulates amyloid precursor protein processing by BACE1, the Alzheimer’s beta-secretase’, *The Journal of cell biology*, 163(1), pp. 97–107. doi: 10.1083/JCB.200303059.

Schuitemaker, A. *et al.* (2012) ‘Microglial activation in healthy aging’, *Neurobiology of aging*, 33(6), pp. 1067–1072. doi: 10.1016/J.NEUROBIOLAGING.2010.09.016.

Schumacher, J. *et al.* (2018) ‘Functional connectivity in dementia with Lewy bodies: A within- and between-network analysis’, *Human Brain Mapping*, 39(3), pp. 1118–1129. doi: 10.1002/HBM.23901.

Seeger, G. *et al.* (1994) ‘Mapping of perineuronal nets in the rat brain stained by colloidal iron hydroxide histochemistry and lectin cytochemistry’, *Neuroscience*, 58(2), pp. 371–388. doi: 10.1016/0306-4522(94)90044-2.

Serlin, Y. *et al.* (2015) ‘Anatomy and Physiology of the Blood-Brain Barrier’, *Seminars in cell & developmental biology*, 38, p. 2. doi: 10.1016/J.SEMCDB.2015.01.002.

Setiawan, E. *et al.* (2015) ‘Increased Translocator Protein Distribution Volume, A Marker of Neuroinflammation, in the Brain During Major Depressive Episodes’, *JAMA psychiatry*, 72(3), p. 268. doi: 10.1001/JAMAPSYCHIATRY.2014.2427.

Shackman, A. J. *et al.* (2011) ‘The Integration of Negative Affect, Pain, and Cognitive Control in the Cingulate Cortex’, *Nature reviews. Neuroscience*, 12(3), p. 154. doi: 10.1038/NRN2994.

Shah, N. H. and Aizenman, E. (2014) ‘VOLTAGE-GATED POTASSIUM CHANNELS AT THE CROSSROADS OF NEURONAL FUNCTION, ISCHEMIC TOLERANCE, AND NEURODEGENERATION’, *Translational stroke research*, 5(1), p. 38. doi: 10.1007/S12975-013-0297-7.

Shahmoradian, S. H. *et al.* (2019) ‘Lewy pathology in Parkinson’s disease consists of crowded organelles and lipid membranes’, *Nature Neuroscience 2019 22:7*, 22(7), pp. 1099–1109. doi: 10.1038/s41593-019-0423-2.

Sharaf, A., Krieglstein, K. and Spittau, B. (2013) ‘Distribution of microglia in the postnatal murine nigrostriatal system’, *Cell and tissue research*, 351(3), pp. 373–

382. doi: 10.1007/S00441-012-1537-Y.

Sheehan, B. (2012) ‘Assessment scales in dementia’, *Therapeutic Advances in Neurological Disorders*, 5(6), p. 349. doi: 10.1177/1756285612455733.

Shen, J. *et al.* (2014) ‘α-Synuclein amino terminus regulates mitochondrial membrane permeability’, *Brain Research*, 1591(1), pp. 14–26. doi: 10.1016/J.BRAINRES.2014.09.046.

Sheng, J. G., Mrak, R. E. and Griffin, W. S. T. (1998) ‘Enlarged and phagocytic, but not primed, interleukin-1 alpha-immunoreactive microglia increase with age in normal human brain’, *Acta neuropathologica*, 95(3), pp. 229–234. doi: 10.1007/S004010050792.

Shenhav, A., Botvinick, M. M. and Cohen, J. D. (2013) ‘The expected value of control: An integrative theory of anterior cingulate cortex function’, *Neuron*, 79(2), p. 217. doi: 10.1016/J.NEURON.2013.07.007.

Sherman, L. S. *et al.* (2002) ‘Hyaluronate-based extracellular matrix: keeping glia in their place’, *Glia*, 38(2), pp. 93–102. doi: 10.1002/GLIA.10053.

Sherman, L. S. *et al.* (2015) ‘Hyaluronan Synthesis, Catabolism, and Signaling in Neurodegenerative Diseases’, *International Journal of Cell Biology*, 2015. doi: 10.1155/2015/368584.

Shi, W. *et al.* (2019) ‘Perineuronal nets protect long-term memory by limiting activity-dependent inhibition from parvalbumin interneurons’, *Proceedings of the National Academy of Sciences of the United States of America*, 116(52), pp. 27063–27073. doi: 10.1073/PNAS.1902680116.

Shi, W. *et al.* (2022) ‘Whole-brain mapping of efferent projections of the anterior cingulate cortex in adult male mice’, *Molecular Pain*, 18, pp. 1–12. doi: 10.1177/17448069221094529.

Shibasaki, K. *et al.* (2017) ‘Glycine release from astrocytes via functional reversal of GlyT1’, *Journal of neurochemistry*, 140(3), pp. 395–403. doi: 10.1111/JNC.13741.

Shimojo, M. *et al.* (2020a) ‘Selective Disruption of Inhibitory Synapses Leading to Neuronal Hyperexcitability at an Early Stage of Tau Pathogenesis in a Mouse Model’, *Journal of Neuroscience*, 40(17), pp. 3491–3501. doi:

10.1523/JNEUROSCI.2880-19.2020.

Shimojo, M. *et al.* (2020b) ‘Selective Disruption of Inhibitory Synapses Leading to Neuronal Hyperexcitability at an Early Stage of Tau Pathogenesis in a Mouse Model’, *Journal of Neuroscience*, 40(17), pp. 3491–3501. doi: 10.1523/JNEUROSCI.2880-19.2020.

Shiri, Z. *et al.* (2015) ‘Interneuron activity leads to initiation of low-voltage fast-onset seizures’, *Annals of neurology*, 77(3), pp. 541–546. doi: 10.1002/ANA.24342.

Shiri, Z. *et al.* (2016) ‘Activation of specific neuronal networks leads to different seizure onset types’, *Annals of Neurology*, 79(3), pp. 354–365. doi: 10.1002/ANA.24570.

Sica, A. and Mantovani, A. (2012) ‘Macrophage plasticity and polarization: in vivo veritas’, *The Journal of Clinical Investigation*, 122(3), p. 787. doi: 10.1172/JCI59643.

Siddiqui, S. V. *et al.* (2008) ‘Neuropsychology of prefrontal cortex’, *Indian Journal of Psychiatry*, 50(3), p. 202. doi: 10.4103/0019-5545.43634.

Siegel, M., Donner, T. H. and Engel, A. K. (2012) ‘Spectral fingerprints of large-scale neuronal interactions’, *Nature Reviews Neuroscience 2012 13:2*, 13(2), pp. 121–134. doi: 10.1038/nrn3137.

Sigal, Y. M. *et al.* (2019) ‘Structural maturation of cortical perineuronal nets and their perforating synapses revealed by superresolution imaging’, *Proceedings of the National Academy of Sciences of the United States of America*, 116(14), pp. 7071–7076. doi: 10.1073/PNAS.1817222116/-/DCSUPPLEMENTAL.

Silva Albequerque, M. *et al.* (2015) ‘Regional and sub-regional differences in hippocampal GABAergic neuronal vulnerability in the TgCRND8 mouse model of Alzheimer’s disease’, *Frontiers in aging neuroscience*, 7(FEB). doi: 10.3389/FNAGI.2015.00030.

Singer, W. (2001) ‘Consciousness and the Binding Problem’, *Annals of the New York Academy of Sciences*, 929(1), pp. 123–146. doi: 10.1111/J.1749-6632.2001.TB05712.X.

Sofroniew, M. V. (2009) ‘Molecular dissection of reactive astrogliosis and glial scar formation’, *Trends in neurosciences*, 32(12), pp. 638–647. doi:

10.1016/J.TINS.2009.08.002.

Sofroniew, M. V. (2015) ‘Astrogliosis’, *Cold Spring Harbor Perspectives in Biology*, 7(2). doi: 10.1101/CSHPERSPECT.A020420.

Söllvander, S. *et al.* (2016) ‘Accumulation of amyloid-β by astrocytes result in enlarged endosomes and microvesicle-induced apoptosis of neurons’, *Molecular neurodegeneration*, 11(1). doi: 10.1186/S13024-016-0098-Z.

Somjen, G. G. (2002) ‘Ion Regulation in the Brain: Implications for Pathophysiology’, *http://dx.doi.org/10.1177/1073858402008003011*, 8(3), pp. 254–267. doi: 10.1177/1073858402008003011.

Song, I. and Dityatev, A. (2018) ‘Crosstalk between glia, extracellular matrix and neurons’, *Brain Research Bulletin*, 136, pp. 101–108. doi: 10.1016/J.BRAINRESBULL.2017.03.003.

Sorg, B. A. *et al.* (2016) ‘Casting a Wide Net: Role of Perineuronal Nets in Neural Plasticity’, *Journal of Neuroscience*, 36(45), pp. 11459–11468. doi: 10.1523/JNEUROSCI.2351-16.2016.

Souter, L. and Kwok, J. C. F. (2020) ‘Visualization of Perineuronal Nets in Central Nervous System Tissue Sections’, *Methods in molecular biology (Clifton, N.J.)*, 2043, pp. 251–260. doi: 10.1007/978-1-4939-9698-8_20.

Southwell, D. G. *et al.* (2010) ‘Cortical Plasticity Induced by Inhibitory Neuron Transplantation’, *Science (New York, N.Y.)*, 327(5969), p. 1145. doi: 10.1126/SCIENCE.1183962.

Spangenberg, E. E. *et al.* (2016) ‘Eliminating microglia in Alzheimer’s mice prevents neuronal loss without modulating amyloid-β pathology’, *Brain : a journal of neurology*, 139(Pt 4), pp. 1265–1281. doi: 10.1093/BRAIN/AWW016.

Specht, C. G. *et al.* (2005) ‘Subcellular localisation of recombinant alpha- and gamma-synuclein’, *Molecular and cellular neurosciences*, 28(2), pp. 326–334. doi: 10.1016/J.MCN.2004.09.017.

Spillantini, M. G. *et al.* (1997) ‘Alpha-synuclein in Lewy bodies’, *Nature*, 388(6645), pp. 839–840. doi: 10.1038/42166.

Stark, A. K. *et al.* (2004) ‘Glial cell loss in the anterior cingulate cortex, a subregion of the prefrontal cortex, in subjects with schizophrenia’, *The American journal of psychiatry*, 161(5), pp. 882–888. doi: 10.1176/APPI.AJP.161.5.882.

Stefanidou, M. *et al.* (2020) ‘Bi-directional association between epilepsy and dementia: The Framingham Heart Study’, *Neurology*, 95(24), p. e3241. doi: 10.1212/WNL.0000000000011077.

Von Stein, A. and Sarnthein, J. (2000) ‘Different frequencies for different scales of cortical integration: from local gamma to long range alpha/theta synchronization’, *International Journal of Psychophysiology*, 38(3), pp. 301–313. doi: 10.1016/S0167-8760(00)00172-0.

Stephenson, J. *et al.* (2018) ‘Inflammation in CNS neurodegenerative diseases’, *Immunology*, 154(2), pp. 204–219. doi: 10.1111/IMM.12922.

Steullet, P. *et al.* (2014) ‘Fast oscillatory activity in the anterior cingulate cortex: Dopaminergic modulation and effect of perineuronal net loss’, *Frontiers in Cellular Neuroscience*, 8(AUG), p. 244. doi: 10.3389/FNCEL.2014.00244/BIBTEX.

Stevens, B. *et al.* (2007) ‘The Classical Complement Cascade Mediates CNS Synapse Elimination’, *Cell*, 131(6), pp. 1164–1178. doi: 10.1016/j.cell.2007.10.036.

Stokholm, M. G. *et al.* (2017) ‘Assessment of neuroinflammation in patients with idiopathic rapid-eye-movement sleep behaviour disorder: a case-control study’, *The Lancet. Neurology*, 16(10), pp. 789–796. doi: 10.1016/S1474-4422(17)30173-4.

Stossel, T. P. (1993) ‘On the Crawling of Animal Cells’, *Science*, 260(5111), pp. 1086–1094. doi: 10.1126/SCIENCE.8493552.

Stoyka, L. E. *et al.* (2020) ‘Behavioral defects associated with amygdala and cortical dysfunction in mice with seeded α-synuclein inclusions’, *Neurobiology of disease*, 134. doi: 10.1016/J.NBD.2019.104708.

Streit, W. J. *et al.* (2004) ‘Dystrophic microglia in the aging human brain’, *Glia*, 45(2), pp. 208–212. doi: 10.1002/GLIA.10319.

Streit, W. J. (2006) ‘Microglial senescence: does the brain’s immune system have an expiration date?’, *Trends in Neurosciences*, 29(9), pp. 506–510. doi: 10.1016/j.tins.2006.07.001.

Streit, W. J. *et al.* (2008) ‘Microglial degeneration in the aging brain--bad news for neurons?’, *Frontiers in bioscience : a journal and virtual library*, 13(9), pp. 3423–3438. doi: 10.2741/2937.

Streit, W. J. and Xue, Q. S. (2016) ‘Microglia in dementia with Lewy bodies’, *Brain, Behavior, and Immunity*, 55, pp. 191–201. doi: 10.1016/J.BBI.2015.10.012.

Stylianou, M. *et al.* (2020) ‘Early Disruption of Cortical Sleep-Related Oscillations in a Mouse Model of Dementia With Lewy Bodies (DLB) Expressing Human Mutant (A30P) Alpha-Synuclein’, *Frontiers in Neuroscience*, 14, p. 983. doi: 10.3389/FNINS.2020.579867/BIBTEX.

Sugino, K. *et al.* (2005) ‘Molecular taxonomy of major neuronal classes in the adult mouse forebrain’, *Nature Neuroscience 2005 9:1*, 9(1), pp. 99–107. doi: 10.1038/nn1618.

Sugitani, K. *et al.* (2021) ‘Hyaluronan degradation and release of a hyaluronan-aggrecan complex from perineuronal nets in the aged mouse brain’, *Biochimica et biophysica acta. General subjects*, 1865(2). doi: 10.1016/J.BBAGEN.2020.129804.

Sultana, R. *et al.* (2021) ‘Perineuronal Nets in the Prefrontal Cortex of a Schizophrenia Mouse Model: Assessment of Neuroanatomical, Electrophysiological, and Behavioral Contributions’, *International Journal of Molecular Sciences*, 22(20). doi: 10.3390/IJMS222011140.

Summerfield, C. *et al.* (2005) ‘Structural Brain Changes in Parkinson Disease With Dementia: A Voxel-Based Morphometry Study’, *Archives of Neurology*, 62(2), pp. 281–285. doi: 10.1001/ARCHNEUR.62.2.281.

Surendranathan, A. *et al.* (2018) ‘Early microglial activation and peripheral inflammation in dementia with Lewy bodies’. doi: 10.1093/brain/awy265.

Suttkus, A. *et al.* (2012) ‘Neuroprotection against iron-induced cell death by perineuronal nets - an in vivo analysis of oxidative stress’, *American Journal of Neurodegenerative Disease*, 1(2), p. 122. Available at: /pmc/articles/PMC3560462/ (Accessed: 24 September 2024).

Suttkus, A. *et al.* (2016) ‘The neuronal extracellular matrix restricts distribution and internalization of aggregated Tau-protein’, *Neuroscience*, 313, pp. 225–235. doi:

10.1016/J.NEUROSCIENCE.2015.11.040.

Szaflarski, J. P. (2021) ‘Epilepsy and Neurodegeneration: A Bidirectional Relationship’, *Epilepsy Currents*, 21(2), p. 102. doi: 10.1177/1535759721989668.

Szego, É. M. *et al.* (2013) ‘Impairment of the septal cholinergic neurons in MPTP-treated A30P α-synuclein mice’, *Neurobiology of Aging*, 34(2), pp. 589–601. doi: 10.1016/J.NEUROBIOLAGING.2012.04.012.

Tachibana, M. *et al.* (2019) ‘Clasmatodendrosis is associated with dendritic spines and does not represent autophagic astrocyte death in influenza-associated encephalopathy’, *Brain & development*, 41(1), pp. 85–95. doi: 10.1016/J.BRAINDEV.2018.07.008.

Taguchi, K. *et al.* (2014) ‘Differential expression of alpha-synuclein in hippocampal neurons’, *PloS one*, 9(2). doi: 10.1371/JOURNAL.PONE.0089327.

Takahashi, H. *et al.* (2010) ‘Hippocampal interneuron loss in an APP/PS1 double mutant mouse and in Alzheimer’s disease’, *Brain structure & function*, 214(2–3), p. 145. doi: 10.1007/S00429-010-0242-4.

Takashima, H. *et al.* (2022) ‘In vivo Illustration of Altered Dopaminergic and GABAergic Systems in Early Parkinson’s Disease’, *Frontiers in Neurology*, 13, p. 880407. doi: 10.3389/FNEUR.2022.880407/BIBTEX.

Takata, K. *et al.* (2010) ‘Galantamine-induced amyloid-{beta} clearance mediated via stimulation of microglial nicotinic acetylcholine receptors’, *The Journal of biological chemistry*, 285(51), pp. 40180–40191. doi: 10.1074/JBC.M110.142356.

Takata, N. and Hirase, H. (2008) ‘Cortical Layer 1 and Layer 2/3 Astrocytes Exhibit Distinct Calcium Dynamics In Vivo’, *PLoS ONE*, 3(6), p. 2525. doi: 10.1371/JOURNAL.PONE.0002525.

Tambuyzer, B. R., Ponsaerts, P. and Nouwen, E. J. (2009) ‘Microglia: gatekeepers of central nervous system immunology’, *Journal of Leukocyte Biology*, 85(3), pp. 352–370. doi: 10.1189/JLB.0608385.

Tang, Y. *et al.* (2014) ‘Cortical plasticity induced by transplantation of embryonic somatostatin or parvalbumin interneurons’, *Proceedings of the National Academy of Sciences of the United States of America*, 111(51), pp. 18339–18344. doi:

10.1073/PNAS.1421844112/-/DCSUPPLEMENTAL.

Tang, Y. and Le, W. (2016) ‘Differential Roles of M1 and M2 Microglia in Neurodegenerative Diseases’, *Molecular neurobiology*, 53(2), pp. 1181–1194. doi: 10.1007/S12035-014-9070-5.

Tanti, A. *et al.* (2022) ‘Child abuse associates with increased recruitment of perineuronal nets in the ventromedial prefrontal cortex: a possible implication of oligodendrocyte progenitor cells’, *Molecular psychiatry*, 27(3), pp. 1552–1561. doi: 10.1038/S41380-021-01372-Y.

Tarasov, V. V. *et al.* (2019) ‘Alterations of Astrocytes in the Context of Schizophrenic Dementia’, *Frontiers in Pharmacology*, 10. doi: 10.3389/FPHAR.2019.01612.

Tarkowski, E. *et al.* (2003) ‘Intrathecal inflammation precedes development of Alzheimer’s disease’, *Journal of Neurology, Neurosurgery, and Psychiatry*, 74(9), p. 1200. doi: 10.1136/JNNP.74.9.1200.

Taylor, J. P. *et al.* (2011) ‘Visual hallucinations in dementia with Lewy bodies: transcranial magnetic stimulation study’, *The British Journal of Psychiatry*, 199(6), p. 492. doi: 10.1192/BJP.BP.110.090373.

Taylor, T. N. *et al.* (2014) ‘Region-specific deficits in dopamine, but not norepinephrine, signaling in a novel A30P α-synuclein BAC transgenic mouse’, *Neurobiology of Disease*, 62, pp. 193–207. doi: 10.1016/J.NBD.2013.10.005.

Tchieu, J. *et al.* (2019) ‘NFIA is a gliogenic switch enabling rapid derivation of functional human astrocytes from pluripotent stem cells’, *Nature biotechnology*, 37(3), p. 267. doi: 10.1038/S41587-019-0035-0.

Teaktong, T. *et al.* (2005) ‘Muscarinic M2 and M4 receptors in anterior cingulate cortex: relation to neuropsychiatric symptoms in dementia with Lewy bodies’, *Behavioural brain research*, 161(2), pp. 299–305. doi: 10.1016/J.BBR.2005.02.019.

Testa, D., Prochiantz, A. and Di Nardo, A. A. (2019) ‘Perineuronal nets in brain physiology and disease’, *Seminars in cell & developmental biology*, 89, pp. 125–135. doi: 10.1016/J.SEMCDB.2018.09.011.

Tewari, B. P. *et al.* (2018) ‘Perineuronal nets decrease membrane capacitance of peritumoral fast spiking interneurons in a model of epilepsy’, *Nature*

Communications, 9(1). doi: 10.1038/S41467-018-07113-0.

Tewari, B. P. and Sontheimer, H. (2019) 'Protocol to quantitatively assess the structural integrity of Perineuronal Nets ex vivo', *Bio-protocol*, 9(10). doi: 10.21769/BIOPROTOC.3234.

Théry, M. *et al.* (2005) 'The extracellular matrix guides the orientation of the cell division axis', *Nature Cell Biology 2005 7:10*, 7(10), pp. 947–953. doi: 10.1038/ncb1307.

Timofeev, I., Grenier, F. and Steriade, M. (2004) 'Contribution of intrinsic neuronal factors in the generation of cortically driven electrographic seizures', *Journal of Neurophysiology*, 92(2), pp. 1133–1143. doi: 10.1152/jn.00523.2003.

Tiraboschi, P. *et al.* (2000) 'Cholinergic dysfunction in diseases with LEWY bodies', *Neurology*, 54(2), pp. 407–411. doi: 10.1212/WNL.54.2.407.

Tomimoto, H. *et al.* (1997) 'Regressive changes of astroglia in white matter lesions in cerebrovascular disease and Alzheimer's disease patients', *Acta neuropathologica*, 94(2), pp. 146–152. doi: 10.1007/S004010050686.

Tranel, D., Cooper, G. and Rodnitzky, R. L. (2003) 'Higher Brain Functions', *Neuroscience in Medicine*, pp. 621–639. doi: 10.1007/978-1-59259-371-2_29.

Traynelis, S. F. and Dingledine, R. (1988) 'Potassium-induced spontaneous electrographic seizures in the rat hippocampal slice', *https://doi.org/10.1152/jn.1988.59.1.259*, 59(1), pp. 259–276. doi: 10.1152/JN.1988.59.1.259.

Tremblay, M. È. *et al.* (2012) 'Effects of aging and sensory loss on glial cells in mouse visual and auditory cortices', *Glia*, 60(4), p. 541. doi: 10.1002/GLIA.22287.

Tremblay, R., Lee, S. and Rudy, B. (2016) 'GABAergic Interneurons in the Neocortex: From Cellular Properties to Circuits', *Neuron*. Cell Press, pp. 260–292. doi: 10.1016/j.neuron.2016.06.033.

Trushina, E. and McMurray, C. T. (2007) 'Oxidative stress and mitochondrial dysfunction in neurodegenerative diseases', *Neuroscience*, 145(4), pp. 1233–1248. doi: 10.1016/J.NEUROSCIENCE.2006.10.056.

Tsigelny, I. F. *et al.* (2012) ‘Role of α-synuclein penetration into the membrane in the mechanisms of oligomer pore formation’, *The FEBS Journal*, 279(6), pp. 1000–1013. doi: 10.1111/J.1742-4658.2012.08489.X.

Tweedy, C. *et al.* (2021) ‘Hippocampal network hyperexcitability in young transgenic mice expressing human mutant alpha-synuclein’, *Neurobiology of Disease*, 149. doi: 10.1016/J.NBD.2020.105226.

Twohig, D. and Nielsen, H. M. (2019) ‘α-synuclein in the pathophysiology of Alzheimer’s disease’, *Molecular Neurodegeneration 2019 14:1*, 14(1), pp. 1–19. doi: 10.1186/S13024-019-0320-X.

Tzeng, S. F., Hsiao, H. Y. and Mak, O. T. (2005) ‘Prostaglandins and cyclooxygenases in glial cells during brain inflammation’, *Current drug targets. Inflammation and allergy*, 4(3), pp. 335–340. doi: 10.2174/1568010054022051.

Ueno, H. *et al.* (2017) ‘Parvalbumin neurons and perineuronal nets in the mouse prefrontal cortex’, *Neuroscience*, 343, pp. 115–127. doi: 10.1016/j.neuroscience.2016.11.035.

Ueno, H. *et al.* (2018) ‘Expression of aggrecan components in perineuronal nets in the mouse cerebral cortex’, *IBRO Reports*, 4, pp. 22–37. doi: 10.1016/J.IBROR.2018.01.002.

Ueno, H., Suemitsu, S., *et al.* (2019) ‘Alteration of Extracellular Matrix Molecules and Perineuronal Nets in the Hippocampus of Pentylenetetrazol-Kindled Mice’, *Neural Plasticity*, 2019. doi: 10.1155/2019/8924634.

Ueno, H., Fujii, K., *et al.* (2019) ‘Alteration of parvalbumin expression and perineuronal nets formation in the cerebral cortex of aged mice’, *Molecular and Cellular Neuroscience*, 95, pp. 31–42. doi: 10.1016/J.MCN.2018.12.008.

Ueno, S. *et al.* (1997) ‘Bicuculline and Gabazine Are Allosteric Inhibitors of Channel Opening of the GABAA Receptor’, *The Journal of Neuroscience*, 17(2), p. 625. doi: 10.1523/JNEUROSCI.17-02-00625.1997.

Ullsperger, M. *et al.* (2014) ‘Neural mechanisms and temporal dynamics of performance monitoring’, *Trends in cognitive sciences*, 18(5), pp. 259–267. doi: 10.1016/J.TICS.2014.02.009.

Umpierre, C. C., Little, S. A. and Mirkes, P. E. (2001) ‘Co-localization of active caspase-3 and DNA fragmentation (TUNEL) in normal and hyperthermia-induced abnormal mouse development’, *Teratology*, 63(3), pp. 134–143. doi: 10.1002/TERA.1024.

Vargas, M. R. *et al.* (2008) ‘Nrf2 activation in astrocytes protects against neurodegeneration in mouse models of familial amyotrophic lateral sclerosis’, *The Journal of neuroscience : the official journal of the Society for Neuroscience*, 28(50), pp. 13574–13581. doi: 10.1523/JNEUROSCI.4099-08.2008.

Vasile, F., Dossi, E. and Rouach, N. (2017) ‘Human astrocytes: structure and functions in the healthy brain’, *Brain Structure & Function*, 222(5), p. 2017. doi: 10.1007/S00429-017-1383-5.

Vasili, E., Dominguez-Meijide, A. and Outeiro, T. F. (2019) ‘Spreading of α-synuclein and tau: A systematic comparison of the mechanisms involved’, *Frontiers in Molecular Neuroscience*, 12, p. 107. doi: 10.3389/FNMOL.2019.00107/BIBTEX.

Vasudevaraju, P. *et al.* (2012) ‘New evidence on α-synuclein and Tau binding to conformation and sequence specific GC* rich DNA: Relevance to neurological disorders’, *Journal of Pharmacy & Bioallied Sciences*, 4(2), p. 112. doi: 10.4103/0975-7406.94811.

Vaughan, D. W. and Peters, A. (1974) ‘Neuroglial cells in the cerebral cortex of rats from young adulthood to old age: an electron microscope study’, *Journal of neurocytology*, 3(4), pp. 405–429. doi: 10.1007/BF01098730.

Vedunova, M. *et al.* (2013) ‘Seizure-like activity in hyaluronidase-treated dissociated hippocampal cultures’, *Frontiers in Cellular Neuroscience*, 7(SEP), p. 149. doi: 10.3389/FNCEL.2013.00149/BIBTEX.

Végh, M. J. *et al.* (2014) ‘Reducing hippocampal extracellular matrix reverses early memory deficits in a mouse model of Alzheimer’s disease’, *Acta Neuropathologica Communications*, 2(1). doi: 10.1186/S40478-014-0076-Z.

Verguts, T., Vassena, E. and Silvetti, M. (2015) ‘Adaptive effort investment in cognitive and physical tasks: a neurocomputational model’, *Frontiers in Behavioral Neuroscience*, 9, p. 57. doi: 10.3389/FNBEH.2015.00057.

Verhoog, Q. P. *et al.* (2020) ‘Astrocytes as Guardians of Neuronal Excitability: Mechanisms Underlying Epileptogenesis’, *Frontiers in Neurology*, 11, p. 591690. doi: 10.3389/FNEUR.2020.591690.

Verkhratsky, A. *et al.* (2010) ‘Astrocytes in Alzheimer’s Disease’, *Neurotherapeutics*, 7(4), pp. 399–412. doi: 10.1016/J.NURT.2010.05.017.

Vesikansa, A. *et al.* (2007) ‘Activation of kainate receptors controls the number of functional glutamatergic synapses in the area CA1 of rat hippocampus’, *Journal of Physiology*, 583(1), pp. 145–157. doi: 10.1113/JPHYSIOL.2007.133975.

Vezzani, A. *et al.* (2011) ‘The role of inflammation in epilepsy’, *Nature Reviews. Neurology*, 7(1), p. 31. doi: 10.1038/NRNEUROL.2010.178.

Vezzani, A. and Viviani, B. (2015) ‘Neuromodulatory properties of inflammatory cytokines and their impact on neuronal excitability’, *Neuropharmacology*, 96(Pt A), pp. 70–82. doi: 10.1016/J.NEUROPHARM.2014.10.027.

Vicente, M., Addo-Osafo, K. and Vossel, K. (2024) ‘Latest advances in mechanisms of epileptic activity in Alzheimer’s disease and dementia with Lewy Bodies’, *Frontiers in Neurology*, 15, p. 1277613. doi: 10.3389/FNEUR.2024.1277613.

Viitanen, T. *et al.* (2010) ‘The K+-Cl cotransporter KCC2 promotes GABAergic excitation in the mature rat hippocampus’, *The Journal of physiology*, 588(Pt 9), pp. 1527–1540. doi: 10.1113/JPHYSIOL.2009.181826.

Vogt, B. A. *et al.* (2013) ‘Cingulate area 32 homologies in mouse, rat, macaque and human: Cytoarchitecture and receptor architecture’, *Journal of Comparative Neurology*, 521(18), pp. 4189–4204. doi: 10.1002/cne.23409.

Vogt, B. A. and Paxinos, G. (2014) ‘Cytoarchitecture of mouse and rat cingulate cortex with human homologies’, *Brain Structure and Function*, 219(1), pp. 185–192. doi: 10.1007/s00429-012-0493-3.

Volterra, A. and Meldolesi, J. (2005) ‘Astrocytes, from brain glue to communication elements: the revolution continues’, *Nature reviews. Neuroscience*, 6(8), pp. 626–640. doi: 10.1038/NRN1722.

Vossel, K. A. *et al.* (2013) ‘Seizures and Epileptiform Activity in the Early Stages of Alzheimer Disease’, *JAMA Neurology*, 70(9), pp. 1158–1166. doi:

10.1001/JAMANEUROL.2013.136.

Vosskuhl, J., Strüber, D. and Herrmann, C. S. (2018) ‘Non-invasive Brain Stimulation: A Paradigm Shift in Understanding Brain Oscillations’, *Frontiers in Human Neuroscience*, 12, p. 344261. doi: 10.3389/FNHUM.2018.00211/BIBTEX.

De Waal, F. B. M. and Preston, S. D. (2017) ‘Mammalian empathy: behavioural manifestations and neural basis’, *Nature Reviews Neuroscience 2017 18:8*, 18(8), pp. 498–509. doi: 10.1038/nrn.2017.72.

Wakabayashi, K. *et al.* (1988) ‘Parkinson’s disease: the presence of Lewy bodies in Auerbach’s and Meissner’s plexuses’, *Acta neuropathologica*, 76(3), pp. 217–221. doi: 10.1007/BF00687767.

Wakabayashi, K. *et al.* (2000) ‘NACP/alpha-synuclein-positive filamentous inclusions in astrocytes and oligodendrocytes of Parkinson’s disease brains’, *Acta neuropathologica*, 99(1), pp. 14–20. doi: 10.1007/PL00007400.

Wakabayashi, K. *et al.* (2007) ‘The Lewy body in Parkinson’s disease: molecules implicated in the formation and degradation of alpha-synuclein aggregates’, *Neuropathology : official journal of the Japanese Society of Neuropathology*, 27(5), pp. 494–506. doi: 10.1111/J.1440-1789.2007.00803.X.

Wakabayashi, K. *et al.* (2013) ‘The Lewy body in Parkinson’s disease and related neurodegenerative disorders’, *Molecular neurobiology*, 47(2), pp. 495–508. doi: 10.1007/S12035-012-8280-Y.

Wake, H. *et al.* (2009) ‘Resting microglia directly monitor the functional state of synapses in vivo and determine the fate of ischemic terminals’, *J Neurosci*, 29, pp. 3974–3980.

Walker, D. G. *et al.* (2013) ‘Changes in Properties of Serine 129 Phosphorylated α-Synuclein with Progression of Lewy Type Histopathology in Human Brains’, *Experimental neurology*, 240(1), p. 190. doi: 10.1016/J.EXPNEUROL.2012.11.020.

Walker, D. G. and Lue, L. F. (2015) ‘Immune phenotypes of microglia in human neurodegenerative disease: challenges to detecting microglial polarization in human brains’, *Alzheimer’s Research & Therapy*, 7(1). doi: 10.1186/S13195-015-0139-9.

Waller, R. *et al.* (2019) ‘Iba-1-/CD68+ microglia are a prominent feature of age-

associated deep subcortical white matter lesions', *PLoS ONE*, 14(1). doi: 10.1371/JOURNAL.PONE.0210888.

Wang, C. *et al.* (2023) 'The effects of microglia-associated neuroinflammation on Alzheimer's disease', *Frontiers in Immunology*, 14, p. 1117172. doi: 10.3389/FIMMU.2023.1117172/BIBTEX.

Wang, D. D. and Bordey, A. (2008) 'The Astrocyte Odyssey', *Progress in neurobiology*, 86(4), p. 342. doi: 10.1016/J.PNEUROBIO.2008.09.015.

Wang, D. and Fawcett, J. (2012) 'The perineuronal net and the control of CNS plasticity', *Cell and tissue research*, 349(1), pp. 147–160. doi: 10.1007/S00441-012-1375-Y.

Wang, H. *et al.* (2008) 'Chondroitin-4-sulfation negatively regulates axonal guidance and growth', *Journal of cell science*, 121(Pt 18), pp. 3083–3091. doi: 10.1242/JCS.032649.

Wang, J. *et al.* (2020) 'Effect of Fasudil on remyelination following cuprizone-induced demyelination', *CNS Neuroscience & Therapeutics*, 26(1), p. 76. doi: 10.1111/CNS.13154.

Wang, L. *et al.* (2006) 'Changes in hippocampal connectivity in the early stages of Alzheimer's disease: evidence from resting state fMRI', *NeuroImage*, 31(2), pp. 496–504. doi: 10.1016/J.NEUROIMAGE.2005.12.033.

Wang, W., Wang, J. and Li, F. (2017) 'Hyaluronidase and chondroitinase', *Advances in Experimental Medicine and Biology*, 925, pp. 75–87. doi: 10.1007/5584_2016_54/FIGURES/4.

Wang, X. *et al.* (2006) 'Astrocytic Ca2+ signaling evoked by sensory stimulation in vivo', *Nature neuroscience*, 9(6), pp. 816–823. doi: 10.1038/NN1703.

Watrous, A. J. *et al.* (2015) 'More than spikes: common oscillatory mechanisms for content specific neural representations during perception and memory', *Current Opinion in Neurobiology*, 31, pp. 33–39. doi: 10.1016/J.CONB.2014.07.024.

Wen, T. H. *et al.* (2018) 'The Perineuronal "Safety" Net? Perineuronal Net Abnormalities in Neurological Disorders', *Frontiers in Molecular Neuroscience*, 11, p. 270. doi: 10.3389/FNMOL.2018.00270/BIBTEX.

Wennström, M. *et al.* (2015) ‘Cerebrospinal fluid levels of IL-6 are decreased and correlate with cognitive status in DLB patients’, *Alzheimer’s Research & Therapy*, 7(1). doi: 10.1186/S13195-015-0145-Y.

Whittington, M. A. *et al.* (2011) ‘Multiple origins of the cortical gamma rhythm’, *Developmental Neurobiology*, 71(1), pp. 92–106. doi: 10.1002/DNEU.20814.

Whittington, M. A., Traub, R. D. and Jefferys, J. G. R. (1995) ‘Synchronized oscillations in interneuron networks driven by metabotropic glutamate receptor activation’, *Nature 1995 373:6515*, 373(6515), pp. 612–615. doi: 10.1038/373612a0.

Wilhelmsson, U. *et al.* (2006) ‘Redefining the concept of reactive astrocytes as cells that remain within their unique domains upon reaction to injury’, *Proceedings of the National Academy of Sciences of the United States of America*, 103(46), p. 17513. doi: 10.1073/PNAS.0602841103.

Womelsdorf, T. and Fries, P. (2006) ‘Neuronal coherence during selective attentional processing and sensory–motor integration’, *Journal of Physiology-Paris*, 100(4), pp. 182–193. doi: 10.1016/J.JPHYSPARIS.2007.01.005.

Wu, Z. *et al.* (2021) ‘Cell death of hippocampal CA1 astrocytes during early epileptogenesis’, *Epilepsia*, 62(7), pp. 1569–1583. doi: 10.1111/EPI.16910.

Wu, Z. Z. *et al.* (2009) ‘Aminopyridines Potentiate Synaptic and Neuromuscular Transmission by Targeting the Voltage-activated Calcium Channel β Subunit’, *The Journal of Biological Chemistry*, 284(52), p. 36453. doi: 10.1074/JBC.M109.075523.

Wyss-Coray, T. and Mucke, L. (2002) ‘Inflammation in neurodegenerative disease - A double-edged sword’, *Neuron*, 35(3), pp. 419–432. doi: 10.1016/S0896-6273(02)00794-8.

Xu, P. *et al.* (2019) ‘Translational Physiology: Medial prefrontal cortex in neurological diseases’, *Physiological Genomics*, 51(9), p. 432. doi: 10.1152/PHYSIOLGENOMICS.00006.2019.

Xue, M. *et al.* (2022) ‘Mapping thalamic-anterior cingulate monosynaptic inputs in adultmice’, *Molecular Pain*, 18, pp. 1–13. doi: 10.1177/17448069221087034.

Xue, M., Atallah, B. V and Scanziani, M. (2014) ‘Equalizing excitation-inhibition ratios across visual cortical neurons’, *Nature*. 2014/07/22, 511(7511), pp. 596–600. doi:

10.1038/nature13321.

Yamada, J., Ohgomori, T. and Jinno, S. (2015) ‘Perineuronal nets affect parvalbumin expression in GABAergic neurons of the mouse hippocampus’, *The European journal of neuroscience*, 41(3), pp. 368–378. doi: 10.1111/EJN.12792.

Yamada, K. M. *et al.* (2019) ‘Extracellular matrix dynamics in cell migration, invasion and tissue morphogenesis’, *International Journal of Experimental Pathology*, 100(3), pp. 144–152. doi: 10.1111/IEP.12329.

Yamakage, Y. *et al.* (2019) ‘Reducing ADAMTS-3 Inhibits Amyloid β Deposition in App Knock-in Mouse’, *Biological and Pharmaceutical Bulletin*, 42(3), pp. 354–356. doi: 10.1248/BPB.B18-00899.

Yamasaki, T. R. *et al.* (2019) ‘Parkinson’s disease and multiple system atrophy have distinct α-synuclein seed characteristics’, *The Journal of Biological Chemistry*, 294(3), p. 1045. doi: 10.1074/JBC.RA118.004471.

Yan, J. *et al.* (2017) ‘Quantitative proteomics in A30P*A53T α-synuclein transgenic mice reveals upregulation of Sel1l’, *PLOS ONE*, 12(8), p. e0182092. doi: 10.1371/JOURNAL.PONE.0182092.

Yan, L.-J. *et al.* (2013) ‘Metabolic Dysfunction of Astrocyte: An Initiating Factor in Beta-amyloid Pathology?’, *Aging and neurodegeneration*, 1(1), p. 7. Available at: /pmc/articles/PMC3891850/ (Accessed: 12 March 2024).

Yang, H. *et al.* (2019) ‘C-Fos mapping and EEG characteristics of multiple mice brain regions in pentylenetetrazol-induced seizure mice model’, *Neurological Research*, 41(8), pp. 749–761. doi: 10.1080/01616412.2019.1610839.

Yang, S. *et al.* (2015) ‘Perineuronal net digestion with chondroitinase restores memory in mice with tau pathology’, *Experimental neurology*, 265, pp. 48–58. doi: 10.1016/J.EXPNEUROL.2014.11.013.

Yang, S. *et al.* (2017) ‘Antibody recognizing 4-sulfated chondroitin sulfate proteoglycans restores memory in tauopathy-induced neurodegeneration’, *Neurobiology of aging*, 59, pp. 197–209. doi: 10.1016/J.NEUROBIOLAGING.2017.08.002.

Yang, S. *et al.* (2021) ‘Chondroitin 6-sulphate is required for neuroplasticity and

memory in ageing', *Molecular Psychiatry 2021 26:10*, 26(10), pp. 5658–5668. doi: 10.1038/s41380-021-01208-9.

Yang, Z. and Wang, K. K. W. (2015) 'Glial Fibrillary acidic protein: From intermediate filament assembly and gliosis to neurobiomarker', *Trends in neurosciences*, 38(6), p. 364. doi: 10.1016/J.TINS.2015.04.003.

Yao, J. A. and Tseng, G. N. (1994) 'Modulation of 4-AP block of a mammalian A-type K channel clone by channel gating and membrane voltage.', *Biophysical Journal*, 67(1), p. 130. doi: 10.1016/S0006-3495(94)80462-X.

Ye, T. *et al.* (2023) 'Theta oscillations in anterior cingulate cortex and orbitofrontal cortex differentially modulate accuracy and speed in flexible reward learning', *Oxford open neuroscience*, 2. doi: 10.1093/OONS/KVAD005.

Yekhlef, L. *et al.* (2015) 'Selective activation of parvalbumin- or somatostatin-expressing interneurons triggers epileptic seizurelike activity in mouse medial entorhinal cortex', *Journal of Neurophysiology*, 113(5), pp. 1616–1630. doi: 10.1152/jn.00841.2014.

Yener, G. G. and Başar, E. (2013) 'Biomarkers in Alzheimer's disease with a special emphasis on event-related oscillatory responses', *Supplements to Clinical Neurophysiology*, 62, pp. 237–273. doi: 10.1016/B978-0-7020-5307-8.00020-X.

Yin, F., Boveris, A. and Cadenas, E. (2014) 'Mitochondrial energy metabolism and redox signaling in brain aging and neurodegeneration', *Antioxidants & redox signaling*, 20(2), pp. 353–371. doi: 10.1089/ARS.2012.4774.

Yong, S. W. *et al.* (2007) 'A comparison of cerebral glucose metabolism in Parkinson's disease, Parkinson's disease dementia and dementia with Lewy bodies', *European journal of neurology*, 14(12), pp. 1357–1362. doi: 10.1111/J.1468-1331.2007.01977.X.

Yoon, B. E. and Lee, C. J. (2014) 'GABA as a rising gliotransmitter', *Frontiers in Neural Circuits*, 8(DEC). doi: 10.3389/FNCIR.2014.00141.

Yu, C., Deng, X. jun and Xu, D. (2023) 'Microglia in epilepsy', *Neurobiology of disease*, 185. doi: 10.1016/J.NBD.2023.106249.

Yu, P., Pearson, C. S. and Geller, H. M. (2018) 'Flexible Roles for Proteoglycan

Sulfation and Receptor Signaling', *Trends in neurosciences*, 41(1), pp. 47–61. doi: 10.1016/J.TINS.2017.10.005.

Yuan, Y. *et al.* (2008) 'Overexpressed alpha-synuclein regulated the nuclear factor-kappaB signal pathway', *Cellular and molecular neurobiology*, 28(1), pp. 21–33. doi: 10.1007/S10571-007-9185-6.

Yuko, S. *et al.* (2003) 'Accumulation of phosphorylated alpha-synuclein in aging human brain', *Journal of neuropathology and experimental neurology*, 62(6), pp. 644–654. doi: 10.1093/JNEN/62.6.644.

Zeisel, A. *et al.* (2018) 'Molecular Architecture of the Mouse Nervous System', *Cell*, 174(4), pp. 999-1014.e22. doi: 10.1016/j.cell.2018.06.021.

Zhang, J. *et al.* (2002) 'c-fos regulates neuronal excitability and survival', *Nature Genetics 2002 30:4*, 30(4), pp. 416–420. doi: 10.1038/ng859.

Zhang, J. M. *et al.* (2003) 'ATP Released by Astrocytes Mediates Glutamatergic Activity-Dependent Heterosynaptic Suppression', *Neuron*, 40(5), pp. 971–982. doi: 10.1016/S0896-6273(03)00717-7.

Zhang, L. and McBain, C. J. (1995) 'Potassium conductances underlying repolarization and after-hyperpolarization in rat CA1 hippocampal interneurones.', *The Journal of Physiology*, 488(Pt 3), p. 661. doi: 10.1113/JPHYSIOL.1995.SP020998.

Zhang, S. *et al.* (2018) 'Intercellular transfer of pathogenic α-synuclein by extracellular vesicles is induced by the lipid peroxidation product 4-hydroxynonenal', *Neurobiology of aging*, 61, p. 52. doi: 10.1016/J.NEUROBIOLAGING.2017.09.016.

Zhang, W. *et al.* (2016) 'Hyperactive Somatostatin Interneurons Contribute to Excitotoxicity in Neurodegenerative Disorders', *Nature neuroscience*, 19(4), p. 557. doi: 10.1038/NN.4257.

Zhang, Wei *et al.* (2005) 'Aggregated alpha-synuclein activates microglia: a process leading to disease progression in Parkinson's disease', *FASEB journal : official publication of the Federation of American Societies for Experimental Biology*, 19(6), pp. 533–542. doi: 10.1096/FJ.04-2751COM.

Zhao, W. *et al.* (2006) 'Protective effects of an anti-inflammatory cytokine,

interleukin-4, on motoneuron toxicity induced by activated microglia', *Journal of neurochemistry*, 99(4), pp. 1176–1187. doi: 10.1111/J.1471-4159.2006.04172.X.

Zheng, C. *et al.* (2016) 'Fast Gamma Rhythms in the Hippocampus Promote Encoding of Novel Object–Place Pairings', *eNeuro*, 3(2), pp. 3089–3096. doi: 10.1523/ENEURO.0001-16.2016.

Zhou, H. J. *et al.* (2017) 'Leukemia Inhibitory Factor Contributes to Reactive Astrogliosis via Activation of Signal Transducer and Activator of Transcription 3 Signaling after Intracerebral Hemorrhage in Rats', *Journal of neurotrauma*, 34(8), pp. 1658–1665. doi: 10.1089/NEU.2016.4711.

Zhou, J. *et al.* (2012) 'Predicting regional neurodegeneration from the healthy brain functional connectome', *Neuron*, 73(6), pp. 1216–1227. doi: 10.1016/J.NEURON.2012.03.004.

Zhou, X.-H. *et al.* (2001) 'Neurocan is dispensable for brain development', *Molecular and cellular biology*, 21(17), pp. 5970–5978. doi: 10.1128/MCB.21.17.5970-5978.2001.

Zhuo, M. and Hawkins, R. D. (1995) 'Long-term depression: a learning-related type of synaptic plasticity in the mammalian central nervous system', *Reviews in the neurosciences*, 6(3), pp. 259–278. doi: 10.1515/REVNEURO.1995.6.3.259.

Zingg, B. *et al.* (2014) 'Neural networks of the mouse neocortex', *Cell*, 156(5), pp. 1096–1111. doi: 10.1016/j.cell.2014.02.023.

Zweier, J. L. *et al.* (1995) 'Enzyme-independent formation of nitric oxide in biological tissues', *Nature medicine*, 1(8), pp. 804–809. doi: 10.1038/NM0895-804.